

**ADVANCED TECHNOLOGIES FOR
IMPROVED DISCOVERY OF DNA APTAMERS
AND CHARACTERIZATION OF BIOLOGIC
AFFINITY REAGENTS**

by

ERIC OUELLET

B.Sc. (Honours), University of Ottawa, 2006

A THESIS SUBMITTED IN PARTIAL FULFILLMENT OF
THE REQUIREMENTS FOR THE DEGREE OF

DOCTOR OF PHILOSOPHY

in

THE FACULTY OF GRADUATE AND POSTDOCTORAL STUDIES
(Biomedical Engineering)

**THE UNIVERSITY OF BRITISH COLUMBIA
(Vancouver)**

July 2015

ABSTRACT

Biological reagents that recognize target molecules with high affinity and specificity are widely used as capture agents, diagnostic reagents, and therapeutics. Through their ability to adopt structures that confer binding affinity for a target, aptamers represent one major class of such reagents. However, their use is limited by the general inability of current selection methods to reliably discover high-quality aptamers. Inefficiencies in their selection are due in part to a lack of fundamental understanding of the mechanisms underpinning each step in the screening process.

This thesis reports on a series of studies conducted to define the factors and mechanisms currently limiting aptamer selections. That knowledge is then used to create highly effective strategies and technologies for ameliorating each limitation affecting their selection. The resulting collection of improvements is integrated into a novel selection workflow termed “Hi-Fi SELEX”. Those improvements include i) application of a novel “competent library” that eliminates fixed-region interference effects during selection, ii) development of effective chemistries to optimally retain desirable library members, iii) invention of simple methods to accurately quantify retained library diversity and mean binding affinity after each selection round, and iv) development of emulsion PCR methods to eliminate generation of amplification artifacts and v) achieve stoichiometric recovery of the desired single-stranded aptamer library. The resulting discovery platform greatly improves the reliability and speed in which useful panels of lead aptamers against several clinically-relevant targets are discovered.

Following initial selection of candidate aptamers based on binding affinity, further screening is typically required, in part to ensure target-specific binding – a performance need shared by antibodies selected against specific targets. However, moderate to high-throughput methods to efficiently screen panels of candidates for binding specificity are lacking. A new technology enabling label-free specificity screening of antibody or aptamer populations at suitable throughputs was therefore established at the proof-of-concept level. The novel microfluidic SPRi arrays described permit multiplexed detection of lead candidates by quantifying both equilibrium binding constants and binding kinetics for each interaction in an element-addressable fashion. The technology offers the ability to independently interrogate candidate affinity reagents and then recover those samples for downstream analysis.

PREFACE

“In research, you really have to love and be committed to your work because things have more of a chance of going wrong than right. But when things go right, there is nothing more exciting”

— Michael Smith (1993)¹

A version of Chapter 2 from this dissertation has been published as:

Ouellet E, et al. (2014) A simple method for eliminating fixed-region interference of aptamer binding during SELEX. *Biotechnology and Bioengineering*, 111: 2265-79

As first author, I designed the research together with my principle supervisor Dr. Charles Haynes, and performed all of the experimental work as described. In addition, I drafted the initial manuscript and further contributions to it were made by Dr. Charles Haynes. Valuable input from both committee members and advisors Drs. Karen Cheung and Eric Lagally were also received prior to publication.

A version of Chapter 3 from this dissertation has been published as:

Ouellet E, et al. (2015) Hi-Fi SELEX: A high-fidelity digital-PCR based therapeutic aptamer discovery platform. *Biotechnology and Bioengineering*, 112: 1506-22.

This work stems from a collaboration with members of the Conway group at the Centre for Blood Research (CBR; Vancouver, BC). As first author, I formulated the basis of the research along with significant intellectual input from Dr. Charles Haynes, Dr. Jonathan Foley (CBR) and Dr. Edward Conway (CBR). Drs. Foley and

Conway were instrumental in providing guidance in choosing clinically-relevant targets for investigation. During the course of the research, I performed all of the experimental work as described, with the exception of the haemolytic assays to evaluate complement pathway inhibition. That work was conducted by Dr. Foley in the Conway group with the help of Alice O'Byrne and Victor Lei. In addition, I drafted the initial manuscript and contributions to it were made by Drs. Haynes, Foley and Conway.

A version of Chapter 4 from this dissertation has been published as:

Ouellet E, et al. (2010) Parallel microfluidic surface plasmon resonance imaging arrays. *Lab on a Chip* **10**, 581-88.

This work results from a collaboration with members from the Institute for Systems Biology (ISB; Seattle, WA). As first author, I designed the basis of the research along with significant intellectual input and contributions from Christopher Lausted (ISB), Drs. Leroy Hood (ISB) and Eric Lagally. Contributions to the initial design of the microfluidic SPRi array were provided by Dr. Lagally. Bernard Coquinco and Dr. Lagally also significantly contributed to the design schematics and assembly of the constant LED driver used for the SPR imager. I performed all of the experimental work as described, including the fabrication of PDMS microfluidic devices (Appendix A), and the assembly of the SPR imager (Appendix B) along with developing its operating software (Appendix C). Dr. Lagally provided guidance throughout the research, and input from Cheng Wei Tony Yang and Tao Lin were also contributed ideas related to the work

TABLE OF CONTENTS

ABSTRACT	ii
PREFACE	iv
TABLE OF CONTENTS	vi
LIST OF TABLES	xi
LIST OF FIGURES	xiii
LIST OF SYMBOLS AND ABBREVIATIONS	xxv
ACKNOWLEDGEMENTS	xxix
DEDICATION	xxxii
Chapter 1: INTRODUCTION	1
1.1 THESIS OVERVIEW	1
1.2 PROPERTIES OF RELEVANT BIOLOGICAL AFFINITY REAGENTS	3
1.2.1 APTAMERS	4
1.2.1.1 CHEMISTRY AND STRUCTURE	5
1.2.1.2 BASIS FOR MOLECULAR RECOGNITION	8
1.2.1.2.1 COULOMBIC FORCES	9
1.2.1.2.2 DIPOLE-DIPOLE AND HIGHER-ORDER POLAR FORCES	10
1.2.1.2.3 HYDROPHOBIC INTERACTIONS	11
1.2.1.2.4 DISPERSION FORCES	12
1.2.1.3 ANALYTICAL AND CLINICAL APPLICATIONS	12
1.2.2 ANTIBODIES	15

1.2.2.1	CHEMISTRY AND STRUCTURE	15
1.2.2.2	BASIS FOR MOLECULAR RECOGNITION	18
1.2.2.3	ANALYTICAL AND CLINICAL APPLICATIONS.....	19
1.2.3	COMPARATIVE ADVANTAGES AND LIMITATIONS	20
1.3	CURRENT METHODS FOR DISCOVERING APTAMERS AND OTHER BIOAFFINITY REAGENTS	23
1.3.1	GENERAL APTAMER SELECTION STRATEGY	27
1.3.1.1	THE DNA OLIGONUCLEOTIDE LIBRARY.....	28
1.3.1.2	LIBRARY INCUBATION.....	30
1.3.1.3	PARTITION AND RECOVERY OF BOUND MEMBERS	31
1.3.1.4	AMPLIFICATION OF RETAINED MEMBERS	33
1.3.1.5	DNA LIBRARY REGENERATION	33
1.3.1.6	ROUND-BY-ROUND AND POST-SELEX APTAMER ANALYSIS AND PROCESSING.....	34
1.3.2	LIMITATIONS OF SELEX-BASED SCREENINGS	35
1.3.2.1	LIBRARY DESIGN AND PRESENTATION LIMITATIONS	36
1.3.2.2	IMPROVING INCUBATION AND PARTITION CONDITIONS	38
1.3.2.3	PCR AMPLIFICATION LIMITATIONS AND ARTIFACTS.....	42
1.3.2.4	LIBRARY REGENERATION ISSUES.....	43
1.3.2.5	CUMBERSOME RETAINED POOL CHARACTERIZATIONS.....	46
1.3.2.6	THROUGH-PUT: THE TIME REQUIRED TO COMPLETE A SELECTION	46
1.4	THESIS SCOPE AND OUTLINE	47
Chapter 2:	A SIMPLE METHOD FOR ELIMINATING FIXED-REGION INTERFERENCE OF APTAMER BINDING DURING SELEX.....	50
2.1	SYNOPSIS.....	50
2.2	EXPERIMENTAL METHODS	53
2.2.1	DNA LIBRARIES SYNTHESIS AND PURIFICATION.....	53
2.2.2	ISOTHERMAL TITRATION CALORIMETRY	56
2.2.3	SELEX-BASED SCREENINGS.....	56
2.2.4	REAL-TIME AMPLIFICATIONS OF ELUTED POOLS	59
2.2.5	QPCR-BASED BULK AFFINITY DETERMINATION	59

2.3	RESULTS AND DISCUSSION	60
2.3.1	SECONDARY STRUCTURES FORMED WITHIN FIXED REGIONS CAN INTERFERE WITH APTAMER BINDING THROUGH STERIC HINDRANCE EFFECTS	61
2.3.2	FIXED REGIONS CAN ELIMINATE APTAMER FOLD AND FUNCTION THROUGH HYBRIDIZATION WITH COMPLEMENTARY SEQUENCES WITHIN THE CORE REGION.	64
2.3.3	BLOCKING FIXED REGIONS WITH COMPLEMENTARY SEQUENCES RESTORES BINDING BY ELIMINATING INTERFERENCES DUE TO STERIC HINDRANCE OR LOSS OF REQUIRED APTAMER STRUCTURE.	66
2.3.4	PRE-BLOCKING FIXED REGIONS DOES NOT INTERFERE WITH OTHERWISE PROPERLY FUNCTIONING LIBRARY MEMBERS	69
2.3.5	PRE-BLOCKING FIXED REGIONS IS EQUALLY EFFECTIVE ON OTHER LIBRARY FORMATS	70
2.3.6	PRE-BLOCKING FIXED REGIONS PROVIDES A NOVEL AVENUE FOR SUCCESSFUL ENRICHMENT OF HIGH-AFFINITY APTAMERS DURING THE CRUCIAL FIRST ROUND OF SELEX.....	72
2.3.7	PRE-BLOCKING FIXED REGIONS ACCELERATES THE ENRICHMENT OF HIGH-AFFINITY APTAMERS AS MEASURED BY A SIMPLE NEW QPCR-BASED METHOD FOR MEAN-AFFINITY DETERMINATION	76
2.4	CONCLUDING REMARKS.....	81
Chapter 3:	DEVELOPMENT OF A HIGH-FIDELITY THERAPEUTIC APTAMER DISCOVERY PLATFORM.....	84
3.1	PLATFORM OVERVIEW	84
3.2	EXPERIMENTAL METHODS	87
3.2.1	MATERIALS.....	87
3.2.2	LIBRARY DESIGN AND SYNTHESIS.....	88
3.2.3	PREPARATION OF TARGET-IMMOBILIZED MAGNETIC BEADS	88
3.2.4	SURFACE PASSIVATION OF AND TARGET-IMMOBILIZATION ON NUNC WELLS	89
3.2.5	ELONA-TYPE ASSAY FOR DETECTING APTAMER BINDING TO HUMAN α -THROMBIN.....	91
3.2.6	HUMAN α -THROMBIN ENZYMATIC ACTIVITY ASSAY	92
3.2.7	HIGH-FIDELITY SELEX: LIBRARY SCREENING	93
3.2.8	HIGH-FIDELITY SELEX: DROPLET-DIGITAL PCR AMPLIFICATION	93
3.2.9	SINGLE-STRAND SELEX LIBRARY REGENERATION	94
3.2.10	APTAMER SELECTION BY CONVENTIONAL SELEX.....	95

3.2.11	AFFINITY AND SPECIFICITY CHARACTERIZATION OF ELUTED POOLS.....	96
3.2.12	ESTIMATING THE SEQUENCE DIVERSITY OF RETAINED POOLS.....	96
3.2.13	INDIVIDUAL APTAMER CLONING, PRODUCTION, AND BINDING CHARACTERIZATION	98
3.2.14	INHIBITION OF ACTIVATION OF THE ALTERNATIVE COMPLEMENT PATHWAY (FUNCTIONAL) ASSAY	98
3.2.15	ISOTHERMAL TITRATION CALORIMETRY.....	99
3.3	RESULTS AND DISCUSSION	100
3.3.1	HI-FI SELEX LIBRARY AND TARGET PRESENTATION METHODS IMPROVE ENRICHMENT OF HIGH-AFFINITY MEMBERS.	100
3.3.2	DROPLET DIGITAL PCR ENSURES PRECISE END-POINT AMPLIFICATION OF ELUTED LIBRARY MEMBERS.....	112
3.3.3	HI-FI SELEX PERMITS RAPID IDENTIFICATION OF HIGH-AFFINITY APTAMER POOLS	125
3.3.4	COMPETENT LIBRARIES RETAIN GREATER SELECTION DIVERSITY.....	129
3.3.5	FUNCTIONAL APTAMER SCREENING WITHIN THE HI-FI SELEX WORKFLOW PROVIDES A BOTTOM-UP APPROACH TO LEAD COMPOUND IDENTIFICATION.....	133
3.4	CONCLUDING REMARKS.....	140
Chapter 4:	PARALLEL MICROFLUIDIC SURFACE PLASMON RESONANCE IMAGING ARRAYS.....	142
4.1	SYNOPSIS.....	142
4.2	EXPERIMENTAL METHODS	146
4.2.1	CHEMICALS AND REAGENTS.....	146
4.2.2	DEVICE DESIGN OVERVIEW	146
4.2.3	MICROFABRICATION	148
4.2.4	INSTRUMENTATION.....	150
4.2.5	SPRI MEASUREMENTS	150
4.2.6	SAMPLE RECOVERY	151
4.3	RESULTS AND DISCUSSION	152
4.3.1	MICROSYSTEM DESIGN AND PERFORMANCE	152
4.3.2	MICRODILUTION NETWORK.....	152
4.3.3	PROOF-OF-CONCEPT: A-THROMBIN IMMUNOASSAY	153
4.3.4	MULTIPLE INTERACTIONS WITH SAMPLE RECOVERY.....	158
4.4	CONCLUDING REMARKS.....	162

Chapter 5: CONCLUSIONS AND OUTLOOK	164
5.1 PROPOSED FUTURE DEVELOPMENTS	168
BIBLIOGRAPHY	171
Appendix A: PROTOCOLS AND PROCEDURES	211
A.1 SPRI DEVICE MOLD DESCRIPTION	211
A.2 PDMS DEVICE FABRICATION	212
A.3 GOLD SUBSTRATE FABRICATION	215
A.4 IRREVERSIBLE SPRI DEVICE BONDING	218
Appendix B: CUSTOM-DESIGNED INSTRUMENTATION	219
B.1 SURFACE PLASMON RESONANCE IMAGER	219
B.2 CONSTANT CURRENT LED DRIVER	229
Appendix C: LABVIEW™ CODE FOR SPR IMAGER	231
C.1 DESCRIPTION OF LABVIEW™	231
C.2 THE MAIN VI	233
C.3 AVERAGE SPR IMAGES.VI	266
C.4 DRAW ROI.VI	267
C.5 FLAT-FIELD ACQUISITION.VI	269
C.6 FLAT-FIELD CORRECTION.VI	271
C.7 INTENSITY CORRECTION.VI	272
C.8 LABEL GOLD ROI.VI	274
C.9 MASK TO ROI.VI	276
C.10 ROI MASK.VI	277
C.11 ROI TRANSFORM.VI	279
C.12 ROTATION CONTROL.VI	281
C.13 SPR CALCULATIONS.VI	286
C.14 SPR CURVE.VI	288

LIST OF TABLES

Table 1-1	Brief overview of SELEX performance for aptamers partitioned using a variety of methods.....	40
Table 2-1	DNA primers, blockers and Library-1 sequences used in this study	54
Table 2-2	DNA primers, blockers and Library-2 sequences used in this study	54
Table 2-3	DNA aptamer sequences used in this study.....	55
Table 2-4	Thermodynamic data for binding of aptamers to their respective targets ^a measured by isothermal titration calorimetry.....	63
Table 3-1	ssDNA SELEX library, primers and blocker sequences used in this study	89
Table 3-2	Mean dissociation binding constants (K_d) measured by qPCR for enriched pools selected ^a against human α -thrombin using two different partition methods. The K_d values and their standard deviations are reported in nM units from duplicate experiments.	111
Table 3-3	Round-by-round mean dissociation constants (K_d) and standard deviations measured by duplicate qPCR experiments for 80-mer ssDNA aptamer and competent aptamer pools selected against human α -thrombin using the complete Hi-Fi SELEX platform described in Figure 3-1	126
Table 3-4	Round-by-round mean dissociation constants (K_d) and standard deviations measured by duplicate qPCR experiments for enriched pools selected against various therapeutic targets using either competent or standard library formats. All K_d values are reported in nM units.....	128
Table 3-5	Sequence diversity of aptamer pools selected against different targets using Hi-Fi SELEX and either competent or standard libraries. Diversity values and standard deviations reported from duplicate experiments represent the total number of unique aptamer sequences at the completion of the third round of selection.	130

Table 3-6 Core (random region) sequences of the top factor D-mediated inhibitors of complement activation (alternative pathway) recovered from the demonstration aliquot containing 40-60 of the unique aptamer sequences within the final retention pool after 3 rounds of Hi-Fi SELEX. Each isolated sequence (clone) reported in the Table are listed in order of % inhibition observed^a 136

Table 3-7 Isothermal titration calorimetry (ITC) data for binding of human factor D to either the full-length (full length) library sequence or the random-region (truncated) sequence of clones 19 and 29. Standard deviations for fitting both the equilibrium binding affinity and enthalpy are reported... 136

LIST OF FIGURES

Figure 1-1	Molecular structure of a single-stranded DNA polynucleotide chain (5'-AGCT-3'). Watson-Crick base pairing between complementary nucleotides (inset). Dashed lines indicate hydrogen bonds.	6
Figure 1-2	Representative molecular structures capable of being adopted by DNA aptamers. Black circles (●) indicate any of the 4 nucleotides. Blue lines (—●—) indicate Watson-Crick base pairing and grey lines (—) indicate Hoogsteen hydrogen bonds between G tetrads.	7
Figure 1-3	Depiction of a theophylline-binding RNA aptamer ⁷⁸ demonstrating exceptionally high discrimination against caffeine (inset) due to its additional sterically hindered N-7 methyl group. Molecular structures were created with PyMOL, accessed from the Protein Data Bank (entry 1O15).	9
Figure 1-4	Model representation of the Macugen (Pegaptanib) RNA aptamer's secondary and associated tertiary structure. Red circles indicate 2'-O-methylated purines, and 2'-fluorine-modified pyrimidines are shown in blue. Unmodified adenosines are also shown. Additional modifications to the aptamer include the 5' attachment of a 40 kDa polyethylene glycol (PEG) moiety and the attachment of an inverted thymine at the 3' end. Tertiary structure prediction was performed using the Assemble2 program (http://bioinformatics.org/assemble) interfaced with UCSF Chimera software (http://www.cgl.ucsf.edu/chimera) and represented via PyMol.	13
Figure 1-5	Common nucleic-acid modifications to aptamers discovered by SELEX to improve circulation half-life and stability.	14
Figure 1-6	Molecular assembly and structure of a protein. Monomeric amino acids are covalently tethered to form a polypeptide displaying various side chains (R _n) displaying a free amino (N-terminus) and carboxyl group (C-terminus). The primary structure of a polypeptide chain can fold into secondary α -helices and/or β -sheets to maximize the formation of H-bonds as well as other random coils for linking these structures. Tertiary and quaternary structural arrangements between individual or multiple polypeptides form functional proteins.	16

Figure 1-7	Schematic of an IgG antibody molecule with constant (black) and variable regions shown. The light chain variable region is encoded by the available combination of genes for the Variable and Joining segments, while the heavy chain is encoded with an additional gene for the Diverse segment.	18
Figure 1-8	Molecular size comparison between a (A) 15 nt anti-thrombin aptamer ¹⁷² (~5 kDa) and (B) an IgG-2a immunoglobulin (~150 kDa). Structures ^{173,174} were created with PyMOL, accessed from the Protein Data Bank (entries 148D and 1IGT, respectively) and are not drawn to scale.	23
Figure 1-9	General schema for library-based identification and characterization of novel aptamer products. When properly performed, each step further adds to the likelihood in identifying suitable members for use in research and diagnostics or as lead compounds for further therapeutic development. The standard SELEX platform does not provide data characterizing aptamer or retained pool specificity (N.D.)	26
Figure 1-10	Schematic of a standard SELEX process for DNA-based aptamer libraries	28
Figure 1-11	Schematic of an individual member of a DNA aptamer library shown with core variable region flanked by constant regions (black). The variable region is encoded by a combinatorially synthesized sequence of random nucleotides.	29
Figure 1-12	Schematic of various ssDNA library regeneration methods based upon either physical removal (streptavidin capture, gel electrophoresis) or enzymatic digestion (lambda exonuclease) of the anti-sense strands of dsDNA amplicons.	34
Figure 1-13	Putative high-molecular weight by-product conversion mechanism within a heterogeneous population of library members.	43
Figure 1-14	Graphical representation of available methods for PCR amplification of retained aptamer pools depicting possible outcomes.	45

Figure 2-1	Comparison of standard and proposed protocols for SELEX-based selection of aptamers. (Top box) Aptamers bind their target with high affinity through the specific fold of their consensus sequence. A typical aptamer library construct used in SELEX contains a random core region flanked by ~20 nt fixed regions to facilitate PCR amplification. Mechanisms by which the flanking regions can interfere with conventional SELEX, but which are ameliorated by the proposed method are then highlighted. In the proposed method, the fixed regions are blocked using complementary sequences. The aptamer fold is therefore confined within the random region and is able to bind its target with high affinity, allowing for efficient SELEX-type enrichment of high-affinity aptamers.....	52
Figure 2-2	Unwanted hybridization of sequences within the fixed regions can impede aptamer binding through steric hindrance effects. (A) The 15nt thrombin-binding consensus sequence (TBA15) folds into a G-quadruplex structure (top panel) that binds thrombin with nanomolar affinity as measured by isothermal titration calorimetry (bottom). Both the raw titration data and the differential heats fitted to a single-site binding model are shown in the bottom panel. (B) The 80 nt thrombin aptamer library construct (TBA15-L1) containing the TBA15 consensus sequence (highlighted) is predicted by Mfold to adopt a structure that includes two stem-loops adjacent to the G-quadruplex binding site formed through hybridization of nucleotides from the fixed (bold face type) and core regions. ITC data show that TBA15-L1 binds human α -thrombin very weakly at most (bottom). ITC experiments were performed in duplicate, from which average K_d values and standard errors were computed and reported. All base-pairing and secondary structure predictions were determined using the program Mfold. ³⁵²	62
Figure 2-3	Unwanted hybridization between complementary regions of the flanking sequences and the core sequence can eliminate aptamer fold and function. (A) The 29-mer streptavidin aptamer consensus sequence (SBA29) adopts a characteristic bulge-hairpin structure (top panel) that ITC data (bottom panel) show binds streptavidin with nanomolar affinity at physiological conditions. (B) The 80 nt aptamer library construct (SBA29-L1) containing the 29-mer consensus sequence (highlighted) is predicted by Mfold to have a structure that is devoid of the bulge-hairpin required for binding due to hybridization of nucleotides within the fixed regions (bold face) to nucleotides within the SBA29 consensus sequence itself (top). ITC data (bottom) show that SBA29-L1 does not bind to streptavidin. ITC experiments were performed in duplicate, from which average K_d values and standard errors were computed and reported.	65

- Figure 2-4** Blocking of sequences within the fixed regions can restore binding affinity by removing interferences due to steric hindrance. Addition and hybridization of either 5'-Comp-L1 (A) or 3'-Comp-L1 (B) results in partial restoration of binding affinity. (C) Hybridization of both complementary sequences results in complete restoration of binding affinity. ITC experiments were performed in duplicate, from which average K_d values and standard errors were computed and reported. All base-pairing and secondary structure predictions were determined using the program Mfold. 67
- Figure 2-5** Blocking of sequences within the fixed regions can restore binding affinity by removing interferences due to loss of structure. (A) The 29-mer streptavidin aptamer consensus sequence (SBA29) adopts a characteristic bulge-hairpin structure (top panel) that ITC data (bottom panel) show binds streptavidin with nanomolar affinity at physiological conditions. (B) Hybridization of both complementary sequences to the fixed regions of SBA29-L1 is predicted by Mfold to restore SBA29's characteristic bulge-hairpin secondary structure (top), and ITC data (bottom) show that binding affinity is restored and identical to that for SBA29. ITC experiments were performed in duplicate, from which average K_d values and standard errors were computed and reported. 68
- Figure 2-6** Application of methodology described in **Figure 2-5** to the 29-mer thrombin aptamer consensus sequence (TBA29). (A) TBA29 folds into a G-quadruplex structure (top panel). ITC data (bottom panel) showing TBA29 binds human α -thrombin with nanomolar affinity at physiological conditions. (B) When the flanking regions are replaced with those from Library-2, the resulting 80 nt aptamer library construct (TBA29-L2) containing the 29-mer consensus sequence (highlighted) is predicted by Mfold to contain base-pairing that interferes with the known G-quadruplex structure required for binding. This result is significantly different from the Library-1 version of the same aptamer (TBA29-L1), which retains the G-quadruplex structure. ITC data (bottom) show that TBA29-L2 binds thrombin with greatly weakened affinity compared to its Library-1 counterpart. (C) Hybridization of both complementary sequences to the fixed regions of TBA29-L2 is predicted by Mfold to eliminate all base pairs that serve to interfere with the G-quadruplex secondary structure (top), and ITC data (bottom) show full restoration of binding affinity to TBA29 or TBA29-L1 (**Table 2-4**). ITC experiments were performed in duplicate, from which average K_d values and standard errors were computed and reported. 71

- Figure 2-7** Pre-blocking the fixed regions of a library permits successful enrichment of high affinity aptamers during the early rounds of SELEX. (A) Conventional SELEX screening was performed using an aptamer library containing SBA29-L1 to permit detection and tracking of this representative high- affinity aptamer during the first round of SELEX. Magnetic beads coated with the target protein (streptavidin) were equilibrated with the library and then washed with binding buffer. Elutions were carried out in a denaturing buffer at 85°C containing 3.5 M urea. A parallel SELEX screening using the blocking method described here was also performed. Real-time amplification with a TaqMan™ probe generated against the target aptamer was used to characterize aptamer loss and the level of enrichment. Real-time amplification using SYBR green as readout was used to determine the total quantity of library members retained and eluted using each method. The relative quantity of SBA29-L1 in each fraction (wash at 140 mM NaCl and pooled elutions) was determined using the difference in threshold cycle value relative to the control (where no streptavidin was added). (B) Results for corresponding screenings of the L1 aptamer library containing TBA15-L1 against immobilized α -thrombin. 74
- Figure 2-8** Pre-blocking the fixed regions permits successful enrichment of both benchmark thrombin aptamers during the first round of SELEX against immobilized α -thrombin. (A) Partitioning of TBA15-L1 and TBA29-L1 in a conventional SELEX screening of Library 1 against magnetic beads coated with human α -thrombin. (B) Partitioning of TBA15-L1 and TBA29-L1 in a parallel SELEX screening of the same system using the pre-blocking method described. The pre-blocking strategy successfully enriches both thrombin aptamers at the completion of the first selection round..... 78
- Figure 2-9** Validation of the qPCR-based affinity-binding assay for the SELEX Library-1 version of the 29- mer thrombin benchmark aptamer. (A) Quantified bound fractions θ of TBA29-L1 were amplified by qPCR and plotted against the corresponding incubation concentration C . The equilibrium dissociation constant K_d was then estimated through data regression to the Langmuir isotherm equation. Amplification reactions were conducted in duplicates, in 20 μ l volumes, with the average value of C_q used to determine the bound fractions. (B) ITC results for titrating the same aptamer in a solution of thrombin at physiological conditions (top). The resulting fit to a single binding site model (bottom) yields the same binding affinity as measured by the qPCR-based assay..... 79

Figure 2-10 Changes in the bulk affinity of the retained aptamer pool in successive rounds of SELEX screenings of Library-2 against thrombin using either the conventional SELEX method or the proposed pre-blocking method. Three rounds of each SELEX method were conducted in parallel and average affinities of retained aptamer pools were measured by qPCR after each round. (A) When the fixed regions of the library are left unblocked, the average affinity of the enriched aptamer pool falls below the assay threshold after the second round (Table; Round 2, Unblocked), and lies in the μM K_d range at the end of the third round (Table; Round 3, Unblocked). (B) Pre-blocking the fixed regions of the library before every selection round results in greater enrichment of high-affinity aptamers..... 80

Figure 3-1 General workflow schema for the Hi-Fi SELEX platform. Potential interference effects due to the fixed regions common to all library members are first blocked using complementary sequences, leading to a “competent” starting library that contains a larger percentage of functionally active aptamer sequences. Targets immobilized on the surface of a microtitre-plate well coated with an adsorption-passivating polyglycol brush and surfactant are used to select library members at a theoretically preferred 100 to 1000:1 aptamer:target ratio with minimal non-specific aptamer retention. Retained members are recovered and amplified by dPCR using a protocol that eliminates formation of amplification by-products to preserve the relative abundances of retained library members while improving end-point yields and concentrations. The dPCR method also ensures that all amplicons are present in their fully complementary duplexed form, permitting stoichiometric conversion of amplified material into ssDNA using lambda exonuclease. The binding affinity of the enriched and dPCR-concentrated ssDNA pool is measured at every round of selection using a cost-effective label-free method based on qPCR. This process is then repeated by adding equimolar amounts of complementary oligonucleotides to form an enriched competent library until no appreciable increase in binding affinity can be detected. The final enriched pool is screened for functional members as well as for specificity before being sequenced, creating an integrated bottom-up approach to therapeutic aptamer discovery..... 86

Figure 3-2 General schema for electrophile-mediated immobilization of proteins onto the reactive Nunc well surface, followed by excess reactive group neutralization and surface passivation as described in the text. (Not drawn to scale) 91

- Figure 3-3** Relative amounts of SELEX library members that were irreversibly retained on Nunc Immobilizer™ plates which had undergone various surface treatments to block reactive sites and eliminate non-specific adsorption. No target was immobilized on the plates. (A) Comparison of amounts of library members that were non-specifically and irreversibly retained on the standard (commercial) Nunc Immobilizer™ plate surface (control), and after that surface has been pre-treated with 1 M ethanolamine, 1% Ficoll (w/v), 1% Ficoll and 1% polyvinyl alcohol (w/v), or Tris-containing aptamer folding (AF) buffer supplemented with 0.005 % Tween-20. (B) Comparison of levels of non-specific adsorption observed after blocking the Nunc Immobilizer™ plate surface with 1X AF buffer supplemented with 0.005 % Tween 20 for either 1 hr or 16 hrs. Standard deviations are reported for quadruplicate absorbance readings from duplicate experiments. For all ELONA-assay values reported, the background colorimetric signal when no SELEX library was incubated with the passivated surface was first subtracted.... 104
- Figure 3-4** Comparison of the performance of conventional SELEX and the proposed method in mitigating non-specific retention of library members during aptamer selection both in the absence and presence of 0.005% Tween-20. In each case, no target was immobilized and reactive coupling sites were blocked before incubating the surface with 1.2×10^{14} library members for 1 hr. The surfaces were then washed extensively with 1X AF buffer alone or supplemented with 0.005% Tween-20, and retained members were eluted and quantified via qPCR. Error bars reported represent the standard deviations from triplicate experiments .. 105
- Figure 3-5** Identification of reaction conditions for immobilizing a target protein on the modified display surface at densities most suitable for Hi-Fi SELEX. (A) Relative amounts of human α -thrombin immobilized on the display surface at different reaction pH..... 106
- Figure 3-6** Effect of surface passivation chemistry (A) and immobilization conditions (B) on the functional (serine protease) activity of immobilized target (human α -thrombin). Activities were determined by monitoring (Ex=370 nm, Em= 450 nm) the cleaving rate of a fluorogenic substrate. In both data sets, negative controls indicate the spontaneous cleavage rate measured for each passivated surface containing no immobilized α -thrombin. Standard deviations are reported from quadruplicate fluorescence readings from triplicate experiments. 109

- Figure 3-7** Effect of incubation time during a selection round on (A) competent library partitioning to the immobilized target (α -thrombin) phase, and (B) non-specific partitioning of the competent library to the same surface, but without immobilized target. Absorbance values reported reflect the quantity of aptamer recovered from the surface following selection and washing. Statistically significant differences in adsorbed amounts are reflected in the *p*-values reported, where a *p*-value > 0.1 is reported as not significant (n.s.), calculated from the standard deviations reported for quadruplicate absorbance readings from duplicate experiments. 110
- Figure 3-8** Comparison of PCR amplification methods for eluted aptamer pools. PCR amplification of (A) 10^8 or (B) 10^5 library members in a conventional bulk reaction. At either retained library abundance, self-priming and mis-priming of individual members leads to rapid conversion of the desired 80 bp amplified material towards aberrant high-molecular-weight by-products. Amplification must therefore be terminated at a low cycle number to avoid loss of product, leading to decreased yields. (C) When optimized for heterogeneous pools of retained library members, droplet PCR amplification avoids these artifacts by sequestering sufficiently small numbers of library members in isolated nL-sized droplets containing amplification reagents. The amplification process can be carried to end-point with minimal by-product accumulation, leading to much higher yields and less contamination of the desired 80 bp product..... 115
- Figure 3-9** Dependence of ddPCR performance in amplifying 10^8 unique library members on the mean copies-per-droplet (CPD) value used. Gel documentation and associated band-intensity analyses show that significant by-products formation occurs at CPD values above 50..... 116
- Figure 3-10** Schema depicting the principal duplex structure of amplicons, and the resulting action of λ -exonuclease on the 5'-phosphorylated reverse strand following PCR amplification of ssDNA SELEX libraries of low (Left column) and high (Right column) sequence diversity. 119
- Figure 3-11** Normalized melting curve data for amplicon pools (10^{14} total amplicons) generated from ssDNA SELEX libraries of different sequence diversity. The sequence diversity of the library is reported for each melting curve reported. Transitions (peaks) centered at a T_m of $\sim 81^\circ\text{C}$ and $\sim 67^\circ\text{C}$ correspond to melting of fully complemented homo-duplexes and partially complemented hetero-duplexes, respectively. 120

- Figure 3-12** Real-time λ -exonuclease-mediated hydrolysis of 5' phosphorylated anti-sense strands as a function of the sequence diversity of the initial amplification pool. Data for sequence diversities ranging from a single amplicon sequence to 10^9 unique sequences are reported along with that for a negative control (Negative) in which no λ -exonuclease was added. The data show that both the initial hydrolysis rate and the total extent of hydrolysis decrease with increasing sequence diversity. 121
- Figure 3-13** Relationship between the sequence diversity of the ssDNA SELEX library and the fraction f_{hetDNA} of those sequences participating in a hetero-duplex structure following amplification. (A) Normalized areas of the melting transitions (**Figure 3-11**) for the hetero-duplexes and homo-duplexes within the pool within the 10^{14} amplicons. (B) Fraction of all amplicons that are in a hetero-duplex structure, computed from the data in (A). Standard deviations are reported from quadruplicate experiments. 122
- Figure 3-14** Characterization of the amplification of a retained aptamer library containing 10^8 unique sequences by conventional bulk PCR (SELEX) or by the optimized ddPCR protocol. (A) Following end-point ddPCR at a CPD of 50, the resulting amplicon pool is reformed by breaking the droplet emulsion. Melt analysis of that pool shows a single transition centered at $T_m = 81^\circ\text{C}$, indicative of the formation of only fully-duplexed amplicons. In contrast, bulk PCR amplification of the retained library, as is commonly done in SELEX, results in a lower-concentration pool of amplicons that, when melted, exhibit two melting transitions centered at 67°C and 81°C whose areas correlate with the fraction of hetero-duplexed and homo-duplexed amplicons, respectively. (B) Conversion of ddPCR amplicons back into single-stranded library members using λ -exonuclease. When fully-duplexed ddPCR amplicons are processed (left-most gel), stoichiometric conversion of all dsDNA amplicons into ssDNA library members is achieved in no more than 60 min, a result identical to that observed for processing of a single amplicon (library) sequence at the same starting concentration (middle gel). In contrast, incomplete conversion occurs during processing of bulk-PCR amplified samples, where an abundance of hetero-duplexed members prevents complete enzymatic conversion into the desired single-stranded library (right-most gel). 124

- Figure 3-15** Schema and results for the alternative PCR/PicoGreen™ method for quantifying the sequence diversity of a retained aptamer pool. (A) Eluted library members are PCR amplified. (B) Calibration standards (10^8 to 10^0 individual members) generated by PCR amplification are then used to define the slope of fluorescently quantified double-stranded regions (generated by PicoGreen™ staining) of serially diluted amplicons. (C) The sequence diversity of an eluted pool can be quantified using this information. The data show that for library diversities spanning 6 orders of magnitude, the slope is inversely proportional to the sequence diversity due to the increased proportion of hetero-duplexes formed at higher diversities. Standard deviations are reported for slopes quantified by quadruplicate fluorescence readings from duplicate experiments. 131
- Figure 3-16** Comparison of diversities from eluted aptamer pools selected using competent (blocked) or standard (unblocked) libraries after the third round of Hi-Fi SELEX. (A) Raw data used to estimate pool diversity by the melting curve method defined in **Figure 3-11** and **Figure 3-13**. (B) Quantification of pool diversities by the PCR/PicoGreen™ fluorometric assay described in **Figure 3-15**. Standard deviations are reported for quadruplicate fluorescence readings from duplicate experiments..... 132
- Figure 3-17** SPR sensorgrams for binding of human factor D to immobilized biotinylated aptamers from (A) the entire round 3 pool ($K_d = 1.17 \pm 0.63$ nM) or (B) the representative factor D inhibiting aliquot generated from that pool and containing 40 – 60 unique aptamer sequences ($K_d = 0.97 \pm 0.43$ nM). Experiments were performed on a Biacore 3000 using an SA chip. Several concentrations of Factor D were injected, and the results fitted to a 1:1 Langmuir isotherm. 137
- Figure 3-18** M-fold predicted secondary structures for the full-length blocked aptamers sequences in **Table 3-6**. Several of the clones exhibit a common bulge-loop motif..... 138
- Figure 3-19** Human factor D binding affinities and specificities of individual aptamers (library form) competently selected in three rounds of Hi-Fi SELEX and present in a small aliquot containing 40 to 60 of the retained library sequences that together inhibit factor D mediated activation of complement. (A) Binding affinities were measured using the full-length library form of the aptamer sequence. The binding isotherm for an 80 bp double-stranded DNA is also shown as a negative control. (B) Specificities measured using binding affinity to human serum albumin (HSA) as a metric. Data are reported for clone 28, as it was the only aptamer (library form) showing a measurable affinity for HSA. 139

Figure 4-1	Mask design of the microfluidic device. The chip consists of a top control layer and a bottom flow layer. The array consists of 264 individually addressable chambers, each with a volume of 700 pL. The row multiplexer (top left) selects a particular group of 4 chambers by setting a 4-bit gray code. Sample is then loaded into a particular group of chambers. The selected group of chambers (top middle) is divided into 4 individual chambers by a series of compartmentalization valves. Here, the valves of chamber 1 are opened to let sample through. After loading the sample, the device operation switches to washing mode, in which all chamber valves are closed and the wash loop is opened. Wash buffer is introduced, flushing any remaining sample in the channel. A series of micromixers (top right) allow serial dilutions of samples into 6 different concentrations.....	148
Figure 4-2	Photograph of the microfluidic chip bonded to a gold patterned glass slide. (Inset) A close-up of the marked region of the microarray; scale bar: 650 μm	149
Figure 4-3	Serial dilutions from the chaotic advection micromixers on the chip. Top: schematic diagram of the serial dilution network. Bottom: fluorescence images and intensities of six different concentrations of fluorescein created by the dilution network from a stock solution of fluorescein (45 mM). The mean intensity of fluorescence was determined for all 4 chambers within a group.....	154
Figure 4-4	SPR images collected with the microfluidic chip (A) before the injection of anti-thrombin IgG; (B) after injection of anti-thrombin IgG; (C) difference image obtained for anti-human α -thrombin. Human α -thrombin was loaded in a pattern (D) to confirm the element addressability of the design (E) Intensity profile of the region marked in (C).....	156
Figure 4-5	SPRi sensorgrams of anti-human α -thrombin binding to surface-immobilized thrombin on the microfluidic chip. The fitted curves yield an equilibrium dissociation constant of 5.0 ± 1.9 nM.....	157
Figure 4-6	Residual plot of fittings for SPRi data shown in Figure 4-5	157
Figure 4-7	Recovery of surface-bound fluorescently-labeled antibodies from the microfluidic SPRi chip. (A) SPRi sensorgram of the interaction process and collected fraction marked as I, II and III. Step 1 – protein immobilization on the gold surface, Step 2a,b – association and dissociation phase of the protein-IgG complex, Step 3 – regeneration phase.	159
Figure 4-8	Standard curves for fluorescence quantitation of recovered labelled-antibody fractions from microfluidic SPRi arrays.....	161

Figure B-1 Initial SPRi setup for mounting optical breadboards, rotation stages and optical rails. Depiction adapted from publicly available CAD drawings obtained from ThorLabs and Newport Corporation..... 221

Figure B-2 Summary of SPRi optical components and their mounting order on the optical rails. Depiction adapted from publicly available CAD drawings obtained from ThorLabs and Newport Corporation..... 223

Figure B-3 Custom-built prism holder depiction with equilateral prism and clamping arm..... 224

Figure B-4 SPR imager enclosure construction. (A) Construction rails are fastened together to form an enclosure large enough to contain the entire optical setup. (B) Blackout material is cut to dimension and inserted to enclose the imager. Depiction adapted from publicly available CAD drawings obtained from ThorLabs and Newport Corporation..... 225

Figure B-5 Final depiction of the fully enclosed SPR imager with corresponding lid, providing access to the prism surface. The rotation stages and CCD camera are connected to a computer and the LED to a constant current source (not shown). Depiction adapted from publicly available CAD drawings obtained from ThorLabs and Newport Corporation 226

Figure B-6 LED constant current driver schematic. This was developed in collaboration with Bernard Coquinco and Dr. Eric Lagally (Michael Smith Laboratories – UBC Vancouver)..... 230

Figure B-7 LED driver circuit board diagram and electronic components. (A) Top view: Copper Layer (Blue), Vias (Green) and Connectors (Grey). Bottom view showing the ground mounting hole: Copper Layer (Blue), Vias (Green). Dimensions 20 mm X 35mm. (B) Representation of the assembled printed circuit board. 230

LIST OF SYMBOLS AND ABBREVIATIONS

Abbreviations

λ -exonuclease	Lambda Exonuclease
3'-Comp	Complementary sequence of the 3' fixed region
5'-Comp	Complementary sequence of the 5' fixed region
A	Adenine
AF	Aptamer folding
aHUS	Atypical hemolytic-uremic syndrome
AMD	Age-related macular degeneration
B cell	Lymphocyte produced in the bone marrow of humans
bp	Base pair
C	Cytosine
C _H	Constant region of the heavy chain of an IgG
C _L	Constant region of the light chain of an IgG
C3b	Oponin resulting from cleaving complement component C3
C5	Complement component 5
C6	Complement component 6
C5b	Initiator of the terminal complement complex; cleaved from C5
C7	Complement component 7
C8	Complement component 8
C9	Complement component 9
C5b-9	Terminal complement complex comprising of C5b, C6, C7, C8 and C9
CAD	Computer-aided design
CCD	Charge-coupled device
CDR	Complementarity determining region
CE	Capillary electrophoresis
CPD	Copies per droplet
DNA	Deoxyribonucleic Acid
ddPCR	Droplet digital PCR
dNTP	Deoxynucleotide triphosphate

dPCR	Digital PCR
dsDNA	Double-stranded DNA
dUTP	Deoxyuridine triphosphate
<i>E. coli</i>	<i>Escherichia coli</i>
ELONA	Enzyme-linked oligonucleotide assay
Fc	Crystallizable (constant) fragment of an IgG
F _v	Variable fragment of an IgG
Fab	Antigen-binding fragment of an IgG
FDA	US Food and Drug Administration
FOR	Forward primer
FQ	Fluorescence quencher
FWMH	Full width at half maximum
G	Guanine
Hi-Fi	High fidelity
HMW	High molecular weight
HPLC	High-performance liquid chromatography
HRP	Horseradish peroxidase
HSA	Human serum albumin
Ig	Immunoglobulin
IgG	Immunoglobulin isotype G
ITC	Isothermal titration calorimetry
L1	Library 1 format
L2	Library 2 format
LED	Light-emitting diode
LNA	Locked nucleic acid
LOD	Limit of detection
M-SELEX	Microfluidic SELEX
mAb	Monoclonal antibody
Macugen	Pegaptanib sodium – PEG modified anti-VEGF ₁₆₅ aptamer
mRNA	Messenger RNA
MW	Molecular weight
MWCO	Molecular weight cut-off
N	Random nucleotide
N.D.	No data available
NGS	Next-generation sequencing
nt / -mer	Nucleotide
pAb	Polyclonal antibody
PCB	Printed circuit board
PCR	Polymerase chain reaction
qPCR	Quantitative PCR

R	Amino acid side chain
REV	Reverse primer
RNA	Ribonucleic Acid
ROI	Region of interest
RPM	Revolutions per minute
S/N	Signal to noise ratio
SBA29	29 nt streptavidin-binding aptamer
SELEX	Systematic evolution of ligands by exponential enrichment
siRNA	Small interfering RNA
SOIC	Small outline integrated circuit
SPR	Surface plasmon resonance
SPRi	Surface plasmon resonance imaging
ssDNA	Single stranded DNA
ssRNA	Single stranded RNA
SW	Stringent wash
T	Thymine
Taq	<i>Thermus aquaticus</i>
TBA15	15 nt thrombin-binding aptamer
TBA29	29 nt thrombin-binding aptamer
V _H	Variable region of the heavy chain of an IgG
V _L	Variable region of the light chain of an IgG
VBA25	25 nt VEGF-binding aptamer
VEGF	Vascular endothelial growth factor
VI	Virtual instrument

Chemical Names

EDC	1-ethyl-3-(3-dimethylaminopropyl) carbodiimide hydrochloride
EDTA	Ethylenediaminetetraacetic acid
FAM	6-Carboxyfluorescein
FITC	Fluorescein isothiocyanate
GVB	Gelatin veronal buffer
HRP	Horseradish peroxidase
MES	2-[N-morpholino]ethane sulfonic acid
NHS	N-hydroxysuccinimide
PBS	Phosphate buffered saline
PDMS	Polydimethylsiloxane
PEG	Poly-ethylene glycol
PVA	Poly (vinyl alcohol)
TEG	Tri-ethylene glycol

TMB	3,3',5,5'-tetramethylbenzidine
Tris	Hydroxyl-methyl-aminomethane
Tween-20	Polyoxyethylene (20) sorbitan monolaurate

Greek Letters and Symbols

A	Total fraction of aptamers
$A_{67^{\circ}\text{C}}$	Area beneath melt peak at 67°C
$A_{81^{\circ}\text{C}}$	Area beneath melt peak at 81°C
A_i	Aptamer fraction i
A_j	Aptamer fraction j
C	Concentration; M
C_q	Threshold cycle number
ΔC_q	Difference in C_q
f_{hetDNA}	Fraction of heteroduplexed DNA amplicons
g	Gravitational force
kDa	Kilodalton; kg mol⁻¹
K_d	Equilibrium dissociation constant ; M
k_{off}	Dissociation rate constant ; s⁻¹
k_{on}	Association rate constant; M⁻¹ s⁻¹
n	Stoichiometry
n_d	Refractive Index
P	Molecular target
PE	Partition efficiency
t	Time
T	Temperature; K
T_m	Melting temperature ; °C
ΔG	Change in Gibb's free energy; kcal mol⁻¹
ΔH	Change in enthalpy; kcal mol⁻¹
ΔS	Change in entropy; kcal mol⁻¹
θ	Bound fraction
θ_i	Bound fraction occupied by aptamer i
λ	Wavelength; nm
σ	Standard deviation

ACKNOWLEDGEMENTS

“Alone we can do so little; together we can do so much”

— Helen Keller (c.a. 1920)²

My recent marriage to Julie Villeneuve was by far my greatest accomplishment here at UBC, for without her unconditional love and support, none of this would have been possible. Knowing that I could lean on her during the most difficult times gave me the capacity to venture this far. Julie is the most genuine person I know and her eternal optimism makes any daunting task seem routine. As a pillar of support, she gave me a much deeper understanding of the important things in life; the rest is simply just details.

My ability to formulate ideas and devise solutions continues to evolve and has largely been developed by interacting with some of the greatest scientific and engineering minds here at UBC. Collectively, these individuals have helped shape my graduate career while showing genuine interest in seeing me succeed.

My initial advisor, Dr. Eric Lagally gave me the greatest opportunity to become one of the initial members of his research group. During my short amount of time with him, I was fortunate enough to meet an expert in integrated microsystems with an extraordinary vision for developing advanced tools for accelerating discoveries. Moreover, Dr. Lagally provided me with unique opportunities to present my work at international conferences. I fondly remember my time spent in his lab, which enabled me to develop new perspectives and an exciting set of skills that continue to provide motivation for exploring unique ideas and areas of research.

The most fruitful discussions I had were with one of the greatest minds at UBC, Dr. Charles Haynes, for which the majority of ideas presented in this thesis originated. I am immensely grateful to have had the opportunity to continue my doctoral degree under his guidance, where he devoted countless hours to my graduate education and research. More importantly, the frequent advice and unwavering support I received from Professor Haynes has enabled significant expansions to my intellectual repertoire, where I continue to learn and benefit from his teachings. He provided multiple opportunities in making sure I took full advantage of the creative environment here at UBC by facilitating open discussions and collaborations. And thanks to Dr. Louise Creagh for dedicating significant time and effort with the details of research. I am particularly grateful for her willingness in providing me with learning and teaching opportunities while working in the Centre for Biothermodynamics and the CHBE graduate laboratories. Both are genuine and loving people whose generosity is eclipsed only by their kind words.

I have also benefited from several discussions with Dr. Jayachandran (Jay) Kizhakkedathu, Dr. Edward Conway and Dr. Jonathan Foley. I wish to express my sincere gratitude for their significant time investments in providing guidance and opportunities for applying this research toward more clinically-relevant settings. I am also fortunate to have been granted the opportunity by Dr. Conway to present this research at the Earl W. Davie Symposium. And thanks to Alice O'Byrne and Victor Lei for their technical support.

I also had the immense pleasure in having both Dr. Karen Cheung and Dr. Carl Hansen by my side from the very beginning. In particular, my affinity for developing new tools and technologies in Biomedical Engineering was amplified by having numerous fulfilling discussions with them and their contagious enthusiasm for pushing the limits of research continues to be a source of motivation. Their honesty and support in guiding my research direction has largely contributed to my success.

I also wish express my deepest gratitude to Dr. Jim Kronstad, Darlene Crowe and Pal Bains for having provided support throughout my journey here at the Michael Smith Laboratories, in particular during the transition period following the Lagally Lab decommission.

I am also very grateful to have shared this experience with several friends, namely Roza Bidsharhi and Louise Lund, Dr. Curtis Hughesman, Kareem Fakhfakh, Dr. Patrick Francis and Dr. Derek Choy. Your friendship has made this research experience fulfilling, often enlightening and always fun.

I also wish to thank several colleagues, namely former Lagally lab members Tony Yang, Tony Lam, Jie Yu, Bernard Coquinco, Christina Kwok and Antonio Villegas. Additionally, my earliest and fondest memories of my time at UBC will always include those who have helped shape my initial graduate experience, Darek Sikorski, Adam White, Anupam Singhal, Adriana Cajiao, Sonia Lala, Jake McIvor, Kyle Eckhardt, Andrew Ibey, Tim Leaver, Kevin Heyries, Véronique Lecault, and countless others.

I am also grateful to my family members who have supported me through this journey. Particularly, my grandparents Marcel and Margo, as well as Joanne, Josée, Sébastien, Christine and Richard: your kind words and constant encouragement have helped me venture this far.

And finally, to my parents: while I believe that I have reached the limits of schooling, my education continues to expand as a result of your patience and devotion in planting the early seeds of personal and intellectual growth. I am grateful to have had some of the best teachers during my early years of life.

TO MY WIFE

JULIE

...the eternal optimist

YOUR GENTLE NUDGES DURING THESE PAST YEARS
HAS MADE IT ALL POSSIBLE

Chapter 1

INTRODUCTION

“Science sometimes requires courage, at the very least the courage to question the conventional wisdom”

— Carl Sagan (1979)³

1.1 THESIS OVERVIEW

Biological reagents that recognize target molecules with both high affinity and specificity are routinely required in the life sciences and clinics, where in the latter case they often serve as diagnostic or therapeutic agents. Amongst the available classes of affinity reagents, antibodies currently represent the gold standard. Applications of antibodies as molecular recognition agents pre-date the 1950's,^{4,5} but their ubiquitous use follows largely from development of the hybridoma technology by Kohler and Milstein⁶ in 1975. This landmark in modern biotechnology has enabled scientists to produce monoclonal antibodies (mAbs) with desired properties in a more routine and reproducible manner. Antibodies, including mAbs, often bind antigens with high affinities; equilibrium dissociation constants (K_d values) less than order nM are frequently reported.⁷ Moreover, binding is often highly selective, as demonstrated by the ability of mAbs to discriminate post-translational modifications of proteins, as well as among more subtle protein isoforms.^{8,9} These exquisite binding properties can serve to maximize therapeutic mAb potency and minimize off-target effects, while their large size enables relatively long circulation half-lives.^{10,11} Many advances in medicine and

molecular biology are therefore inextricably linked to antibody science, including the explosive growth in mAbs as therapeutic agents over the past 25 years.^{12,13}

However, while remarkable, antibodies are nonetheless limited in certain important aspects. As large complex multimeric proteins, they are sensitive to environmental conditions, and can rapidly be inactivated under acidic conditions or at elevated temperatures. Though significant advances have been made toward their manufacture, mAbs remain expensive to produce and purify at larger scales, especially when being developed for research and diagnostic applications, as opposed to more valuable therapeutic molecules. When used as therapeutic agents, most mAbs are incapable of permeating cells efficiently, which effectively restricts their application to extracellular antigens. Moreover, though humanized-antibody technology has greatly reduced immune responses, therapeutic mAbs often do not escape immune surveillance completely, further challenging their long-term efficacy.¹⁴

As a result, the development of mAb alternatives for use as affinity tools and therapeutic agents has gained considerable interest in recent years.¹⁵ A number of simplified antibody forms including nanobodies, V_H and V_L antibody domains, and single-chain variable fragments have proven effective as mAb surrogates.¹⁶ In addition, a particular class of nucleic acids, known as aptamers^a, has emerged as a potent option.¹⁷ Each comprised of a short single-stranded (ss) oligonucleotide, aptamers can be inexpensively produced at large scale with high precision. The discovery of useful aptamers is likewise facilitated by the ability to easily and cost-effectively synthesize large semi-combinatorial libraries of ssDNA or ssRNA that can be subjected to *in vitro* Darwinian-type selection strategies to enrich sequences that exhibit high affinity and specificity for a target as a result of their unique

^a The definition of aptamers in this thesis is applied in accordance with the more general notion of being comprised of nucleic acid molecules, as originally described. However, aptamers can also be comprised of amino acids, commonly referred to as peptide aptamers, and will not be discussed any further.

tertiary structures. However, current aptamer selection methods are not sufficiently robust to ensure the timely and cost-effective discovery of aptamers useful as analytic/diagnostic reagents or lead candidates for therapeutic development.¹⁸ Existing aptamer discovery platforms would therefore benefit from development of higher-throughput methods to more accurately and comprehensively screen for desired attributes, including binding affinity and specificity. The technologies and methods reported in this thesis are collectively aimed at providing the ability to more efficiently discover and characterize analytic or therapeutic aptamers. One of those technologies is a microfluidic platform enabling highly multiplexed characterization of analyte binding to immobilized affinity reagents, or vice versa. Developed to the proof-of-concept level, this technology can be applied to panels of either aptamers or mAbs to, for instance, characterize binding specificity.

1.2 PROPERTIES OF RELEVANT BIOLOGICAL AFFINITY REAGENTS

The successful completion of the Human Genome Project^{19,20} has advanced medical research in part by reporting new genes and gene mutations that have since been linked to a range of life-threatening disorders.^{21,22} The companion Human Proteome Project^{23,24} is in turn providing greater understanding of the manner in which germ-line and somatic mutation of a genome alter the functions and abundances of the associated gene products, including enzymatic activities and biological pathways that regulate cell proliferation, differentiation and apoptosis. The study of (somatic) variations in gene/peptide sequences, gene copy numbers and protein expression levels has enabled the discovery of mutational drivers and reliable biomarkers of disease progressions,^{25,26} enhancing our knowledge of fundamental causes to a number of hereditary and acquired disorders,²⁷⁻²⁹ as well as the associated inventory of potential targets for diagnostics and therapeutics development. Establishing more rapid and reliable methods for identifying and

screening large libraries of potential lead compounds, including aptamer and antibody-based compounds, will therefore become increasingly significant for continued development of novel prognostic and therapeutic pathways to personalized and preventative medicine.

Work described in this thesis is aimed at improving technologies for discovering and/or characterizing two major classes of biological affinity reagents: primarily (i) nucleic acid aptamers, and in certain cases (ii) monoclonal antibodies. Structures, clinical uses and bio/chemical properties of each class of molecules are therefore described with the aim of providing insight into mechanisms of selective molecular recognition, as well as defining requirements a screening assay must offer in order to achieve robust discovery of useful molecules.

1.2.1 APTAMERS

The discovery of aptamers in 1990 by three independent laboratories³⁰⁻³² spawned their now rapidly growing use as diagnostic³³ and biopharmaceutical³⁴ agents. These short (< 60 nt) single-strand oligonucleotide ligands selectively bind their respective target with an affinity mirroring those typically achieved by antibodies. As a growing class of biological affinity reagents, aptamers possess several unique advantages and potential limitations, particularly when applied as a therapeutic. High-affinity aptamers have been reported for diverse types of targets including proteins, peptides, carbohydrates, small organic molecules, and even whole cells.³⁵⁻⁴² At the time of writing of this thesis, over 2000 DNA and RNA aptamers have been discovered against ca. 500 different targets.⁴³ Currently, nine of these aptamers are either approved or in clinical trials for treatment of various ailments, including age-related macular degeneration (AMD), coronary disease, bleeding disorders and cancers,^{44,45} with several others shown to be of potential clinical significance.^{46,47}

1.2.1.1 CHEMISTRY AND STRUCTURE

Nucleic acids are versatile molecules despite their relatively limited natural chemistry when compared to, say, proteins. Deoxyribonucleic acid (DNA) adopts a protective double-stranded helical structure in its equilibrium state within the nucleus. Ribonucleic acid (RNA), a primarily single-stranded oligonucleotide, mediates the translation of genes into polypeptides (e.g. proteins). However, both DNA and RNA can function in ways unrelated to their role in encoding or transferring genetic information. In particular, the discovery of ribozymes^{48,49} in the early 1980's and subsequent seminal studies on deoxyribozymes (DNA-enzymes)⁵⁰ have proven that DNA and RNA molecules can serve as more than simple passive carriers of genetic information; they have the capacity to adopt sequence-specific tertiary structures that permit their participation in biological processes as catalysts or binding partners.

Both DNA and RNA are naturally occurring polymers built from monomeric units called nucleotides. Each nucleotide is comprised of three chemically and structurally distinct components: a phosphate group, a cyclic pentose sugar and an aromatic nitrogenous base. Nucleotides differ from each other in both their natural sugars (D-deoxyribose in DNA and ribose in RNA) and their aromatic bases. Four different bases naturally occur in DNA: the purines, adenine (A) and guanine (G), and the pyrimidines, cytosine (C) and thymine (T). A single-stranded DNA chain is formed by linking nucleotides (A, G, C and T) via a phosphodiester bond between the 3' carbon of the deoxyribose from the first nucleotide to the 5' carbon of the next via its ionized phosphate group. Each polynucleotide chain is therefore comprised of a linear sequence of nucleotides that is denoted and read in the 5' to 3' direction (**Figure 1-1**).

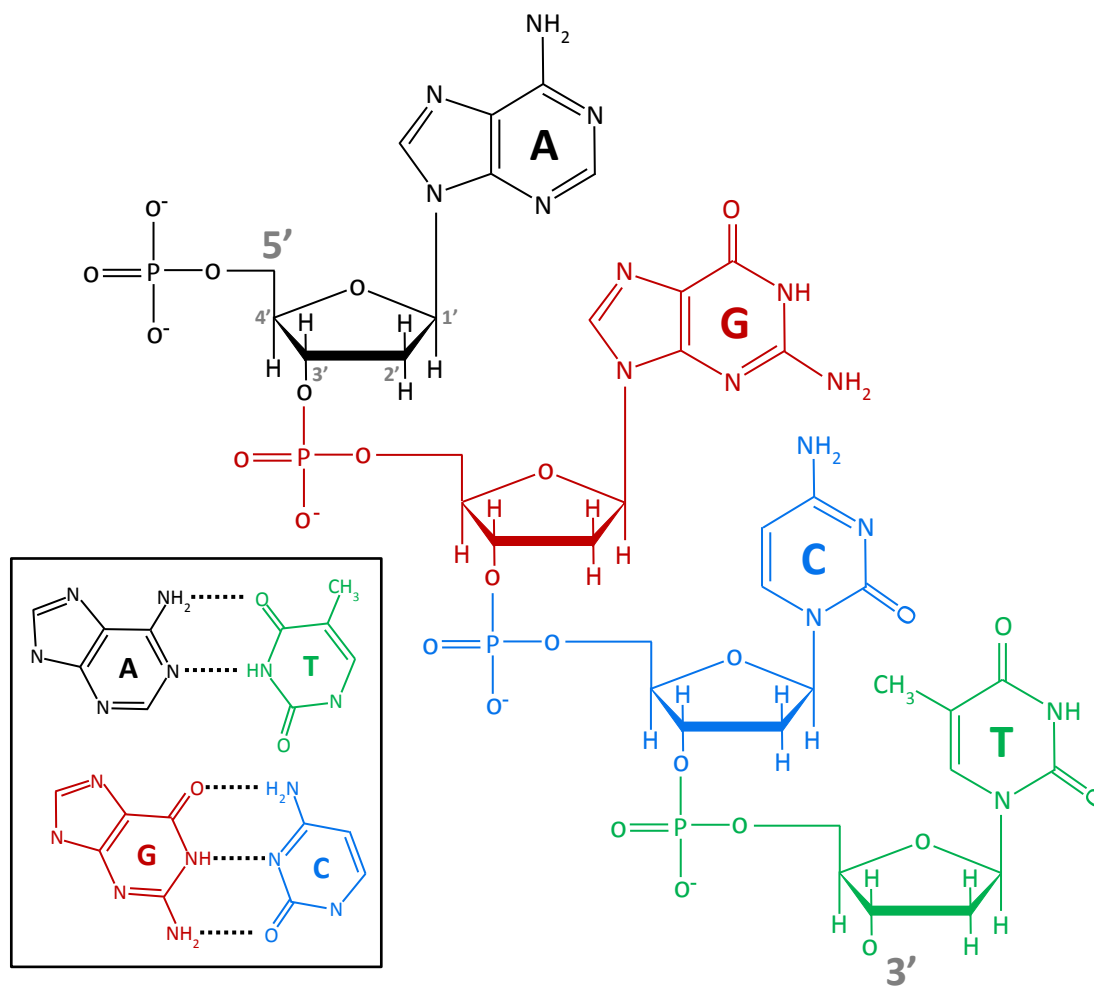


Figure 1-1 Molecular structure of a single-stranded DNA polynucleotide chain (5'-AGCT-3'). Watson-Crick base pairing between complementary nucleotides (inset). Dashed lines indicate hydrogen bonds.

Single-stranded DNA or RNA can also form stable three-dimensional structures via intra-molecular Watson-Crick base pairings as well as other non-canonical interactions⁵¹⁻⁵³ between nucleotides contained within the sequence. Aptamers^b are single stranded oligonucleotides that exploit this capacity to recognise a ligand by folding into a specific structure that confers binding affinity. The intra-molecular interactions that dictate aptamer fold include the hydrogen bonds and base-

^b Unless otherwise specified, the remainder of this thesis will refer to 'aptamer' as being comprised of DNA nucleotides.

stacking interactions of Watson-Crick base pairs—where A pairs with T, and G pairs with C (**Figure 1-1**, inset). Oligonucleotide length and nucleotide sequence define the double-stranded helical segments formed and the resulting stable secondary and tertiary structure adopted by an aptamer. However, as aptamers are highly charged polyanions, their structure, flexibility and binding properties are also influenced by the large negative charge density generated by the phosphodiester backbone. Repulsive Coulombic forces are therefore present and can act to destabilize structure to a magnitude modulated by the dipole shielding effects of the solvating water molecules, and the Debye electrostatic shielding and ion-pairing contributions of monovalent (e.g. Na⁺, K⁺) and divalent (e.g. Mg²⁺, Ca²⁺) cations present through dissociation of salts. Direct association of counter-ions to an aptamer can neutralize its negative charge density, permitting adoption of (more) stable base-pairing conformations and higher-order structures including any combinations of stem-loops^{54,55} or hairpins^{56,57}, bulges^{58,59}, pseudoknots^{60,61}, kissing-complexes^{62,63} or quadruplexes^{64,65} (**Figure 1-2**).

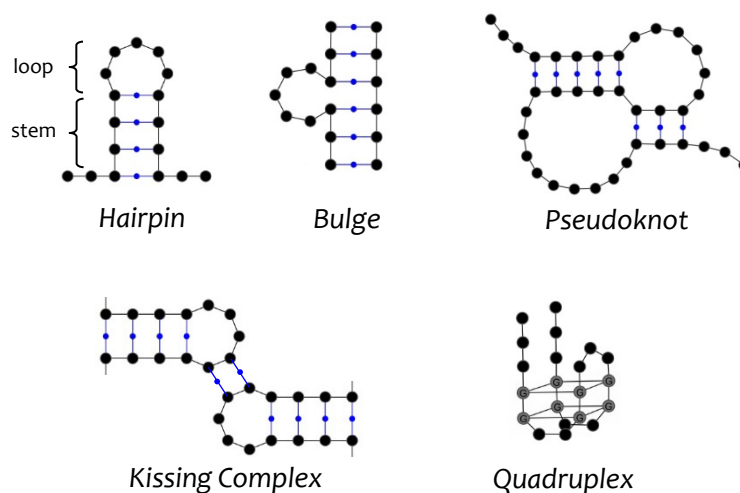


Figure 1-2 Representative molecular structures capable of being adopted by DNA aptamers. Black circles (●) indicate any of the 4 nucleotides. Blue lines (—●) indicate Watson-Crick base pairing and grey lines (—) indicate Hoogsteen hydrogen bonds between G tetrads.

Generally, divalent cations such as magnesium (Mg^{2+}) are much more effective in stabilizing dsDNA helices^{66,67} than are monovalent cations such as sodium (Na^+) or potassium (K^+), while high concentrations of the latter ions can increase the flexibility of ssDNA as evidenced by a shortened persistence length.^{68,69}

1.2.1.2 BASIS FOR MOLECULAR RECOGNITION

Due to their ability to tightly bind molecular targets in a very specific fashion, aptamers may be considered synthetic analogues to antibodies. Aptamers generally possess a higher degree of structural plasticity that allows binding of targets through subtle perturbations in fold to accommodate the surface topology presented on the epitope.⁷⁰⁻⁷² Their molecular recognition mechanism can therefore differ somewhat from the 'lock and key' binding model usually associated with antibodies. Aptamers capable of binding structurally ill-defined (conformationally degenerate) targets strongly and specifically are rare,⁷³ although ones capable of binding denatured targets through an induced affinity mechanism have been reported.^{74,75} But, like antibodies, aptamers are able to discriminate between minor chemical variants/isoforms.^{76,77} A particularly salient example of this is provided in **Figure 1-3**, which describes binding of an RNA aptamer to theophylline via hydrogen bonding and stacking interactions.⁷⁸ The bulge-loop motif of this aptamer confers a 10,000-fold higher binding affinity to theophylline compared to caffeine, which differs from theophylline in chemistry by a single methyl group. The presence of this methyl group sterically hinders caffeine binding by disrupting the pseudo-base pair formed between the adjacent cytosine and the purine-rich binding-region of the aptamer.^{79,80} Steric repulsion is one of many intermolecular forces by which aptamer specificity is conferred.^{79,81,82} Other important forces are described below. Their variety and unique dependencies on intermolecular separation distances and solvent effects serve to make rationale design of aptamers

forces will contribute to binding recognition either favourably, including through the formation of intermolecular ion pairs and bridges, unfavourably, through charge-charge repulsion, or a combination thereof.

In aptamer-protein complexes, ion pairs may form between the univalent phosphate groups of the aptamer backbone and positively charged moieties of proteins, including the ϵ -amino group of lysine, the guanidinium group of arginine, the protonated imidazole ring of histidine, and the α -terminal amine.⁸⁴ Additionally, intra- and inter-molecular salt bridges formed through a charge-neutralizing free ion may also contribute to aptamer affinity.⁸⁵ However, good specificity is generally not achieved when aptamer binding is dominated by electrostatic forces, as aptamers then tend to behave as more aspecific ion-exchange ligands, such as those employed in classic ion-exchange chromatography. Aptamer selection processes are therefore likely to enjoy greater success if they include steps to disfavour retention and enrichment of ion-exchange-dominated binders. Fortunately, therapeutic aptamers typically achieve binding specificity and affinity through a complex ensemble of intermolecular forces.^{86,87}

1.2.1.2.2 DIPOLE-DIPOLE AND HIGHER-ORDER POLAR FORCES

Compared to that between two ions of opposite charge, attraction between permanent dipoles, of which the hydrogen bond is the best known and among the strongest, decreases more rapidly with separation distance. Nevertheless the considerable hydrogen bonding potential of nucleosides, along with the presence of water as the primary solvent, ensures that dipole-dipole interactions will contribute, often significantly, to the sequence specificity and stability of an aptamer-target complex.⁷⁹ For example, hydrogen bonds involving the oxygen atoms of the phosphate groups as well as the hydroxyl groups of the deoxyribose sugars of an aptamer are often observed. The hydrogen bonding potential of unpaired purine or pyrimidine bases is, in general, even stronger⁸⁸ due to the

greater density of electron donors and acceptors, the generally higher configurational freedom of these moieties, and their generally better chemical mapping to H-bond donors and acceptors presented on amino-acid side chains of proteins.

Dipole – induced dipole, induced dipole – induced dipole, and the various dipole – quadrupole and quadrupole – quadrupole forces also contribute to aptamer binding affinity and specificity.^{88,89}

1.2.1.2.3 HYDROPHOBIC INTERACTIONS

The hydrophobic effect is an important physicochemical property of most receptor-ligand interactions. It is mainly an entropic phenomenon that arises due to changes in the density and organization of water molecules at an interface that offers relatively low hydrogen-bonding potential. Water molecules therefore re-orient upon interacting with non-polar surface so as to maintain a maximum number of hydrogen bonds, resulting in a loss in degrees of freedom.^{90,91} Complexes formed between hydrophobic surfaces/residues, including those between an aptamer and aliphatic or aromatic side-chains of proteins, can result in a partial or full dehydration of the interface. Structured water released gains entropy, while the system as a whole loses heat capacity, the two experimental hallmarks of hydrophobic dehydration.^{92,93} As such, dehydration as a binding mechanism tends to favour aptamers whose three-dimensional shape is directly complementary to the surface of the target; entropy may then make substantial contributions to the overall stability of the complex.^{94,95} Single-stranded regions of aptamers have a greater propensity for interacting with aromatic side-chains of amino acids in proteins due to the availability of exposed bases.

1.2.1.2.4 DISPERSION FORCES

Though dispersion forces, including Van der Waals and base-stacking interactions, are short range in nature (proportional to the inverse sixth-power of the separation distance),⁸³ they tend to make significant contributions to aptamer binding affinity and specificity. Dispersion forces are only weakly attractive, but the total density of intermolecular contacts stabilized by dispersion forces tends to be relatively large in macromolecular complexes due to their large contact areas. For aptamers, such interactions can, for instance, occur between side chains of amino acids and bases that remain unstacked,⁹⁶ resulting in a complex and dense topography of aptamer-target contact. Increases in monovalent or divalent cation concentrations can strengthen that contact by dehydrating surfaces and reducing electrostatic repulsion forces.⁹⁷

1.2.1.3 ANALYTICAL AND CLINICAL APPLICATIONS

Although the discovery of new aptamers—especially those able to recognize a disease-associated molecular target and properly modulate its activity—is difficult, a number of important examples of success exist. Macugen (Pegaptanib), a 28-nucleotide RNA aptamer (**Figure 1-4**) approved to treat wet age-related macular degeneration (AMD) by selectively inhibiting the 165 amino acid isoform of the vascular endothelial growth factor (VEGF₁₆₅),⁹⁸ highlights the potential of aptamers to improve patient outcomes. Moreover, aptamers have been applied in other important ways to aid both basic and clinical research. For example, several DNA and RNA aptamers have been discovered and used to better understand the functions of disease-related proteins by selectively inhibiting the relevant epitope, as opposed to eliminating the gene-product entirely by using more traditional siRNA or knockdown/knockout-based strategies.⁹⁹ Recently, an application for the efficient extraction of (bio)molecules from complex fluid mixtures has been described.¹⁰⁰ The system leverages the use of microfluidics and reversible folding

capabilities of aptamers to capture thrombin from human serum via a target-specific aptamer, attached to flexible microstructures embedded within a pH-responsive hydrogel. As such, several cycles of selective capture and release of thrombin could be achieved by modulating the chemical environments within the microchannel.

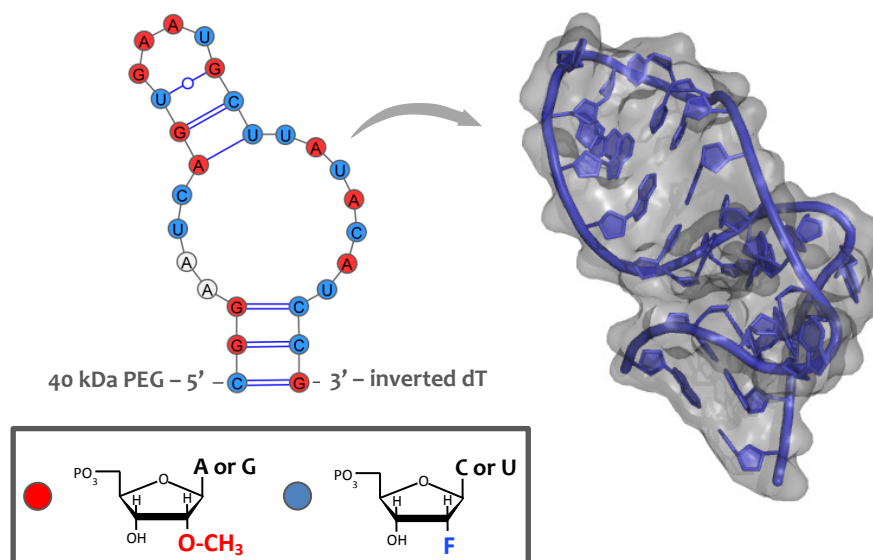


Figure 1-4 Model representation of the Macugen (Pegaptanib) RNA aptamer's secondary and associated tertiary structure. Red circles indicate 2'-O-methylated purines, and 2'-fluorine-modified pyrimidines are shown in blue. Unmodified adenosines are also shown. Additional modifications to the aptamer include the 5' attachment of a 40 kDa polyethylene glycol (PEG) moiety and the attachment of an inverted thymine at the 3' end. Tertiary structure prediction was performed using the Assemble2 program (<http://bioinformatics.org/assemble>) interfaced with UCSF Chimera software (<http://www.cgl.ucsf.edu/chimera>) and represented via PyMol.

Amongst the classes of pharmaceutical agents available, aptamers provide significant value by harnessing both the advantages of small molecule inhibitors and the specificity of antibody-based therapeutics. Aptamers are relatively homogeneous molecules that can be cheaply manufactured to high purity at any required scale. Batch-to-batch variations are negligible, creating the assurance that product quality and efficacy are maintained.¹⁰¹ The nucleic acid chemistry of

aptamers provides additional advantages that will be discussed later, but can also be concerning due to its propensity for rapid degradation and fairly rapid renal clearance in the body. Specific chemical modifications have therefore been established to reduce or even eliminate these concerns and thereby create aptamer products exhibiting remarkable stabilities and circulation half-lives. In particular, modifications^{102,103} that serve to alter the chirality (e.g. Spiegelmers) and structures (locked nucleic acids) of nucleotides (**Figure 1-5**) have been utilized to improve both the thermal stability and nuclease resistance of aptamers.¹⁰⁴ Indeed, these strategies were successful in improving Macugen's half-life 100-fold to 131 hrs following parenteral administration.¹⁰⁵ Additionally, the inclusion of base-modified nucleic acids within an aptamer sequence has been explored in certain cases to expand the chemical diversity of the starting library.¹⁰⁶

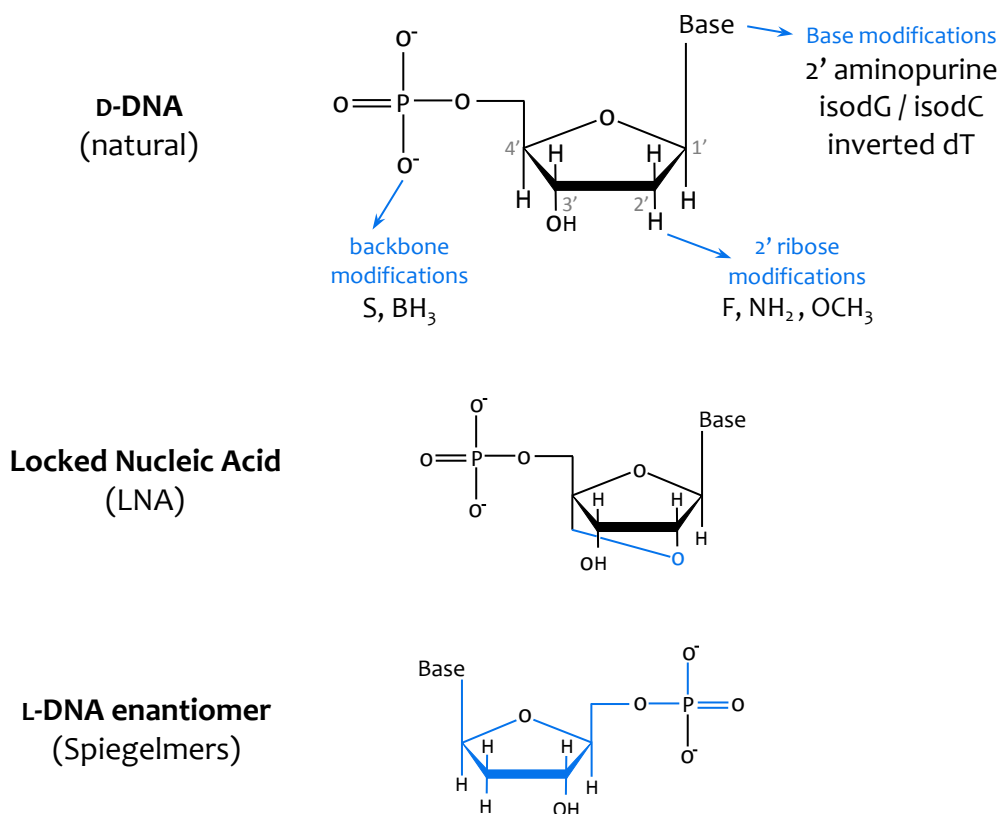


Figure 1-5 Common nucleic-acid modifications to aptamers discovered by SELEX to improve circulation half-life and stability.

1.2.2 ANTIBODIES

The discovery of antibodies at the end of the 19th century,¹⁰⁷⁻¹⁰⁹ and the subsequent development of the hybridoma technology⁶ in 1975 heralded new opportunities in both the analytical and clinical domains. These large (> 150 kDa) immunoglobulin (Ig) protein complexes play an essential role in the adaptive immune system of mammals, in part by selectively binding their respective antigens with high affinities (ca. order-nM K_d). Antibodies have also found applications in the laboratory, being routinely used in chromatography,¹¹⁰ histochemistry¹¹¹ and various other immunoassays.¹¹²⁻¹¹⁴ Their dominant position as biological therapeutic agents includes more than 425 antibodies currently being developed, and 41 received FDA-approval as the time of writing of this thesis,^{115,116} for treating multiple ailments ranging from inflammation¹¹⁷ to cancers¹¹⁸.

1.2.2.1 CHEMISTRY AND STRUCTURE

Proteins are a functionally versatile class of biological molecules that ensures the proper functioning of a cell. Several classes exist in the body, including those that provide (i) structural rigidity to the cell, (ii) transport of materials across the cell membrane, (iii) regulation of genes and pathways, (iv) catalytic function and (v) signaling capabilities to other biomolecules. Antibodies, for example, function with other protective agents within the immune system to maintain the body's integrity.

As with all proteins, antibodies (**Figure 1-6**) are translated from mRNA and assembled from monomeric units called amino acids, each having a chemical backbone structure comprising a central α -carbon atom flanked by an amino (NH_2) and a carboxyl (COOH) group. The 20 amino acids commonly found in proteins differ from each other by the physical (e.g. size) and chemical (e.g. polarity, charge) properties of their carbon-containing side chain (R) appended to the α -carbon atom. A polypeptide chain (referred to as the primary structure) is formed by

linking amino acids via a peptide bond: a covalent attachment between the deprotonated carboxyl group of the first and the protonated amino group of the next. The secondary structure (i.e. α -helix, β -strand or random coil) adopted by a particular segment of a polypeptide chain is dictated by the sequence of its amino acid side chains. Folding of an antibody into its stable tertiary and quaternary structure is then achieved by a highly cooperative process performed via a sequence of spontaneous non-covalent stabilizations and intrinsic quality control mechanisms¹¹⁹ overseen by the cell's endoplasmic reticulum (ER) chaperone machinery. These stable three-dimensional structures, as well as specific post-translational modifications, are integral to the proper function of an antibody.

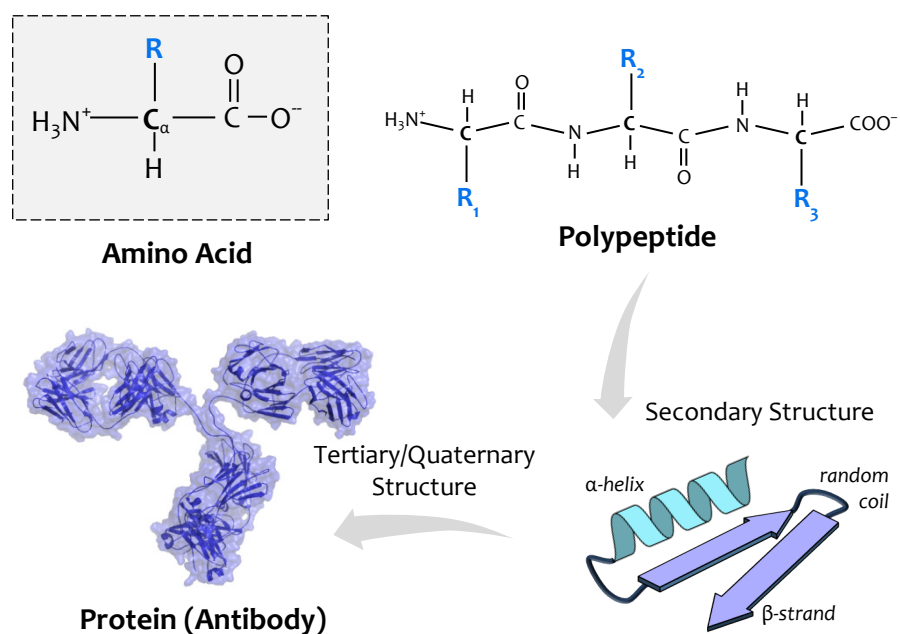


Figure 1-6 Molecular assembly and structure of a protein. Monomeric amino acids are covalently tethered to form a polypeptide displaying various side chains (R_n) displaying a free amino (N-terminus) and carboxyl group (C-terminus). The primary structure of a polypeptide chain can fold into secondary α -helices and/or β -sheets to maximize the formation of H-bonds as well as other random coils for linking these structures. Tertiary and quaternary structural arrangements between individual or multiple polypeptides form functional proteins.

The most abundant antibody isotype is that of the IgG family of immunoglobulins (**Figure 1-7**). IgGs are Y-shaped molecules having a molecular weight of about 150 kDa and comprised of four polypeptide chains: two identical heavy chains (ca. 50 kDa each) and two identical light chains (ca. 25 kDa each).¹²⁰ Each light chain of an IgG contains a variable (V_L) domain near the N-terminus and a constant (C_L) domain at the C-terminus. Similarly, each heavy chain contains a single variable (V_H) domain near the N-terminus, and three constant domains (C_{H1} , C_{H2} , C_{H3}) extending towards the C-terminus. Both antigen-recognizing variable regions (V_L and V_H) are contained within the combinatorially generated antigen-binding fragment (Fab) presented on each arm of the antibody. The tip of each arm contains those portions of the V_L and V_H chains comprising the F_v region, and those portions each contain three variable loops that together are responsible for binding to the antigen. These loops are known as the complementarity determining regions, (CDRs) or idiotypes, and their structures have been clustered and classified.^{121,122} The adaptive immune system is thought to be regulated by interactions between idiotypes.¹²³ Finally, the constant fragment (Fc) of an antibody contains species-specific information for enabling the IgG to bind surface receptors on circulating effector cells,¹²⁴ such as white blood cells and macrophages in the blood plasma that can engulf and destroy bound antigens.

In mammals, antibodies are assembled in B cells,¹²⁵ a specific type of lymphocyte (white blood cell) residing in the bone marrow (total population ranging from 10^{10} to 10^{11}).¹²⁶ Each B cell can produce a specific antibody by combinatorially encoding the **V**ariable, **D**iverse and **J**oining segments of the antibody's variable region by a genetic recombination process¹²⁷ that in principle enables well over 10^{14} combinations of unique antibody molecules to be assembled. Those produced by clones of an individual B-cell are referred to as monoclonal antibodies (mAbs) and are specific for a single epitope of an antigen. Alternatively, a collection of antibodies secreted by a population of cells are referred to as polyclonal antibodies (pAbs) and may recognize multiple epitopes of the same

antigen. However, significant concerns over cross-reactivity with other molecules containing similar epitopes are usually associated with pAb preparations, especially when used in therapeutic applications.¹²⁸

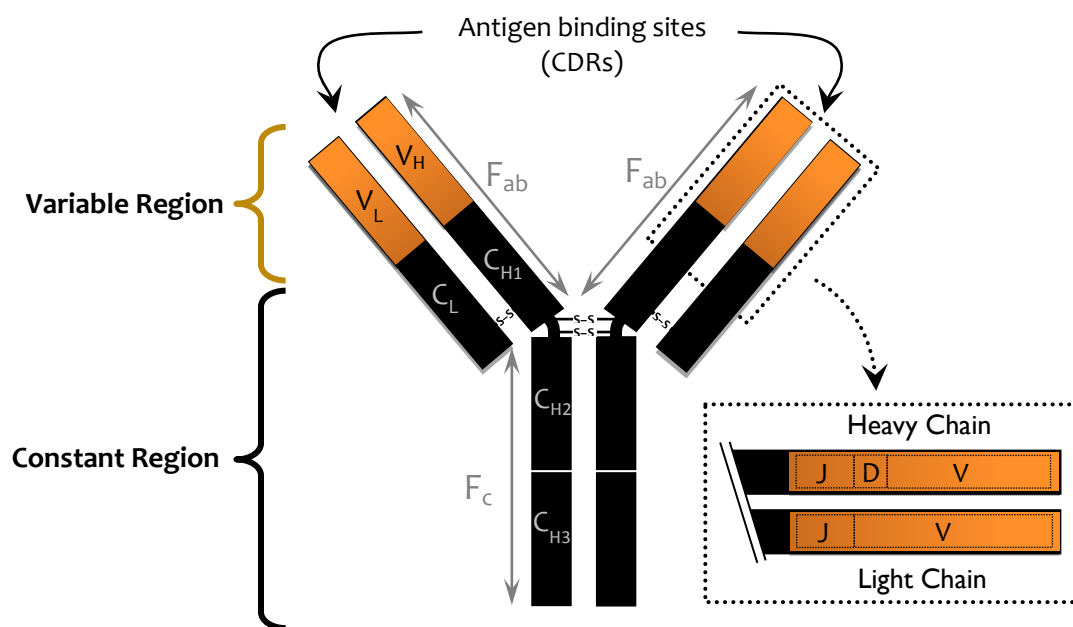


Figure 1-7 Schematic of an IgG antibody molecule with constant (black) and variable regions shown. The light chain variable region is encoded by the available combination of genes for the Variable and Joining segments, while the heavy chain is encoded with an additional gene for the Diverse segment.

1.2.2.2 BASIS FOR MOLECULAR RECOGNITION

The ability to recognize and bind an antigen is conferred by the CDRs of an IgG. These non-contiguous loop structures, presented by the β -sheets forming the structural framework of the variable regions, are positioned in close proximity so as to present clusters of amino acid side chains that directly interact with complementary regions on the surface of an antigen. Other portions of the variable regions can also provide a binding surface.¹²⁹ CDRs may recognize an epitope

present on the solvent-exposed surface of a folded protein, or bind contiguous peptide fragments of a protein under native or denatured conditions.¹³⁰

Analogous to that described for aptamers, an ensemble of long and short-range intermolecular forces enables the specific and tight interaction of an antibody with its antigen. A high degree of complementarity between the two surfaces is usually achieved, resulting in almost complete dehydration of the interface; those water molecules that remain typically provide further stability by facilitating the formation of hydrogen bonds¹³¹ and solvating associated ions.¹³² Antibody-antigen recognition can occur via a relatively inflexible mechanism (i.e. lock-and-key model)¹³³ that is usually associated with high affinity and specificity, or through variations in conformation (i.e. induced-fit model)¹³⁴ that can result in a broadening of specificities. Extrinsic factors, including deviations from physiological conditions (e.g. temperature, pH, ionic strength), can serve to weaken and disrupt antibody-antigen complexes.¹³⁵

1.2.2.3 ANALYTICAL AND CLINICAL APPLICATIONS

Antibodies are widely used in research laboratories as analytical reagents for conducting routine assays, and in clinics to detect proteins, including those that present mutations and variations that are indicative of cancer, infectious diseases, sepsis, and other life-threatening indications.¹³⁶⁻¹³⁹ In addition, mAbs are highly effective therapeutics against a variety of ailments, currently serving as front-line agents against cancer (e.g. Avastin, Erbitux, Herceptin, Removab, Rituxan), rheumatoid arthritis (e.g. Enbrel, Remicade), Crohn's disease (e.g., Humira), psoriasis (e.g. Raptiva) and pathogen infections (e.g. Aurexis), to name a few. However, administration of these humanized chimeric molecules—often of murine origin—carries some risks associated with undesired immune responses and other side effects that can serve to neutralize their benefits;¹⁴⁰ major efforts are therefore underway to address these issues.¹⁴¹ Methods to improve “humanization” of

antibodies are thereby being realized, for example, by substituting various murine segments with the corresponding human variants, which have led to next-generation antibody-based therapeutics¹⁴² displaying far less immunogenicity. Transgenic mice able to produce fully human antibodies,¹⁴³ and surrogate molecules such as mAbs fragments¹⁴ and bicyclic peptides,¹⁴⁴ are further improving therapeutic performance.

By virtue of their specificities, mAbs also lend themselves very well to being used as targeted therapy agents,¹¹⁸ as do aptamers.¹⁴⁵ Immuno-conjugates capable of binding antigens while simultaneously locally administering drug payloads¹⁴⁶ or providing *in vivo* imaging capabilities^{147,148} have been described.

1.2.3 COMPARATIVE ADVANTAGES AND LIMITATIONS

Due to their large multi-domain structures and post-translational modification requirements (e.g. glycosylation), antibodies are, in general, difficult and expensive to manufacture. Their *in vivo* production is usually accomplished by culturing highly engineered mammalian cell lines under tightly regulated conditions. Deviations in culture or storage environment (e.g. temperature, pH, ionic strength) can result in batch-to-batch variations of antibody quality, or even render the antibody non-functional (e.g. irreversibly denatured/aggregated).¹⁴⁹ Additionally, antigens that are poorly or non-immunogenic may not elicit the immune response needed to produce antibodies,¹⁵⁰ though that problem can often be addressed through the use of immunogenic carrier molecules. Alternatively, antigens that are extremely immunogenic or even toxic may kill the host prior to production and recovery of the antibody repertoire.^{151,152} Nevertheless, the science of antibody production, particularly mAbs, has matured to the point that these complex therapeutic agents can be reliably produced at all scales. Costs remain high,¹⁴ and other issues including poor antigen immunogenicity are a concern, but these limitations are being addressed through improvements to phage-display

technology,^{153,154} humanization methods,^{153,155} genetic engineering of antibody fragments,¹⁵⁶⁻¹⁵⁸ as well as streamlined *in vivo* and *in vitro* production technologies.^{159,160} Through these approaches, mAbs having long and modulatable half-lives,^{161,162} afforded by their ability to exceed the renal clearance threshold, are being created. These advances, particularly when combined with the exquisite selectivity and generally low immunogenicity of humanized cell-culture derived mAbs, suggest that antibodies will likely remain the dominant class of affinity reagents used as human therapeutics.

Like antibodies, aptamers can exhibit exquisite affinity and specificity for their target. By virtue of their nucleic acid chemistry, they can be produced far more economically. Moreover, that chemistry generally results in their reversible folding, permitting aptamers to be subjected to more adverse conditions during selection or processing without loss of function. Longer shelf-lives may therefore also be realized.¹⁷ Such unique attributes, including low cost manufacturing, provide aptamers with important opportunities for use in more cost-constrained technologies (e.g. chromatography columns, diagnostic tests), as well as in stringent environments and conditions commonly found in laboratory, industrial and diagnostic applications where use of mAbs is not optimal.

However, the smaller size (**Figure 1-8**) of aptamers generally allows for faster and more efficient tissue penetration.¹⁶³ Their use in immuno-conjugates is therefore an active field of research, as their chemistry and *in vitro* production permit facile tethering to a wide variety of functional groups¹⁶⁴ (e.g. dyes, isotopes, biomolecules) and payloads¹⁶⁵ (e.g. drugs, toxins, particles). As therapeutics, nucleic acid aptamers are not immunogenic,¹⁶⁶⁻¹⁶⁸ even when compared to their antibody counterparts, but they are susceptible to chemical and enzymatic degradation, typically necessitating their extensive modification to establish sufficient resistance as noted above. Moreover, when compared to the immune system's ability to produce mAbs, current aptamer discovery platforms are not

nearly as efficient, often taking months to complete and delivering a panel of candidate aptamers that do not meet performance requirements. This has no doubt limited their use, particularly as therapeutics.

Addressing these limitations could prove very beneficial. As a versatile class of affinity molecules, aptamers are more cost-effectively produced at industrial scales (ca. USD \$20 per gram for those containing modified bases)³⁴ compared to cGMP monoclonal antibodies (typically around USD \$300 per gram).¹⁶⁹ This suggests they will find increasing use as industrial (e.g., ligands for affinity chromatography), diagnostic and analytical reagents, as exemplified by their recent commercialization in hot-start activations of Taq DNA polymerase (e.g. EpiMark®; NEB and AptaTaq™; Roche)¹⁷⁰ and the development of aptamer libraries for proteome screening applications.¹⁷¹ Their general applicability as a class of therapeutic reagents capable of delivering the specificities and affinities required to compete with mAbs remains to be seen.^{46,47}

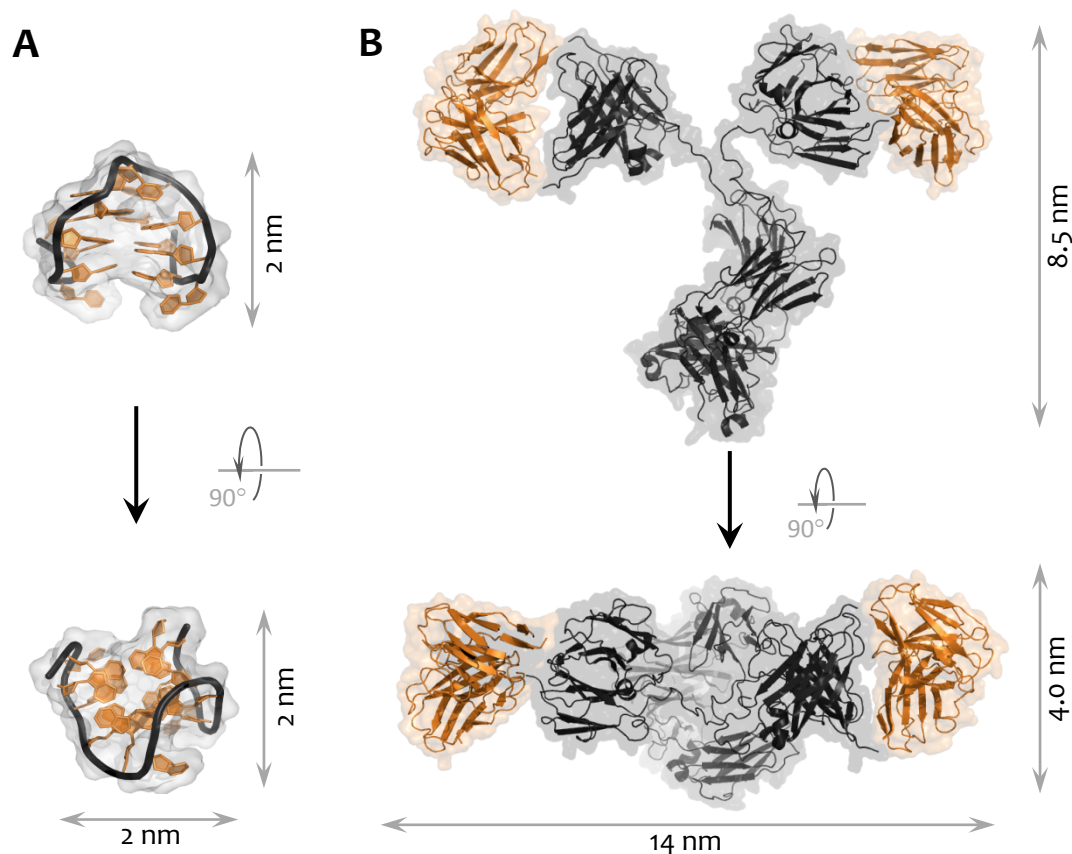


Figure 1-8 Molecular size comparison between a (A) 15 nt anti-thrombin aptamer¹⁷² (~5 kDa) and (B) an IgG-2a immunoglobulin (~150 kDa). Structures^{173,174} were created with PyMOL, accessed from the Protein Data Bank (entries 148D and 1IGT, respectively) and are not drawn to scale.

1.3 CURRENT METHODS FOR DISCOVERING APTAMERS AND OTHER BIOAFFINITY REAGENTS

Current platforms for identifying either aptamer or antibody class affinity reagents usually rely on high-throughput experimental approaches that sample large, often semi-combinatorial libraries of molecules to systematically screen for binding affinity/kinetics against a molecular target or antigen. Although these methods have some well-recognized practical limitations, such as the non-exhaustive diversity of the initial population of sequences (the library), the more rational method of selecting lead candidates based on *de novo* designs performed *in*

silico (e.g., molecular docking simulations, molecular dynamics simulations, etc.) is not sufficiently advanced to permit its reliable use. As a result, *in vivo* and *in vitro* screening methods that require no prior knowledge of a target's interaction with a specific sequence continue to represent the best strategy to discovering new aptamers and antibodies to an expanding array of targets.

Efficient screening of a large number of sequences against a molecular target to identify lead compounds generally requires isolation and enrichment of sequences that display proper complementarity to the relevant epitope on the target surface. The *in vivo* Darwinian-type evolutionary process of selecting antibody repertoires against antigens represents one means by which Nature accomplishes this. What is remarkable about that natural process is its nearly absolute reliability in delivering antibodies having the required affinity, specificity and functional action toward the antigen. The hybridoma technique has allowed this strategy to be partially transferred to *in vitro* screening platforms, but with considerably reduced rates of success due, in large part, to the vastly smaller number of antibodies that are then typically screened.

Recently, Singhal et al.¹⁷⁵ and others,¹⁷⁶⁻¹⁸² have described high-throughput *in vitro* antibody discovery platforms that eliminate the low (fusion) efficiency hybridoma process by enabling high-density multiplexed screening of the unique antibody produced by each antibody-secreting plasma cell or memory B cell collected by fluorescence-activated cell sorting (FACS) following repeated immunizations. In principal, these emerging platforms should greatly increase the number of antibodies screened against a particular antigen. At present, that screening process is limited to determination of the binding affinity/kinetics and RT-PCR derived coding sequence of each antibody. As a result, the platforms do not necessarily insure discovery of antibodies displaying the required specificity and functional activity toward the target.

Seminal work¹⁸³ by Sol Spiegelman has shown that evolutionary-type selection processes can also be applied *in vitro* to populations of nucleic acid molecules. That work laid the foundation for development of the systematic evolution of ligands by exponential enrichment (SELEX) method, a moderate-throughput technique developed in 1990³⁰⁻³² for screening large combinatorial libraries of single-strand oligonucleotides (aptamers). This *in vitro* strategy is designed to partition and enrich library members based on their binding affinity; binding specificity and functional activity are generally not evaluated in the SELEX process.

Thus, on their own, these current selection platforms do not provide a general means to effectively isolate and identify a small, fully vetted (i.e., good affinity, specificity, activity) panel of lead antibodies or aptamers suitable for further development into therapeutics. Additional knowledge is required, as indicated in **Figure 1-9** for the case of discovering therapeutic aptamers.

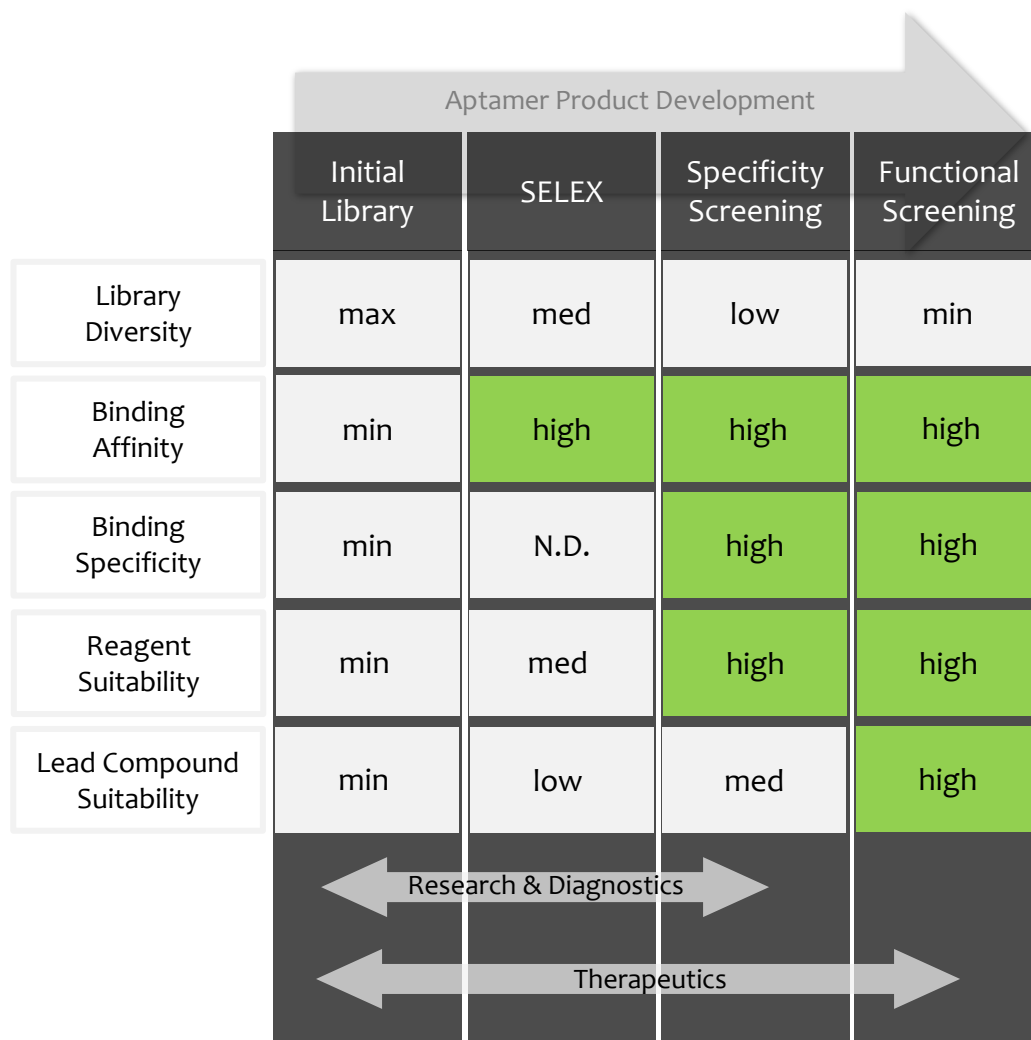


Figure 1-9 General schema for library-based identification and characterization of novel aptamer products. When properly performed, each step further adds to the likelihood in identifying suitable members for use in research and diagnostics or as lead compounds for further therapeutic development. The standard SELEX platform does not provide data characterizing aptamer or retained pool specificity (N.D.)

1.3.1 GENERAL APTAMER SELECTION STRATEGY

As initially described by Tuerk et.al.,³⁰ Ellington et.al.³¹ and Robertson et. al.,³² SELEX enriches a subset of short single-stranded RNA or DNA sequences from an initial synthetic library comprised of a semi-combinatorial population of such sequences (ca. 10^{14} unique sequences) whose total diversity is similar to the body's own antibody repertoire.¹⁸⁴ As the screenings are performed *in vitro*, SELEX provides the capacity to modulate the nature and stringency of the conditions used so as to more efficiently select library members showing high affinity to a target.

When applied to DNA-based aptamers, the standard SELEX process (**Figure 1-10**) is comprised of the following sequence of operations: (i) **incubation** of the semi-combinatorial **library** with a **target** molecule that is typically displayed on a surface, (ii) **partitioning** and retention of members that bind the target using washing cycles to remove unbound members, (iii) elution (recovery) and **amplification** of retained members to generate an enriched pool of binding members, and (iv) **regeneration** of the enriched single-stranded library by digestion and removal of the anti-sense strand of each amplicon to permit the next round of selection. Several (typically 8 to 20) rounds of SELEX are generally performed to gradually isolate from the initial library a pool of high-affinity binders.

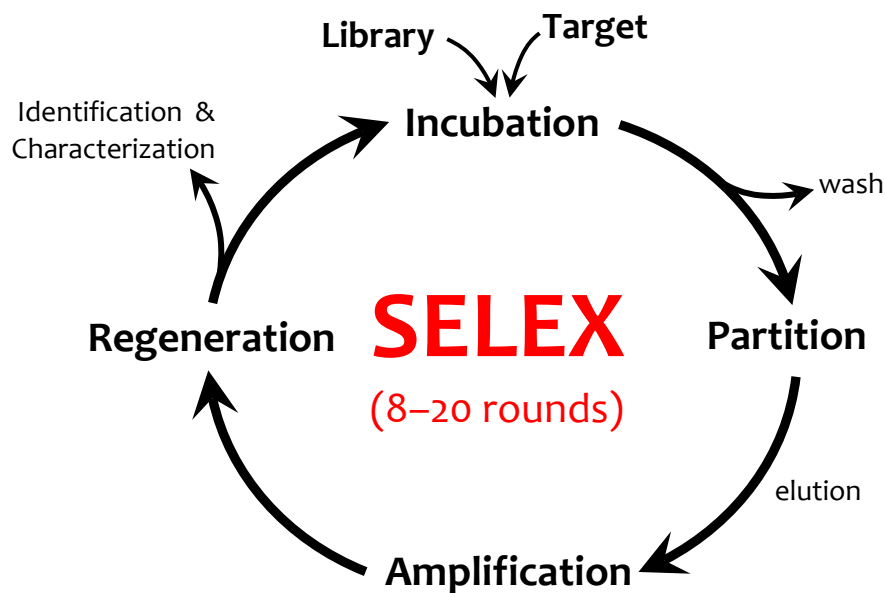


Figure 1-10 Schematic of a standard SELEX process for DNA-based aptamer libraries

1.3.1.1 THE DNA OLIGONUCLEOTIDE LIBRARY

SELEX can operate on either a DNA or RNA library, with the choice typically made by carefully examining the intended application of the aptamer and the associated requirements. RNA-based aptamers have a more flexible backbone that allows them to adopt a wider range of complex secondary and tertiary structures; however, they are more susceptible to chemical and enzymatic degradation. Though built on a less flexible backbone, DNA-based aptamers have higher chemical stability and their selection is more straightforward due to the relative simplicity of the amplification and regeneration steps. The technological advances presented in this thesis pertain to DNA-based aptamer selections.

Single-stranded DNA SELEX libraries typically contain 10^{14} unique members of equivalent length in which a random 40 to 60 nt oligonucleotide sequence within a central core region is flanked by universal fixed sequences at the 5' and 3' termini (**Figure 1-11**). The libraries are synthesized chemically in quantities (typically

several μmoles)¹⁸⁵ and using methods that satisfy the DNA quality (e.g. uniform length) and diversity requirements of the SELEX process. Library diversity is largely encoded in the variable region, with the two fixed regions facilitating operations core to the SELEX process, as described in more detail below.

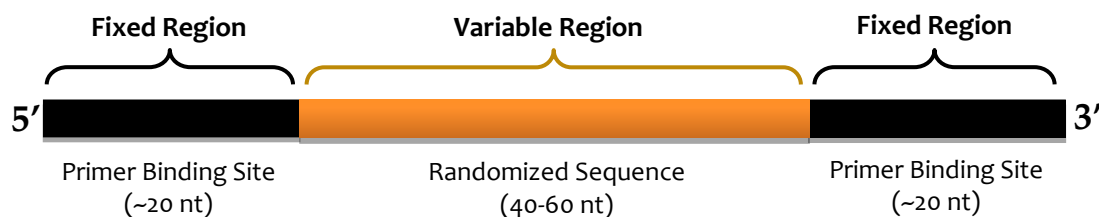


Figure 1-11 Schematic of an individual member of a DNA aptamer library shown with core variable region flanked by constant regions (black). The variable region is encoded by a combinatorially synthesized sequence of random nucleotides.

The sequences of the universal fixed regions (typically 20 nt each) at the 5' and 3' ends of each library member are specifically engineered to achieve high-fidelity amplification of retained library members by eliminating, or at least minimizing, self-association and primer-dimer pairing reactions that can promote formation of unwanted by-products during PCR. In addition, the flanking regions add to the overall sequence diversity of the library, but the net contribution is quite small (arguably negligible) in relation to that provided by the variable core region.

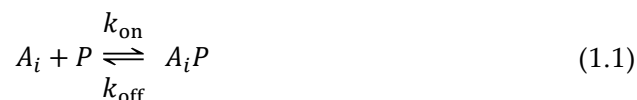
The variable core region can be created utilizing different types of randomization and nucleotide chemistry. Most often, chemical syntheses that equally weight the frequency of each naturally occurring nucleotide are employed, but variable regions comprised of partially-randomized sequences,¹⁸⁶ genomic DNA inserts^{187,188} and chemically-modified nucleotides^{104,189,190} have also been used with success. Traditionally, a random region that is 40 to 60 nt in length is used, as a fixed length in this range offers a good balance between structural complexity and low-cost/high-fidelity synthesis. Shorter randomization windows (i.e. < 20) can be problematic¹⁹¹ due to libraries becoming structurally and diversity constrained.

Alternatively, while consistent with the general aim of SELEX to identify a reasonably short and stable aptamer candidate that can be cost-effectively synthesized, somewhat longer randomizations (i.e. > 60 nt) that could permit discovery of more complex and stable structural motifs have traditionally been avoided.^{192,193}

1.3.1.2 LIBRARY INCUBATION

Prior to SELEX, the library is subjected to a thermal denaturation/renaturation cycle designed to promote folding of each member into its thermodynamically favourable conformation at incubation conditions.¹⁹⁴ One round of screening in the absence of the molecular target is sometimes then conducted to remove (or at least reduce in number) those members of the library that might be retained through mechanisms unrelated to the target.¹⁹⁵ The library is then equilibrated with the molecular target (e.g. a protein) at solution conditions that in principle are defined to favour preferential binding of high-affinity members within the library.^{196,197} Identifying such incubation conditions can be challenging,¹⁹⁸ as a significant fraction of library members will exhibit some degree of affinity for the target. Selective enrichment of tight binders is therefore often promoted by setting library to target concentration ratios at 100:1 or greater.^{199,200} During the incubation step, sufficient target molecules are then present to allow the vanishingly small fraction of high-affinity binders to compete for binding partners, while reducing to acceptable levels the associated carry-over of more weakly binding members present in greater collective abundance within the initial library.

The binding interaction for any given library member can be represented by the following equation:



where A_i denotes a given free aptamer (i) in solution, P is the molecular target available for binding and A_iP is the resulting aptamer:target bound complex. The rate of change in the concentration of an aptamer:target complex is given by

$$\frac{d[A_iP]}{dt} = k_{\text{on}}[A_i][P] - k_{\text{off}}[A_iP] \quad (1.2)$$

where k_{on} ($\text{M}^{-1} \text{s}^{-1}$) and k_{off} (s^{-1}) are the forward and reverse rate constants, respectively. At equilibrium, that rate of change is zero, and solution of eq. (1.2) then yields

$$\frac{[A_i][P]}{[A_iP]} = \frac{k_{\text{off}}}{k_{\text{on}}} = K_d \quad (1.3)$$

where the equilibrium dissociation constant (K_d) is a measure of affinity (in molar concentration), determined by the ratio of rate constants. Therefore, library members that associate quickly (large k_{on}) and remain complexed for long periods of time (small k_{off}) have much higher affinity than those that bind the same target more transiently. Identifying aptamers that form stable complexes having a long complex half-life is of particular interest when they are to be used as therapeutics.²⁰¹

1.3.1.3 PARTITION AND RECOVERY OF BOUND MEMBERS

Following the incubation step, bound library members are physically segregated from unbound members. This is usually achieved by extensively washing the system to remove both unbound and weakly bound members. As these

washing steps are non-equilibrium by nature, care must be taken to avoid removing desirable higher-affinity aptamers from the retained pool. As a result, unwanted lower-affinity aptamers will be co-retained during each selection round. Practitioners of SELEX have attempted to quantify the overall quality of a given selection step through the creation of a parameter PE known as the “partition efficiency”:

$$PE = \frac{[A]}{[AP]} \quad (1.4)$$

where,

$$[A] = \sum_{i=1}^n [A_i] \quad (1.5)$$

and denotes the total molar concentration of all aptamers collected in the wash (i.e. the total unbound fraction); likewise $[AP]$ is the molar concentration of all aptamers recovered in the elution fraction (i.e. the total bound fraction). In standard SELEX, per round PE values generally range from 10 to 1000, with values as high as 10,000 observed on occasion; elimination of all weakly/non-specifically retained members and reduction of the starting population of 10^{14} members to a manageable number of candidate aptamers, say $\leq 10^4$, therefore typically requires a relatively large number of successful selection rounds (generally identified by an improvement in the mean K_d of the retained pool). New techniques and strategies that improve preferential retention of members that form tight sequence-specific interactions, and thus result in significant increases in PE , would therefore be of considerable value to SELEX-based aptamer selections.

1.3.1.4 AMPLIFICATION OF RETAINED MEMBERS

SELEX leverages the polymerase chain reaction (PCR) to amplify the population of retained library members to concentrations needed for the next selection round. The ability to amplify each recovered member is conferred by the presence of the universal fixed regions flanking the core region of each member (**Figure 1-11**). A small-scale “pilot” PCR reaction²⁰²⁻²⁰⁴ is generally performed to determine the number of PCR cycles (typically ranging from 10 to 15) that can be conducted before significant amounts of reaction by-products are accumulated. Those high-molecular weight (HMW) contaminants²⁰⁵ are known to adversely affect the selection process and must therefore be removed, typically using gel electrophoresis.

1.3.1.5 DNA LIBRARY REGENERATION

The amplification step generates dsDNA products (amplicons) from which the sense strands must be recovered in order to continue the SELEX process. A number of purification methods have been established for stoichiometrically removing the antisense strand from the sense (aptamer) strand of amplicons (**Figure 1-12**), including alkaline denaturation followed by streptavidin capture of biotinylated anti-sense strands (generated by chemically modifying the reverse primer)²⁰⁶ or electrophoretic separation of poly-T-labelled anti-sense strands.^{207,208} However, methods relying on enzymatic digestion of 5'-phosphorylated (PO₄) anti-sense strands with lambda exonuclease constitute the most efficient and reliable strategy for producing high-quality ssDNA library members,²⁰⁹ and are therefore amongst the most frequently applied.²¹⁰⁻²¹⁶

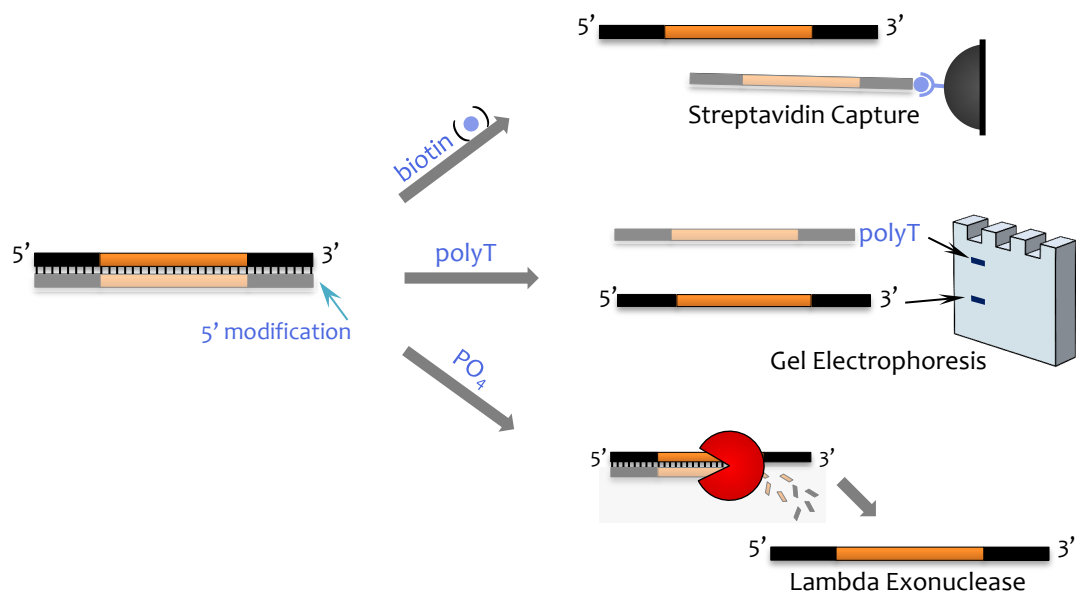


Figure 1-12 Schematic of various ssDNA library regeneration methods based upon either physical removal (streptavidin capture, gel electrophoresis) or enzymatic digestion (lambda exonuclease) of the anti-sense strands of dsDNA amplicons.

1.3.1.6 ROUND-BY-ROUND AND POST-SELEX APTAMER ANALYSIS AND PROCESSING

With increasing round number, incubation and partitioning of the enriched pool of library members is sometimes conducted at progressively more stringent conditions. This usually entails either increasing the library to target concentration ratio during incubation²¹⁷⁻²²¹ or changing the wash/elution conditions during the partition step.²²²⁻²²⁵ Either change is thought to contribute to the gradual enrichment of oligonucleotides exhibiting increased affinity for the target.

In a successful SELEX screening, the mean bulk affinity of the enriched library will increase by several orders of magnitude over the course of several rounds of selection. The SELEX process is then terminated when the mean bulk affinity of retained members either remains unchanged for additional consecutive rounds or

has reached a suitable value for a particular application. Typically, aptamers in the final enriched pool are sequenced and aligned to identify common sequence and predicted structural motifs^{58,226,227} among tight-binding members. Aptamers of interest are then produced individually (often by cloning in *E. coli*) in quantities that permit measurement of their binding affinity—typically using either surface-plasmon resonance (SPR) or isothermal titration calorimetry (ITC)—and/or binding kinetics (SPR). Though clearly essential to discovery of useful aptamers, binding specificities are generally not included in this initial analysis, in large part because methods of sufficient throughput for completing such analyses are not readily available. The same is true for current antibody discovery platforms, creating potential in current screening methods for both classes of affinity reagents to deliver molecules that do not satisfy basic performance requirements.

1.3.2 LIMITATIONS OF SELEX-BASED SCREENINGS

The conventional SELEX method²²⁸ outlined in **Figure 1-10** can, and has produced aptamers of therapeutic or diagnostic utility.^{45,229,230} However, significant issues limiting the performance and reliability of the method are known,^{198,231-233} and those limitations have motivated the development of a number of process modifications.²³⁴⁻²⁵⁰ Useful changes to standard SELEX have included the application of alternative oligonucleotide libraries,²⁵¹ including ones employing non-natural nucleotide chemistries²⁵²⁻²⁵⁴, and changes in the operating conditions used in specific process steps (e.g. partition, regeneration). Most of these alternative screening methods perform well for specific targets, but have not been shown to provide a markedly more robust general strategy for aptamer discovery.²³³ More significant alterations and alternatives to the SELEX platform have also been proposed. Most of these advances are specifically designed to improve round-by-round *PE* values,^{255,256} and do not address other significant limitations to successful aptamer selection. The following sections outline these

technical advances, as well as those shortcomings to SELEX that have not been addressed effectively either in isolation or within an integrated selection platform.

1.3.2.1 LIBRARY DESIGN AND PRESENTATION LIMITATIONS

Library design, chemistry, starting diversity and presentation all impact the quality of an aptamer selection process. Simple loop (hairpin) structures formed via single-strand self-complementarity typically contain at least 12 nucleotides, while the more complex secondary structures (e.g. G-quadruplex, bulge-loops, etc.) that provide aptamers their affinity and specificity for a target are typically longer in length. Variable-region lengths of at least 40 nt are therefore generally employed,²⁵⁷ but arguments have been made that screening of libraries comprised of longer length random regions could yield new and more target-specific fold motifs.²⁵⁸ The most compelling evidence supporting that argument has been provided by Bartel et. al.,²⁵⁹ who were successful in selecting from an initial library, containing a core region of 220 random nucleotides, a functional RNA molecule (i.e. a ribozyme) capable of performing ligations. Although ribozymes are functionally different from aptamers (the latter usually not associated with catalytic activity), this example underlines the potential in selecting nucleic acid molecules within large randomization windows.

More substantial efforts to improve library diversity and aptamer performance have been made by introducing non-natural nucleotide chemistries.¹⁰⁴ For example, Shoji et al.²⁶⁰ discovered a powerful aptamer against *R*-thalidomide by applying SELEX to a non-natural DNA library in which T was replaced with a modified deoxyuridine bearing a cationic group displayed at the C5 position through a methylene linker. Other modifications have been realized by adding functional groups to nucleic acid analogs that mimic the side-chains of proteins.²⁶¹ These advances have been conducive to the selection of aptamers exhibiting slow

off-rates and high specificity for their cognate ligand in continued efforts to identify novel protein biomarkers.^{261,262}

The impact of the fixed regions of an aptamer library on the selection process has also been studied.^{193,263,264} Beyond their prescribed function as primer annealing sites, these fixed regions can participate in or interfere with aptamer fold. Basic combinatorial statistics predict that, although possible, it is unlikely that candidate aptamers discovered by a SELEX-based library screen will contain fixed-region components, simply due to the invariance of those flanking sequences.¹⁹³ Thus, the potential for the fixed regions to disrupt the fold, and therefore the function, of an aptamer sequence presented within the random-region of a library member is of greater concern. In particular, portions of the fixed regions can either self-hybridize or anneal to complementary sequences in the core region to create unwanted secondary structures that compromise the selection of potentially useful aptamers.²⁶⁵⁻²⁶⁸ Several strategies have therefore been proposed to minimize or even remove these unwanted effects on the aptamer selection process. The most frequently applied include (i) minimizing the length of each fixed region,^{264,269} (ii) completely removing and regenerating the fixed regions before and after each selection step using restriction digest and ligation reactions, respectively,^{270,271} and (iii) replacing the fixed regions with different sequences following each or certain selection round(s).²⁷² Though sometimes effective, this collection of strategies has known limitations, including, but not limited to, the potential for a reduction in PCR efficiency when short priming sites are used, and a loss of library material during the cleavage and re-ligation of the new fixed regions between selection rounds. Additionally, replacement of single-strand fixed regions during the selection process does not abrogate the potential for losing a tight-binding aptamer, particularly during early selection rounds, through binding interference effects involving those regions.

1.3.2.2 IMPROVING INCUBATION AND PARTITION CONDITIONS

Large *PE* values are desirable for screening high-affinity aptamers as they can ultimately lead to more efficient and better selections due to the underlying significantly reduced co-partitioning of inappropriate library members. *PE* values are dependent on several factors, including the medium/method used to display the target, and the stringency of the solution conditions applied in the incubation and the partition steps of a particular round of selection. As a result, many strategies for improving the *PE* of a SELEX round have been described, primarily through changes to the target-display media and solid-phase environments used to conduct SELEX, or the solvent compositions and volumes used in the incubation and wash (partition) steps. Only a brief overview is provided here, as detailed review articles on this topic are available.^{18,192,195,232,256,273-277}

Standard SELEX typically filters target-bound aptamer complexes through a nitrocellulose membrane or immobilizes targets on a microbead.²⁷³ However, the nitrocellulose membrane system is known to suffer from significant non-specific retention of library members,²⁷⁸ which reduces *PE* (typically to less than 100) and usually then necessitates a larger number (> 10) of selection rounds (**Table 1-1**). Classic strategies to block non-specific adsorption sites, such as with > 1% (w/v) bovine serum albumin, have therefore been applied,^{223,225,279,280} but they do not in general improve *PE* significantly. These findings likewise apply to bead-based target-display systems (e.g. *PE* < 1000 observed and > 10 selection rounds typically required), though they generally provide better control over both the density of target displayed and the degree of non-specific binding by leveraging the abundant surface chemistries (e.g. carboxyl, amine, hydroxyl, epoxy, or thiol groups), as well as various affinity tags (e.g. glutathione, nickel-charged nitrilotriacetic acid, polyhistidine) available for target immobilization and surface passivation.²⁸¹⁻²⁸⁴ As a result, bead-based selections requiring a fewer number of rounds have been achieved on occasion (**Table 1-1**). Overall, however, performance data for current

SELEX platforms indicate the potential to better passivate target-display surfaces against non-specific retention mechanisms that contribute to overall decreases in *PE* and, in many cases, total failure of the selection process to isolate/enrich aptamers that bind the target specifically and tightly.^{204,285,286}

In conventional SELEX, the incubation step is designed to let the system come to equilibrium, so that the fraction θ_i of target binding sites occupied by each bound aptamer i is effectively determined by the multi-sorbate form of the Langmuir isotherm:

$$\theta_i = \frac{K_{d,i}^{-1}[A_i]}{1 + \sum_j K_{d,j}^{-1}[A_j]} \quad (1.6)$$

As noted above, performing the incubation under non-equilibrium conditions could allow for the preferential selection of tight binders characterized by fast association kinetics, slow dissociation kinetics, or possibly both. Both affinity chromatography^{300,301} and capillary electrophoresis (CE) systems^{302,303} have been exploited for this purpose, with the resulting CE-SELEX technology now finding widespread use due to the fact that per-round *PE* values as high as 10^5 can be obtained for systems where the size of the target is large, or whose electrophoretic mobility and charge are favorable.³⁰⁴ In this case, high-affinity aptamer pools may be generated in as few as 3 rounds of selection. However, *PE* values obtained by CE-SELEX tend to fall with decreasing net charge and/or size of the target, resulting in the identification of lower affinity aptamers³⁰⁵ in comparison to those identified using traditional methods.³⁰⁶ Furthermore, libraries of relatively low initial diversity (typically $\sim 10^{12}$ members) work best for CE-based selections.^{304,307,308} And finally, the solvent compositions that may be used are limited, as they must show electrophoretic compatibility. As a result, the stringent solvents typically required to minimize retention of undesirable library members can be difficult or impossible to implement.³⁰⁹

Table 1-1 Brief overview of SELEX performance for aptamers partitioned using a variety of methods.

Partition Method	Target	Size (kDa)	Rounds	Affinity (nM)	Ref.
Nitrocellulose (Conventional SELEX)	Complement C5	210	12	20	287
Nitrocellulose (Conventional SELEX)	α -Thrombin	36.7	11	2.0	288
Nitrocellulose (Conventional SELEX)	Vascular endothelial growth factor	38.2	11	0.14	289
Beads – Polystyrene (Conventional SELEX)	CD4 glycoprotein	55	15	1.5	290
Beads – Agarose (Conventional SELEX)	Epidermal growth factor receptor-3 (unglycosylated)	40	12	30	291
Beads – Agarose (Conventional SELEX)	Complement C5a	9	10	1.4	292
Beads – Magnetic (Conventional SELEX)	Neurotensin receptor 1	45.1	7	1.0	293
Beads – Magnetic (Conventional SELEX)	Prostate-specific membrane antigen	88.8	6	2.1	294
Beads – Magnetic (M-SELEX)	α -Thrombin	36.7	3	0.33	295
Beads – Magnetic (M-SELEX)	Platelet-derived growth factor	25.4	3	2.5	296
Beads – Magnetic (M-SELEX)	C-reactive protein	115	5	3.5	297
Capillary Electrophoresis (CE-SELEX)	Protein Kinase C delta	104	9	122	298
Capillary Electrophoresis (CE-SELEX)	Neuropeptide Y	4.2	4	300	299

Methods and technologies to improve *PE* by increasing the stringency of the wash steps used to remove unbound and less strongly bound library members have also been described. Most SELEX platforms, including conventional SELEX and the M-SELEX system (see below), perform increasingly stringent wash steps using larger volumes of the same buffer as was applied during the incubation step.^{203,223,295,310-312} However, though supporting data are scarce, improvements in *PE* have been realized using strategies that fully or gradually replace the aptamer folding/incubation buffer as the wash medium with a solvent that shifts the binding equilibrium more towards the desorbed state; a smaller, higher affinity population of library members is thereby retained.^{313,314} Microfluidic platforms (e.g. M-SELEX,²⁰³ QPASS¹⁷¹) designed to permit washing of bound library members with large volumes of fluid applied under continuous-flow conditions have also been described. These more advanced technologies have been successful in attaining *PE* values approaching 10^6 . As a result, significant reductions in the number of selection rounds (≤ 5) needed to isolate a pool of candidates offering a mean K_d of order nM have been realized. However, at present, these microfluidic platforms are challenging to construct and operate robustly. Moreover, they are not commercially available, but are instead used by a few select groups that have the capabilities and expertise to fabricate, operate and fine-tune the associated equipment. Therefore, there is a clear need for improvements to the incubation and partition steps of SELEX that permit *PE* values $\geq 10^5$ and a concomitant reduction in rounds to be realized using equipment that is available and used in nearly all labs with interest in SELEX-based screenings.³¹⁵

Irrespective of the target-display incubation and partition strategies employed, *PE* values will depend on both the target concentration and library-to-target concentration ratio used.^{304,316} In particular, though rarely acknowledged, selection quality and efficiency depend on the surface density of an immobilized target.³¹⁷ Macromolecular crowding due to an excessive density of immobilized target molecules can sterically hinder aptamer binding to specific epitopes (leading to

losses in high-affinity members) or promote bridged binding of library members between proximal target molecules (leading to confounding avidity effects). Alternatively, too low a relative concentration of target can thwart aptamer discovery by introducing unproductive levels of selection pressure within the system. Partition stringency is therefore generally increased round-by-round by sequential decreases in target concentration during the library incubation step.

1.3.2.3 PCR AMPLIFICATION LIMITATIONS AND ARTIFACTS

Stoppage of PCR amplification of the retained pool at ≤ 15 cycles is used in virtually all SELEX platforms to avoid excessive accumulation of high-molecular-weight (HMW) by-products. However, it creates the disadvantage of needing to perform the amplification at a relatively large scale (several mL total), typically by partitioning that large reaction volume across several (≥ 96) parallel reactions, then pooling together the gel-purified amplification products in order to gather enough material (ca. 10^{14} members) for the next round of selection.²⁶⁴ HMW by-product accumulation can arise via several mechanisms, including through (i) oligonucleotide stretches within the universal primer regions mis-priming library members, (ii) improperly extended products acting as primers on a heterologous sequence, or via combinations thereof (**Figure 1-13**). Through these spurious priming and extension events, HMW by-products generally start accumulating when the amplicon concentration reaches ca. 20-50 nM (ca. $10^{11} - 10^{12}$ members).²⁰⁵

Alternative strategies have also been described, including amplification-free variations of SELEX,^{286,318,319} in which methods capable of realizing high *PE* values (CE or affinity chromatography) are employed. Although this approach has been successful in circumventing HMW contaminants formation, the abolition of PCR amplifications between selection rounds is known to greatly increase the chances of losing entire representations of library members to stochastic effects.³¹⁹

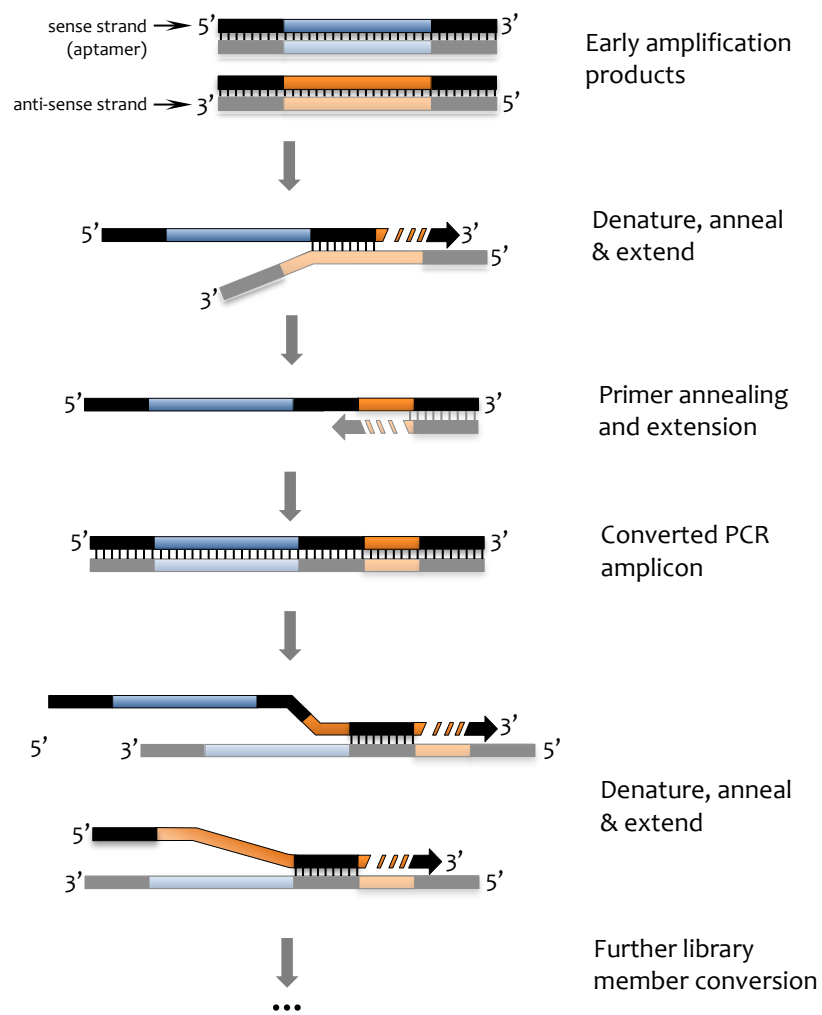


Figure 1-13 Putative high-molecular weight by-product conversion mechanism within a heterogeneous population of library members.

1.3.2.4 LIBRARY REGENERATION ISSUES

The relative performance of available methods for regenerating the ssDNA library from the purified dsDNA amplicons has been studied by Civit et al.³²⁰ and others,^{210,213,321} who collectively showed that enzymatic digestion of 5'-phosphorylated (PO₄) anti-sense strands with lambda exonuclease generally works

best. Overall, however, relatively little effort has been made to fully understand and thereby improve this critical step. The presence of universal primer regions is known to contribute to the formation of heteroduplexes between amplicons. In such cases, the sense strand of a library member (encoding the aptamer sequence) anneals to complementary flanking regions of an anti-sense strand showing only partial complementarity within the core region. This can cause issues for downstream amplicon processing. In particular, gel-electrophoresis purification is complicated by altered migration patterns created by these heteroduplexes which, as a result, can be interpreted as by-products and removed (reducing yields). Moreover, though it has not received attention in the aptamer community, λ -exonuclease hydrolysis activity is appreciably lower on ssDNA than on complementary dsDNA.³²² This raises the question as to whether enzymatic regeneration of the library goes to completion and, if not, what might be the impact on the selection process. Likewise, heteroduplex formation might impact cloning of individual members of the final pool, since the mismatch repair system³²³ of host cells (e.g. *E. coli*) can arbitrarily create new composite sequences derived from the two strands, effectively deleting and/or shuffling retained high-affinity aptamer sequences. Though all of these issues deserve study, they share the common feature of (potentially) arising due to heteroduplex formation during PCR amplification of the retained library. Identifying ways to eliminate heteroduplexes during amplification could therefore be of particular benefit.

The use of emulsions to isolate and amplifying single templates by PCR is well established,³²⁴ and it is known that the resulting partitioning of single templates into individual droplets reduces formation of unwanted by-products when co-amplifying mixtures of different sequences (e.g. multiple genes).^{325,326} Spurious priming events are greatly reduced within a single reaction vessel (droplet), in part because competition between different amplicons and biases resulting from differences in amplification efficiencies are avoided.³²⁷ Moreover, post amplification, the emulsions can be broken to recover the full set of amplicons in an

aqueous phase suitable for downstream processing. Commercial emulsion PCR-based instruments are available (e.g. QX100 droplet digital PCR system (Bio-Rad), RainDrop digital PCR system (RainDance)), but the method has not yet been applied to or optimized for the amplification of retained library members. In addition to mitigating formation of unwanted HMW products, the method could provide a means to eliminate formation of heteroduplexes during amplification, as reactions in each droplet could be designed to amplify a single library member (Figure 1-14).

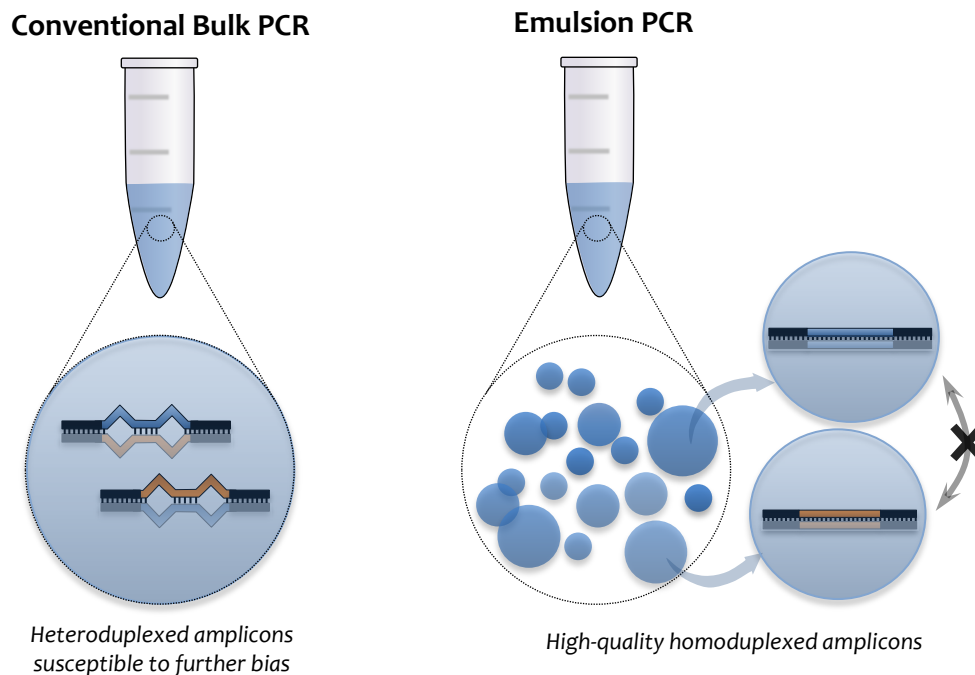


Figure 1-14 Graphical representation of available methods for PCR amplification of retained aptamer pools depicting possible outcomes.

1.3.2.5 CUMBERSOME RETAINED POOL CHARACTERIZATIONS

In conventional SELEX, the aptamer selection process is typically monitored by measuring the mean binding affinity of retained pools after blindly conducting a few SELEX rounds in order to enrich sufficient amounts of high-affinity binders to make K_d determination (typically by SPR or fluorescence spectroscopy) possible. Parallel PCR amplifications, followed by anti-sense strand removal, are typically required to generate the required quantities of modified (e.g. fluorescently-labelled or biotinylated for spectroscopy) or unmodified (for SPR) retained library pools. This widely-adopted strategy is time consuming, fails to provide information in the critical early rounds of selection, and can be costly if SPR is used for analysis of mean K_d values. Moreover, a risk of altered binding properties that bias selection is created if modification of library members is required.

Regrettably, the omission of such characterization steps can lead to the over-selection of aptamer pools, which often results in significantly reduced high-affinity aptamer diversities at the conclusion of SELEX.²³² In general, a proper balancing of retained member diversity and mean binding affinity must be maintained across selection rounds for SELEX to prove successful. Understanding and maintaining that balance would benefit from the development of a simpler, less expensive approach to quantify both the mean K_d and the total sequence diversity of retained pools after every selection round. Currently, enriched library diversities are determined using next-generation sequencing, which is neither fast nor inexpensive.^{171,328,329} However, no suitable alternatives currently exist.

1.3.2.6 THROUGH-PUT: THE TIME REQUIRED TO COMPLETE A SELECTION

Conventional SELEX operations generally take weeks to months to complete, with no assurance the operation will yield a useful aptamer.¹⁶⁴ M-SELEX and CE-SELEX can cut that timeline in half,^{297,330} but further advances are required to

increase throughput to desired levels (days),^{171,331-334} including through the use of robotic liquid-handling platforms that operate on either 96 or 384-well microtitre plates. Traditionally used in quantitative analytical assays, these auto-manipulated plate systems can in principle provide a facile and cost-effective route to aptamer selection. The plate format offers an abundance of available surface chemistries for immobilizing target molecules on the well surface.³³⁵ To date, target immobilization has largely been achieved by physical adsorption to plate well surfaces; but limitations to that strategy have emerged, including poor control of surface densities that confounds aptamer selections by virtue of several issues related to the slow release (leaching) or lateral migration (clustering) of the target biomolecules.³³⁵⁻³³⁷ Therefore, strategies involving covalent attachment chemistries may prove more effective in controlling target density and non-specific binding, in the latter case by using the reactive sites to also create effective passivation layers.

1.4 THESIS SCOPE AND OUTLINE

The discovery of aptamer (and antibody) products generally requires three key connected elements: (i) initial identification of members that present high binding affinity, followed by screening of that sub-population for required (ii) specificity and (iii) analytical or biological function in order to identify small panels of lead compounds suitable for further development. As noted in section 1.3, technological limitations to this standard approach are known when applied to either class of affinity reagent.

Current and emerging mAb discovery pipelines, including those based on multiplexed analysis of individual antibody secreting plasma cells,^{178,338-340} offer highly efficient strategies for screening binding affinity. However, comparable tools for accurate screening of binding specificity at appropriate throughputs are lacking. Challenges related to the affinity and specificity screening of aptamers by the SELEX method likewise exist, sometimes leading to complete failure of the

approach. However, the mechanistic causes of those failures are not fully understood. Therefore, this thesis aims to first address those knowledge gaps, and then combine the resulting better understanding with technological advances to improve both the reliability and overall performance of nucleic acid aptamer discovery platforms. Where possible, these advances are expected to improve characterization of either aptamers or antibodies. Specific objectives include:

- Understand the primary mechanisms limiting per-round partition efficiencies and overall performance of SELEX technology
- Establish strategies or new technologies to ameliorate each of those mechanisms
- Integrate those capabilities into a new platform that greatly improves the reliability and speed by which useful DNA aptamers can be discovered
- Establish a new label-free microfluidic technology that enables screening of either aptamer or antibody populations for binding specificity at throughputs commensurate with current selection platforms

Interferences to robust aptamer selection caused by the fixed regions of an aptamer library are identified and described in Chapter 2, “A Simple Method for Eliminating Fixed-Region Interference of Aptamer Binding during SELEX”, along with a new method to eliminate them. The method efficiently isolates aptamer function to the core random region by blocking the ability of the flanking sequences to interfere with aptamer fold or binding. Incorporation into current SELEX methodologies is shown to greatly enhance retention and enrichment of tight-binding aptamers during the selection process.

Additional factors affecting SELEX performance are identified in Chapter 3, “Development of a High-Fidelity Therapeutic Aptamer Discovery Platform”, and then used to develop methods and technologies to (i) improve target-display chemistry and geometry so as to minimize non-specific binding, (ii) establish

incubation and partition methods that greatly enhance partition efficiency, (iii) enable high-fidelity amplification of retained library members to concentrations suitable for conducting the next selection round, (iv) achieve stoichiometric regeneration of DNA aptamer libraries from amplicons, and (v) achieve rapid and accurate measurements of the mean affinity and sequence diversity of aptamer pools following each selection round. Finally, the methodological and technological advances made are used to create a greatly improved platform for reliable and rapid selection of high-affinity aptamers. The platform, which includes technology described in Chapter 2, is shown to rapidly, efficiently and reliably isolate high-affinity aptamers against several clinically-relevant targets.

Finally, in Chapter 4, “Parallel Microfluidic Surface Plasmon Resonance Imaging Arrays”, a novel moderate-throughput technology that enables label-free analysis of the specificity of an affinity reagent is described at the proof-of-concept level. The technology utilizes custom microfluidic arrays for SPRi-based detection of binding, and the sample workflow and operating conditions required to measure binding affinities and kinetics are described.

Chapter 2

A SIMPLE METHOD FOR ELIMINATING FIXED-REGION INTERFERENCE OF APTAMER BINDING DURING SELEX

“Simplicity is prerequisite for reliability”

— Sir Charles Antony Hoare (1974)³⁴¹

2.1 SYNOPSIS

This chapter reports results for a strategy that involves annealing the complementary sequence to each fixed region of an aptamer library during the selection process in order to reduce artifacts that might compromise or eliminate the discovery of a tight-binding ligand within the combinatorial random region of the library. The inspiration for this idea was provided by Shtatland and coworkers²⁷² and also by Wen and Gray who mentioned its potential application to genomic SELEX libraries.³⁴² However, neither group conducted an analysis of the concept’s utility, due in part to their concerns that the double-stranded tails formed might sterically interfere with aptamer structure, binding or selection. As a result, the value and possible limitations of this flanking-region blocking strategy on aptamer selection are not known. A set of model studies specifically designed to evaluate the merits of the idea on combinatorially synthesized aptamer libraries—

which are known to possess much larger diversities than their genomic counterparts—is first reported in order to establish an effective protocol for incorporating the concept into the screening process. The goal of this work is therefore not the discovery of a new aptamer, but rather the refinement and evaluation of a protocol that might improve aptamer discovery. When applied to a set of benchmark aptamers, the new protocol proves very effective in minimizing unwanted interference effects caused by the fixed regions, allowing for efficient selection of tight-binding ligands that might otherwise be lost from the library during the early critical rounds of selection. The general workflow for the method is outlined in **Figure 2-1**, along with that for a standard selection step of SELEX for comparison. Because it eliminates any single-strand structures within the fixed regions, the technique isolates aptamer fold and function to within the random region of the library members. The protocol therefore complements standard and modified SELEX approaches by offering a non-enzymatic route to minimizing fixed-regions interference during aptamer selection.

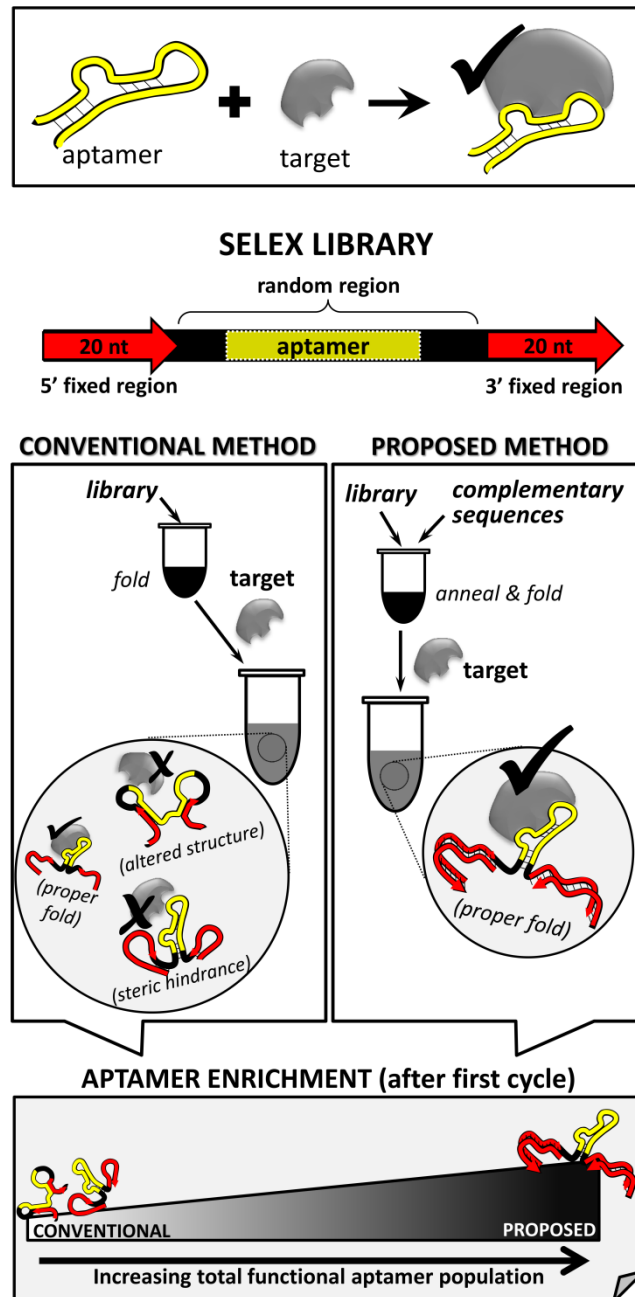


Figure 2-1 Comparison of standard and proposed protocols for SELEX-based selection of aptamers. (Top box) Aptamers bind their target with high affinity through the specific fold of their consensus sequence. A typical aptamer library construct used in SELEX contains a random core region flanked by ~20 nt fixed regions to facilitate PCR amplification. Mechanisms by which the flanking regions can interfere with conventional SELEX, but which are ameliorated by the proposed method are then highlighted. In the proposed method, the fixed regions are blocked using complementary sequences. The aptamer fold is therefore confined within the random region and is able to bind its target with high affinity, allowing for efficient SELEX-type enrichment of high-affinity aptamers.

2.2 EXPERIMENTAL METHODS

2.2.1 DNA LIBRARIES SYNTHESIS AND PURIFICATION

Each member of the ssDNA aptamer library was comprised of a core 40-mer random region (N_{40}) flanked by a 5' universal 20-mer flanking sequence and a 3' universal 20-mer primer binding sequence. Two libraries were synthesized, differing in the sequences of the two flanking regions used. In each, the random region was created combinatorially by mixing A:C:G:T at a molar ratio of 3:3:2:2.4 in order to achieve equal probability incorporation of each nucleotide within the core region.³⁴³ The two independent sets of 20-mer flanking sequences used in this study are among the most frequently applied to SELEX-based aptamer selection.^{307,310,344-347} Indeed, the selection of each of the current benchmark aptamers against thrombin, streptavidin and VEGF used engineered 80-mer libraries comprised of one of these two flanking sequence pairs and associated library templates, hereafter referred to as L1 and L2. Both flanking sequences of each library format had their complement synthesized, where the complement to the 3' flanking sequences (3'-Comp-L1 or 3'-Comp-L2) also served as the reverse primer (REV-L1 or REV-L2) for PCR amplification. All oligonucleotides were synthesized and HPLC purified by Integrated DNA Technologies, Inc. (IDT; Coralville, IA), and reconstituted in 1X AF buffer. **Table 2-1** and **Table 2-2** summarize the two library formats used in this study, as well as the primers and blockers applied to them. Engineered aptamer sequences used in this study, which include the 29 nt streptavidin aptamer (SBA29), the 15 nt and 29 nt thrombin aptamers (TBA15 and TBA29, respectively), and the 25 nt vascular endothelial growth factor aptamer (VBA25), are summarized in **Table 2-3**. For certain selection studies identified in the Results and Discussion, the appropriate library form of either SBA29 (10^{12} sequences added), TBA15 (10^{12} sequences added), or TBA15 and TBA29 (10^6 sequences of each added), was introduced into the ssDNA library (1 nmole; 10^{14} sequences) to permit detection of the aptamer in the bound and unbound pools during the first round of selection.

Otherwise, the basic unsupplemented library in either blocked or unblocked form was used.

Table 2-1 DNA primers, blockers and Library-1 sequences used in this study

Name	Sequence (5' – 3')	Comments
FOR-L1	AGCAGCACAGAGGTCAGATG	5' amplification primer
5'-Comp-L1	CATCTGACCTCTGTGCTGCT	5' complementary blocker
REV-L1 / 3'-Comp-L1	Phos – TTCACGGTAGCACGCATAGG	3' amplification primer / complementary blocker
Library-1 (L1) (80nt)	AGCAGCACAGAGGTCAGATG–N(40)– CCTATGCGTGCTACCGTGAA	N(40) = 40 randomized nucleotides

Table 2-2 DNA primers, blockers and Library-2 sequences used in this study

Name	Sequence (5' – 3')	Comments
FOR-L2	TCGCACATTCCGCTTCTACC	5' amplification primer
5'-Comp-L2	GGTAGAAGCGGAATGTGCGA	5' complementary blocker
REV-L2 / 3'-Comp-L2	Phos – TTCGCACACACGGACTTACG	3' amplification primer / complementary blocker
Library-2 (L2) (80nt)	TCGCACATTCCGCTTCTACC–N(40)– CGTAAGTCCGTGTGTGCGAA	N(40) = 40 randomized nucleotides

Table 2-3 DNA aptamer sequences used in this study

Name	Sequence (5' – 3') ^a	Comments
TBA15 (15nt)	GGTTGGTGTGGTTGG	Thrombin aptamer ¹⁷²
TBA15-L1 (80nt)	AGCAGCACAGAGGTCAGATG – GCTGCTGAATT <u>CGGTTGGTGTGGTTGGGAATT</u> CTACGGAT–CCTATGCGTGCTACCGTGAA	Library 1 80-mer form of TBA15
TBA29 (29nt)	AGTCCGTGGTAGGGCAGGTTGGGGTGACT	Thrombin aptamer ²⁸⁸
TBA29-L1 (80nt)	AGCAGCACAGAGGTCAGATG – TTCAGTCCGTGGTAGGGCAGGTTGGGGTGACT GTTACCGT–CCTATGCGTGCTACCGTGAA	Library 1 80-mer form of TBA29
TBA29-L2 (80nt)	TCGCACATTCCGCTTCTACC – TTCAGTCCGTGGTAGGGCAGGTTGGGGTGACT GTTACCGT–CGTAAGTCCGTGTGTGCGAA	Library 2 80-mer form of TBA29
SBA29 (29nt)	ATTGACCGCTGTGTGACGCAACACTCAAT	Streptavidin aptamer ³⁴⁸
SBA29-L1 (80nt)	AGCAGCACAGAGGTCAGATG – ACTACTATTGACCGCTGTGTGACGCAACACTC <u>AAITTCAC</u> –CCTATGCGTGCTACCGTGAA	Library 1 80-mer form of SBA29
VBA25 (25nt)	CCGTCTTCCAGACAAGAGTGCAGGG	Vascular endothelial growth factor aptamer ³⁴⁹
VBA25-L1 (80nt)	AGCAGCACAGAGGTCAGATG – GGCTGAT <u>CCGTCTTCCAGACAAGAGTGCAGG</u> <u>GATCGAGCC</u> –CCTATGCGTGCTACCGTGAA	Library 1 80-mer form of VBA25

a: Primer sites in bold; aptamer binding sequence underlined.

2.2.2 ISOTHERMAL TITRATION CALORIMETRY

Human α -thrombin, purified from human plasma and resuspended in phosphate buffer (20 mM Sodium Phosphate, 150 mM NaCl, pH 7.4), was purchased from Haematologic Technologies (Essex Junction, VT). Streptavidin was purchased from Sigma-Aldrich (Oakville, ON, Canada) and recombinant human VEGF-165 from BioLegend (San Diego, CA). All proteins were either exchanged or reconstituted in 1X aptamer folding (AF) buffer (1X AF buffer is 20 mM Tris-HCl pH 7.4, 140 mM NaCl, 5 mM KCl, 1 mM MgCl₂, 1 mM CaCl₂). All aptamers with the exception of the anti-VEGF aptamers were diluted to a final concentration of 30 μ M in 1X AF buffer. VEGF aptamers were diluted to a final concentration of 20 μ M. Prior to ITC measurements, working concentrations of aptamers were heated to 95°C and slowly cooled down to 25°C at a rate of 0.5°C min⁻¹ in a Mastercycler® ep thermocycler (Eppendorf, Mississauga, ON, Canada) to ensure proper folding. In cases where complementary oligonucleotides were added, this folding protocol also ensured their proper annealing to the flanking regions. ITC measurements were performed at 25°C using a MicroCal iTC₂₀₀ system (GE Healthcare, Piscataway, NJ). The sample cell contained 200 μ L of target protein (3 μ M; 2 μ M for VEGF) also prepared in 1X AF buffer. The injection syringe contained 40 μ L of diluted aptamer. A first injection of 0.4 μ L preceded the 15 injections of 2.5 μ L. Run parameters were set for an injection rate of 0.5 μ L s⁻¹ with a 150 s time interval between injections. The syringe rotation speed was set at 1000 rpm. The results were analyzed using Origin 7.0 software (OriginLab Corp., Northampton, MA) by fitting to a single-site binding model. Where duplicate experiments were done, standard errors were reported.

2.2.3 SELEX-BASED SCREENINGS

MyOne carboxylic acid and streptavidin C1 Dynabeads from Invitrogen Life Technologies (Burlington, ON, Canada) were supplied as a 10 mg ml⁻¹ stock

solution. 1-ethyl-3-(3-dimethylaminopropyl) carbodiimide hydrochloride (EDC), N-hydroxysuccinimide (NHS) and ethanolamine were obtained from Sigma-Aldrich (Oakville, ON, Canada). Carboxylic acid beads (0.5 mg) were washed 3X in MES buffer (25 mM 2-[N-morpholino]ethane sulfonic acid, pH 6.0), and the beads were then recovered using a magnetic particle separator (Magna-Sep, Invitrogen Life Technologies) before being activated in a 250 μ l solution of 400 mM EDC and 100 mM NHS for 30 min at room temperature. After activation, the beads were washed 3X in MES buffer and incubated in a solution containing 50 μ g human α -thrombin, incubating for 2 hrs. After incubation, the beads were washed 3X in 2 M NaCl Tris-buffer (20 mM Tris-HCl pH 7.4, 2 M NaCl, 5 mM KCl, 1 mM MgCl₂, 1 mM CaCl₂), followed by 3X wash in MES buffer. The modified beads were then blocked in a 250 μ l solution of 1 M ethanolamine for 30 min, before being subjected to a final wash sequence 3X in MES buffer containing 0.02% Tween-20. The thrombin-modified beads were stored at a 10 mg ml⁻¹ concentration at 4°C until further use.

The 80-mer library form of the streptavidin binding aptamer (SBA29-L1), where the 29-mer consensus sequence is fully contained within the core region, was spiked into the ssDNA library (1 nmole; 10¹⁴ sequences) at a 1% molar ratio to permit detection of the aptamer in the bound and unbound pools during the first round of selection. Equimolar amounts of the complementary oligonucleotides 5'- and 3'-Comp-L1 to the flanking sequences were added to and equilibrated with the spiked library prior to permit hybridization and aptamer folding.

Selection of streptavidin-binding aptamers is described in full here as an example of the general protocol employed. A 2 μ l portion of washed MyOne streptavidin C1 Dynabeads (~10⁶ beads) was incubated with 1 nmole (~10¹⁴ sequences) of the selected folded aptamer library supplemented with equimolar amounts of its respective complementary oligonucleotides 5'- and 3'-Comp in 500 μ l of 1X binding buffer (20 mM Tris-HCl pH 7.4, 140 mM NaCl, 5 mM KCl,

1 mM MgCl₂, 1 mM CaCl₂, 0.02% Tween-20) for 1 hr at room temperature with gentle rotation. Unbound and weakly bound aptamers, including the library form of the 29 nt streptavidin aptamer (SBA29-L1), were removed by conducting a series of 500 µl washes in 1X binding buffer. All remaining bound aptamers and oligonucleotides were eluted from the beads in 1X denaturing buffer (40 mM Tris-HCl pH 8.0, 3.5 M urea, 10 mM EDTA, 0.02% Tween-20) at 85°C. All wash and elution steps were performed three times for 5 min in a total volume of 500 µl. Each collected fraction was desalted using centrifugal filter units (Amicon Ultra-0.5 MWCO 10K, Millipore) and the aptamers recovered in nanopure water (18.2 MΩ-cm) according to the manufacturer's instructions. Conventional SELEX cycles²³² were also performed exactly as described above, but without addition of the complementary blocking sequences to the library prior to folding.

Similarly, pre-blocked and standard SELEX-based screens of the 80 nt Library-1 or Library-2 containing the 15 nt thrombin aptamer (TBA15-L1) and/or the 29 nt thrombin aptamer (TBA29-L1) were also performed as described above, but using carboxylic acid functionalized beads displaying immobilized human α-thrombin prepared according to the protocol described above.

Recovered members were desalted and amplified in 50 µl PCR reactions containing 1X PCR buffer, 1.5 mM MgCl₂, 200 µM dNTP, 250 nM each of FOR-L2 and phosphorylated REV-L2 primer, as well as 2 units of Platinum Taq DNA polymerase. Amplification was stopped at the maximum number of cycles before artifact formation was observed on a one-dimensional agarose gel (i.e. the maximum number of cycles where no higher molecular weight amplification products could be observed). Thermal cycling conditions were as follows: initial denaturation at 95°C for 3 min, followed by an optimal number of cycles (10-18) comprised of denaturation at 94°C for 15 s, annealing at 64°C for 20 s and extension at 72°C for 30 s, with a final extension at 72°C for 3 min. PCR reactions were pooled, ran on a 1.5% TBE agarose gel, and purified using a QIAEXII Gel Extraction

Kit (Qiagen, Toronto, ON) following the manufacturer's protocol. The purified double-stranded product was digested with 5 units of lambda exonuclease (NEB; Whitby, ON) in the supplied buffer for 60 min at 37°C. The resulting single stranded product was then purified by phenol extraction and ethanol precipitation for the next round of selection.

2.2.4 REAL-TIME AMPLIFICATIONS OF ELUTED POOLS

Desalted eluted library fractions were amplified in a CFX Real-Time PCR detection system (Bio-Rad, Mississauga, ON) in the presence of either SYBR Green or a TaqMan™ probe against the target aptamer (e.g., the hydrolysis probe 5'-FAM-CCG CTG TGT GAC GCA ACA CTC AA-Iowa Black FQ -3' was used for the SBA29-L1 aptamer). For the latter real-time amplification, a 5 µl aliquot of each eluted library fraction was mixed with iQ Supermix (Bio-Rad), 300 nM each of the forward and reverse primers, as well as 200 nM of the respective TaqMan™ hydrolysis probe to form a 25 µl reaction volume. Quantification of total library levels eluted in each fraction was achieved by mixing a 5 µl aliquot of each eluted fraction with iQ SYBR Green Supermix (Bio-Rad) and 300 nM of each required primer (**Table 2-1** and **Table 2-2**). The thermal cycling conditions were as follows: initial denaturation for 3 min at 95°C, then 50 PCR cycles each comprised of denaturation at 95°C for 30 s and annealing/extension at 59.5°C for 30 s. For the TBA29-L1 primer pair, the annealing/extension temperature was 55°C for 30 s. All results were analyzed using CFX Manager Software (Bio-Rad), which automatically computes and reports a threshold cycle value for each real-time amplification curve.

2.2.5 QPCR-BASED BULK AFFINITY DETERMINATION

A new qPCR-based method was developed to permit rapid and inexpensive determination of the mean binding affinity, recorded in terms of the equilibrium

dissociation constant K_d , of the eluted library to the target. Briefly, the protein target (e.g., human α -thrombin) was immobilized on Nunc Immobilizer Amino plates (Thermo Fisher; Edmonton, AB) according to the manufacturer's instructions³⁵⁰ at a concentration of 90 nM in 100 mM sodium phosphate buffer pH 7.4. Eluted aptamer pools were serially diluted into 8 different concentrations (2-fold dilutions starting at 100 nM) and the set incubated in functionalized wells for 1 hr at 25°C with gentle mixing at 300 rpm. Aptamer pools in the equilibrated wells were successively washed three times with 300 μ l 1X binding buffer and the retained members then eluted in 50 mM NaOH at 70°C and neutralized with 20 mM Tris pH 7.4 containing 50 mM HCl. The neutralized material was mixed with iQ SYBR Green supermix (Bio-Rad) containing 250 nM of each required primer (**Table 2-1** and **Table 2-2**). Thermal cycling conditions were as follows: initial denaturation for 3 min at 95°C, then 40 cycles each comprised of denaturation at 95°C for 30 s and annealing/extension at 64.0°C for 30 s. Bound aptamer fractions were determined through comparison to a standard curve constructed from C_q data for serially diluted Library-2 members. The resulting binding isotherm data were nonlinearly fitted to the Langmuir equation to determine the dissociation constant of the pool of eluted members.³⁵¹

2.3 RESULTS AND DISCUSSION

Building on the arguments first proposed by Shtatland et al.,²⁷² it was postulated that each fixed-region sequence within a given selection library can interfere with aptamer fold and function through its potential to adopt stable secondary structures created through either 1) self-association, or 2) association with complementary nucleotides within the random core region, the opposing fixed region, or both. Each of these types of unwanted structures can occur either within an individual aptamer or between complementary regions of different members of the library. Below, examples of these possible interference effects are

provided, followed by demonstrating how pre-blocking fixed regions can serve to eliminate their occurrence.

2.3.1 SECONDARY STRUCTURES FORMED WITHIN FIXED REGIONS CAN INTERFERE WITH APTAMER BINDING THROUGH STERIC HINDRANCE EFFECTS

Arguably the most extensively studied of all known aptamers, the 15 nt thrombin binding aptamer (TBA15) tightly and specifically binds the fibrinogen exosite of the serine protease human α -thrombin.¹⁷² **Figure 2-2A** reports ITC data (**Table 2-4**) that show that TBA15 binds α -thrombin with nanomolar affinity at physiological conditions through an enthalpically driven reaction that is compensated by a loss in entropy. Insertion of the TBA15 consensus sequence into the 40 nt core region of the 80 nt SELEX Library-1 template results in a sequence (TBA15-L1) that is predicted by Mfold³⁵² to form no base pairs that *directly* interfere with TBA15's known G-quadruplex structure required for thrombin binding (**Figure 2-2B**). However, Mfold also predicts a large stem loop formed within the 5' flanking region adjacent to the aptamer binding sequence, as well as a second moderate-sized stem loop within the 3' flanking region. ITC data for titrating this 80-mer library version of the thrombin aptamer (TBA15-L1) into a solution of human α -thrombin show evidence of, at most, very weak binding (**Figure 2-2B**, bottom), indicating that the presence of the flanking regions strongly inhibits binding, presumably through steric hindrance imposed by the two stem loop structures. Thus, although Mfold predictions are two-dimensional and therefore rather crude, they correlate well with ITC data by identifying changes in library-aptamer fold or other structural aspects that may influence aptamer function.

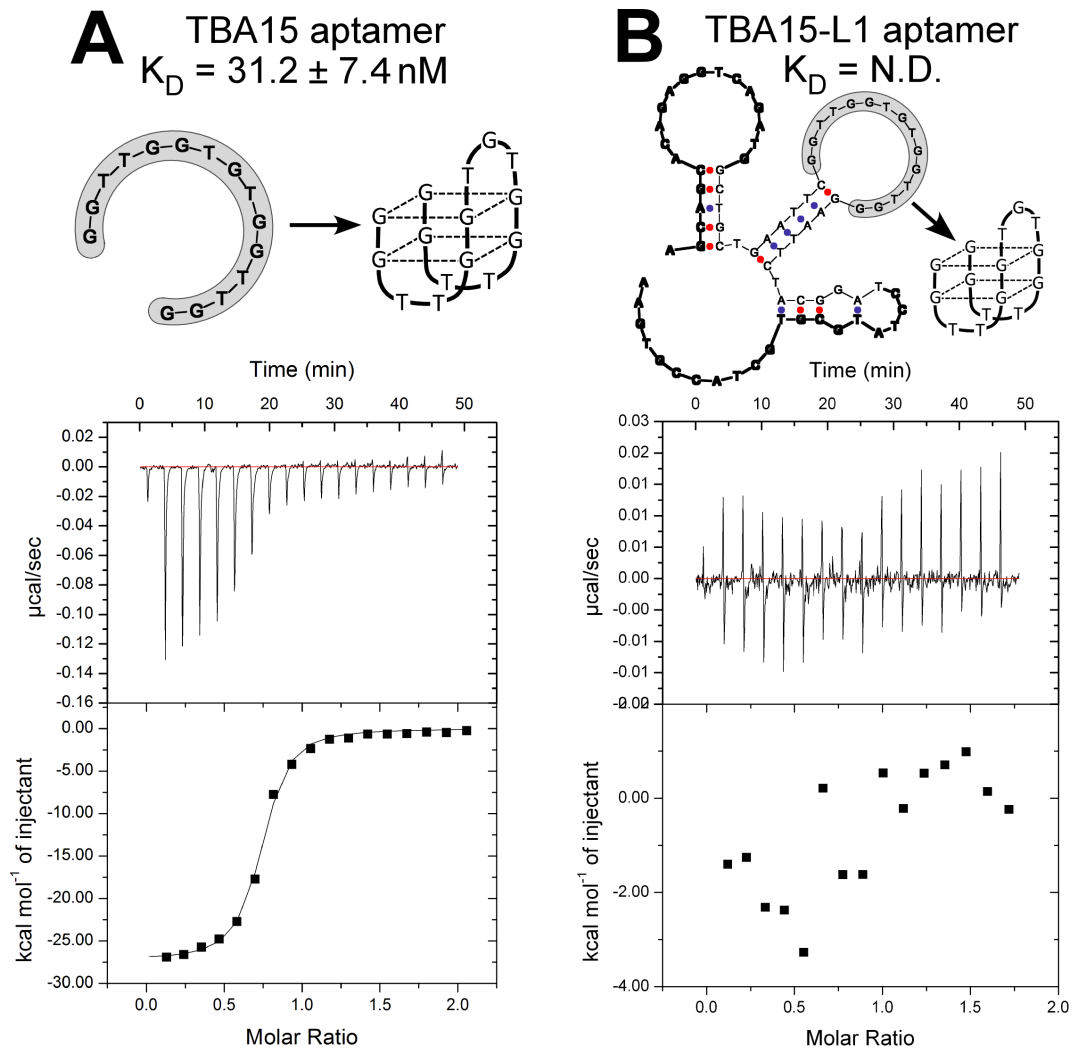


Figure 2-2 Unwanted hybridization of sequences within the fixed regions can impede aptamer binding through steric hindrance effects. (A) The 15nt thrombin-binding consensus sequence (TBA15) folds into a G-quadruplex structure (top panel) that binds thrombin with nanomolar affinity as measured by isothermal titration calorimetry (bottom). Both the raw titration data and the differential heats fitted to a single-site binding model are shown in the bottom panel. (B) The 80 nt thrombin aptamer library construct (TBA15-L1) containing the TBA15 consensus sequence (highlighted) is predicted by Mfold to adopt a structure that includes two stem-loops adjacent to the G-quadruplex binding site formed through hybridization of nucleotides from the fixed (bold face type) and core regions. ITC data show that TBA15-L1 binds human α -thrombin very weakly at most (bottom). ITC experiments were performed in duplicate, from which average K_d values and standard errors were computed and reported. All base-pairing and secondary structure predictions were determined using the program Mfold.³⁵²

Table 2-4 Thermodynamic data for binding of aptamers to their respective targets^a measured by isothermal titration calorimetry.

Aptamer	K_d (nM)^b	ΔH (kcal mol⁻¹)	$-T\Delta S$ (kcal mol⁻¹)	ΔG (kcal mol⁻¹)
TBA15	31.2 ± 7.4	-27.2 ± 0.3	17.0	-10.2
TBA15-L1	n.d.	n.d.	n.d.	n.d.
TBA15-L1+Comp-L1's	20.0 ± 2.7	-23.5 ± 0.1	13.0	-10.5
SBA29	20.8 ± 2.2	-38.1 ± 0.1	27.6	-10.5
SBA29-L1	n.d.	n.d.	n.d.	n.d.
SBA29-L1+Comp-L1's	20.8 ± 2.4	-34.1 ± 0.1	23.6	-10.5
VBA25	36.8 ± 4.9	-24.8 ± 0.2	14.6	-10.2
VBA25-L1	34.5 ± 3.2	-10.9 ± 0.1	0.70	-10.2
VBA25-L1+Comp-L1's	35.5 ± 7.0	-11.8 ± 0.1	1.6	-10.2
TBA29	3.9 ± 0.8	-18.7 ± 0.1	7.2	-11.5
TBA29-L1	5.5 ± 1.5	-12.6 ± 0.1	1.4	-11.3
TBA29-L1+Comp-L1's	5.7 ± 2.3	-9.9 ± 0.1	-1.3	-11.3
TBA29	3.9 ± 0.8	-18.7 ± 0.1	7.2	-11.5
TBA29-L2	454 ± 61	-28.4 ± 0.7	19.8	-8.64
TBA29-L2+Comp-L2's	4.0 ± 1.1	-10.8 ± 0.1	-0.7	-11.5

a: Experiments were performed at 25°C in 20 mM Tris-HCl (pH 7.4), 140 mM NaCl, 5 mM KCl, 1 mM MgCl₂, and 1 mM CaCl₂.

b: no detectable binding; the iTC200 instrument does not detect binding weaker than 10² M⁻¹

2.3.2 FIXED REGIONS CAN ELIMINATE APTAMER FOLD AND FUNCTION THROUGH HYBRIDIZATION WITH COMPLEMENTARY SEQUENCES WITHIN THE CORE REGION.

Known aptamers having nanomolar affinity to streptavidin share a 29 nt consensus sequence (SBA29) that folds into a bulge-hairpin motif (**Figure 2-3A**).³⁴⁸ ITC data for titrating SBA29 into a streptavidin solution (**Figure 2-3A; Table 2-4**) show that the strong affinity is derived from a very favorable binding enthalpy that is only modestly compensated by entropy. Presentation of SBA29 within the random region of the standard 80 nt SELEX Library-1 template results in a ssDNA sequence (SBA29-L1) that is predicted by Mfold to no longer display the bulge-hairpin motif of SBA29 due to the formation of more stable secondary structures comprised of regions of the 29 nt aptamer and complementary sequences within both the 5' and 3' fixed regions of the library (**Figure 2-3B**). As a result, ITC data for titrating the 80-mer library version of the streptavidin aptamer (SBA29-L1) into a solution of streptavidin show no evidence of a binding interaction (**Figure 2-3B**). Thus, the SELEX protocol, in its standard configuration, can preclude the enrichment and identification of desired tight-binding aptamers through a number of mechanisms involving the single-stranded flanking regions.

2.3.3 BLOCKING FIXED REGIONS WITH COMPLEMENTARY SEQUENCES RESTORES BINDING BY ELIMINATING INTERFERENCES DUE TO STERIC HINDRANCE OR LOSS OF REQUIRED APTAMER STRUCTURE.

To test this hypothesis, the effect of annealing 5'-Comp-L1, 3'-Comp-L1 or both oligonucleotides to the library form of the 15-mer thrombin aptamer (TBA15-L1), with each Comp-L1 sequence added to a concentration equimolar to that of TBA15-L1. ITC data (**Figure 2-4A, B and C**) show that the hybridization of both blocking oligonucleotides to TBA15-L1 completely restores binding affinity to that of the original consensus aptamer (TBA15) ($K_d = 20.0 \pm 2.7$ nM; it is in fact seen to be slightly improved, albeit to a nearly insignificant degree when experimental errors are taken into account), while adding only one of the oligonucleotides (**Figure 2-4A, B**) partially restores affinity ($K_d = 48.3 \pm 13.8$ nM for 5'-Comp-L1 or $K_d = 45.0 \pm 11.6$ nM for 3'-Comp-L1). These results therefore suggest that interferences from the flanking regions can be eliminated through pre-blocking with the respective complementary oligonucleotides.

Similarly, when 5'-Comp-L1 and 3'-Comp-L1 are added in equimolar amounts to the Library-1 version of the streptavidin aptamer (SBA29-L1), Mfold predicts full recovery of SBA29's bulge-hairpin motif required for binding, which is corroborated with ITC data showing a full restoration of binding affinity ($K_d = 20.8 \pm 2.4$ nM) to streptavidin (**Figure 2-5**). Thus, it is found that pre-blocking can serve to eliminate the most obvious and worrisome mechanisms by which the single-stranded fixed regions of a library interfere with or eliminate binding, and therefore selection, of desired tight-binding aptamers.

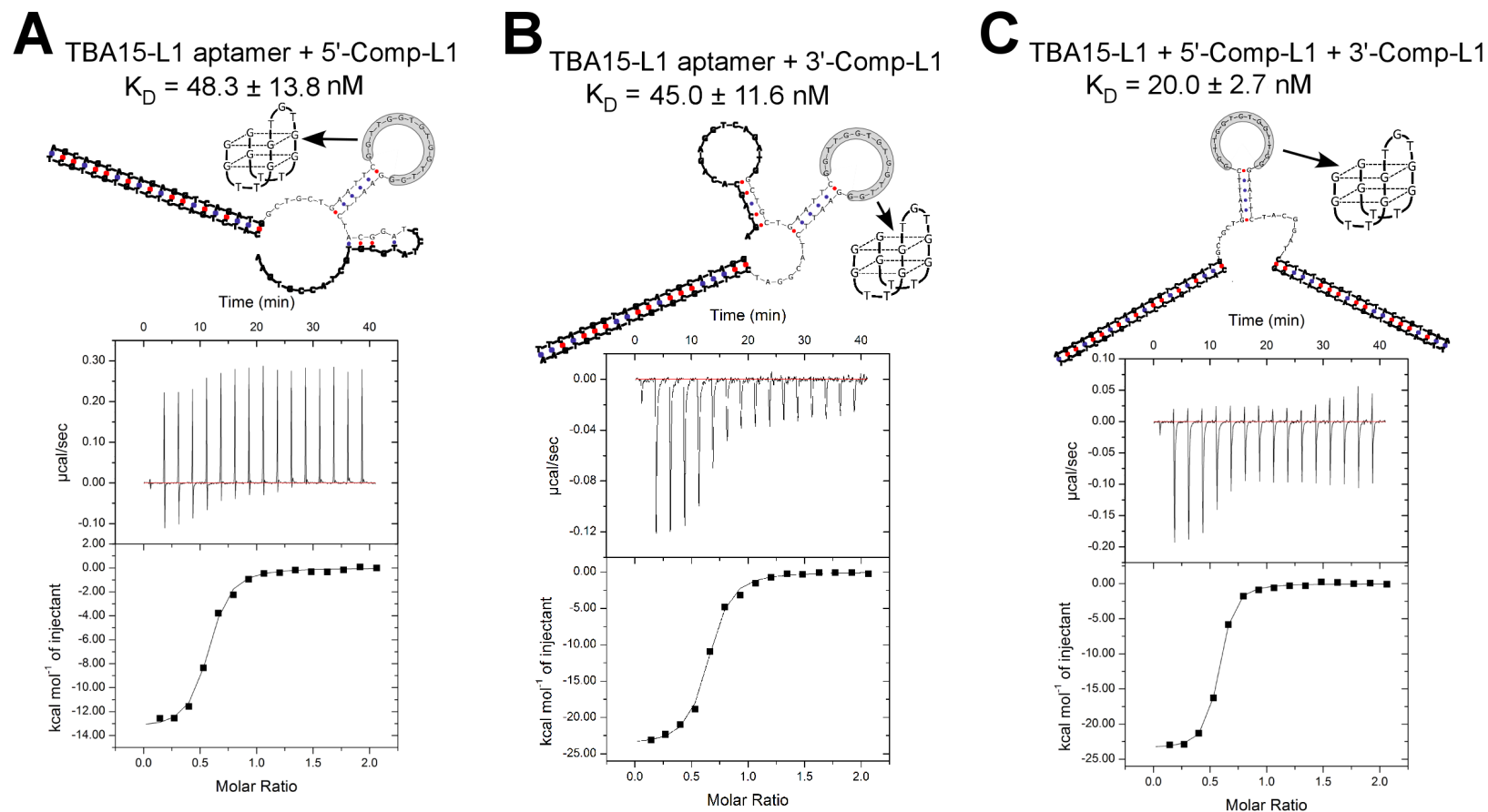


Figure 2-4 Blocking of sequences within the fixed regions can restore binding affinity by removing interferences due to steric hindrance. Addition and hybridization of either 5'-Comp-L1 (A) or 3'-Comp-L1 (B) results in partial restoration of binding affinity. (C) Hybridization of both complementary sequences results in complete restoration of binding affinity. ITC experiments were performed in duplicate, from which average K_d values and standard errors were computed and reported. All base-pairing and secondary structure predictions were determined using the program Mfold.

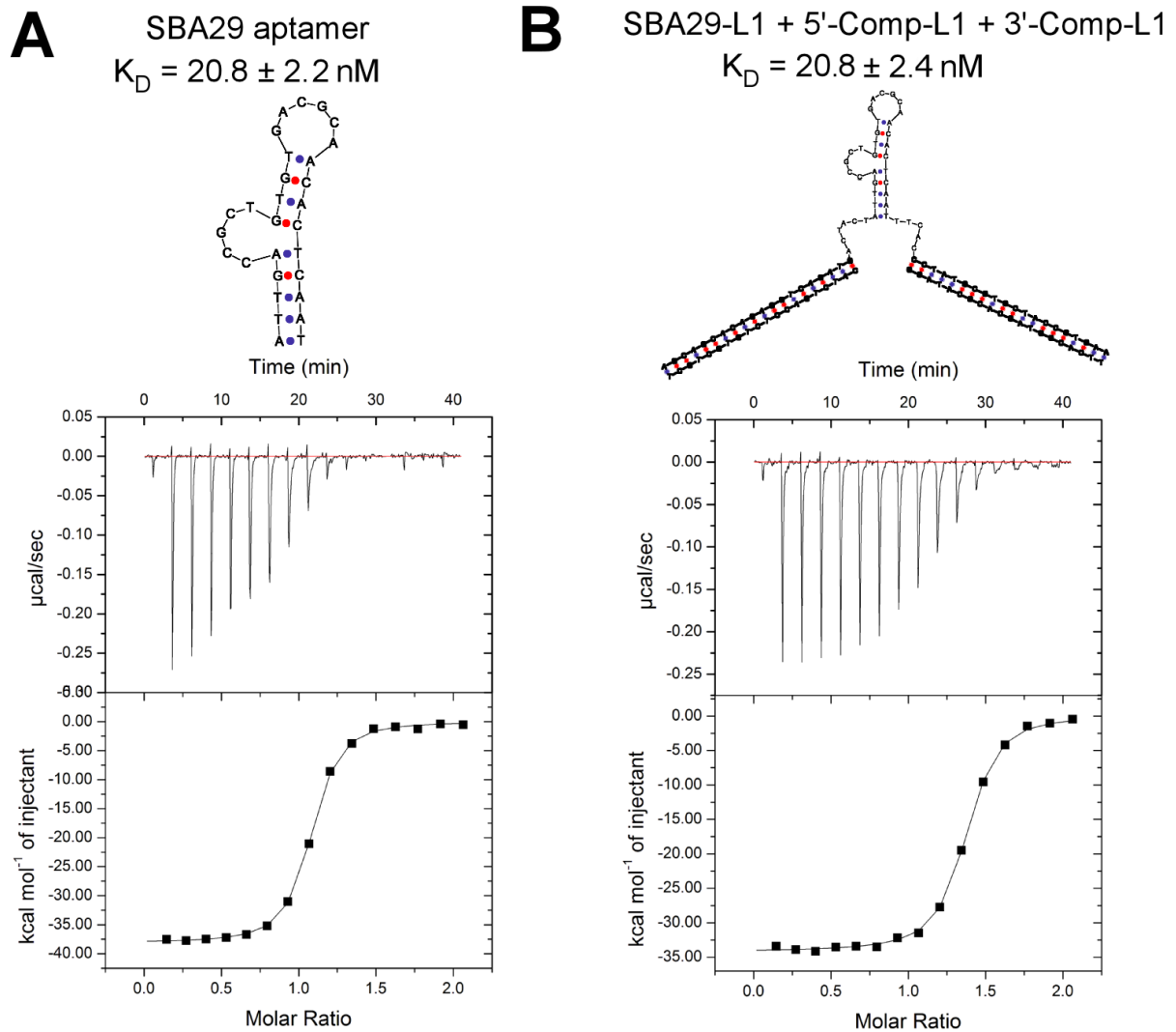


Figure 2-5 Blocking of sequences within the fixed regions can restore binding affinity by removing interferences due to loss of structure. (A) The 29-mer streptavidin aptamer consensus sequence (SBA29) adopts a characteristic bulge-hairpin structure (top panel) that ITC data (bottom panel) show binds streptavidin with nanomolar affinity at physiological conditions. (B) Hybridization of both complementary sequences to the fixed regions of SBA29-L1 is predicted by Mfold to restore SBA29's characteristic bulge-hairpin secondary structure (top), and ITC data (bottom) show that binding affinity is restored and identical to that for SBA29. ITC experiments were performed in duplicate, from which average K_D values and standard errors were computed and reported.

2.3.4 PRE-BLOCKING FIXED REGIONS DOES NOT INTERFERE WITH OTHERWISE PROPERLY FUNCTIONING LIBRARY MEMBERS

To investigate the general utility of pre-blocking in rendering a combinatorial aptamer library suitable for SELEX-based screening, studies were extended to include two additional aptamers: VBA25 and TBA29. VBA25, a 25 nt DNA aptamer against the vascular endothelial growth factor (VEGF),³⁵³ is among the first aptamers approved for therapeutic use by the FDA. It therefore serves as a benchmark for therapeutic aptamers.³⁵⁴ The 29 nt aptamer TBA29 binds to the heparin binding site of human α -thrombin, as opposed to the fibrinogen exosite targeted by TBA15.²⁸⁸ ITC data (**Table 2-4**) show that each of these consensus aptamers binds its target with nanomolar affinity at physiological conditions ($K_d = 3.9 \pm 0.8$ nM for TBA29; $K_d = 36.8 \pm 4.9$ nM for VBA25). Insertion of either TBA29 or VBA25 into the 40 nt random region of the 80 nt SELEX Library-1 template results in a sequence (TBA29-L1 or VBA25-L1, respectively) where the flanking regions are predicted by Mfold to not alter directly the known structures of the two aptamers. ITC data for titration of TBA29-L1 or VBA25-L1 into a solution of human α -thrombin or VEGF₁₆₅ (**Table 2-4**), respectively, reveal a binding affinity that is equivalent to the isolated consensus sequence ($K_d = 5.5 \pm 1.5$ nM for TBA29-L1; $K_d = 34.5 \pm 3.2$ nM for VBA25-L1), indicating that, in these cases, the stem-loop structures formed within the flanking regions do not inhibit aptamer function. Here, the addition of both complementary oligonucleotides yields no significant change in binding affinity ($K_d = 5.7 \pm 2.3$ nM for TBA29-L1; $K_d = 35.5 \pm 7.0$ nM for VBA25-L1), demonstrating that the proposed protocol eliminates pathways for significant loss of promising aptamers without adversely affecting the properties and selection of otherwise properly functioning library members.

2.3.5 PRE-BLOCKING FIXED REGIONS IS EQUALLY EFFECTIVE ON OTHER LIBRARY FORMATS

The various SELEX library designs successfully used to date differ both in library member length and in the sequences of the fixed regions employed. In addition, fixed-region sequences can be replaced after each or a selected panning round to reduce persistent interference to aptamer fold.²⁷² To be of general utility, this pre-blocking of fixed regions strategy must therefore be effective on different libraries and library formats. For the 29 nt thrombin aptamer TBA-29, **Figure 2-6A** and **B** (see also **Table 2-4**) show that when the flanking regions of TBA29-L1 are replaced with those of Library-2, the resulting sequence (TBA29-L2) is predicted by Mfold to form base pairs between random and fixed sequences that serve to inhibit formation of the G-quadruplex structure required for binding to thrombin. ITC data (**Figure 2-6B**) for titrating this 80-mer Library-2 version of the thrombin aptamer into a solution of human α -thrombin shows evidence of greatly weakened binding affinity ($K_d = 454 \pm 61$ nM) at physiological condition, compared to that of TBA29 alone ($K_d = 3.9 \pm 0.8$ nM).

As with Library 1, when 5'-Comp-L2 and 3'-Comp-L2 are added in equimolar amounts to the Library-2 version of this thrombin aptamer (TBA29-L2) and allowed to anneal to their complementary fixed regions, Mfold predicts recovery of TBA29's G-quadruplex structure required for binding. More importantly, ITC data show full restoration of binding affinity ($K_d = 4.0 \pm 1.1$ nM) to thrombin (**Figure 2-6C**). The results in **Figure 2-2** to **Figure 2-6** therefore show that unblocked flanking regions will impact the structures and affinities of a fraction of library members presenting a functional aptamer sequence within the random region, and that pre-blocking of the flanking regions can provide a general strategy to eliminate those deleterious effects on aptamer fold and function, regardless of the chosen target, library format or fixed region sequences employed.

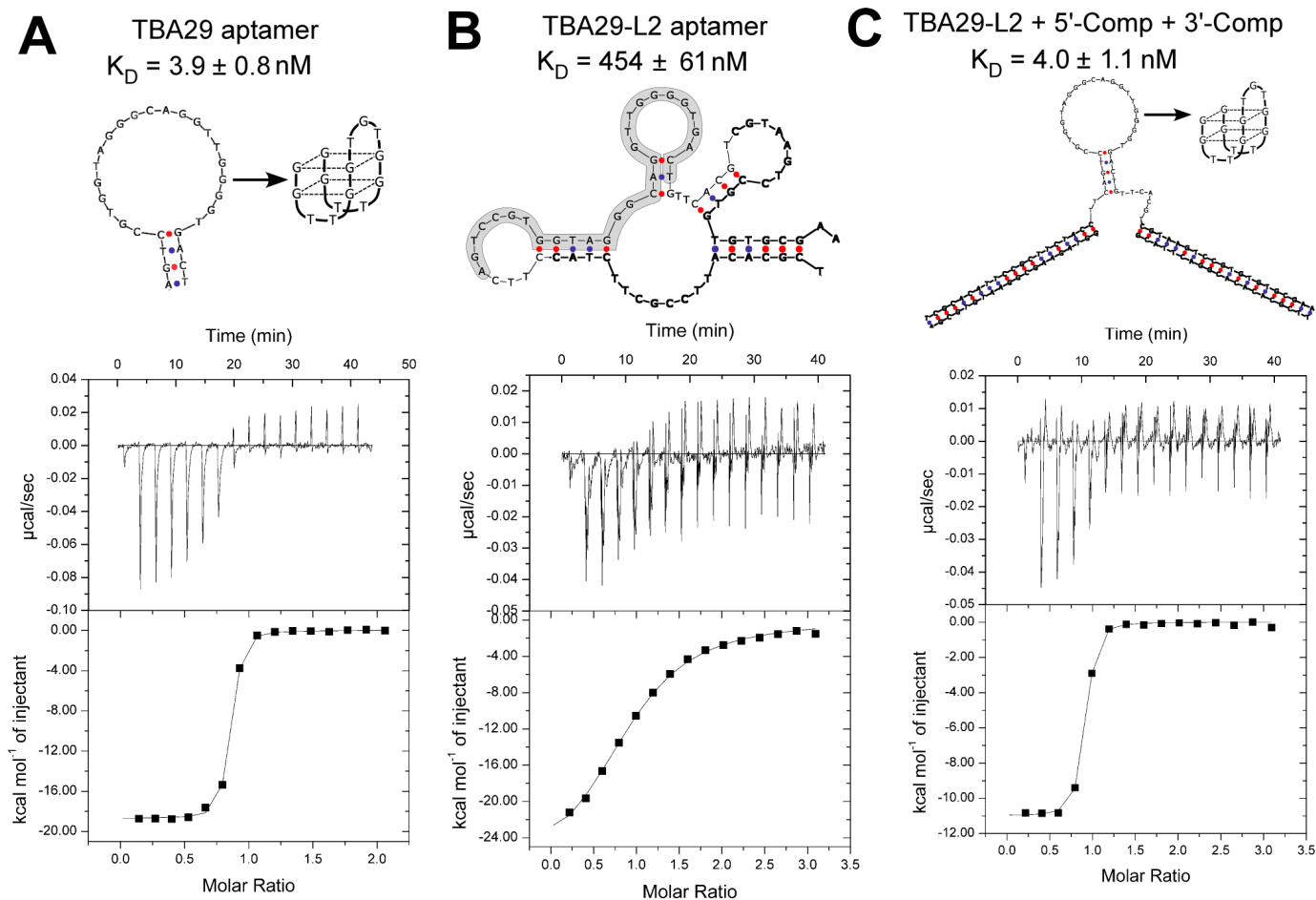


Figure 2-6 Application of methodology described in **Figure 2-5** to the 29-mer thrombin aptamer consensus sequence (TBA29). (A) TBA29 folds into a G-quadruplex structure (top panel). ITC data (bottom panel) showing TBA29 binds human α -thrombin with nanomolar affinity at physiological conditions. (B) When the flanking regions are replaced with those from Library-2, the resulting 80 nt aptamer library construct (TBA29-L2) containing the 29-mer consensus sequence (highlighted) is predicted by Mfold to contain base-pairing that interferes with the known G-quadruplex structure required for binding. This result is significantly different from the Library-1 version of the same aptamer (TBA29-L1), which retains the G-quadruplex structure. ITC data (bottom) show that TBA29-L2 binds thrombin with greatly weakened affinity compared to its Library-1 counterpart. (C) Hybridization of both complementary sequences to the fixed regions of TBA29-L2 is predicted by Mfold to eliminate all base pairs that serve to interfere with the G-quadruplex secondary structure (top), and ITC data (bottom) show full restoration of binding affinity to TBA29 or TBA29-L1 (**Table 2-4**). ITC experiments were performed in duplicate, from which average K_d values and standard errors were computed and reported.

2.3.6 PRE-BLOCKING FIXED REGIONS PROVIDES A NOVEL AVENUE FOR SUCCESSFUL ENRICHMENT OF HIGH-AFFINITY APTAMERS DURING THE CRUCIAL FIRST ROUND OF SELEX.

In SELEX, the potential for inadvertent loss of desired tight-binding aptamers is highest in the first round of selection since there are, at most, only a few (< 10) representations of each sequence in the starting pool. Establishing methods that provide more efficient partitioning, retention and subsequent amplification of strong-binding aptamers in the first round of SELEX are therefore likely to enhance the quality of the selection process.

Currently there are several methods³⁵⁵⁻³⁵⁷ by which panning can be performed, each having specific advantages and disadvantages. Among the most often used are those based on magnetic particles,^{310,311,358,359} which offer a facile and reproducible means of controlling stringency during the selection process. They also allow for simple handling and a modest level of parallelization.¹⁹⁵ To evaluate the impact of pre-blocking on aptamer retention and amplification, an initial round of SELEX on aptamer library 1 (L1) supplemented with either SBA29-L1 or TBA15-L1 was performed, using as the target either streptavidin or α -thrombin attached to super-paramagnetic beads. Parallel selections were performed either in a conventional manner (where the complementary sequences were omitted) (**Figure 2-1**; left panel) or using the proposed method with both complementary sequences (5'-Comp-L1 and 3'-Comp-L1) added to and equilibrated with the supplemented L1 library ($\sim 10^{14}$ members) prior to the selection (**Figure 2-1**; right panel). For both selections, the molar ratio of target to library members was set at 1:100. Real-time amplification results for the detection of SBA29-L1 within the wash and elution pools for the first round of library L1 panning against immobilized streptavidin are presented in **Figure 2-7A**. Relative quantities were calculated using ΔC_q values after correcting for fluorescence drift, where ΔC_q is defined as the difference in

threshold cycle value between the test sample and the negative control sample (where no streptavidin-coated beads were added). The results are expressed as the fold difference relative to the control sample, assuming 100% amplification efficiency. For the conventional screening (L1 aptamer library without addition of complementary sequences), the wash fraction – identical to the binding/wash conditions most often used in SELEX – removes essentially all (97.2 (\pm 6.0)% at 95% confidence) of the SBA29-L1 from the pool of retained library members, consistent with the loss in binding affinity when the flanking regions are left unblocked (**Figure 2-7A**). Consequently, a vanishingly small amount of SBA29-L1 is detected in the final elution fraction (2.8 (\pm 1.2)% at 95% confidence), indicating that this benchmark high-affinity aptamer could be falsely screened out of the binding pool of library members in the initial round of SELEX.

When both 5'-Comp-L1 and 3'-Comp-L1 are added to the L1 aptamer library prior to first-round SELEX-based screening (**Figure 2-1**; right panel) real-time amplification results indicate that little (1.1 (\pm 0.15)% at 95% confidence) of the now properly folded high-affinity SBA29-L1 is removed in the wash fraction of the L1 library (**Figure 2-7A**). Virtually all of the SBA29-L1 binds to the target and is therefore recovered in the elution fraction (98.9 (\pm 11.7)% at 95% confidence), resulting in significant enrichment of SBA29-L1 within the retained and eluted L1 library members. The results therefore support the ITC data that show recovery of aptamer binding when 5'-Comp-L1 and 3'-Comp-L1 are used to eliminate fixed-region interference effects (**Figure 2-5**).

First-round SELEX screening of aptamer library L1 against thrombin-coated magnetic beads yielded similar results, with the corresponding qPCR data sets showing significant enrichment of TBA15-L1 in the bound fraction of the L1 aptamer library when the fixed-region blocking strategy is applied (**Figure 2-7B**).

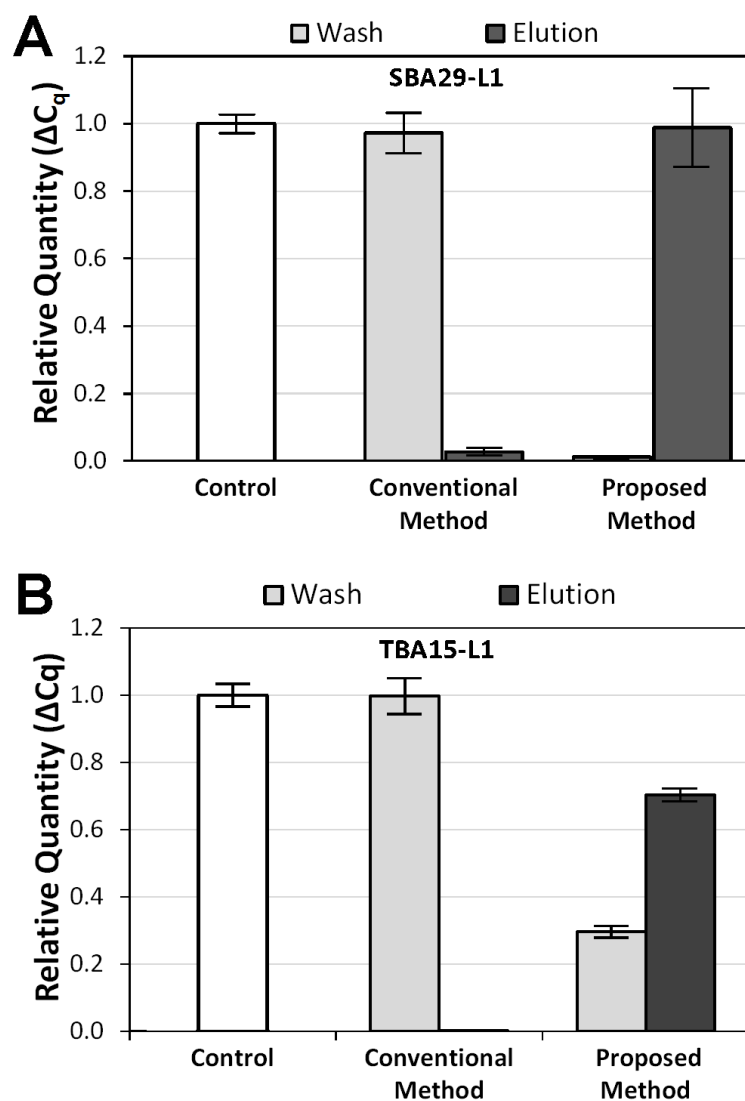


Figure 2-7 Pre-blocking the fixed regions of a library permits successful enrichment of high affinity aptamers during the early rounds of SELEX. (A) Conventional SELEX screening was performed using an aptamer library containing SBA29-L1 to permit detection and tracking of this representative high-affinity aptamer during the first round of SELEX. Magnetic beads coated with the target protein (streptavidin) were equilibrated with the library and then washed with binding buffer. Elutions were carried out in a denaturing buffer at 85°C containing 3.5 M urea. A parallel SELEX screening using the blocking method described here was also performed. Real-time amplification with a TaqMan™ probe generated against the target aptamer was used to characterize aptamer loss and the level of enrichment. Real-time amplification using SYBR green as readout was used to determine the total quantity of library members retained and eluted using each method. The relative quantity of SBA29-L1 in each fraction (wash at 140 mM NaCl and pooled elutions) was determined using the difference in threshold cycle value relative to the control (where no streptavidin was added). (B) Results for corresponding screenings of the L1 aptamer library containing TBA15-L1 against immobilized α -thrombin.

As recently outlined,³⁶⁰ nearly all high-affinity aptamers discovered to date are selective toward a single epitope on the corresponding target, with the most documented exception being the pair of DNA aptamers selective towards the fibrinogen (TBA15) and heparin (TBA29) exosites of human α -thrombin, respectively. This exception provided a particularly useful system to investigate if the proposed protocol generally results in retention and enrichment of tight-binding aptamers irrespective of aptamer sequence or binding exosite. An initial round of SELEX was performed on aptamer library L1 supplemented with the Library-1 forms of the two thrombin aptamers TBA15-L1 and TBA29-L1. Parallel selections were performed (**Figure 2-1**, left and right panels) as previously described. Real-time PCR results for the partitioning of the two thrombin aptamers (TBA15-L1 and TBA29-L1) within the bound and unbound pools are presented in **Figure 2-8A** for conventional SELEX and **Figure 2-8B** for the pre-blocked form of the library.

When conventional SELEX screening was applied (**Figure 2-8A**), 3X washing of the equilibrated beads removes all (99.9 (± 1.6)% at 95% confidence) of TBA15-L1 from the retained pool of library members, a result consistent with the loss in binding affinity when the flanking regions are left unblocked (**Figure 2-2B**). No statistically significant amount of TBA15-L1 was detected in the elution fraction (0.1 (± 0.1)% at 95% confidence), confirming that this benchmark high-affinity aptamer candidate is falsely screened out of the binding pool in the initial round of conventional SELEX. A majority (67.7 (± 10.4)% at 95% confidence) of TBA29-L1 in the starting pool is retained in the first selection round, consistent with the lack of influence of the flanking sequences on the fold and function of this aptamer in its Library-1 form.

As shown in **Figure 2-8B**, addition of 5'-Comp-L1 and 3'-Comp-L1 to the library results in the retention and enrichment of both TBA15-L1 and TBA29-L1 in the first

round of the L1 library selection. Moreover, based on the difference in cycle threshold values from real-time amplification with SYBR green used as a general amplification reporter, pre-blocking of the library also results in the retention and recovery of 3.1 ± 0.8 (p -value < 0.001) times more aptamer sequences than was achieved using the conventional SELEX protocol, a result that suggests that up to two-thirds of potential aptamer sequences embedded within the random core region of the library may be compromised with respect to either fold or function through interference from the flanking regions. It is found that interference effects related to unblocked flanking sequences may therefore severely impact aptamer discovery.

2.3.7 PRE-BLOCKING FIXED REGIONS ACCELERATES THE ENRICHMENT OF HIGH-AFFINITY APTAMERS AS MEASURED BY A SIMPLE NEW QPCR-BASED METHOD FOR MEAN-AFFINITY DETERMINATION

In conventional SELEX, panning is typically terminated if an order-nM K_d is recorded for a pool of library members recovered and amplified after a given cycle. Therefore, the next order of business was to ask if the number of selection cycles required to achieve this metric could be reduced by using the pre-blocking protocol to increase the number and sequence diversity of high-affinity aptamers retained. Three rounds of aptamer selection were performed on Library 2 using thrombin as the target, with the use of Library 2 in this study also serving to confirm that the performance of the protocol is not sensitive to the flanking sequences employed. Here, Library 2 was screened in its basic un-supplemented form to confirm that the new protocol provides rapid enrichment of a target aptamer from a standard SELEX library. In parallel, three selection rounds were also performed in the absence of the blocking agents (i.e. conventional SELEX) as a reference. Retained aptamer fractions were subjected to PCR amplification up to the cycle number after which by-product formation was detected in a pilot PCR run and subsequent gel

electrophoresis. Before proceeding to the next round, the bulk affinity of eluted and amplified material was measured using a new qPCR-based binding assay. That binding assay was initially validated on the Library-1 form of TBA29-L1 by serially diluting and then incubating TBA29-L1 with a constant amount of human α -thrombin immobilized on paramagnetic beads. Following successive wash steps to remove unbound aptamers, bound TBA29-L1 was eluted in 50 mM NaOH at 85°C, neutralized with HCl, and then amplified by qPCR to permit absolute quantification of total bound TBA29-L1 using a standard curve. Bound aptamer fractions (θ) were calculated and plotted against the equilibrium solution concentration (C), the results of which were nonlinearly fitted to the classic 1:1 binding stoichiometry form of the Langmuir equilibrium isotherm to determine the dissociation constant (K_d):

$$\log\left(\frac{\theta}{1-\theta}\right) = \log C - \log K_d \quad (2.1)$$

Due to the low number of human α -thrombin binding sites present in the system, C could be taken as the incubation concentration without error. The isotherm results for this validation assay are presented in **Figure 2-9**, with the regressed binding affinity ($K_d = 5.76 \pm 1.17$ nM; **Figure 2-9A**) matching within experimental error that value measured using ITC (5.49 ± 1.46 nM; **Figure 2-9B**). The advantages of the qPCR-based assay described are that its cost and completion time are at least an order of magnitude less than the SPR or ITC methods more commonly used to determine bulk affinities. It should be noted that while the average K_d for a retained pool determined either by qPCR or SPR/ITC represents a useful metric for monitoring the progress and success of the selection process (which is all that is required during the selection process), it is not a rigorous thermodynamic quantity, since equation 2.1 is not an exact model of the heterogeneous and competitively complex binding phenomena actually occurring.

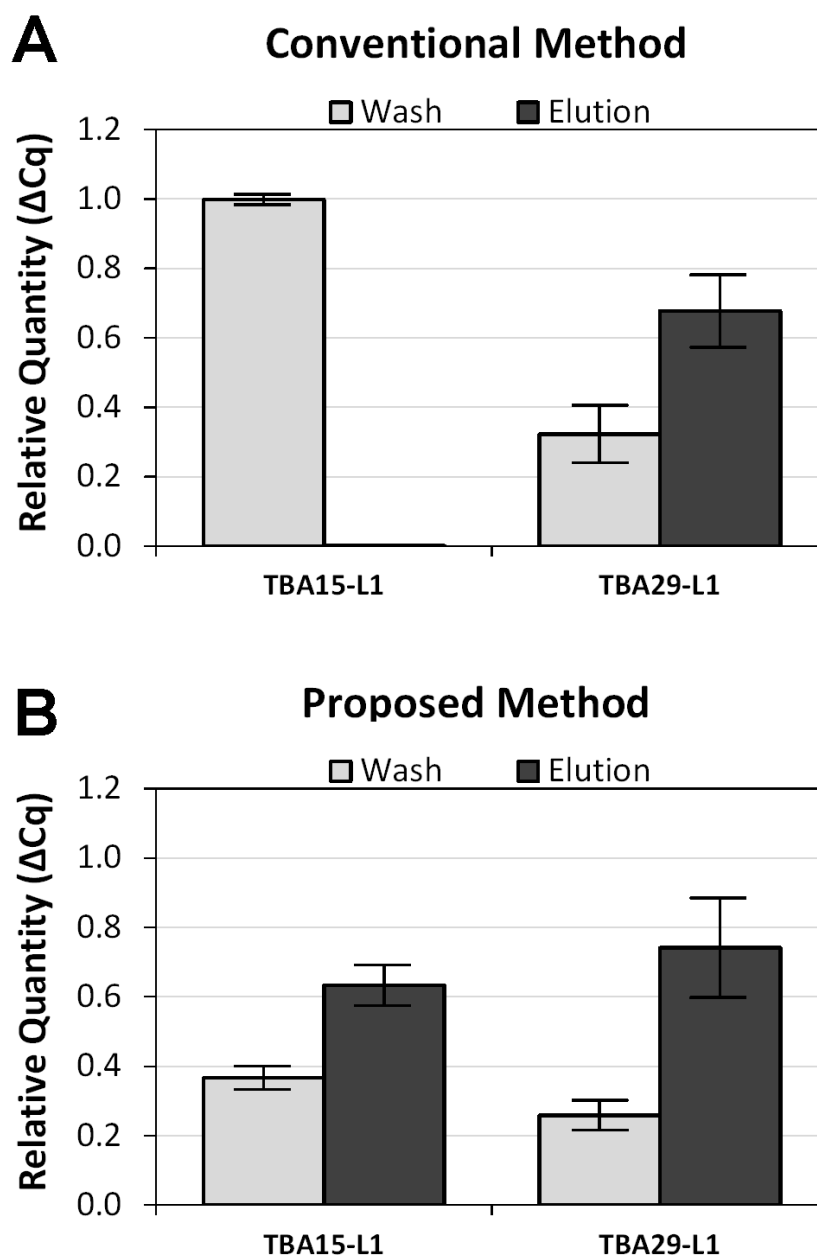


Figure 2-8 Pre-blocking the fixed regions permits successful enrichment of both benchmark thrombin aptamers during the first round of SELEX against immobilized α -thrombin. (A) Partitioning of TBA15-L1 and TBA29-L1 in a conventional SELEX screening of Library 1 against magnetic beads coated with human α -thrombin. (B) Partitioning of TBA15-L1 and TBA29-L1 in a parallel SELEX screening of the same system using the pre-blocking method described. The pre-blocking strategy successfully enriches both thrombin aptamers at the completion of the first selection round.

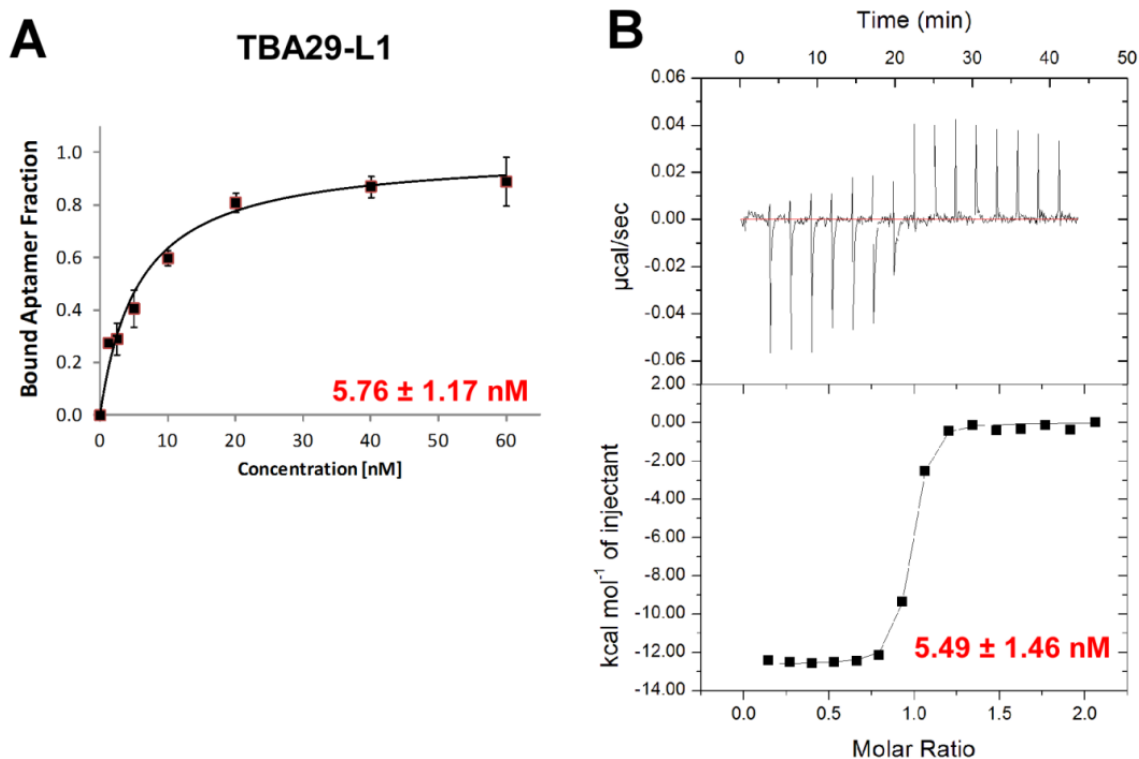


Figure 2-9 Validation of the qPCR-based affinity-binding assay for the SELEX Library-1 version of the 29-mer thrombin benchmark aptamer. (A) Quantified bound fractions θ of TBA29-L1 were amplified by qPCR and plotted against the corresponding incubation concentration C . The equilibrium dissociation constant K_d was then estimated through data regression to the Langmuir isotherm equation. Amplification reactions were conducted in duplicates, in 20 μl volumes, with the average value of C_f used to determine the bound fractions. (B) ITC results for titrating the same aptamer in a solution of thrombin at physiological conditions (top). The resulting fit to a single binding site model (bottom) yields the same binding affinity as measured by the qPCR-based assay.

Using this assay, mean binding affinities of retained Library-2 aptamer pools against thrombin were measured after each round of SELEX conducted either in the absence (conventional) or the presence of fixed-region blocking agents (**Figure 2-10**). For the conventional method, the mean affinity of retained aptamers after the first selection round fell below the detection limit of the assay, indicating relatively modest enrichment of high-affinity binders in the retained pool. A modest enrichment of tight-binding aptamers is consistent with results obtained after two rounds of selection, where binding of the retained aptamer pool could be detected, but not at levels that allowed statistically significant regression of a mean K_d . The third round of selection results in further enrichment of high-affinity members

such that the measured mean affinity for the retained pool is 278.2 ± 80.9 nM (**Figure 2-10A**), indicating that the conventional SELEX method is incrementally progressing toward the isolation of a pool of high-affinity aptamers. This result is consistent with the 8 to 20 rounds of selection that are typically required to identify suitable aptamers using this standard SELEX approach.³⁶¹

When 5'-Comp-L2 and 3'-Comp-L2 are applied to the Library-2 pool before each SELEX round, a significantly greater enrichment of tight-binding aptamers is observed. After the second round of selection, the mean affinity of the retained aptamer pool (344.3 ± 68.2 nM) is comparable to that reached after 3 rounds of the conventional SELEX protocol. Significant further enhancement of the mean binding affinity to 99.6 ± 13.1 nM is then observed after the third round (**Figure 2-10B**).

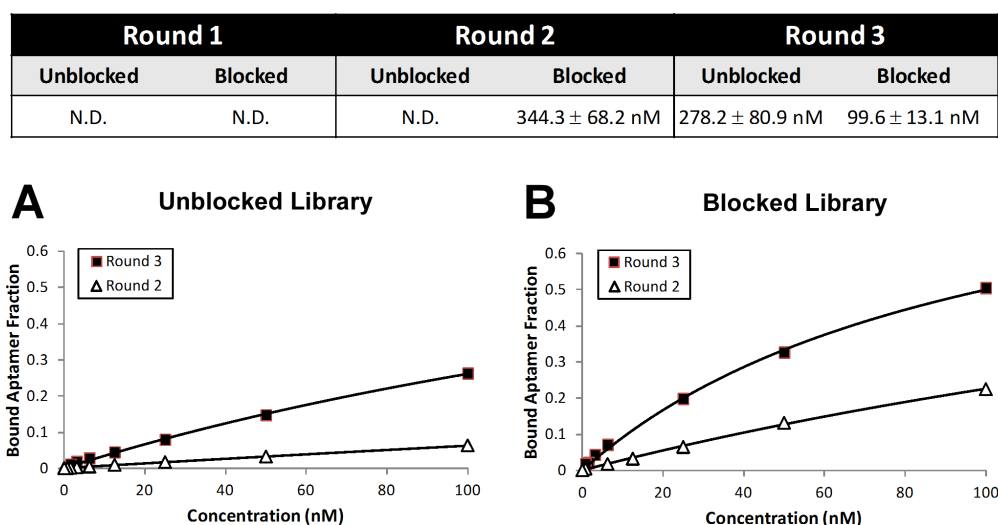


Figure 2-10 Changes in the bulk affinity of the retained aptamer pool in successive rounds of SELEX screenings of Library-2 against thrombin using either the conventional SELEX method or the proposed pre-blocking method. Three rounds of each SELEX method were conducted in parallel and average affinities of retained aptamer pools were measured by qPCR after each round. (A) When the fixed regions of the library are left unblocked, the average affinity of the enriched aptamer pool falls below the assay threshold after the second round (Table; Round 2, Unblocked), and lies in the μM K_d range at the end of the third round (Table; Round 3, Unblocked). (B) Pre-blocking the fixed regions of the library before every selection round results in greater enrichment of high-affinity aptamers.

2.4 CONCLUDING REMARKS

The findings presented here provide an improved understanding of the conditions required for successful enrichment of tight-binding aptamers within a SELEX library. It was shown that the conventional SELEX protocol, and by extension most of the recent improvements to it^{171,286,295,328} do not account for or prevent fixed-region interference effects that can lead to a complete loss of high-affinity aptamers to the wash fraction of the first or subsequent selection rounds. For example, despite the nM affinity of TBA15 to thrombin, the results reported in this chapter show that a standard library version of this high-affinity aptamer (TBA15-L1) is falsely screened out of the binding pool in the early rounds of standard SELEX due to disruption of aptamer fold and a concomitant suppression of binding affinity. Although the severity of these interference effects could be lessened through careful sequence analyses to address self-association within the fixed regions, that strategy will not alleviate losses in aptamer fold and function due to complementarity between fixed and random region sequences.

This inherent limitation to SELEX was addressed through the introduction of a complementary oligonucleotide to each fixed region of the aptamer library. The results obtained collectively show that this concept serves to improve the retention and enrichment of tight-binding aptamers for subsequent rounds of selection by eliminating folding or binding interferences caused by the single-stranded fixed regions of library members. As a result, pools of aptamers retained after successive rounds of selection contain a greater diversity and proportion of high-affinity library members than are observed when the pre-blocking agents are not employed in an otherwise identical selection process. The proposed method may therefore provide a more efficient route to high-affinity aptamer enrichment, particularly when applied to the many variants of the SELEX protocol that do not address fixed-region interference effects fully or in any way.

The method described may further serve to complement currently employed SELEX protocols through its ability to isolate and fully preserve aptamer folds and functions within the random region of the library. Confining candidate sequences to that region of a library should ease the difficult downstream analyses involved in deciphering the minimal binding sequence of newly discovered aptamers. Indeed, challenges in maintaining binding affinity of newly discovered aptamers after truncating the fixed regions are well documented, with complete loss in binding affinity having been reported for a number of aptamers selected against various proteins,³⁶² cells^{346,363} and small molecules³⁶⁴ alike. A particularly salient example is provided by Cho et al., who reported that three of the four most highly represented sequences in a final retained aptamer pool exhibited high affinities when analyzed as full-length library sequences, while much weaker affinities were measured when their corresponding core-region sequences were analyzed.¹⁷¹ This is important because the elegant high-throughput Agilent™ arrays they pioneered and used to analyze the binding properties of selected library members were applicable to the 40 nt core-region sequence but not to the full 80 nt sequence of each retained library member due to limitations in the length of DNA that can be reliably prepared by available surface-initiated synthesis methods.

Along with the strengths and unique attributes noted above, the method has one obvious limitation compared to many of the SELEX-type methods currently employed. Namely, it precludes all aptamers in a library that form their structures from sequences spanning across the core and flanking regions. Though the contribution of such aptamers to the total pool of aptamers within a library is thought to be small, it is not negligible, and some of the high-affinity aptamers discovered to date adopt such structures. In addition, the blocking strategy utilized here can create sites for those proteins known to bind duplex DNA. Thus the method is not likely to be suitable for library screening of those protein families (e.g. transcription factors, nucleases, histones, etc.). The proposed method is therefore viewed as being complementary to other effective SELEX methods by

offering a unique approach to aptamer selection. Towards this last point, a key virtue of the proposed method lies in its ability to be easily incorporated into many of the most widely used SELEX protocols, including those operating on patterned libraries containing universal nucleotides in the random region.³⁶⁵ Little to no changes to the selection conditions or the library design are required and the approach may therefore offer a certain level of standardization to a SELEX-type process. Moreover, although the results provided here were reported for DNA-based libraries, the technique should be applicable to RNA-based libraries. Based on these findings, it can be argued that complementing current SELEX-type protocols to include a selection path utilizing blocking oligonucleotides that minimize flanking-region mediated interference effects can improve aptamer discovery efforts by isolating consensus sequences of aptamers to the random region of the library, thereby preventing the complete and undesirable loss of these potential tight-binding library members.

Chapter 3

DEVELOPMENT OF A HIGH-FIDELITY THERAPEUTIC APTAMER DISCOVERY PLATFORM

“Divide each of the difficulties under examination into as many parts as possible, and as might be necessary for its adequate solution”

— René Descartes (1637)³⁶⁶

3.1 PLATFORM OVERVIEW

This chapter reports the development of Hi-Fi SELEX, a high-fidelity aptamer discovery platform (**Figure 3-1**) that integrates the novel fixed-region blocking elements reported in **Chapter 2** into a new selection process to improve the functional diversity of the starting library. As levels of non-specifically retained members are known to dictate the level of enrichment of useful aptamers achieved in a given round of SELEX,³⁶⁷ Hi-Fi SELEX presents the target on a photo-coupled polyglycol layer, and the library in conditioned equilibration and wash solvents. Together they greatly inhibit non-specific adsorption. At a theoretically optimal aptamer-to-target ratio of 100:1 to 1000:1,^{199,200} high stringency segregation and significant enrichment of specific high-affinity members is achieved in each selection round. The sequence diversity is thereby reduced 10^5 to 10^6 orders of

magnitude through the first selection round, resulting in a round-one partition efficiency (PE) of 8.0×10^5 and retention of 10^8 to 10^9 unique library sequences offering a mean equilibrium dissociation constant $K_d < 100$ nM. This PE exceeds typical values (10 to 100) reported when traditional selection methods (e.g. nitrocellulose filtration, magnetic beads) are employed.^{368,369} and is comparable to per-round PE s reported for modified SELEX methods that rely on more complex fabricated materials (e.g., microfluidics; M-SELEX)²⁰³ or instruments (e.g. capillary electrophoresis; CE-SELEX)^{304,370} that often are not available in standard molecular biology laboratories.

Hi-Fi SELEX then uses digital PCR (dPCR) to achieve ultra-high-fidelity amplification of a selected pool of library members in a manner that ensures each amplicon exists as a fully complementary duplex. This outcome is shown to not be achieved in a conventional bulk PCR of retained library members, which can result in incomplete conversion of dsDNA amplicons back into the desired ssDNA library form using λ -exonuclease. Average template numbers and reaction conditions per droplet are identified so as to minimize formation of unwanted amplification by-products during dPCR that might bias the relative abundances of retained library members, while at the same time permitting large amounts of the desired 80-mer aptamer product to be generated. Tailoring and integration of dPCR into the Hi-Fi SELEX workflow thereby ensures enrichment of high-affinity members in a form and in quantities suitable both for the next round of selection and, as will be shown, for the rapid and reliable determination of the mean K_d of the retained pool using a simple, cost-effective qPCR-based binding-isotherm assay.

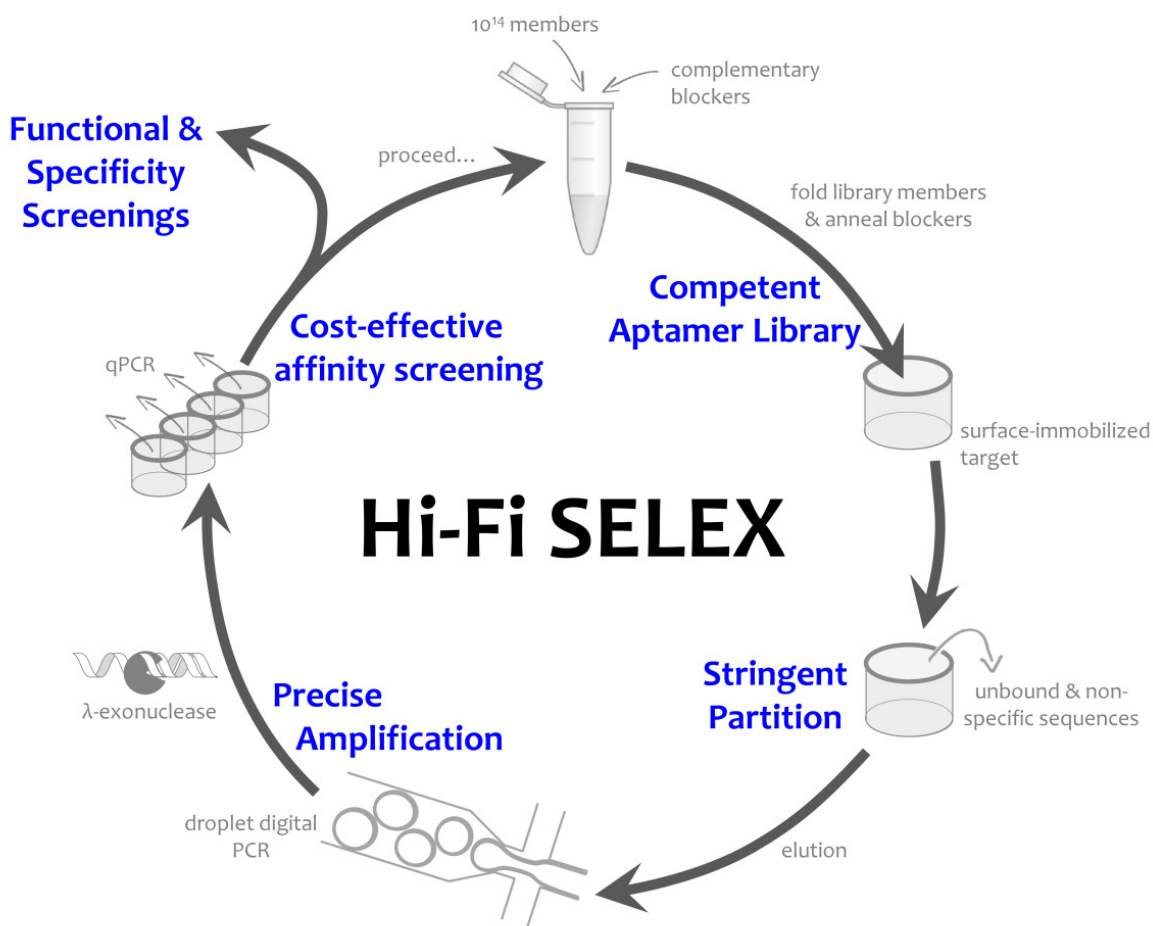


Figure 3-1 General workflow schema for the Hi-Fi SELEX platform. Potential interference effects due to the fixed regions common to all library members are first blocked using complementary sequences, leading to a “competent” starting library that contains a larger percentage of functionally active aptamer sequences. Targets immobilized on the surface of a microtitre-plate well coated with an adsorption-passivating polyglycol brush and surfactant are used to select library members at a theoretically preferred 100 to 1000:1 aptamer:target ratio with minimal non-specific aptamer retention. Retained members are recovered and amplified by dPCR using a protocol that eliminates formation of amplification by-products to preserve the relative abundances of retained library members while improving end-point yields and concentrations. The dPCR method also ensures that all amplicons are present in their fully complementary duplexed form, permitting stoichiometric conversion of amplified material into ssDNA using lambda exonuclease. The binding affinity of the enriched and dPCR-concentrated ssDNA pool is measured at every round of selection using a cost-effective label-free method based on qPCR. This process is then repeated by adding equimolar amounts of complementary oligonucleotides to form an enriched competent library until no appreciable increase in binding affinity can be detected. The final enriched pool is screened for functional members as well as for specificity before being sequenced, creating an integrated bottom-up approach to therapeutic aptamer discovery.

The capacity of Hi-Fi SELEX to improve DNA aptamer selection is first demonstrated using a benchmark target, human α -thrombin. The platform is then applied to three therapeutic targets (human Factor IXa, Factor X, and complement Factor D), in each case resulting in enrichment of a pool of aptamers offering an order-nM mean K_d within three selection rounds. The direct integration of biological function and specificity screens into the Hi-Fi SELEX workflow to identify structurally-related aptamers against Factor D that inhibit alternative pathway complement activation is demonstrated. This family of ssDNA aptamers against Factor D may therefore serve as useful lead compounds for development of therapeutics to treat human diseases in which germ-line or somatic mutations hyper-activate the alternative pathway and thereby stimulate tissue inflammation and organ damage. Renal diseases such as atypical hemolytic-uremic syndrome (aHUS), diseases linked to polymorphisms in complement inhibitors or activating proteins (e.g. age-related macular degeneration), and a variety of major diseases (e.g. rheumatoid arthritis, asthma, lupus nephritis) in which the alternative pathway is known to have a pathophysiologic association may therefore benefit from development of therapeutic aptamers against Factor D.³⁷¹⁻³⁷⁴

3.2 EXPERIMENTAL METHODS

3.2.1 MATERIALS

Human complement factor D was purchased from Complement Technology Inc. (Tyler, TX). Human α -thrombin, human factor IXa and Human factor X were all purchased from Haematologic Technologies (Essex Junction, VT). Nunc Amino Immobilizer plates (Lock Well C8) were purchased from Thermo Fisher (Edmonton, AB). 1-ethyl-3-(3-dimethylaminopropyl) carbodiimide hydrochloride (EDC), N-hydroxysuccinimide (NHS), Ficoll (400 kg mol⁻¹), Poly (vinyl alcohol) (PVA; MW =

9,000 – 10,000) and ethanolamine were obtained from Sigma-Aldrich (Oakville, ON).

3.2.2 LIBRARY DESIGN AND SYNTHESIS

Each member of the ssDNA SELEX library was comprised of an internal variable (random) region 40 nucleotides (N_{40}) in length, flanked by a common 20-mer 5' sequence and by a 20-mer universal 3' primer binding sequence. The 80-mer library was combinatorially synthesized by mixing the DNA nucleotides A:C:G:T at a molar ratio of 3:3:2:2.4 to achieve equal probability incorporation of each nucleotide in the core region.³⁴³ The 20-mer flanking sequences and associated primers (**Table 3-1**) are ones commonly employed in conventional SELEX,^{347,375,376} and were utilized here due to their suitability for SYBR green qPCR amplification.³⁴⁷ For this work, both flanking sequences had their reverse complement synthesized, with the complement to the 5' and 3' flanking sequences denoted in **Table 3-1** as 5'-Comp and 3'-Comp, respectively. The 3'-Comp sequence was 5'-phosphorylated and also used as the reverse primer (REV) for PCR amplification. All oligonucleotides were synthesized and HPLC purified by Integrated DNA Technologies, Inc. (IDT; Coralville, IA) and reconstituted in 1X Aptamer Folding (AF) buffer (20 mM Tris-HCl pH 7.4, 140 mM NaCl, 5 mM KCl, 1 mM MgCl₂, 1 mM CaCl₂).

3.2.3 PREPARATION OF TARGET-IMMOBILIZED MAGNETIC BEADS

A 10 μ l aliquot ($\sim 10^8$) of MyOne carboxylic acid beads was washed 3X in MES buffer (25 mM 2-(N-morpholino)-ethane sulfonic acid, pH 6.0), activated with EDC/NHS for 30 min at room temperature, and further washed 3X in MES buffer before being incubated with 50 μ g human α -thrombin for 2 hrs under gentle agitation (500 rpm). Average protein loadings were ca. 10^7 molecules per bead

using this protocol. After incubation, the beads were washed 3X in 2 M NaCl Tris-buffer (20 mM Tris-HCl pH 7.4, 2 M NaCl, 5 mM KCl, 1 mM MgCl₂, 1 mM CaCl₂) and remaining functional groups then blocked in 1X AF Buffer supplemented with 0.005% Tween-20 for 1 hr. Following a final 3X wash with 1X AF buffer containing 0.005 % Tween-20, the thrombin-modified beads were stored at 10 mg ml⁻¹ and 4°C until further use. The same procedure was used for immobilizing human factor IXa, factor X or factor D and passivating sites. Immobilization methods and surface densities of target protein corresponded to those commonly reported in recent literature using magnetic beads for aptamer selections.^{203,377,378}

Table 3-1 ssDNA SELEX library, primers and blocker sequences used in this study

Name	Sequence (5' – 3')	Comments
Library	TCGCACATTCCGCTTCTACC– N ₄₀ – CGTAAGTCCGTGTGTGCGAA	N ₄₀ = random nucleotide region of library
FOR	TCGCACATTCCGCTTCTACC	5' amplification primer
REV or 3'-Comp	p-TTCGCACACACGGACTTACG	3' phosphorylated amplification primer / complementary blocker
5'-Comp	GGTAGAAGCGGAATGTGCGA	5' complementary blocker

3.2.4 SURFACE PASSIVATION OF AND TARGET-IMMOBILIZATION ON NUNC WELLS

Each protein target was immobilized within wells of Nunc Amino Immobilizer C8 strips (**Figure 3-2**) by incubating overnight at 4°C in 100 µl of 100 mM sodium phosphate (pH 7.5). For human α -thrombin, a series of immobilizations was conducted using protein concentrations in solution ranging from 5 to 180 nM, with

an equilibration concentration of 80 nM proving most effective. Following target immobilization, wells were washed 3X with 300 μ l of 1X AF buffer. During this wash sequence, the amines (Tris (hydroxyl-methyl-aminomethane)) present in AF buffer neutralize unreacted electrophiles displayed on the end-grafted polyglycol surface. The wells were then filled once more with 300 μ l of 1X AF buffer and left to incubate at room temperature for 1 hr under gentle agitation (500 rpm in a Thermomixer fitted with a plate adapter; Eppendorf, Mississauga, ON) to complete this neutralization reaction. The AF buffer used in both the wash and incubation steps was supplemented with 0.005 % Tween-20, which served to further passivate the surface against non-specific adsorption. The incubation buffer was aspirated at the end of the neutralization/passivation process and a final wash sequence was performed (3X 300 μ l 1X AF buffer + 0.005 % Tween-20) before sealing the wells with optical film and storing them at 4°C until further use. Other passivation agents (1% Ficoll (w/v), and 1% Ficoll + 1% PVA (w/v)) were also tested using the same protocol. Proteins immobilized by this procedure included human α -thrombin, and factors IXa, X and D.

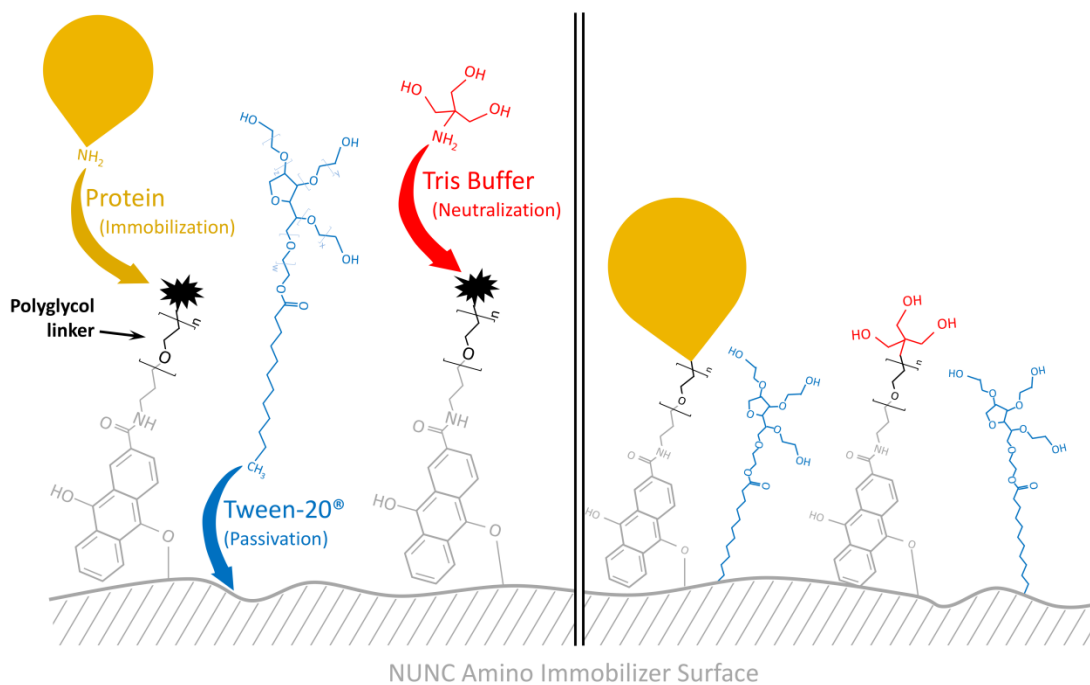


Figure 3-2 General schema for electrophile-mediated immobilization of proteins onto the reactive Nunc well surface, followed by excess reactive group neutralization and surface passivation as described in the text. (Not drawn to scale)

3.2.5 ELONA-TYPE ASSAY FOR DETECTING APTAMER BINDING TO HUMAN α -THROMBIN

Human α -thrombin was immobilized in Nunc wells according to the aforementioned procedure, with the exception of the blocking reagents. In these cases, Nunc wells were incubated with either 300 μ l 1X AF buffer supplemented with 0.005 % Tween-20, 1% Ficoll solution, 1% Ficoll and PVA solution, or 1 M ethanolamine pH 8.0. All blocking incubations were performed for 1 hr with gentle agitation (500 rpm). A final wash sequence was performed before storing the wells at 4°C until further use.

Duplicate electrophile-neutralized and surface-passivated wells (see above) displaying immobilized α -thrombin were prepared along with duplicate wells generated according to the same procedure but not displaying protein. Aliquots

(500 nM) of a biotinylated version of the 29-mer anti-thrombin aptamer (biotin TEG-CAG TCC GTG GTA GGG CAG GTT GGG GTG ACT T) were diluted in 1X AF buffer, heated to 95°C and slowly cooled down to 25°C at a rate of 0.5°C min⁻¹ in a Mastercycler ep thermocycler (Eppendorf, Mississauga, ON, Canada) to ensure proper folding. Folded aptamers were incubated in each well for 2 hrs at 25°C under agitation (500 rpm). All wells were washed 3X following the incubation with 300 µl 1X AF buffer, and further incubated with 10 nM avidin-HRP (Life Technologies, Burlington, ON) for 1 hr. Wells were washed again 3X in 300 µl 1X AF buffer before the addition of 100 µl 3,3',5,5'-tetramethylbenzidine (TMB; Sigma-Aldrich, Oakville, ON). The reaction was allowed to proceed for 10 to 15 min in each well, and then quenched by adding 100 µl 1 M HCl. The concentration of the surface-bound complex was then quantified by measuring absorbance at 450 nm using a plate reader (Tecan Infinite 200 Pro, San Jose, CA). The same procedure was employed for ELONA-type assays performed on magnetic beads blocked using the same conditions: 1X AF buffer supplemented with 0.005 % Tween-20.

3.2.6 HUMAN α -THROMBIN ENZYMATIC ACTIVITY ASSAY

Nunc wells were functionalized with human α -thrombin and then surface neutralized and passivated as described above. A 10 µM solution of Boc-L-FPR-ANSN fluorogenic substrate (SN-20; Hematologic Technologies) was prepared in 1X AF buffer. One hundred microliters of this substrate solution was added to each well and mixed. Fluorescence intensity was then measured (370 nm excitation, 450 nm emission) at regular intervals in a plate reader (Tecan Infinite 200 Pro) incubated at 37°C. Negative control reactions were also measured by adding the substrate to neutralized and passivated wells containing no immobilized α -thrombin.

3.2.7 HIGH-FIDELITY SELEX: LIBRARY SCREENING

One nanomole ($\sim 10^{14}$ sequences) of aptamer library was mixed with equimolar amounts of 5'-Comp and 3'-Comp in 100 μl of 1X AF buffer supplemented with 0.005 % Tween-20 and heated to 95°C for 5 min before being slowly cooled down to 25°C at a rate of 0.5°C min^{-1} in a MasterCycler ep thermocycler (Eppendorf; Mississauga, ON). This step ensures that each library member anneals both complement sequences, and that the variable region of each library member properly folds into its specific structure. The folded library was then added to a functionalized, neutralized and passivated well and incubated for 1 hr at 25°C under gentle agitation (500 rpm) in a Thermomixer equipped with a plate adapter. Unbound and weakly bound members were removed by first washing 3X with 300 μl of 1X AF buffer supplemented with 0.005 % Tween 20. A second more stringent set of 3X washes with 300 μl 1X Stringent Wash (SW) buffer (20 mM Tris-HCl pH 7.4, 4 M NaCl, 5 mM KCl, 1 mM MgCl_2 , 1 mM CaCl_2 , 0.005 % Tween-20) were then applied to remove non-specifically bound members as well as aptamers whose binding is dominated by coulombic interactions. All remaining library members (the retained pool) were eluted by 3X incubation with 1X denaturing buffer (40 mM Tris-HCl pH 8.0, 3.5 M urea, 10 mM EDTA, 0.005 % Tween-20) at 70°C for 10 min, then desalted using a centrifugal filter unit (NanoSep® Omega 10K MWCO; Pall, Ville St. Laurent, QC). Parallel screenings were also performed exactly as described above, but without adding complementary blocking sequences to the library prior to folding.

3.2.8 HIGH-FIDELITY SELEX: DROPLET-DIGITAL PCR AMPLIFICATION

Desalted aptamer pools were quantified by qPCR using iQ SYBR green Supermix (CFX96, Bio-Rad; Mississauga, ON) in order to determine the amount of material that was eluted from each well. The eluted pool was then subjected to

droplet digital PCR amplification (ddPCR) (QX-100, Bio-Rad) where the number of wells required was determined by the quantity of library members eluted. Each ddPCR reaction was carried out in a 20 μ l volume by partitioning the reaction mix (ddPCR Supermix for probes without dUTP) containing the entire eluted pool mixed with 900 nM of each amplification primers (FOR and phosphorylated REV). That mixture was loaded into a well of a DG8 cartridge before addition of fluorinated oil to the corresponding oil wells of the cartridge. Droplets were formed by inserting the cartridge into the droplet generator instrument (cat no: 186-3002; Bio-Rad). The resulting emulsion containing ca. 20,000 droplets per well was transferred into a 96-well PCR plate and subjected to thermocycling in a CFX96 thermocycler (Bio-Rad, Mississauga, ON). Cycles consisted of an initial activation step at 95°C for 5 min, followed by 35 cycles of amplification each comprised of denaturation at 95°C for 30 s and annealing/extension at 64°C for 30 s. The heating and cooling rates were set at 2.5°C s⁻¹ to ensure even heat distribution to all droplets in a single well. Immediately after amplification, all wells were pooled together and spun at 5000g to separate the reaction droplets from the continuous oil phase, which was removed and discarded. Double-stranded DNA amplicons were recovered by subjecting the recovered droplet concentrate to freeze/thaw cycles of 15 min at -80°C, and immediate spinning of frozen droplets at 14,000g for 5 min. The process was repeated three times, and the clear aqueous phase containing the amplified material was recovered.

3.2.9 SINGLE-STRAND SELEX LIBRARY REGENERATION

The recovered amplified material was loaded and run on a 2% agarose gel, then purified using the QIAEXII gel extraction kit according to the manufacturer's instructions (Qiagen, Valencia, CA). Single-stranded products were regenerated from the purified amplicons by reacting with 5 U of λ -exonuclease (New England Biolabs, Whitby, ON) at 37°C for an optimized period (**Figure 3-14**) of 1 hr, followed by heat inactivation at 75°C for 10 min. The digested product was then

purified by phenol chloroform extraction/ethanol precipitation in the standard manner.

3.2.10 APTAMER SELECTION BY CONVENTIONAL SELEX

A 2 μl portion of functionalized MyOne Dynabeads ($\sim 10^6$ beads) was incubated with 1 nmole ($\sim 10^{14}$ sequences) of folded aptamer library supplemented with equimolar amounts of the complementary oligonucleotides 5'- and 3'-Comp. The incubation was performed in a 500 μl volume containing 1X AF buffer supplemented with 0.005 % Tween-20 for 1 hr at room temperature under gentle agitation (500 rpm). Unbound and weakly bound aptamers were removed in a 3X series of 500 μl washes containing 1X AF buffer supplemented with 0.005 % Tween-20. The remaining pool of retained aptamers was then eluted from the beads in 1X denaturing buffer at 70°C as described above. Parallel screenings were also performed without addition of the complementary blocking sequences prior to folding.

Recovered members were amplified by conventional PCR using Platinum Taq DNA polymerase (Life Technologies; Burlington, ON) and 250 nM of each amplification primers (FOR and REV). Thermocycling conditions were as follows: initial activation at 95°C for 5 min followed by 10 to 15 cycles of amplification, each comprised of denaturation at 95°C for 30 s, annealing at 64°C for 30 s, and extension at 72°C for 30 s. A final extension at 72°C for 2 min was performed to repair any damaged amplification products. The amplification was terminated at the cycle number where accumulation of by-products (i.e. higher molecular weight amplification products) could first be observed on a one-dimensional agarose gel as determined by small-scale pilot-PCR runs. Double-stranded DNA amplicons were then purified and digested as previously described.

3.2.11 AFFINITY AND SPECIFICITY CHARACTERIZATION OF ELUTED POOLS

Mean equilibrium dissociation binding constants (K_d) of retained aptamer pools were determined by a qPCR-based method, previously shown to yield identical results to Isothermal Titration Calorimetry (ITC)-based measurements.³⁷⁶ As described above, the protein target was immobilized in 16 wells of a NUNC Amino Immobilizer plate. The regenerated and purified ssDNA SELEX library was then serially diluted to create 8 different concentrations. In duplicate, each concentration was added to a target-displaying well and the mixture equilibrated for 1 hr. Unbound and weakly bound members were removed by washing as described. The retained aptamer fractions were eluted and quantified by qPCR using 2X iQ SYBR Green Supermix (Bio-Rad). By applying a total mass balance, the binding isotherm could thereby be constructed and was fitted to the Hill equation to determine the mean K_d of each retained pool before proceeding to the next round of selection. Specificities of individual aptamers were also determined using this procedure with immobilized human serum albumin serving as a metric for non-specific binding.

3.2.12 ESTIMATING THE SEQUENCE DIVERSITY OF RETAINED POOLS

The sequence diversity of a retained pool of library members was estimated in two different ways. In the first, a small aliquot of a retained pool was amplified by qPCR using iQ SYBR green supermix and thermocycling conditions as previously described (initial activation at 95°C for 5 min followed by an optimal number of amplification cycles, each comprised of denaturation at 95°C for 30 s, annealing at 64°C for 30 s, and extension at 72°C for 30 s with a heating and cooling ramp rate of 3°C s⁻¹). The dye-bearing amplicons were then melted by heating from 55°C to 95°C in 0.5°C increments in a CFX96 Real-Time PCR Thermocycler (Bio-Rad,

Mississauga, ON). The resulting melt curves were analysed by computing the areas beneath the two normalized transition peaks centered at ~ 67°C and 81°C, which represent melting of hetero-duplexed and homo-duplexed amplicons, respectively. The two peak areas were used to compute the fraction f_{hetDNA} of amplicons in the hetero-duplexed state:

$$f_{hetDNA} = \frac{A_{67^{\circ}\text{C}}}{(A_{67^{\circ}\text{C}} + A_{81^{\circ}\text{C}})} \quad (3.1)$$

Melt analyses of serial reductions in the sequence diversity of the starting library were used to create a standard curve relating f_{hetDNA} to sequence diversity. The value of f_{hetDNA} for the retained pool thereby permitted estimation of sequence diversity.

The second method for characterizing pool diversities relies on fluorometric quantitation of dsDNA after amplification. A standard curve of sequence diversities was created by first preparing serial reductions in initial library sequence diversity (ranging from 10^8 to 10^2 unique sequences) and amplifying each to its optimal cycle number (as determined by smaller-scale pilot PCR reactions). A control library having a sequence diversity of 1 was also amplified. Two-fold dilutions of each amplified diversity standard were prepared, then mixed with Quant-IT PicoGreen™ dsDNA reagent (Life Technologies) in 200 μl volumes and fluorescence intensities quantified in a plate reader (Tecan Infinite 200 Pro) using optical black plates. The measured fluorescence for each library standard was plotted and fitted to a straight line, intersecting the origin after background fluorescence subtraction. The resulting slope of each diversity standard was thereby determined and plotted against the starting library diversity, generating a standard curve with statistical significance over 6 orders of magnitude. For the assay, serial dilutions of an amplified pool of retained aptamers were prepared,

mixed with the Quant-IT PicoGreen working reagent, and the fluorescence intensity versus amplicon concentration determined. The sequence diversity of the retained pool was then quantified by determining the slope and applying the standard curve.

3.2.13 INDIVIDUAL APTAMER CLONING, PRODUCTION, AND BINDING CHARACTERIZATION

Amplicons of retained library members were purified as previously described, introduced into the pJET1.2 vector using the CloneJet kit (Thermo Fisher), and the recombinant product used to transform OneShot® chemically competent *E. coli* (Life Technologies, Burlington, ON). Transformed colonies were grown, plated and individually picked. Plasmid DNA containing the aptamer insert was purified using a Miniprep Kit (Qiagen). Colony PCR was performed on each colony prior to isolating the plasmid DNA to determine if inserts were present. Inserts were then amplified with Platinum Taq DNA polymerase and the amplification products purified and digested, as previously described. Dissociation binding constants for individual aptamers, as well as for pools of cloned aptamers, were measured on a Biacore 3000 instrument using a CM-dextran chip modified with streptavidin (Sensor Chip SA) with inserts amplified as described above but using a biotinylated REV primer (biotin TEG–TTC GCA CAC ACG GAC TTA CG).

3.2.14 INHIBITION OF ACTIVATION OF THE ALTERNATIVE COMPLEMENT PATHWAY (FUNCTIONAL) ASSAY

Both individual aptamers and small aliquots comprised of 40-60 members of a retained aptamer pool were assayed for their ability to inhibit activation of the alternative complement pathway as a result of binding human complement factor D. In a 96-well plate, 15 μ L of 3 nM factor D was incubated with 15 μ L of 80 nM aptamer aliquots for 10 min at 37°C. Controls included wells without aptamer.

Gelatin veronal buffer (GVB, pH 7.4, 30 μ L) containing 50 nM C3b (Cobra), 100 nM factor B, 30 nM C5, 50 nM C6 and 7 mM MgCl₂ was added, and the reaction was allowed to proceed for 10 min, generating newly formed C5b,6 in a factor D-dependent manner, i.e., via the alternative pathway. The amount of C5b,6 was then quantified using the “terminal pathway assay”, accomplished by immediately mixing 50 μ L of the preceding reactant with 250 μ L of GVB containing 10 mM EDTA, chicken erythrocytes (cRBC) (3.3×10^8 cells mL⁻¹) and 2% normal human serum (as the source of C7, C8, and C9). This allowed progressive assembly of the lytic C5b-9 membrane attack complex. After 30 min, the unlysed cell pellet was removed by centrifugation. Erythrocyte lysis, reflected by the released hemoglobin in the supernatant, was quantified by measuring the absorbance at 405 nm using the Mithras LB 940 microplate reader from Berthold Technologies (Bad Wildbad, Germany). Percent lysis was relative to the control of 100% lysis with H₂O. A standard curve using known quantities of C5b,6 to initiate the terminal pathway, was established. Percent inhibition of factor D function by aptamers was thereby calculated, based on the C5b,6 levels in the absence of aptamers.

Mixed-aptamer aliquots and individual aptamers exhibiting inhibition activity were thereby identified. Inserts containing candidate aptamers were sequenced on an Applied Biosystems 3730S 48-capillary DNA Analyzer using BigDye Terminator 3.1 chemistry. The sequences were analysed using the UGENE bioinformatics platform (Unipro; Novosibirsk, Russia) and secondary structure predictions were obtained using M-fold.³⁵²

3.2.15 ISOTHERMAL TITRATION CALORIMETRY

Truncated (random-region sequence only) and full-length library versions of identified aptamers were synthesized and HPLC purified by Integrated DNA Technologies, Inc. (IDT; Coralville, IA), and reconstituted in 1X AF buffer. Each aptamer or library member was diluted to a final concentration of 10 μ M. Prior to

ITC measurements, the diluted sequence was heated to 95°C then slowly cooled to 25°C at 0.5°C min⁻¹ in a Mastercycler ep thermocycler (Eppendorf) to ensure proper folding. In cases where the full-length library member was used, complementary oligonucleotides were annealed at equimolar concentrations prior to folding. Human complement factor D was diluted to a final concentration of 1 μM in 1X AF buffer. Isothermal titration calorimetry (ITC) measurements were performed at 25°C in a MicroCal iTC200 (GE Healthcare, Piscataway, NJ). The injection syringe contained 40 μL of the diluted sequence, and the 300 μL sample cell contained factor D. A first injection of 0.4 μL preceded the remaining injections of 3.25 μL. Run parameters were set for an injection rate of 0.5 μL s⁻¹ with a 180 s time interval between injections. The syringe rotation speed was set at 750 rpm, according to the manufacturer's recommendation. Results were analyzed using Origin 7.0 software (OriginLab Corp., Northampton, MA) by fitting to a single-site binding model.

3.3 RESULTS AND DISCUSSION

3.3.1 HI-FI SELEX LIBRARY AND TARGET PRESENTATION METHODS IMPROVE ENRICHMENT OF HIGH-AFFINITY MEMBERS.

Human α -thrombin and two aptamers against it have long served as useful benchmarks for aptamer research and selection-technology development. The first, a 15-mer ssDNA aptamer (anti-Thr-15) isolated in 5 rounds of SELEX,¹⁷² binds the fibrinogen binding epitope of α -thrombin with a K_d of 25 nM. The second, a 29-mer ssDNA aptamer (anti-Thr-29) isolated in 11 rounds,²⁸⁸ binds α -thrombin's heparin binding epitope with higher affinity ($K_d = 1$ nM). The development and initial validation of the Hi-Fi SELEX platform was therefore based on this well-studied target, and the number of rounds of selection needed to isolate an enriched pool of library members having a sub 50-nM mean K_d was applied as a metric of platform performance.

Hi-Fi SELEX works to improve round-by-round *PE* values (where *PE* equals the ratio of aptamers removed in the wash fractions to those collected in the elution fractions) and overall selection efficiencies, in part through careful control of the manner by which the library and the target are presented, equilibrated and washed. To begin, a “competent” SELEX library is prepared using a novel method recently reported that anneals a complementary oligonucleotide to each fixed region to eliminate the various ways in which those common sequences can interfere with the fold or function of aptamers localized within the random region of the library.³⁷⁹ In that work, it was shown that the method is applicable to common SELEX library formats comprised of different flanking region sequences, and results in recovery of function and enrichment of tight-binding library-formatted aptamers otherwise lost due to fold disruption, steric hindrance, or other fixed-region mediated interference mechanisms. However, as the method isolates aptamer fold and function within the random region of the library, it screens out any aptamers comprised of both random and fixed region elements. The net change in the total number of functional aptamers within the initial library is therefore determined by a trade-off between the gain in functional aptamers presented within the random region of the library and the loss of aptamers of hybrid random+fixed region construction. In this work, it will be shown that the net change is quite favourable, serving to increase the total abundance of functionally active aptamer sequences in the initial library and the overall selection efficiency.

Hi-Fi SELEX further improves *PE*s by leveraging chemistry known to passivate surfaces against non-specific adsorption of biologics through a novel preparation process that renders that chemistry equally effective in mitigating retention of undesirable library members during selection rounds. Many groups,^{380,381} including our own,^{382,383} have shown that dendritic or end-grafted layers of polyglycol chains, most notably polyethylene glycol chains 1 kDa or higher, presented at densities near or above those needed for soft brush formation³⁸³ can

effectively passivate a surface against non-specific adsorption of proteins³⁸⁴ or oligonucleotides,^{385,386} even in cases where the zeta potentials of the underlying base surface and sorbate are opposite in sign.^{384,387} Nunc Immobilizer™ plates (Thermo Scientific) employ this type of surface-passivation chemistry,^{388,389} and significant advantages for aptamer selection can be offered when specific target-immobilization and additional surface-modification reactions are employed. The need to further modify the target-presentation surface, as well as the selection conditions required to minimize non-specific retention, were identified using a biotinylated version of the 80-mer aptamer library applied in an enzyme-linked oligonucleotide assay (ELONA) that quantifies non-specifically retained amounts of aptamer using an avidin-HRP (horse radish peroxidase) chimera to detect chromophoric-substrate cleavage. **Figure 3-3A** shows that moderate levels of non-specific library retention are observed on the unmodified Nunc Immobilizer™ plate surface (no target immobilized or surface treatment steps applied). As stated by the manufacturer, treatment with excess ethanolamine to neutralize the reactive electrophiles displayed on the Nunc surface reduces some of this unwanted retention. However, significant amounts of non-specifically bound material remain (**Figure 3-3A**). Methods known to both neutralize unreacted electrophiles through reaction with an appropriate nucleophile, and coat surfaces to passivate them against non-specific adsorption were therefore screened. When compared to the recommended ethanolamine treatment, statistically significant decreases in non-specifically bound library were observed when 1% Ficoll (w/v) polymer served as the nucleophile and passivating agent; no improvement was then seen with added poly(vinyl alcohol), a second oft-used passivating agent. However, greatly reduced non-specific retention of library members was achieved using a method described here that independently addresses electrophile neutralization (via the amines present in Tris (hydroxyl-methyl-)aminomethane buffer) and surface passivation (via coating of the base Nunc Immobilizer™ surface with the non-ionic surfactant, Tween-20). Passivation of and non-specific adsorption on the Nunc plate surface

were systematically investigated as a function of Tris and Tween-20 incubation concentrations and times. Minimum non-specific adsorption of aptamers was achieved using a time and composition optimized reaction at 25°C of 1 hr with AF buffer containing 20 mM Tris-HCl and supplemented with 0.005% Tween-20 (**Figure 3-3A**). No improvement in surface passivation is observed with longer reaction times (**Figure 3-3B**).

Figure 3-4 compares levels of non-specific library retention on the optimally passivated Nunc plate surface to those recorded on magnetic MyOne Carboxylic Dynabeads, the latter of which are widely employed in SELEX screens.^{310,311,358,359} In both systems, no protein target was immobilized, and functional groups were neutralized either according to manufacturer's instructions (MyOne Dynabeads) or using the nucleophilic reaction described above. Non-specifically retained library members were quantified by qPCR after extensive washing in either AF buffer, or AF buffer supplemented with nonionic surfactant. On the MyOne beads, library incubation in the absence of Tween-20 resulted in nonspecific retention of $3.89 \pm 0.85\%$ of the starting library. A significant reduction in bound amount is then observed with added surfactant. However, a further 6-orders of magnitude reduction in non-specifically retained library members is achieved using this surface-passivation protocol. When Tween-20 is added to an optimal concentration of 0.005%, non-specific adsorption on the surface-passivated Nunc plates is effectively reduced to quasi-undetectable levels (**Figure 3-4**). Library members recovered in the pooled incubation + wash solutions are also reported in **Figure 3-4** to verify closure of the total mass balance. The exceptionally low level of library members that are adsorbed to the optimally passivated Nunc-plate surface is strengthened by the fact that the total surface area available for non-specific adsorption was ca. 10-fold higher in the Nunc-surface study (0.95 cm² per treated well) than was available in the corresponding study on the MyOne beads (0.08 cm² displayed on ca. 2.4×10^6 beads).

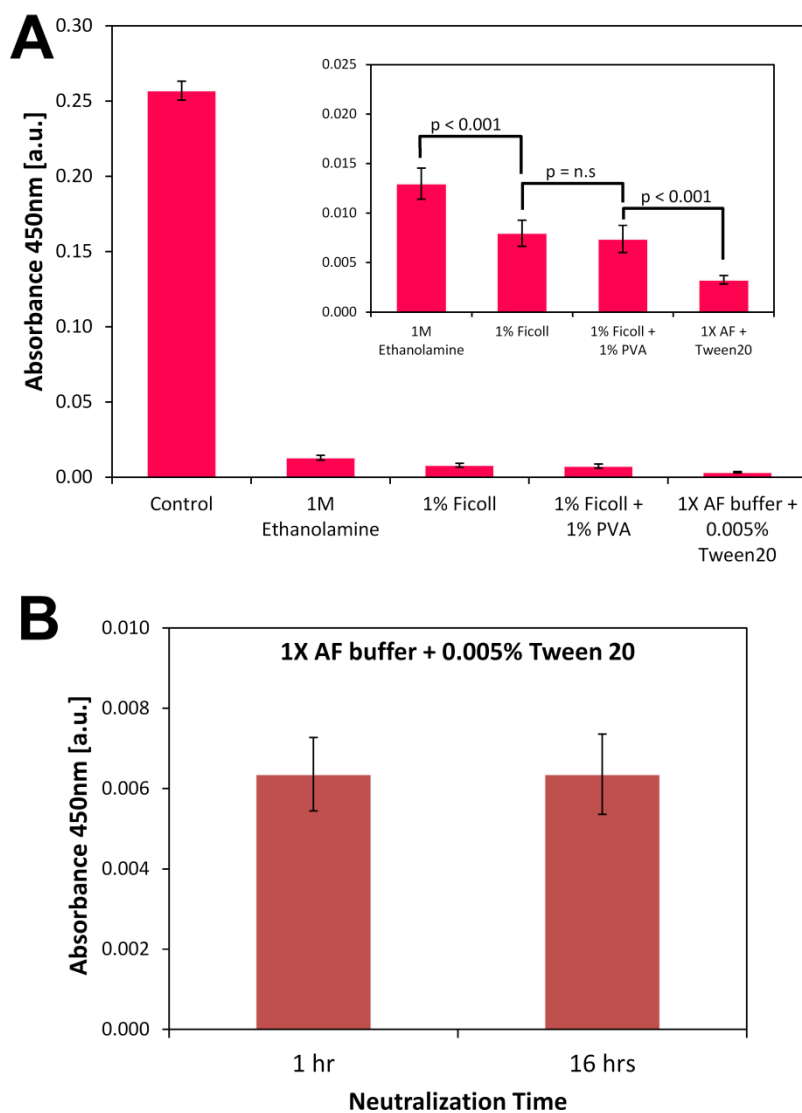


Figure 3-3 Relative amounts of SELEX library members that were irreversibly retained on Nunc Immobilizer™ plates which had undergone various surface treatments to block reactive sites and eliminate non-specific adsorption. No target was immobilized on the plates. (A) Comparison of amounts of library members that were non-specifically and irreversibly retained on the standard (commercial) Nunc Immobilizer™ plate surface (control), and after that surface has been pre-treated with 1 M ethanolamine, 1% Ficoll (w/v), 1% Ficoll and 1% polyvinyl alcohol (w/v), or Tris-containing aptamer folding (AF) buffer supplemented with 0.005 % Tween-20. (B) Comparison of levels of non-specific adsorption observed after blocking the Nunc Immobilizer™ plate surface with 1X AF buffer supplemented with 0.005 % Tween 20 for either 1 hr or 16 hrs. Standard deviations are reported for quadruplicate absorbance readings from duplicate experiments. For all ELONA-assay values reported, the background colorimetric signal when no SELEX library was incubated with the passivated surface was first subtracted.

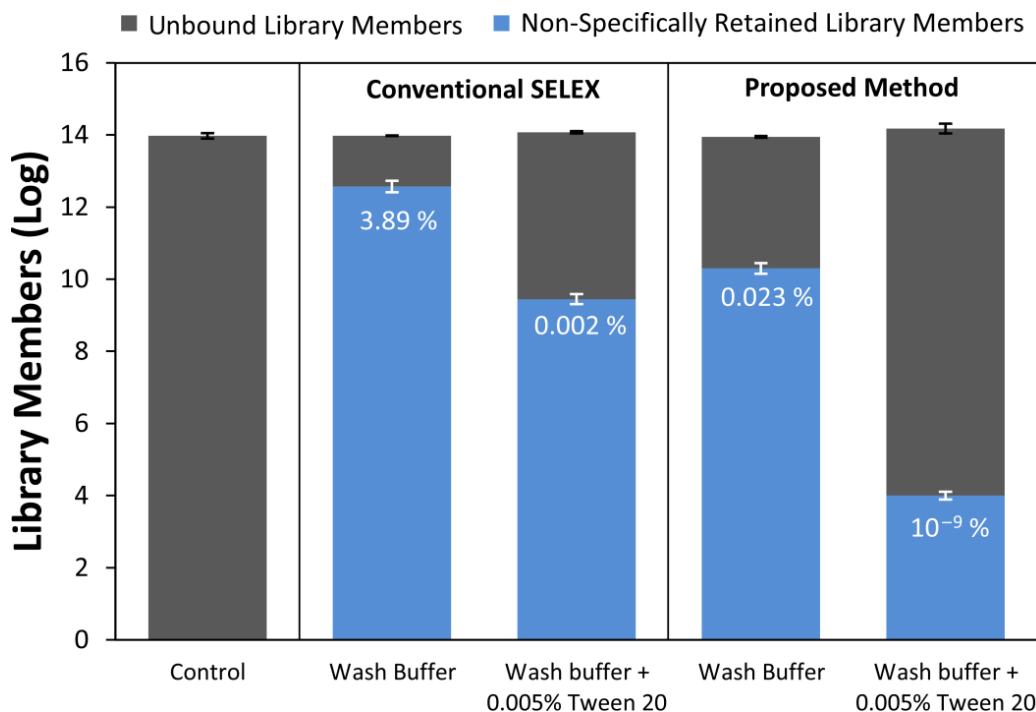


Figure 3-4 Comparison of the performance of conventional SELEX and the proposed method in mitigating non-specific retention of library members during aptamer selection both in the absence and presence of 0.005% Tween-20. In each case, no target was immobilized and reactive coupling sites were blocked before incubating the surface with 1.2×10^{14} library members for 1 hr. The surfaces were then washed extensively with 1X AF buffer alone or supplemented with 0.005% Tween-20, and retained members were eluted and quantified via qPCR. Error bars reported represent the standard deviations from triplicate experiments

Target immobilization and presentation strategies were then explored with the aim of maximizing signal to noise. Method improvements were based on monitoring the amount of biotinylated anti-Thr-29, within an otherwise unlabeled library, that binds to thrombin (ELONA assay) immobilized onto the surface-passivated surface. The effects of the reaction conditions used for thrombin immobilization, as well as the conditions (solution composition, pH, etc.) employed to then neutralize unreacted coupling agents were explored. Covalent immobilization of thrombin onto the target-display surface proceeds through reaction of amino groups or other nucleophiles on the protein with electrophilic coupling agents displayed on polyglycol chain ends. The manufacturer

recommends conducting this reaction at pH 9.6, but the use of a basic pH raises possibilities for chemical modifications (e.g., de-amidation) that alter target protein structure, chemistry and/or activity. Alternative reaction conditions were therefore screened and it was found that efficient coupling could also be achieved through an overnight reaction in 100 mM sodium phosphate buffer (pH 7.5) at 4°C (**Figure 3-5A**). At these milder conditions, surface saturation is realized by reacting with 80 nM thrombin (**Figure 3-5B**) to create a density of immobilized protein having a theoretical mean center-of-mass separation distance of 8.6 nm (**Figure 3-5C**). As the hydrodynamic diameter of a random 80-mer DNA aptamer is ca. 7.9 nm, this surface density permits aptamer screening anywhere within the theoretically preferred 100:1 to 1000:1 aptamer-to-target range, while eliminating the possibility of bridging of aptamers between proximal immobilized targets, an effect that has been shown to confound aptamer selection.³¹⁷

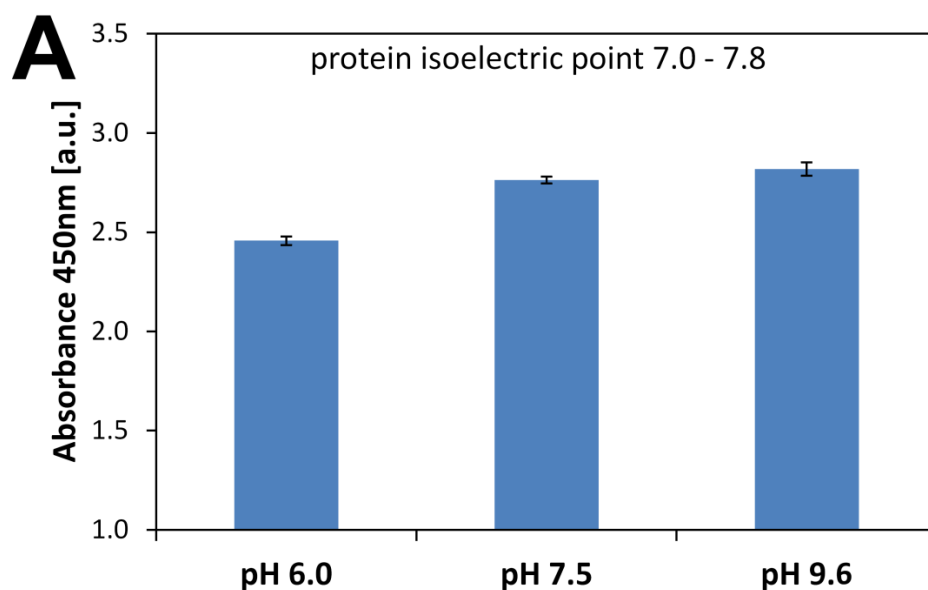


Figure 3-5 Identification of reaction conditions for immobilizing a target protein on the modified display surface at densities most suitable for Hi-Fi SELEX. (A) Relative amounts of human α -thrombin immobilized on the display surface at different reaction pH.

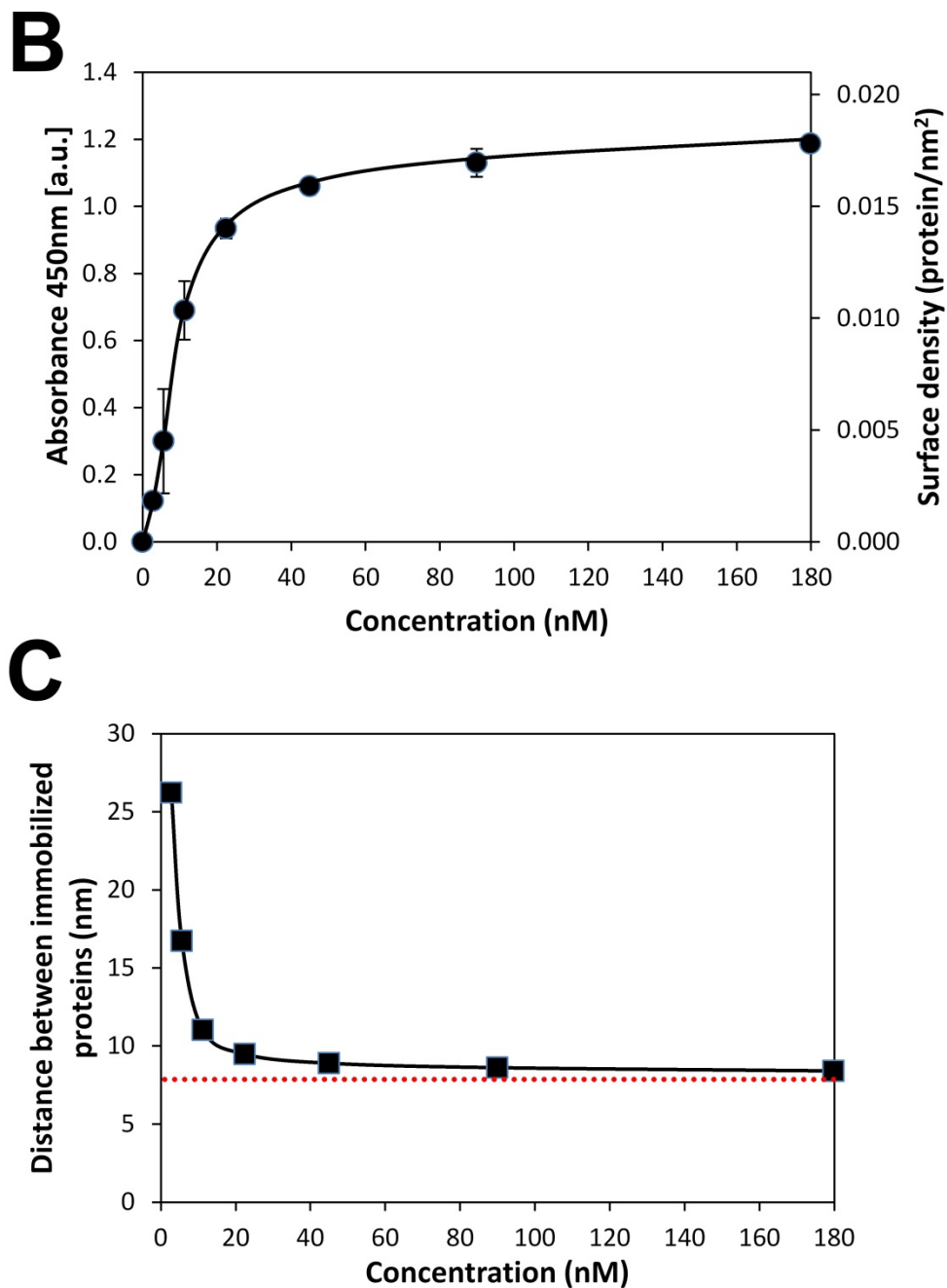


Figure 3-5 [continued from previous] (B) Change in the surface density of immobilized human α -thrombin as a function of the concentration of thrombin in the reacting solution. (C) Computed mean center-of-mass distance of separation of immobilized thrombin as a function of the concentration of the immobilization solution. The dashed line indicates the separation distance below which aptamer bridging effects could theoretically be observed. Standard deviations are reported for quadruplicate absorbance readings from duplicate experiments.

Following target immobilization, neutralization of unreacted coupling agents and passivation of non-specific binding sites is achieved through the 1 hr reaction with 1X AF buffer (pH 7.5) supplemented with 0.005% Tween-20, as described above. The set of target immobilization and surface passivation reactions are sufficiently mild to preserve α -thrombin's activity as measured by fluorogenic substrate conversion rates (**Figure 3-6**). By comparison, though an equivalent loading of α -thrombin can be achieved using the reaction conditions recommended by the manufacturer (immobilization at pH 9.6 followed by passivation with ethanolamine), that reaction results in significantly lower thrombin activity, as do the other methods explored. More importantly, this target-display method also improves signal-to-noise for specific aptamer (anti-Thr-29) binding to α -thrombin by preserving the availability of active immobilized target (**Figure 3-6**) while minimizing non-specific retention of library members on the underlying display surface (**Figure 3-4**).

Finally, library incubation conditions and times were screened and optimal conditions thereby identified (1 nmole resuspended in 1X AF buffer pH 7.5 with 0.005% Tween-20 for 60 min at 25°C with gentle (300 rpm) agitation) so as to permit members to approach equilibrium partitioning (**Figure 3-7A**) in each selection round while minimizing non-specific adsorption (**Figure 3-7B**).

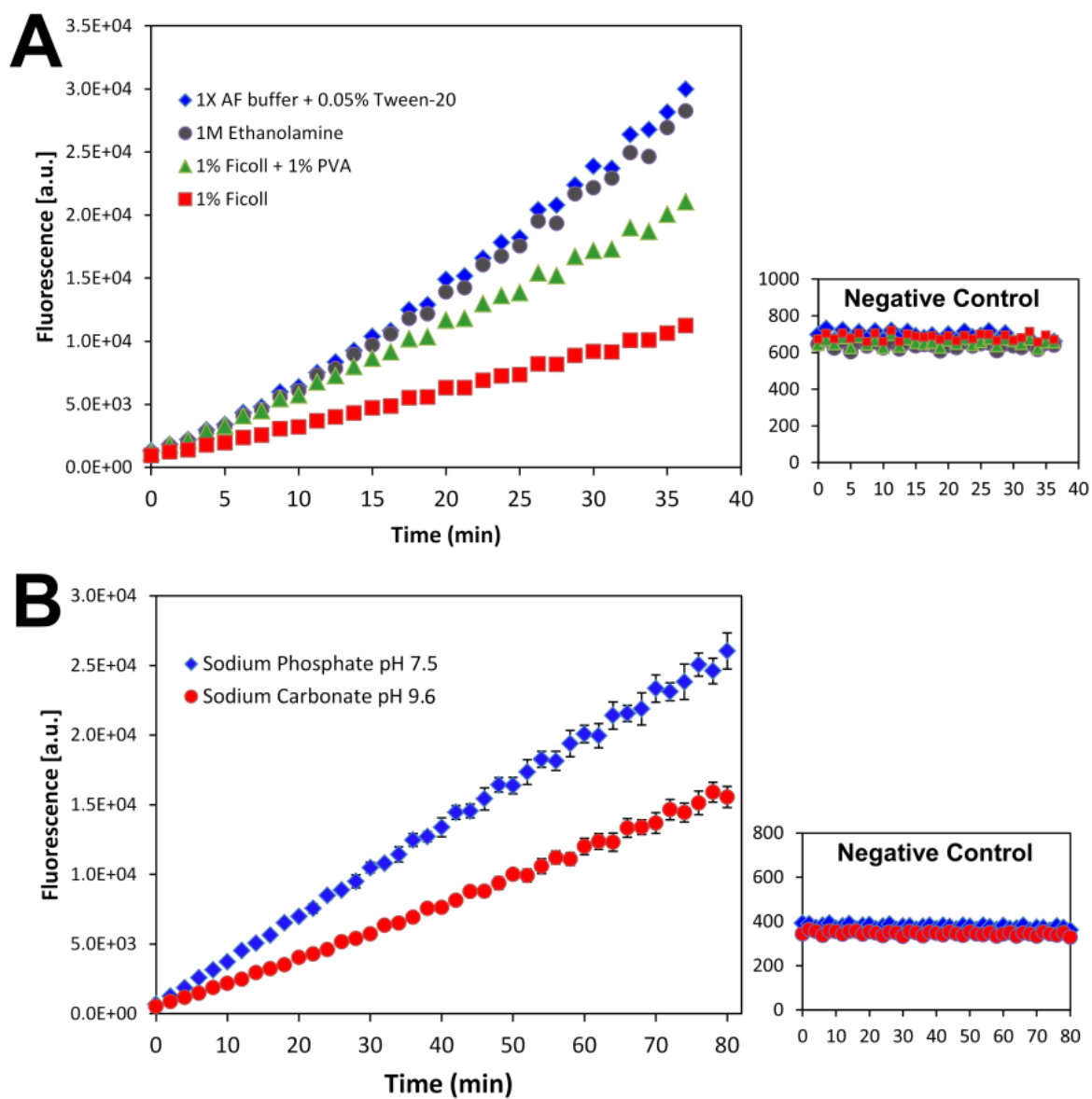


Figure 3-6 Effect of surface passivation chemistry (A) and immobilization conditions (B) on the functional (serine protease) activity of immobilized target (human α -thrombin). Activities were determined by monitoring (Ex=370 nm, Em= 450 nm) the cleaving rate of a fluorogenic substrate. In both data sets, negative controls indicate the spontaneous cleavage rate measured for each passivated surface containing no immobilized α -thrombin. Standard deviations are reported from quadruplicate fluorescence readings from triplicate experiments.

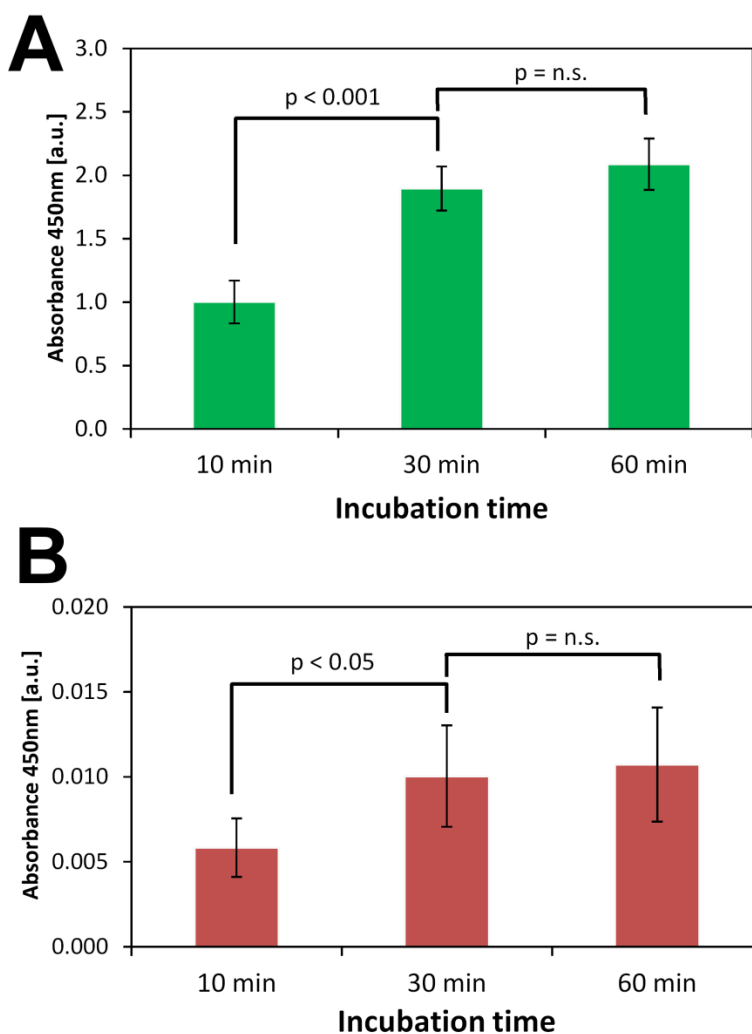


Figure 3-7 Effect of incubation time during a selection round on (A) competent library partitioning to the immobilized target (α -thrombin) phase, and (B) non-specific partitioning of the competent library to the same surface, but without immobilized target. Absorbance values reported reflect the quantity of aptamer recovered from the surface following selection and washing. Statistically significant differences in adsorbed amounts are reflected in the p -values reported, where a p -value > 0.1 is reported as not significant (n.s.), calculated from the standard deviations reported for quadruplicate absorbance readings from duplicate experiments.

The combined impact of the novel target and library presentation method on aptamer selection was then assessed (**Table 3-2**) by measuring round-by-round bulk affinities of retained pools of aptamers selected against human α -thrombin using either a conventional SELEX protocol employing magnetic MyOne Carboxylic Dynabeads³⁷⁹ or the platform described above coupled with the bulk

PCR and λ -exonuclease treatment typically used in SELEX to amplify and reconstitute each retained pool of ssDNA library members. For each system, results are shown for screening of both competent (supplemented with both 5' and 3' blocking agents) and standard 80-mer ssDNA libraries to parse out the performance contribution of the novel library-presentation elements of this approach. In all selections reported in **Table 3-2**, the aptamer:target ratio was set at 100:1. Based on the measured round-by-round mean K_d values for the retained pools, a PE of at least 5.0×10^4 is achieved in the front-end of the proposed method during each early selection round. As a result, significantly greater enrichment of high-affinity library members is realized when compared to standard SELEX screens performed with MyOne magnetic beads ($PE \sim 500$ to 5000). Moreover, when competent libraries are employed, significantly better round-by-round bulk affinities are realized, consistent with previous findings:³⁷⁹ that high-affinity members can be lost during SELEX due to interferences from unblocked flanking regions.

Table 3-2 Mean dissociation binding constants (K_d) measured by qPCR for enriched pools selected^a against human α -thrombin using two different partition methods. The K_d values and their standard deviations are reported in nM units from duplicate experiments.

	Conventional SELEX		Proposed Method and Target-Display Surface	
	Competent ^b	Standard ^b	Competent	Standard
Round 1	N.D. ^c	N.D.	63.0 ± 27.2	236.5 ± 69.1
Round 2	344.3 ± 68.2	N.D.	31.5 ± 7.2	105.7 ± 57.1
Round 3	99.6 ± 13.1	278.2 ± 80.9	10.7 ± 3.5	32.7 ± 7.0

a: Conventional SELEX was performed using MyOne carboxylic acid beads by partitioning and washing retained aptamers in standard 1X AF buffer, and by using conventional bulk PCR to amplify eluted aptamer pools.

b: Library formats used for either partition method included competent libraries (where both flanking regions were blocked) and standard libraries (where flanking regions were left unblocked)

c: N.D.: mean binding affinity of the eluted pool was too weak to measure

3.3.2 DROPLET DIGITAL PCR ENSURES PRECISE END-POINT AMPLIFICATION OF ELUTED LIBRARY MEMBERS.

Following each selection round, PCR is typically used to amplify the diverse ensemble of retained library sequences using universal forward and reverse primers targeting the common flanking sequences. As shown in **Figure 3-8A**, this reaction can prove challenging when performed in bulk on a pool of retained sequences. For a pool of 10^8 library members, amplification begins as desired with exponential accumulation of 80-bp dsDNA amplicons. However, unlike in PCR amplification of a single sequence using template-specific primers, a maximum in the total abundance of the desired 80-bp amplicon pool is reached after a limited number of cycles. Beyond that cycle number, the decreasing primer-to-template ratio no longer strongly favors annealing of universal primers to the common flanking sequences of each template. As a result, unwanted formation of hetero-duplexes comprised of two partially complementary strands, typically exhibiting only end-complementary between the common flanking sequences, occurs through cross-hybridization of amplified library members.^{323,390} The presence of such hetero-duplexed chimera is known to promote spurious priming events,²⁰⁵ and this can result in complete conversion of the library to increasingly aberrant high molecular weight (HMW) by-products in as little as 5 additional PCR cycles (**Figure 3-8A**). Careful monitoring of the reaction is therefore required to ensure amplification is terminated prior to formation of these library-degrading by-products. Regrettably, stopping amplification at a relatively low cycle number typically results in an end-point yield ($\sim 10^{11}$ to 10^{12} 80-bp amplicons) that is several orders of magnitude lower than can be achieved (ca. 10^{14}) in PCR of a homogeneous template. This issue may be and often is addressed in conventional SELEX by multiplexing the PCR step so as to distribute the retained pool amongst a large set of parallel reactions, each amplifying between 10^5 to 10^6 library members. The sequence heterogeneity in a given reaction is thereby reduced. As a result, amplification can proceed to a larger cycle number before incipient formation of

HMW by-products and a maximum in the abundance of the desired 80-bp amplicon pool are observed. For example, by partitioning 10^7 retained members across ca. 100 parallel reactions (i.e. a PCR plate), the pool of $\sim 10^5$ library members in each reaction can be amplified to a final abundance of $\sim 10^{12}$ 80 bp amplicons before significant by-products formation is observed (**Figure 3-8B**). The dilute products from the 100 parallel reactions may then be pooled and concentrated to reach the desired amplicon concentration (i.e. 10^{14} amplicons in 100 μL) for downstream (λ -exonuclease) processing and the next round of SELEX. Weaknesses of this strategy include the need to scout and control the cycle number at which each PCR is terminated, and the potential for variability in the abundance of amplicons produced in each reaction.²⁰⁵ In addition, a further, more significant weakness was identified—namely that dsDNA amplicons produced in this manner are poorly converted by λ -exonuclease back to their desired ssDNA SELEX library form (discussed further below).

Hi-Fi SELEX addresses these limitations to further improve overall selection efficiencies through the incorporation of droplet digital PCR (ddPCR)³⁹¹ into the workflow, a concept that has only very recently been proposed for aptamer selection.³⁹² In this approach, the pool of library members recovered after each selection round is partitioned among a near equivalent number of nanoliter-sized droplets, each of which contains the reagents needed for template amplification. Each droplet therefore contains a small number of templates, keeping the sequence heterogeneity per droplet very low. As a result, amplification of the isolated pool of templates can proceed to its conventional asymptotic end-point abundance without significant formation of HMW by-products or any observed maximum and subsequent decline in the abundance of the desired 80 bp material. This is shown in **Figure 3-8C**, which reports ddPCR results when the same library of 10^5 members is partitioned in a normal distribution among ca. 20,000 droplets in a single reaction, so that each drop contains 5 templates on average (i.e. a mean copies per droplet, CPD, of 5). Unlike during standard bulk amplification (**Figure 3-8B**),

minimal by-products formation is observed over 40 ddPCR cycles, permitting high-fidelity end-point amplification of all 10^5 library members into more than 10^{14} copies of the desired 80 bp dsDNA product.

In Hi-Fi SELEX, ca. 10^8 library members are recovered in each selection round. To minimize the reagents required to amplify sufficiently these library members for the next round of selection, the maximum CPD that could be employed in the ddPCR procedure was determined. At a CPD of 50, complete end-point amplification of the 80 bp library with minimal accumulation of HMW by-products is still achieved (**Figure 3-9**). However, ddPCR at higher CPDs results in by-product formation and a concomitant loss of desired 80-bp product and product quality in a manner similar to that observed in standard bulk PCR of retained library members (**Figure 3-8B**). This CPD limit specifically relates to libraries retained in the first few rounds of selection, where stochastically, each of the 50 templates within each droplet is almost certain to harbour a unique sequence within its random region. In later rounds of selection, duplicate library sequences will increasingly partition into a given drop, diminishing template heterogeneity and the probability of forming unwanted hetero-duplexes during amplification cycles. Higher CPDs may then be used.

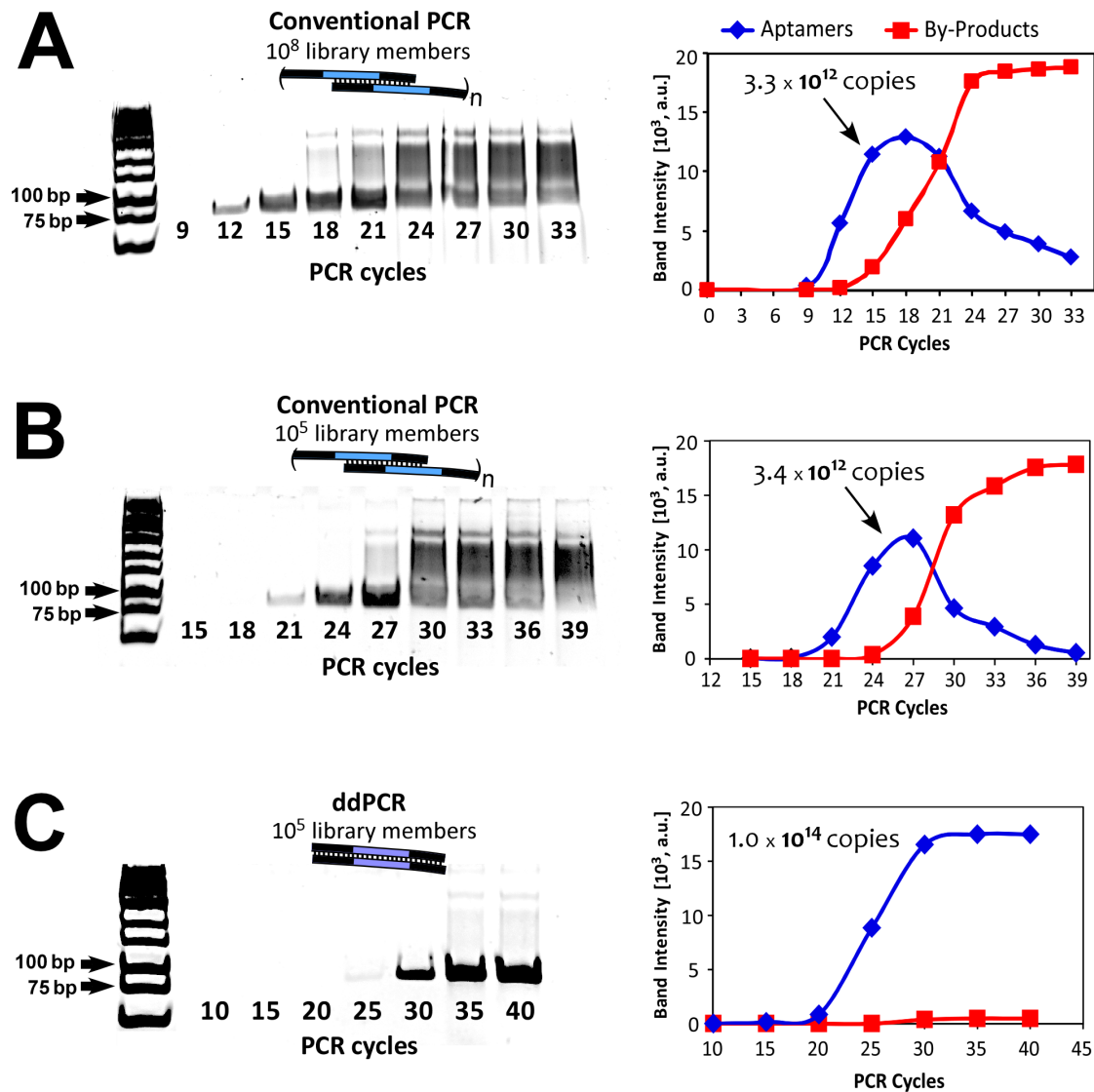


Figure 3-8 Comparison of PCR amplification methods for eluted aptamer pools. PCR amplification of (A) 10^8 or (B) 10^5 library members in a conventional bulk reaction. At either retained library abundance, self-priming and mis-priming of individual members leads to rapid conversion of the desired 80 bp amplified material towards aberrant high-molecular-weight by-products. Amplification must therefore be terminated at a low cycle number to avoid loss of product, leading to decreased yields. (C) When optimized for heterogeneous pools of retained library members, droplet PCR amplification avoids these artifacts by sequestering sufficiently small numbers of library members in isolated nL-sized droplets containing amplification reagents. The amplification process can be carried to end-point with minimal by-product accumulation, leading to much higher yields and less contamination of the desired 80 bp product.

In addition to preventing the accumulation of amplification artifacts, CPD-optimized integration of ddPCR into Hi-Fi SELEX ensures generation of only fully duplexed dsDNA amplicons (i.e., homo-duplexes). Although not addressed in the

literature to date, this was found to be important to maintaining library integrity during selection rounds. DNA-based SELEX libraries utilize the sense strand of dsDNA amplicons, necessitating removal of amplified antisense strands prior to the next round of selection. Alkaline denaturation of amplicons and streptavidin-based removal of the biotinylated antisense strands can be utilized for this purpose. However, antisense strand hydrolysis using λ -exonuclease has been shown to provide a more reliable means to recover ssDNA library members,³²⁰ and is therefore more widely used.²¹⁰⁻²¹² But, in work unrelated to SELEX technology, Lee et al.³²² have shown that the antisense strand hydrolysis activity of λ -exonuclease is diminished when operating on duplexes containing large contiguous regions of mismatch. Exonuclease activity stalls, resulting in partially digested dsDNA products.

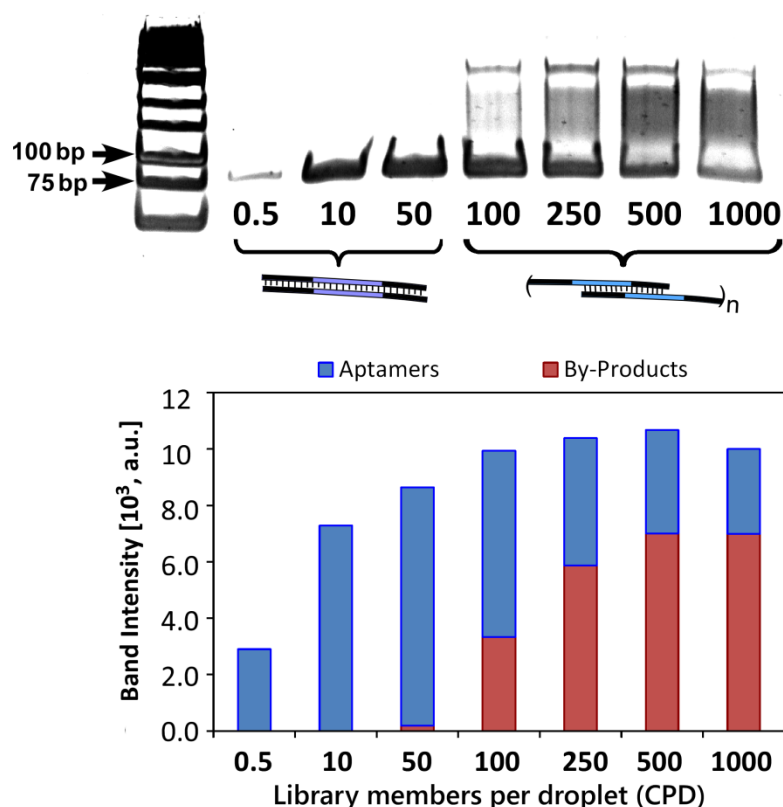


Figure 3-9 Dependence of ddPCR performance in amplifying 10^8 unique library members on the mean copies-per-droplet (CPD) value used. Gel documentation and associated band-intensity analyses show that significant by-products formation occurs at CPD values above 50.

The potential impact of this finding on the round-by-round integrity of SELEX libraries is not known. Lambda-exonuclease eliminates antisense strands of SELEX library amplicons through its preferential hydrolytic activity on the 5'-ends of dsDNA, which is at least 20 times higher than on non-phosphorylated dsDNA 5'-termini.^{393,394} Fluorescently labeled and quenched dsDNA amplicons were therefore generated from 80-bp SELEX libraries of increasing sequence diversity using PLEXOR™ qPCR technology (Promega) and a 5'-phosphorylated universal reverse primer (**Figure 3-10**). The 5'-terminus of each amplicon's antisense strand is therefore phosphorylated, while that of the sense strand is not and instead bears an iso(dC)-FAM group that is quenched by a base-paired dabcyI-iso(dG) group.

When the starting diversity of the ssDNA SELEX library is low (e.g. < 100 unique random-region sequences; **Figure 3-10**, left panel), standard PCR amplification results in only homo-duplexed amplicons, as indicated by the high melting temperature ($T_m = 81.5^\circ\text{C}$) and single Gaussian peak recorded for the amplification product (**Figure 3-11**; bottom right); λ -exonuclease exhibits good anti-sense strand hydrolysis activity in this case (**Figure 3-12**), effectively equivalent to that obtained on amplicons generated from a single library sequence. However, as the sequence diversity of the starting library is increased (**Figure 3-10**, right panel), an increasingly larger percentage of the final amplicon pool is present in the form of hetero-duplexes having only partial complementarity. That hetero-duplexed pool of amplicons collectively exhibits a melting envelope characterized by a much lower T_m (~ 66 to 67°C) (**Figure 3-11**). Lambda-exonuclease processing of that heterogeneous pool results in significant and proportionate reductions in the total quantity of quenching agent (DabcyI) released and the maximum FAM signal recorded (**Figure 3-12**), indicating incomplete digestion of antisense strands within hetero-duplexed amplicons (as illustrated in **Figure 3-10**).

Figure 3-11 indicates that the amount of hetero-duplexed amplicons produced depends on the sequence diversity of the ssDNA SELEX library being amplified.

That dependence can be quantified by determining the area under each melting curve (Gaussian distribution) after correcting for background fluorescence (**Figure 3-13A**), then using those results to compute the fraction of all amplicons in hetero-duplexed form f_{hetDNA} and the dependence of f_{hetDNA} on library diversity. The resulting plot (**Figure 3-13B**) shows that only homo-duplexed amplicons are produced when the sequence diversity of the starting ssDNA SELEX library is less than ca. 50. By partitioning large numbers of templates amongst a nearly equivalent number of order-nL droplets³⁹⁵ or chambers,³⁹⁶ digital PCR can readily achieve CPD values ≤ 50 to permit high-fidelity amplification of a SELEX library having significant sequence diversity. This is illustrated in **Figure 3-14A**, which shows that partitioning of 10^8 different SELEX sequences into droplets having a mean CPD of 50 results in a ddPCR product of greater than 10^{14} amplicons, all of which are present in their desired homo-duplexed form as evidenced by the single melting peak centered at a $T_m = 81^\circ\text{C}$. In contrast, conventional bulk PCR of the same pool of 10^8 unique sequences yields two distinct melting peaks with normalized areas in quantitative accordance with **Figure 3-13A**.

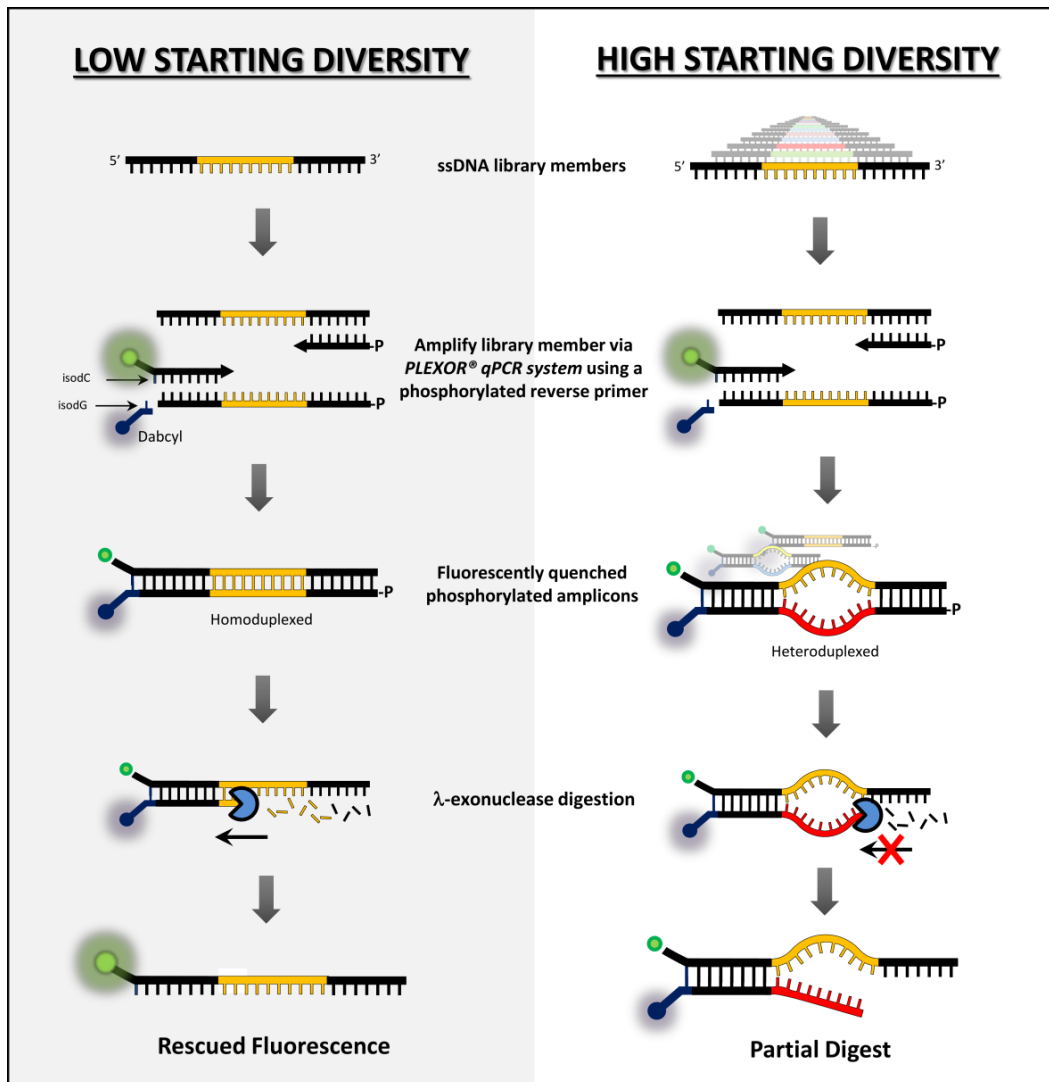


Figure 3-10 Schema depicting the principal duplex structure of amplicons, and the resulting action of λ-exonuclease on the 5'-phosphorylated reverse strand following PCR amplification of ssDNA SELEX libraries of low (Left column) and high (Right column) sequence diversity.

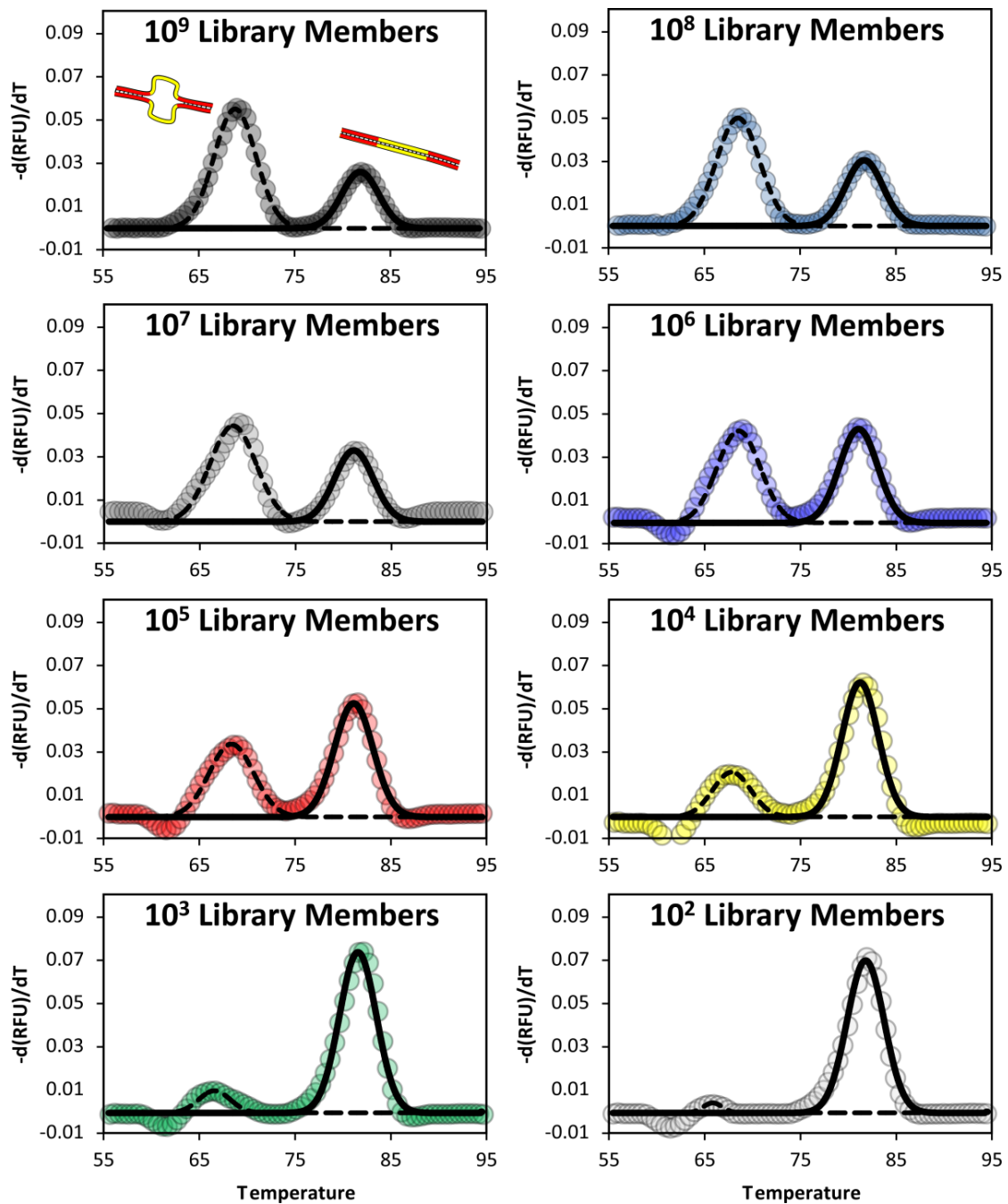


Figure 3-11 Normalized melting curve data for amplicon pools (10^{14} total amplicons) generated from ssDNA SELEX libraries of different sequence diversity. The sequence diversity of the library is reported for each melting curve reported. Transitions (peaks) centered at a T_m of $\sim 81^\circ\text{C}$ and $\sim 67^\circ\text{C}$ correspond to melting of fully complemented homo-duplexes and partially complemented hetero-duplexes, respectively.

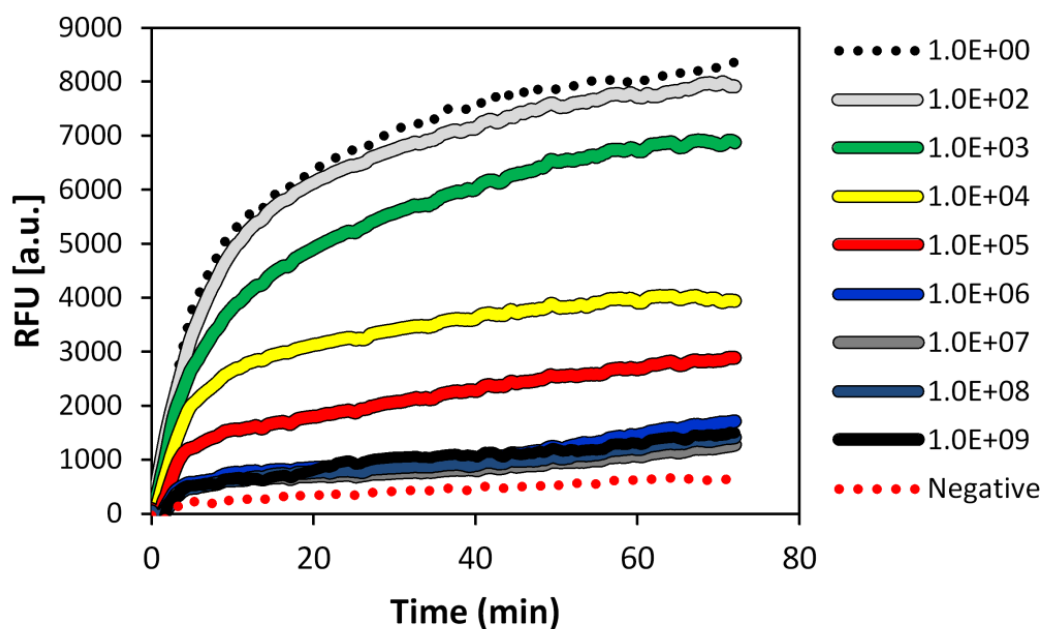


Figure 3-12 Real-time λ -exonuclease-mediated hydrolysis of 5' phosphorylated anti-sense strands as a function of the sequence diversity of the initial amplification pool. Data for sequence diversities ranging from a single amplicon sequence to 10^9 unique sequences are reported along with that for a negative control (Negative) in which no λ -exonuclease was added. The data show that both the initial hydrolysis rate and the total extent of hydrolysis decrease with increasing sequence diversity.

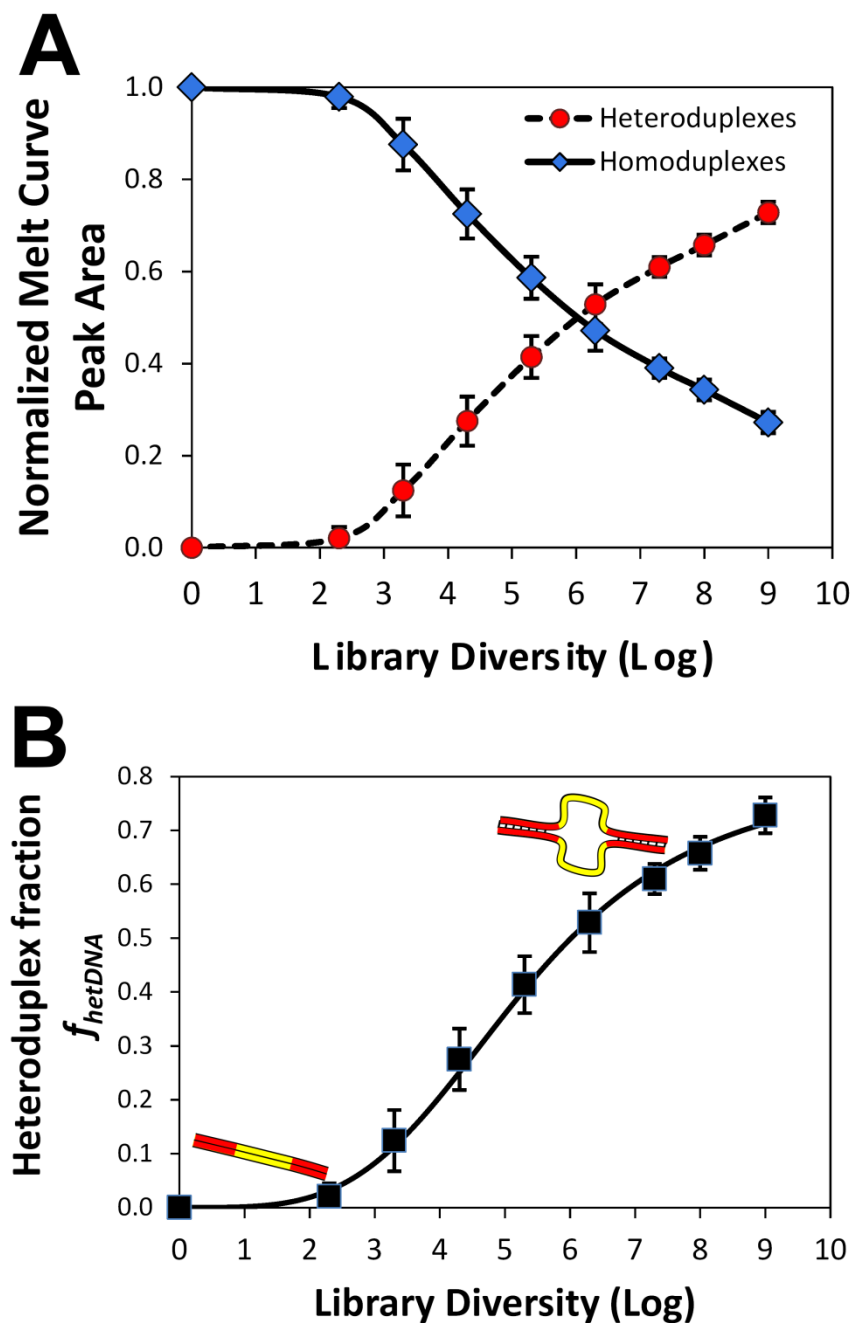


Figure 3-13 Relationship between the sequence diversity of the ssDNA SELEX library and the fraction f_{hetDNA} of those sequences participating in a hetero-duplex structure following amplification. (A) Normalized areas of the melting transitions (Figure 3-11) for the hetero-duplexes and homoduplexes within the pool within the 10^{14} amplicons. (B) Fraction of all amplicons that are in a hetero-duplex structure, computed from the data in (A). Standard deviations are reported from quadruplicate experiments.

By exploiting ddPCR to produce $\geq 10^{14}$ amplicons, all in their homo-duplexed form, the dsDNA product can stoichiometrically be processed using λ -exonuclease to obtain the required ssDNA SELEX library in no more than 60 minutes (**Figure 3-14B**); dsDNA amplicons generated from a single library sequence (a reaction for which hetero-duplex formation is naturally precluded) are likewise fully converted into the desired ssDNA product in less than an hour (positive control). In contrast, appreciable amounts of dsDNA product remain after more than 2 hours of λ -exonuclease-catalyzed hydrolysis when the 10^8 retained SELEX library members are PCR amplified in bulk, confirming that hetero-duplexed amplification products are, at best, very slowly and poorly processed. This is important, as λ -exonuclease exhibits low levels of hydrolytic activity on ssDNA.³⁹⁴ As a result, though longer digestion times could in principle allow for more complete processing of anti-sense strands, it would also result in loss of fully processed ssDNA library members. A reduction in the quality and diversity of a ssDNA SELEX library is therefore expected when library amplification results in the formation of hetero-duplexes.

It was therefore found that ddPCR permits the reliable, high-fidelity amplification of eluted library members. In particular, the ddPCR method described yields significantly higher amplified material concentrations per reaction than can be achieved using a standard bulk PCR. When 2×10^5 unique library members are amplified together in a standard 20 μ l volume, a final 80 bp amplicon concentration of order ~ 300 nM is achieved. But when that same sample is amplified using the optimized ddPCR protocol, a final yield of 9.0 μ M (30X more product) is realized. Moreover, all amplicons produced are in their fully complementary dsDNA state, permitting stoichiometric removal of the antisense strands by λ -exonuclease. As a result, a clean ssDNA library can be created from as little as 10^5 retained members in quantities sufficient to not only proceed to the next selection round, but also, as will be shown, to determine the mean binding affinity of the enriched pool after each selection round, providing a useful metric of how well the overall selection is proceeding.

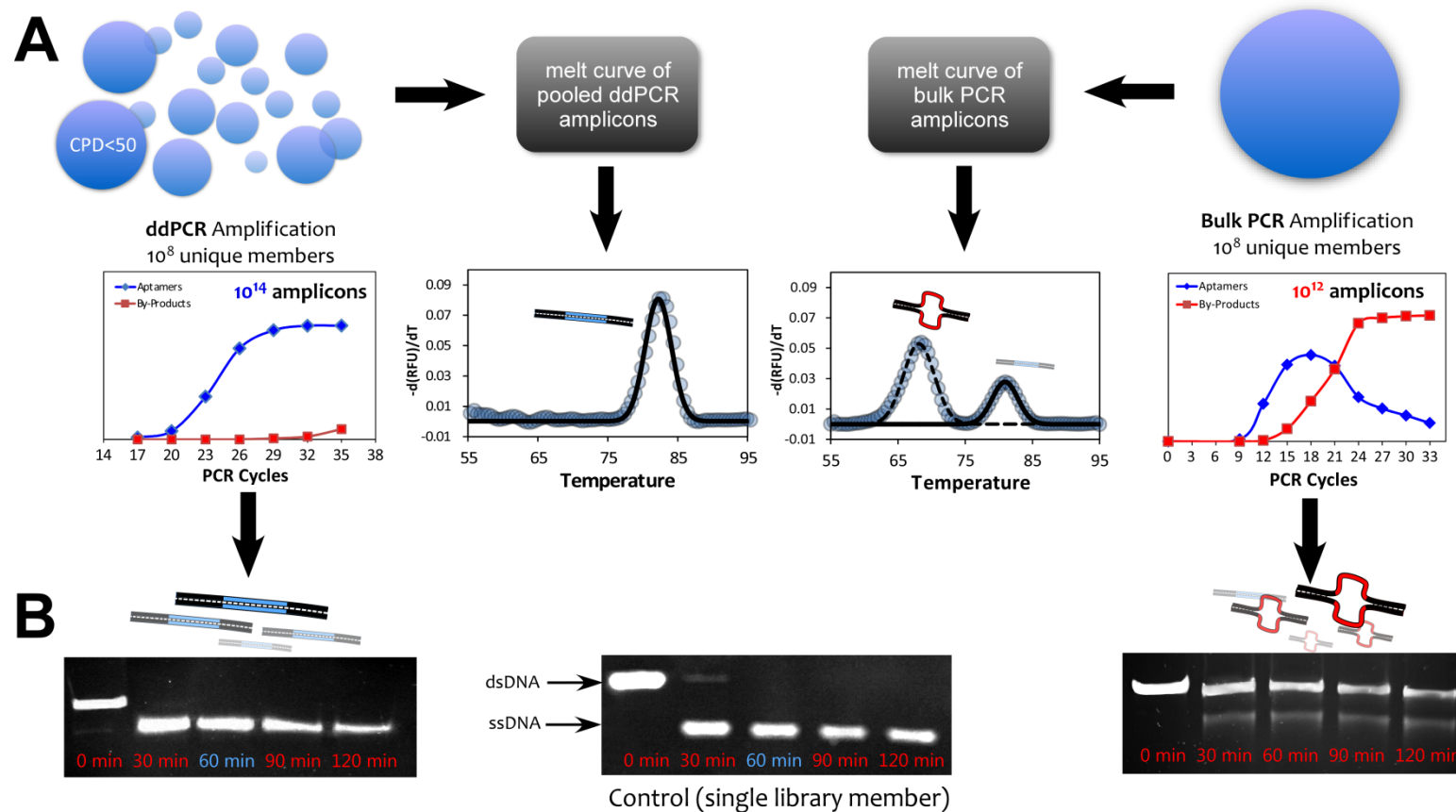


Figure 3-14 Characterization of the amplification of a retained aptamer library containing 10⁸ unique sequences by conventional bulk PCR (SELEX) or by the optimized ddPCR protocol. (A) Following end-point ddPCR at a CPD of 50, the resulting amplicon pool is reformed by breaking the droplet emulsion. Melt analysis of that pool shows a single transition centered at $T_m = 81^\circ\text{C}$, indicative of the formation of only fully-duplexed amplicons. In contrast, bulk PCR amplification of the retained library, as is commonly done in SELEX, results in a lower-concentration pool of amplicons that, when melted, exhibit two melting transitions centered at 67°C and 81°C whose areas correlate with the fraction of hetero-duplexed and homo-duplexed amplicons, respectively. (B) Conversion of ddPCR amplicons back into single-stranded library members using λ -exonuclease. When fully-duplexed ddPCR amplicons are processed (left-most gel), stoichiometric conversion of all dsDNA amplicons into ssDNA library members is achieved in no more than 60 min, a result identical to that observed for processing of a single amplicon (library) sequence at the same starting concentration (middle gel). In contrast, incomplete conversion occurs during processing of bulk-PCR amplified samples, where an abundance of hetero-duplexed members prevents complete enzymatic conversion into the desired single-stranded library (right-most gel).

3.3.3 HI-FI SELEX PERMITS RAPID IDENTIFICATION OF HIGH-AFFINITY APTAMER POOLS

In addition to permitting creation of clean 80 nt ssDNA libraries from retained and amplified pools, ddPCR, by virtue of its ability to increase the degree of amplification without by-products formation, also allows more stringent washing of bound library members to be employed during each selection round so as to reduce non-specific retention and thereby improve per round *PE* values. This might be achieved through washing of bound material with more column volumes of AF buffer, a method previously shown to be effective in both microfluidic SELEX³¹⁰ and micro-column SELEX,³⁵⁷ or by employing a wash buffer that differs compositionally from AF buffer in a manner that serves to alter binding equilibria to select for desirable classes of aptamers. Of particular interest to us was the potential to use wash conditions (e.g. high ionic strength) that favored retention of aptamers whose binding interaction with the target is not dominated by coulombic forces. It was found that washing the retained library following equilibration with AF buffer supplemented with 4 M NaCl strongly shifts towards the desorbed state the binding equilibria of those library members whose surface-retention is largely or exclusively driven by electrostatics (i.e. non-specific or promiscuous ion-exchangers). Aptamers bound through a more balanced ensemble of short- and long-range interactions with the target are thereby preferentially retained.

The combined impact of the high-salt wash and associated ddPCR processing on aptamer selection is illustrated in **Table 3-3**, which reports the per-round mean affinity constant (K_d) for aptamer pools selected against α -thrombin when either a competent or standard 80-mer SELEX library is screened using the full Hi-Fi SELEX platform described in **Figure 3-1**. The results in **Table 3-3** add to this finding by showing per round *PE* values of at least 8×10^5 are achieved in Hi-Fi SELEX. Indeed, comparison with the results reported in **Table 3-2** (where only the front-

end components of the platform are employed) shows that the net benefit to Hi-Fi SELEX of the back-end components (ddPCR, stringent wash) is a further 6 to 10 fold improvement in the mean K_d after the first selection round. More importantly, order-nM K_d values are realized in Hi-Fi SELEX within three rounds of selection, with selections employing competent libraries again proving more effective.

Table 3-3 Round-by-round mean dissociation constants (K_d) and standard deviations measured by duplicate qPCR experiments for 80-mer ssDNA aptamer and competent aptamer pools selected against human α -thrombin using the complete Hi-Fi SELEX platform described in **Figure 3-1**.

	$K_d \pm \sigma$ (nM)	
	Competent	Standard
Round 1	10.7 \pm 2.2	23.5 \pm 1.5
Round 2	7.2 \pm 2.0	17.4 \pm 6.6
Round 3	2.6 \pm 0.6	8.7 \pm 2.5

The K_d values reported in **Table 3-2** and **Table 3-3** were determined by integrating into the workflow a qPCR-based assay that leverages the large amounts of clean by-product free 80-nt aptamer library product generated. The details of that assay are described in a recent publication³⁷⁹ that shows the simple label-free method delivers mean K_d values for retained aptamer pools at higher throughput and lower cost than currently achieved by standard approaches (e.g. fluorescence anisotropy, isotherm data using labelled aptamers, surface plasmon resonance) commonly used in SELEX.

The general utility of Hi-Fi SELEX in identifying aptamer pools against therapeutically-relevant targets was then explored by performing both conventional SELEX and Hi-Fi SELEX screenings against blood coagulation factors

IXa and X, as well as against human complement Factor D. For each target, per-round mean K_d values for screening of either a standard or competent library are presented in **Table 3-4**. Per-round PE values (1400 to 4100) and overall selection efficiencies provided by conventional SELEX screening of standard libraries on magnetic MyOne Carboxylic Dynabeads are consistent with more extensive data on that system available in the literature.^{215,369,397} For all three targets, mean K_d values for retained aptamer pools therefore remain in the μM range after 3 rounds of selection, with some improvement observed when competent libraries are employed. In contrast, Hi-Fi SELEX screenings against each target yield per-round PE values in excess of 8.0×10^5 . As a result, mean K_d values between 2 to 20 nM are achieved after only 3 rounds of selection when competent libraries are used.

Table 3-4 Round-by-round mean dissociation constants (K_d) and standard deviations measured by duplicate qPCR experiments for enriched pools selected against various therapeutic targets using either competent or standard library formats. All K_d values are reported in nM units.

	Standard Library (Unblocked)			Competent Library (Blocked)		
Standard SELEX (MyOne beads)	Round 1	Round 2	Round 3	Round 1	Round 2	Round 3
Factor IXa	N.D.	454.2 ± 270.7	135.2 ± 19.7	N.D.	386.0 ± 161.1	133.5 ± 16.5
Factor X	N.D.	N.D.	211.9 ± 61.7	N.D.	436.0 ± 91.8	125.0 ± 46.5
Factor D	N.D.	N.D.	519.7 ± 79.8	N.D.	N.D.	496.5 ± 66.3
Hi-Fi SELEX	Round 1	Round 2	Round 3	Round 1	Round 2	Round 3
Factor IXa	126.4 ± 28.2	21.6 ± 5.0	22.9 ± 7.1	73.6 ± 21.9	16.6 ± 3.2	17.2 ± 6.4
Factor X	259.1 ± 52.6	59.9 ± 15.3	10.6 ± 3.9	40.1 ± 7.2	26.9 ± 3.6	6.4 ± 1.5
Factor D	140.6 ± 24.8	27.8 ± 9.7	3.8 ± 1.2	62.6 ± 16.8	8.6 ± 4.8	2.9 ± 0.9

3.3.4 COMPETENT LIBRARIES RETAIN GREATER SELECTION DIVERSITY

Tight binding aptamers must also possess correct epitope specificity to elicit a desired therapeutic response.^{105,172,398-400} As SELEX screens for only binding affinity, it is desirable to engineer the selection process to retain the maximum possible diversity of aptamers exhibiting an affinity that equals or exceeds the target's interaction with its natural substrate/binding partner. Determination of enriched library diversities generally relies on next-generation sequencing (NGS) platforms,^{171,328} and is often met with significant challenges, including the current costs associated with round-by-round integration of NGS within the SELEX workflow to avoid over-selection. A simple and more cost-effective alternative method, based on *C₀t* analysis,⁴⁰¹ has therefore recently been described.^{375,402} Due to its sensitivity to *f_{hetDNA}*, it was suspected that the amplicon-melt analysis method demonstrated in **Figure 3-11** might also offer a simple approach to estimating retained pool diversities after each selection round. The calibration curve shown in **Figure 3-13** indicates the proposed method accurately quantifies library diversity for diversities above ca. 10⁴ unique members, with uncertainties increasing below that value. It has the advantage that it is easily integrated into the SELEX workflow to quantify retained library diversities in early selection rounds. To apply the method, **Figure 3-13**, or curves like it constructed for other library formats, are created by qPCR melt analysis of serial reductions in starting library diversity. Background fluorescence is then quantified and subtracted,^{403,404} followed by fitting of the normalized peaks to Gaussian distributions by nonlinear least-squares regression.⁴⁰⁵

Limited available NGS data available in the literature suggest that library diversities at the end of a conventional SELEX process typically fall below 10⁶ unique sequences.^{171,296,328} It would therefore be useful to also establish a

complementary qPCR method that provides good sensitivity for library diversities in that range, so as to permit quantification of diversities in later selection rounds. As shown in **Figure 3-15**, library diversities $\leq 10^6$ may be accurately quantified using a simple fluorescence assay based on the dsDNA minor-groove-binding probe PicoGreen™. PicoGreen™ periodically binds dsDNA at \sim every 4 bp,⁴⁰⁶ and thus the total fluorescence readout is highly sensitive to the total abundance of duplex present in the system. Following correction for background fluorescence, that abundance decreases with increasing f_{hetDNA} , resulting in a concomitant decrease in the slope of the fluorescence intensity versus total amplicon concentration as the diversity of library and thus f_{hetDNA} increases (**Figure 3-15**). If the ddPCR method proposed in this work is used for library amplification, a small amount of the amplification product must first be melted to create the pool containing f_{hetDNA} of heterogeneous duplexes required for the assay.

Both of these new methods were applied to round 3 elution pools reported in **Table 3-3** and **Table 3-4** for Hi-Fi SELEX, employing either standard or competent library formats (**Figure 3-16**). The measured diversities for each target recorded using each method are reported in **Table 3-5**. As expected, the melt-curve analysis method and PicoGreen™ assay provide more precise values for retained libraries of higher and lower diversity, respectively.

Table 3-5 Sequence diversity of aptamer pools selected against different targets using Hi-Fi SELEX and either competent or standard libraries. Diversity values and standard deviations reported from duplicate experiments represent the total number of unique aptamer sequences at the completion of the third round of selection.

	Melt-Curve Analysis		PicoGreen® Assay	
	Competent	Standard	Competent	Standard
α-Thrombin	$5.7 \times 10^4 \pm 4.0 \times 10^4$	$2.1 \times 10^3 \pm 8.8 \times 10^2$	$7.3 \times 10^4 \pm 4.1 \times 10^4$	$5.6 \times 10^3 \pm 2.7 \times 10^3$
Factor IXa	$7.2 \times 10^7 \pm 3.9 \times 10^7$	$1.2 \times 10^5 \pm 9.1 \times 10^4$	$> 10^6$	$3.0 \times 10^5 \pm 1.5 \times 10^5$
Factor X	$9.7 \times 10^4 \pm 6.1 \times 10^4$	$4.0 \times 10^3 \pm 2.9 \times 10^3$	$2.7 \times 10^4 \pm 1.2 \times 10^4$	$8.8 \times 10^3 \pm 4.8 \times 10^3$
Factor D	$2.6 \times 10^4 \pm 1.4 \times 10^4$	$2.2 \times 10^2 \pm 1.1 \times 10^2$	$5.2 \times 10^4 \pm 2.1 \times 10^4$	$3.2 \times 10^2 \pm 1.4 \times 10^2$

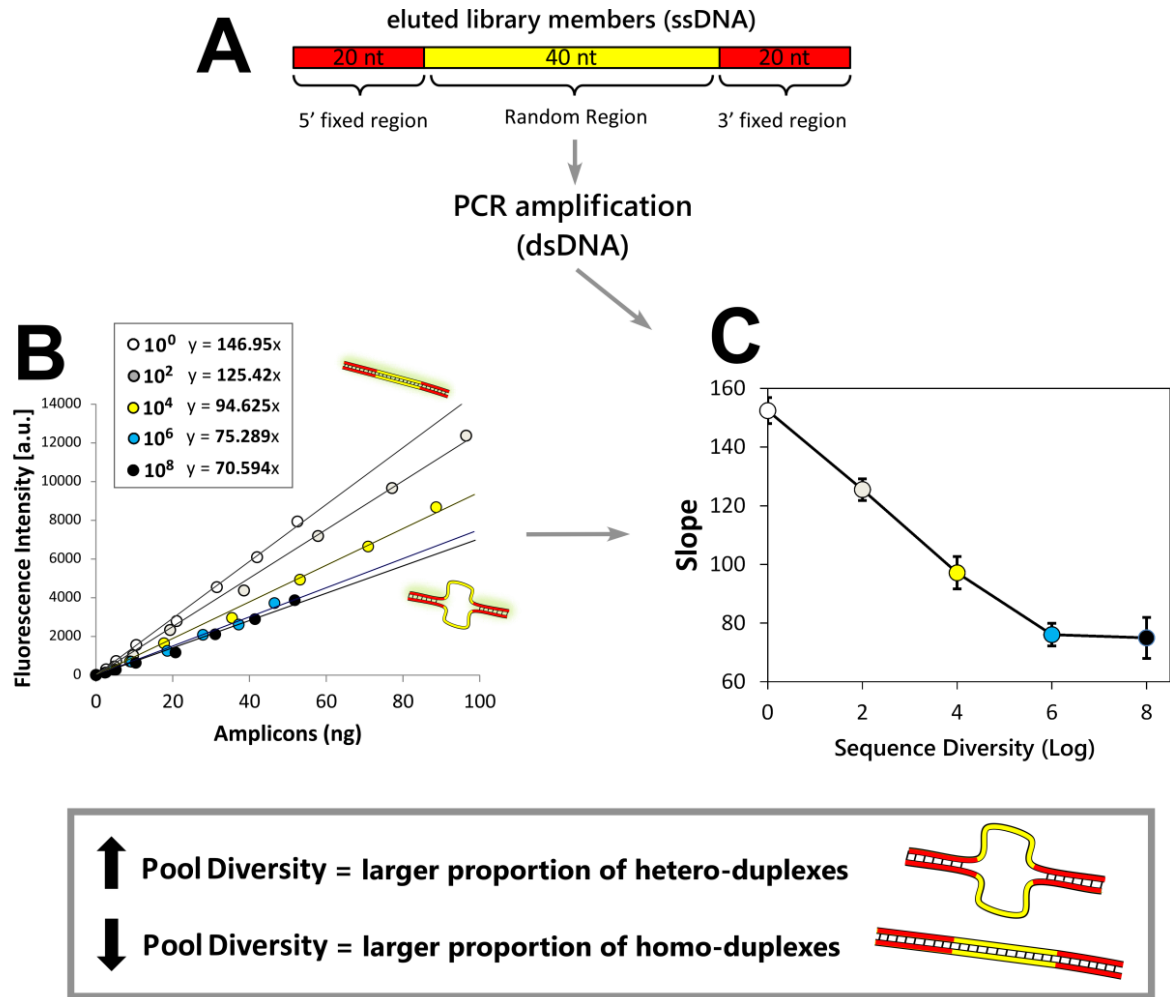


Figure 3-15 Schema and results for the alternative PCR/PicoGreen™ method for quantifying the sequence diversity of a retained aptamer pool. (A) Eluted library members are PCR amplified. (B) Calibration standards (10^8 to 10^0 individual members) generated by PCR amplification are then used to define the slope of fluorescently quantified double-stranded regions (generated by PicoGreen™ staining) of serially diluted amplicons. (C) The sequence diversity of an eluted pool can be quantified using this information. The data show that for library diversities spanning 6 orders of magnitude, the slope is inversely proportional to the sequence diversity due to the increased proportion of hetero-duplexes formed at higher diversities. Standard deviations are reported for slopes quantified by quadruplicate fluorescence readings from duplicate experiments.

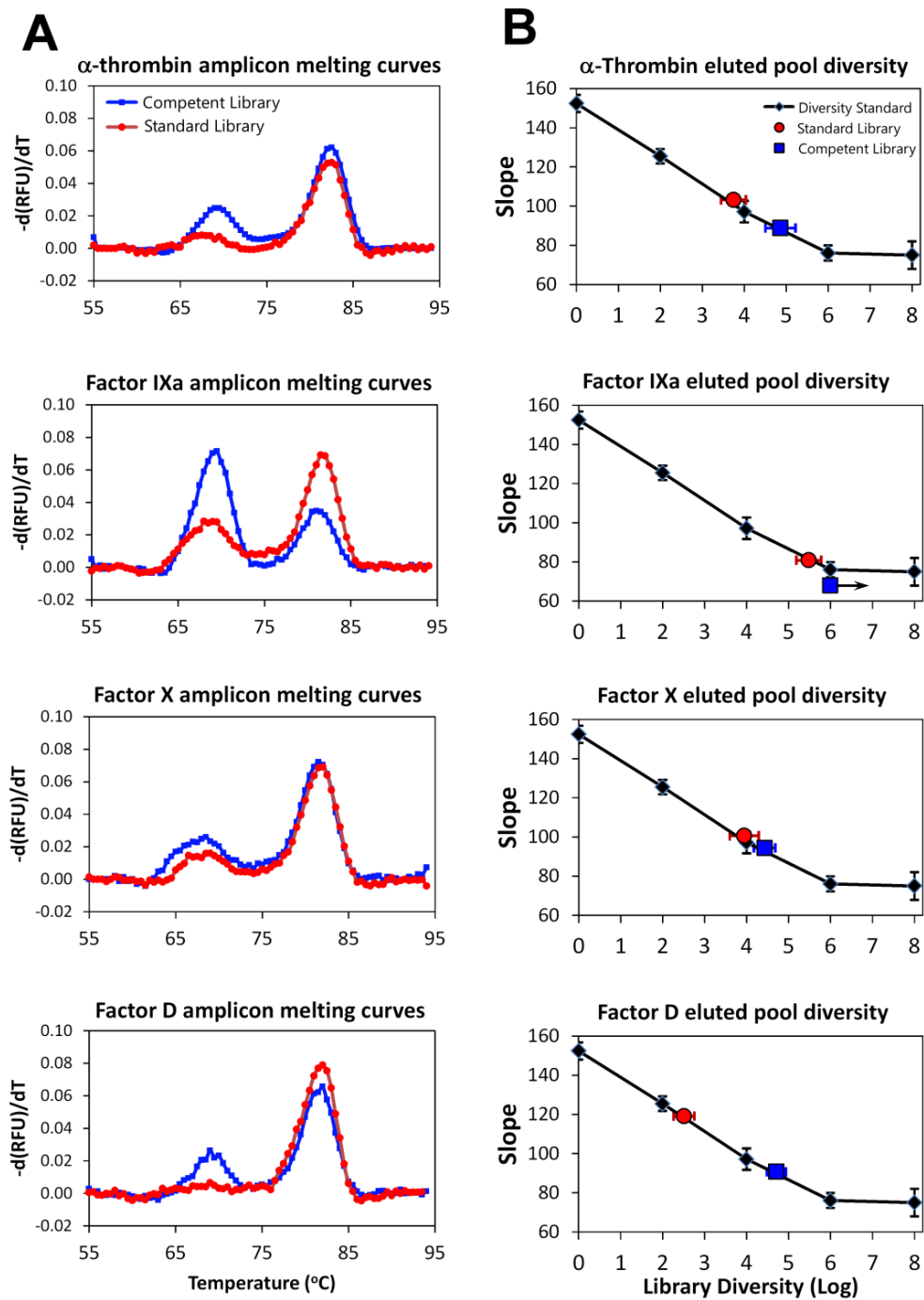


Figure 3-16 Comparison of diversities from eluted aptamer pools selected using competent (blocked) or standard (unblocked) libraries after the third round of Hi-Fi SELEX. (A) Raw data used to estimate pool diversity by the melting curve method defined in **Figure 3-11** and **Figure 3-13**. (B) Quantification of pool diversities by the PCR/PicoGreen™ fluorometric assay described in **Figure 3-15**. Standard deviations are reported for quadruplicate fluorescence readings from duplicate experiments.

The interest here, however, is in the fact that both methods show that three rounds of Hi-Fi SELEX consistently yield a retained pool of greater than 10^4 unique library members offering a mean K_d of < 20 nM. Moreover, while the Hi-Fi selections using standard and competent libraries yield comparable mean K_d values after 3 selection rounds, the sequence diversity of the final library is generally better (never worse, and often much better) when competent libraries are employed, indicating that the use of fixed-region blocking agents increases both the total abundance of functionally active aptamer sequences in the initial library and the overall selection efficiency. These results support recent work where it was shown in independent selections against streptavidin and α -thrombin that the use of a competent library ensures the retention and selection of high-affinity aptamers against these targets that are lost in a standard SELEX screen (**Chapter 2**).³⁷⁶ Together these findings have important implications, especially when considering aptamer selection for the discovery of novel therapeutics, as more diverse libraries of high-affinity aptamers offer a better chance of providing usable lead compounds for further therapeutic development.

3.3.5 FUNCTIONAL APTAMER SCREENING WITHIN THE HI-FI SELEX WORKFLOW PROVIDES A BOTTOM-UP APPROACH TO LEAD COMPOUND IDENTIFICATION

In most SELEX-based strategies employed for aptamer identification, selection rounds are performed until the eluted pool is comprised of a manageable number of unique aptamer sequences exhibiting an acceptable mean K_d . At least a portion of that pool is then serially cloned to produce and sequence the individual aptamers to identify families sharing common sequence and/or fold motifs. Typically, individual representatives from each family are screened for binding affinity and specificity. In more comprehensive studies, the most promising aptamers emerging from the sequence and binding analyses are also screened for functional activity. However, as that cloning process typically represents a

throughput and cost bottleneck, improvements to the speed and success of therapeutic aptamer discovery could be realized by partitioning the retained pool into aliquots of manageable sequence diversity, and then exploiting the fidelity of ddPCR to amplifying each aliquot to produce the $\sim\mu\text{M}$ concentrations needed to screen the aptamers within it for functional activity (i.e. target inhibition or gain-of-function/activity). In this manner, the scope of time-consuming and expensive cloning and sequencing studies can be limited to those aliquots containing aptamers that have been positively pre-screened for the desired biological activity.

Proof of concept of this strategy was applied to aliquots, each comprised of approximately 40 to 60 aptamers, derived from the final retained pool (roughly 25,000 to 50,000 unique aptamers – see **Table 3-5**) competently selected against human complement factor D. Functional screening of ddPCR-amplified aliquots was achieved using an assay in which the amount of C5b,6, generated in a factor D-dependent manner via the alternative pathway C5 convertase, was measured using an erythrocyte hemolytic assay. Thus, in a 96 well plate, a fixed concentration of factor D was preincubated with aliquots of aptamers or individual aptamers isolated from them. This was followed by addition of C3b (Cobra), factor B, and complement factors C5 and C6 in a buffer containing MgCl_2 . The reaction was allowed to proceed for 10 min, during which time the serine protease factor D activates factor B, generating the C5 convertase, C3bBbC3b . This, in turn cleaves C5 in the presence of C6 to yield a stable C5b,6 complex. The amount of C5b,6 was determined by mixing this immediately with a solution containing EDTA, chicken erythrocytes and normal human serum (as a source of the terminal components, C7, C8 and C9), generating the lytic C5b-9 membrane attack complex, the latter measured by release of hemoglobin. A standard curve was generated with known concentrations of C5b,6. Aptamer-mediated suppression of factor D function was reflected by reduced levels of C5b,6 as compared to reactions in which no aptamers were present. Results from one therapeutically promising aliquot are reported here to demonstrate the utility of the strategy, with data from the full panel of aliquots

reserved for a follow-up publication. SPR data indicate that the representative aliquot exhibits a mean K_d that is essentially indistinguishable from that of the final retained pool (**Figure 3-17**). Each aptamer within the representative aliquot was therefore cloned and produced individually in amounts needed to determine sequence, factor D binding affinity and activity suppression, and binding specificity as defined by the affinity of the aptamer to human serum albumin (HSA).

In this manner, several aptamers that suppress factor D activity (complement activation) by at least 40% were discovered within the representative aliquot. Their sequences and M-fold predicted secondary structures are reported in **Table 3-6** and **Figure 3-18**, respectively. The top three inhibitors (clones 19, 28 and 29) within the aliquot were selected for further characterization. For each full-length library member, the K_d for binding to factor D was shown by the qPCR assay described in this work to be better than 20 nM (**Figure 3-19A**), with that for clone 19 being sub-nM. That strong affinity was confirmed by isothermal titration calorimetry ($K_d = 0.714 \pm 0.247$ nM), which further showed that binding occurs in a 1:1 stoichiometry ($n = 0.95$) and is driven both enthalpically ($\Delta H = -8.25$ kcal mol⁻¹) and entropically ($T\Delta S = 4.29$ kcal mol⁻¹), a result that has been reported by Croy et al. to suggest that binding affinity is established through a combination of coulombic forces, favourable hydrogen bonds, and hydrophobic interactions.⁴⁰⁷ The specificities of the full-length version of the selected clones were also investigated using affinity for HSA as a metric of non-specific binding. While clones 19 and 29 exhibited no appreciable affinity for HSA, clone 28 did (145.7 ± 14.1 nM) (**Figure 3-19B**). Clone 28 (as well as clone 5/14 which showed a weak affinity for factor D) was therefore rejected as a factor D specific aptamer, a conclusion that is supported by its secondary structure which M-fold predicts lacks the apparent bulge-loop motif common to clones 19, 29 and other aptamers in the aliquot exhibiting anti-factor D activity (**Figure 3-18**).

Table 3-6 Core (random region) sequences of the top factor D-mediated inhibitors of complement activation (alternative pathway) recovered from the demonstration aliquot containing 40-60 of the unique aptamer sequences within the final retention pool after 3 rounds of Hi-Fi SELEX. Each isolated sequence (clone) reported in the Table are listed in order of % inhibition observed^a

Clone number	Core region sequence (5' – 3')	Factor D Inhibition
28	ACGGAGAAAGAGAGAGTGTAATTGCTAGCATAACCGCTGC	56 %
29	GTAACCACGTTGCCAGACCGAGTCTACCAGCGATCCTCAG	51 %
19	TATGCCCAAATCCCTCAAGTCGGCCAGGATACACCACCGT	44%
21	AATCAAAAGGCTCACGCGGGATTGGTCAACCTTACAACC	39%
35	TCGGCCTTCCCAGACCACCGCAATCCCCAGGGAACAGGCA	36%
13	CATCACACTGTCAACATACCCAGCCTGGGGAAAGACGAAC	35%
36	AACCCGCATGCCGATCGATGTCGTGCCTCGCTCCACGCTC	33%
12	ACCAGGCACCCGACGGACTAACTCATCACTCAGGCGAGGG	33%

a: Inactivation assay was performed using full-length (library) sequences

Finally, the binding affinity of the consensus sequences (**Table 3-7**) of clones 19 ($K_d = 0.627 \pm 0.157$ nM) and 29 ($K_d = 5.44 \pm 0.42$ nM) was investigated by ITC to verify that aptamer fold and function were indeed localized to the random region of the library.

Table 3-7 Isothermal titration calorimetry (ITC) data for binding of human factor D to either the full-length (full length) library sequence or the random-region (truncated) sequence of clones 19 and 29. Standard deviations for fitting both the equilibrium binding affinity and enthalpy are reported.

Aptamer	<i>n</i>	K_d (nM)	ΔH (kcal mol ⁻¹)	$-T\Delta S$ (kcal mol ⁻¹)	ΔG (kcal mol ⁻¹)	
Clone 19	<i>Full Length</i>	0.95	0.714 ± 0.247	-8.25 ± 0.06	-4.29	-12.54
	<i>Truncated</i>	0.90	0.627 ± 0.157	-6.26 ± 0.04	-6.32	-12.58
Clone 29	<i>Full Length</i>	0.93	4.55 ± 0.46	-5.87 ± 0.03	5.52	-11.39
	<i>Truncated</i>	0.95	5.44 ± 0.42	-7.47 ± 0.07	3.82	-11.29

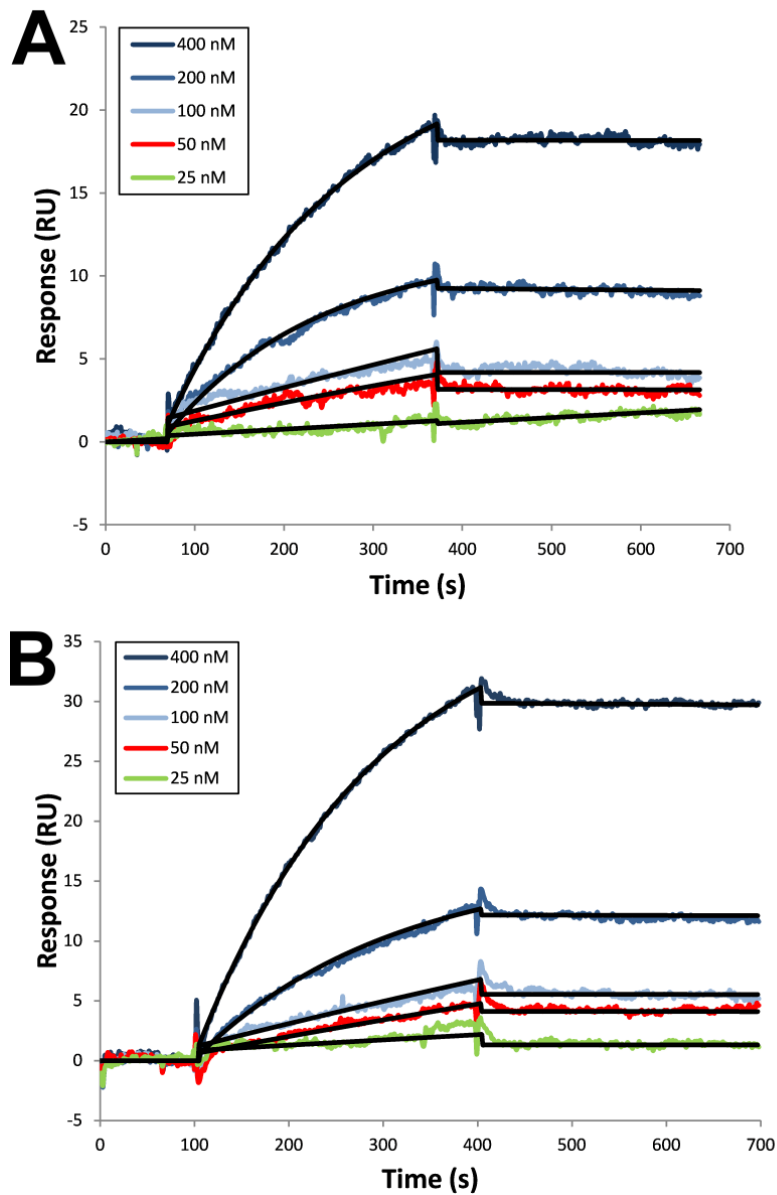


Figure 3-17 SPR sensorgrams for binding of human factor D to immobilized biotinylated aptamers from (A) the entire round 3 pool ($K_d = 1.17 \pm 0.63$ nM) or (B) the representative factor D inhibiting aliquot generated from that pool and containing 40 – 60 unique aptamer sequences ($K_d = 0.97 \pm 0.43$ nM). Experiments were performed on a Biacore 3000 using an SA chip. Several concentrations of Factor D were injected, and the results fitted to a 1:1 Langmuir isotherm.

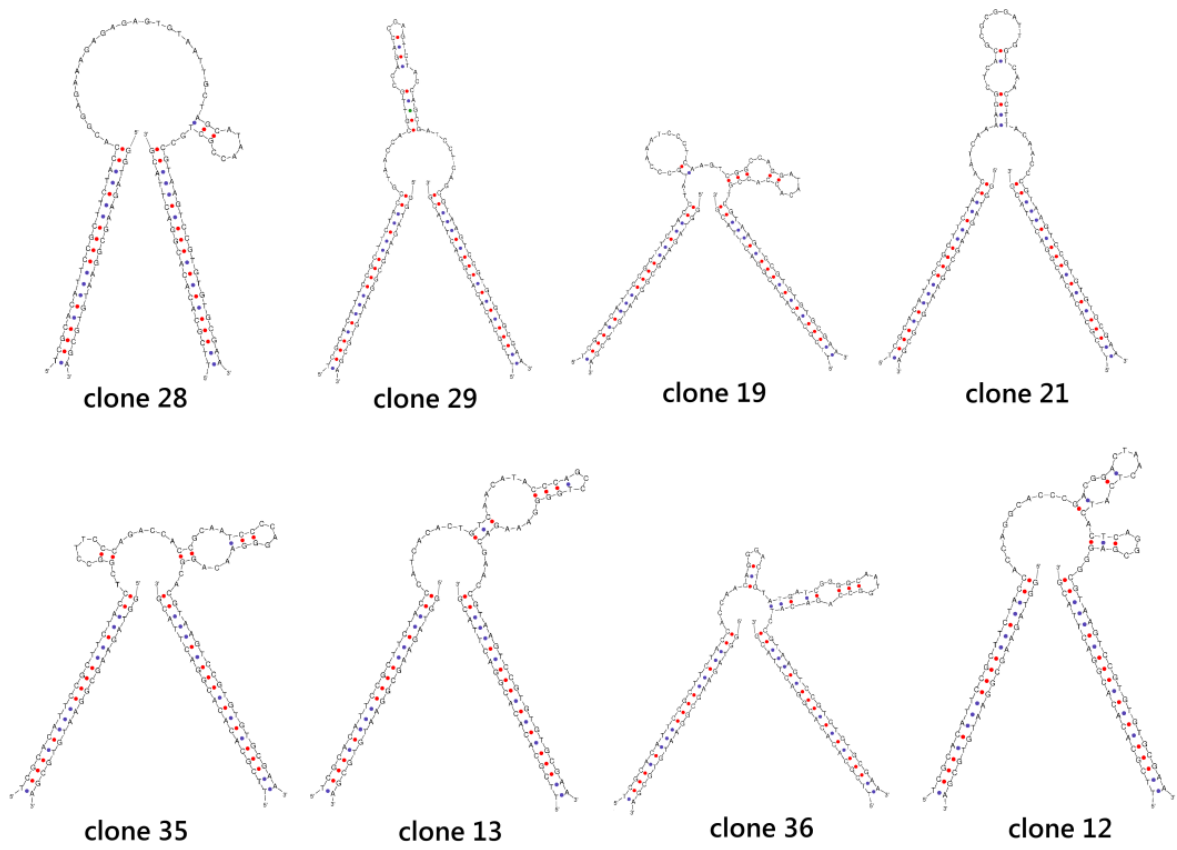


Figure 3-18 M-fold predicted secondary structures for the full-length blocked aptamers sequences in Table 3-6. Several of the clones exhibit a common bulge-loop motif.

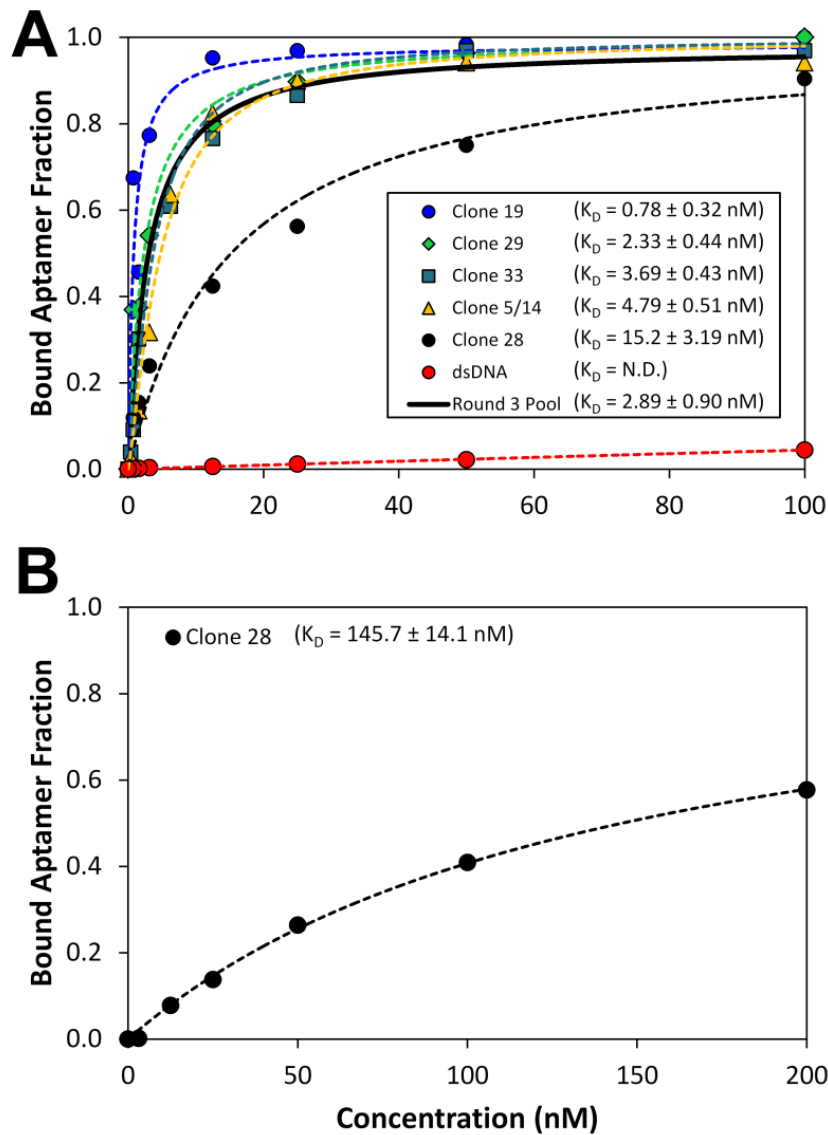


Figure 3-19 Human factor D binding affinities and specificities of individual aptamers (library form) competently selected in three rounds of Hi-Fi SELEX and present in a small aliquot containing 40 to 60 of the retained library sequences that together inhibit factor D mediated activation of complement. (A) Binding affinities were measured using the full-length library form of the aptamer sequence. The binding isotherm for an 80 bp double-stranded DNA is also shown as a negative control. (B) Specificities measured using binding affinity to human serum albumin (HSA) as a metric. Data are reported for clone 28, as it was the only aptamer (library form) showing a measurable affinity for HSA.

3.4 CONCLUDING REMARKS

A new platform, Hi-Fi SELEX, for DNA aptamer selection was presented and its performance in efficiently isolating pools of aptamers exhibiting order-nM binding affinity against three different therapeutically-relevant targets was reported. Hi-Fi SELEX distinguishes itself from other SELEX-based technologies in a number of ways. First, it presents the library in a unique form that maximizes the diversity of functional aptamer sequences displayed in the starting library by eliminating common mechanisms by which the two common flanking sequences can interfere with aptamer fold and function. It then displays the target on a novel chemically modified surface that eliminates nearly all selection artifacts related to non-specific adsorption of aptamers, as well as to bridging of aptamers between proximal target molecules. This eliminates the traditional requirement in SELEX to pre-screen a starting library against the selection surface bearing no target (which is expected to eliminate non-specifically binding members), and thereby maximizes the sequence diversity of the starting pool of library members. Very high stringency washing of bound aptamer pools with a solvent of high ionic strength relative to the selection buffer is used to selectively retain in each selection round $10^7 - 10^8$ distinct aptamers whose binding affinity to the target is not solely driven by coulombic forces. Digital PCR, optimized for application to retained pools of aptamers having high sequence diversity, is then used to achieve very high fidelity amplification by eliminating mis-priming events that plague bulk PCR of aptamers. Moreover, each amplicon produced is comprised of fully complementary duplex DNA, in which it was shown to be essential to proper stoichiometric conversion of amplicons by λ -exonuclease into the corresponding ssDNA aptamer library needed for the next selection round and functional studies. Novel qPCR-based assays are described and integrated into the Hi-Fi SELEX workflow to permit rapid and inexpensive determination of the mean K_d and sequence diversity after each selection round, thereby creating a safeguard against over-selection. Thus, while other selection platforms (e.g., CE-SELEX³⁰⁴, QPASS¹⁷¹) designed to improve therapeutic aptamer

selection have recently been described, none provides the combined advantages of Hi-Fi SELEX. Finally, the potential value in screening small aliquots of retained aptamers for putative therapeutic activity as a means of reducing the total number of candidate sequences that must be cloned, then produced, sequenced and functionally evaluated in pure form was demonstrated.

Chapter 4

PARALLEL MICROFLUIDIC SURFACE PLASMON RESONANCE IMAGING ARRAYS

“Today’s science is tomorrow’s technology”

— Edward Teller (1962)⁴⁰⁸

4.1 SYNOPSIS

This chapter describes the development and application of novel microfluidic arrays for surface plasmon resonance imaging (SPRi), a label-free technique that may be used for the quantitation of binding affinities and specificities for a wide variety of target molecules. The method offers the ability to quantify both the equilibrium binding constant and the kinetics of such interactions, which are of particular importance, especially when screening panels of potential therapeutic aptamer or antibody lead compounds. Surface plasmon resonance (SPR)^{409,410} is a widely used surface-sensitive method for biomolecular interactions analysis (BIA). It is an optical technique that detects molecular binding events at a metal (typically gold) surface by measuring changes in the local refractive index upon mass loading of the sorbate via complex formation with the immobilized target molecule.⁴¹¹ Using this optical signature, SPR can provide real-time label-free detection of

binding kinetics and total mass loading by either monitoring reflectance as a function of time or by monitoring the angle of minimum reflectance as a function of time.⁴¹²

By combining spectral SPR with multiplexed detection, surface plasmon resonance imaging (SPRi)^{413,414} offers the potential for high-throughput binding affinity and specificity studies.⁴¹⁵⁻⁴¹⁷ A CCD detector (camera) outputs microscopic images of the SPR array as a function of time, enabling near real-time monitoring of parallel binding events. SPRi has been used as a detection tool for analyzing DNA hybridization,^{418,419} DNA-RNA binding,⁴²⁰ DNA-protein binding,^{421,422} aptamer-protein binding,⁴²³ and antibody-antigen binding,^{424,425} as well as for detection of proteins in whole blood⁴²⁶ and drugs in saliva specimens.⁴²⁷ Although the most widespread use of SPRi relies on the original Kretschmann optical configuration,⁴²⁸ other plasmonic sensors such as nano-hole arrays^{429,430} are often employed as means to improve throughput. However, these various SPRi strategies, including commercial SPRi instruments, are currently limited to analysis of a single analyte in the fluid stream passed across multiple immobilized ligand registers.⁴³¹ The throughput and versatility of SPRi systems therefore could be improved by creating technology that enables multiplexing of both the surface immobilized targets and the analytes presented in the flowing solution phase. When applied to affinity reagents discovery, this would permit candidate antibodies or aptamers to be arrayed in a surface immobilized form, and subsequent sequential SPR analyses of their individual binding reactions both with the target and with any suitable number of competing analytes so as to probe binding specificity. Moreover, with the publishing of the human genome sequence and the corresponding ever increasing discovery of biomarkers of human disease, high-throughput techniques for measuring biomolecular interactions in a label-free cost-effective fashion are increasingly required.^{415-417,432,433}

SPRi throughput can be improved by forming robust, reproducible arrays of biomolecules on sensors. For example, micro-spotting technologies such as pin printers have been employed in a manner analogous to their widespread use in DNA microarray platforms. However, creating required flow architectures post-spotting can be problematic, and the method generally requires expensive robotic equipment.⁴³⁴

Alternatively, microfluidics has the potential to increase SPRi throughput while retaining a greater level of cost-efficiency by utilizing inexpensive materials and through its inherent ability to reduce the volumes of ligand and analyte required to perform a binding assay. In addition, microfluidic technologies have been demonstrated to accelerate analysis in part due to their smaller footprint, effectively reducing diffusion distances^{435,436} in volumes that permit a better control over the reaction conditions.⁴³⁷ Greater reproducibility and precision are enabled via automated computer-controlled manipulations.⁴³⁸

The integration of SPRi and microfluidics systems has been demonstrated.^{417,425,431,439-443} One-dimensional SPRi microarrays with continuous-flow microfluidic channels on gold-coated glass fabricated in PDMS were first developed and demonstrated for detection of DNA hybridization.⁴⁴⁴ While this approach significantly reduced sample consumption and reaction times, the architecture used only a single set of parallel microchannels, preventing the addressability of individual sensors. Subsequent work using a two dimensional crossed-flow architecture with dedicated valves for each channel intersection to prevent cross-talk between horizontal or vertical channels has somewhat addressed this limitation.⁴³³ In particular, the approach adds an additional level of control, but microchannels are still dedicated to the same analyte stream. Thus, none of these devices allows for simultaneous interrogation of multiple analyte (sorbate) concentrations. Similarly, commercial high-throughput SPR instruments employ either a cross-flow channel geometry, such as Bio-Rad's ProteOn XPR36,⁴⁴⁵ or a

flow-cell based system that permits many ligand spots (up to 400 with Biacore's FlexChip)⁴⁴⁶ but can only interrogate a single analyte in a single experiment.

To address these challenges, an integrated microfluidic array was developed using soft lithography techniques that enable both creation of element-addressable ligand spots and their parallel SPRI-based detection across different analyte concentrations. The device consists of an array of 264 chambers; each of these isolated 700 pL reaction volumes is independently addressable by integrated microvalves. Further functionality is provided by the integration of a serial dilution network that enables simultaneous interrogation of up to six different analyte concentrations without requiring lengthy surface regenerations. Controlled recovery of rare samples for downstream analysis is also facilitated by the use of integrated microvalves.

Here, details of the device design and fabrication are reported along with proof-of-concept studies demonstrating its utility as a tool for multiplexed analysis of the binding properties of affinity reagents. Device performance was initially validated by interrogating human α -thrombin immobilized on the sensor surface against an anti-human α -thrombin IgG, simultaneously injected across the surface at different concentrations. The resulting equilibrium dissociation constant was determined to be 5.0 ± 1.9 nM, which agrees well with values reported in the literature for this antibody. The ability to interrogate multiple mAbs in a single device was then investigated to verify the technology's capability as a general affinity-reagent screening tool. Those studies show not only that accurate binding data can be obtained, but also that samples/analytes of interest can be recovered without cross-contamination. By virtue of its dynamic nature, the microfluidic array is capable of interrogating binding events for up to 264 different immobilized ligands against multiple analytes in a single experiment. The novel microfluidic device presented here therefore allows simultaneous interrogations of multiple ligands against different analytes at different concentrations in parallel.

4.2 EXPERIMENTAL METHODS

4.2.1 CHEMICALS AND REAGENTS

All chemicals and reagents were obtained from commercial sources: Streptavidin and fluorescein from Sigma-Aldrich (Oakville, ON, Canada); biotinylated human α -thrombin, human α -thrombin, human factor IX, anti-human α -thrombin monoclonal antibody and anti-human factor IX monoclonal antibody from Haematologic Technologies, Inc. (Essex Junction, VT); phosphate-buffered saline (PBS) at pH 7.4 from Invitrogen (Burlington, ON, Canada); Shipley SPR220-7 positive photoresist from MicroChem (Newton, MA); PDMS RTV 615 from GE Silicones (Waterford, NY); type TFA gold etchant and type 1020 chromium etchant from Transene Company Inc. (Danvers, MA).

4.2.2 DEVICE DESIGN OVERVIEW

The mask design used for the fabrication of the SPRi chip was adapted from previous work in the Quake laboratory⁴⁴⁷ and is presented in **Figure 4-1**. The device is composed of two layers fabricated using polydimethylsiloxane (PDMS) soft lithography.⁴⁴⁸ The lower layer (flow layer) has microchannels of 100 μm width by 10 μm height where the biomolecular interactions occur. The upper layer (control layer) contains 1132 microvalves (100 μm wide and 150 μm long) that are used to isolate and control the flow of fluids beneath. This layer also contains a micropump that can pump fluid throughout the chip. The chip contains an array of 264 chambers divided into 11 groups of 4 chambers per group. There are 6 stacks (columns) in total on the chip. Each stack has a dedicated flow channel for introduction of channel, which is then subdivided into flow channels for each of the 11 groups within the stack. To control the loading of an individual chamber, a row multiplexer gates the entrance of fluid to a specific group of 4 chambers. A series of 4 chamber valves are then opened or closed to allow loading of a specific

chamber within the group. Upon loading a ligand through the sample input port, fluid flows into the chamber array for loading into a specific chamber. Once loaded, all chamber valves are closed and remaining sample can be flushed to the sample output port via a wash loop. This procedure enables up to 264 different samples to be injected in the system, each in a separate element-addressable chamber.

To perform a binding assay against any of the immobilized ligands, the analytes are injected through the sample port. An analyte can either be introduced directly to a specific chamber or it can be serially diluted via a parallel continuous-flow serial dilution network adapted from work first presented by the Whitesides group.⁴⁴⁹ The on-chip dilution network has two input fluid lines, one for the analyte and the other for the diluent (loaded through the diluent input port). This network contains six parallel channels, five of them containing chaotic advection micromixers.⁴⁵⁰ These micromixers are composed of three sets of 10 chevrons (50 μm width, 4 μm height) in a 200 μm width by 10 μm height square microchannel. The spacing between each chevron in a set is 50 μm , and the spacing between each of the three chevron sets is 400 μm . These five mixers ensure rapid and uniform mixing of sample and diluent. A portion of the diluted sample proceeds directly into the chamber array while the remaining portion is further diluted in a cascade-like fashion, achieving a dynamic range of 32. Upon exiting the dilution network, the analytes are loaded in all chambers of their respective stack. Since there are six dilution channels and six stacks of 44 chambers (11 groups of 4 chambers each), the first stack will contain the undiluted sample, and the last stack will contain the most diluted sample.

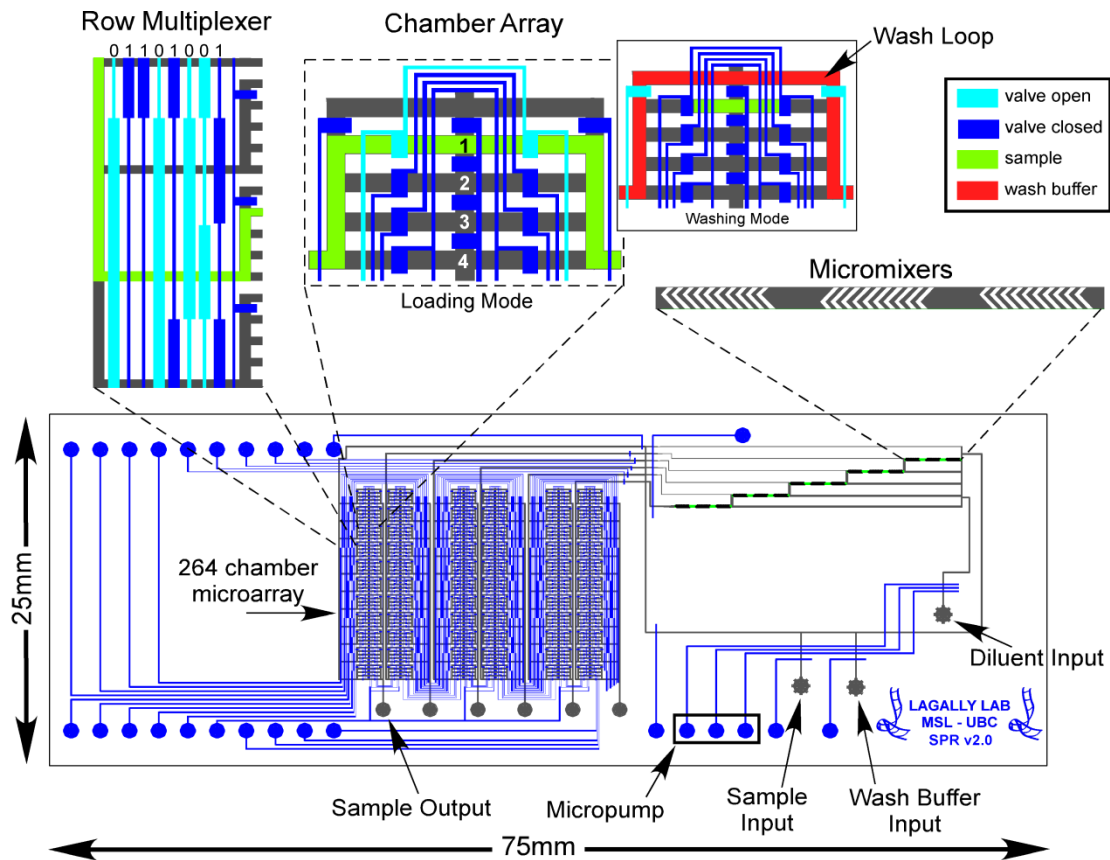


Figure 4-1 Mask design of the microfluidic device. The chip consists of a top control layer and a bottom flow layer. The array consists of 264 individually addressable chambers, each with a volume of 700 pL. The row multiplexer (top left) selects a particular group of 4 chambers by setting a 4-bit gray code. Sample is then loaded into a particular group of chambers. The selected group of chambers (top middle) is divided into 4 individual chambers by a series of compartmentalization valves. Here, the valves of chamber 1 are opened to let sample through. After loading the sample, the device operation switches to washing mode, in which all chamber valves are closed and the wash loop is opened. Wash buffer is introduced, flushing any remaining sample in the channel. A series of micromixers (top right) allow serial dilutions of samples into 6 different concentrations.

4.2.3 MICROFABRICATION

The PDMS device was fabricated using standard soft-lithography procedures as described elsewhere.⁴⁵¹ SF-10 glass substrates (25 mm X 75 mm X 1.1 mm, Specialty Glass Products, Willow Grove, PA) were cleaned and a 47.5 nm gold layer was sputtered onto a 5 nm chromium adhesion layer (UHV Sputtering Inc., Morgan Hill, CA). Prior to use, the gold-coated slides were first cleaned by immersion in acetone, followed by isopropanol, followed by rinsing with Nanopure water

(18 M Ω -cm) and drying in a N₂ stream. Following cleaning, photoresist was spin-coated at 5000 rpm for 40 s and baked for 2 min on a hotplate at 115°C. The film was left to relax for 30 min at room temperature before being exposed with the gold pattern mask using a contact aligner (Canon PLA-501F). A post-exposure bake step was performed for 2 min on a hot plate at 115°C. The film was left to relax at room temperature for 30 min before developing (MF-24A Megaposit Developer) for 2 min. The gold slides were then etched to create the gold spots by sequential immersion in gold and chromium etchant for 17 s and 2 s, respectively, before being rinsed extensively with Nanopure water. The gold spots were revealed by cleaning the slides in acetone to dissolve the photoresist, followed by a wash in piranha solution (5:1 H₂SO₄:H₂O₂) at 80°C for 15 min. Both the PDMS chip and the gold-patterned glass slide were exposed to UV-Ozone (UVO-Cleaner, Model 42, Jelight Co. Inc., CA) for 5 min before being irreversibly bonded (**Figure 4-2**).

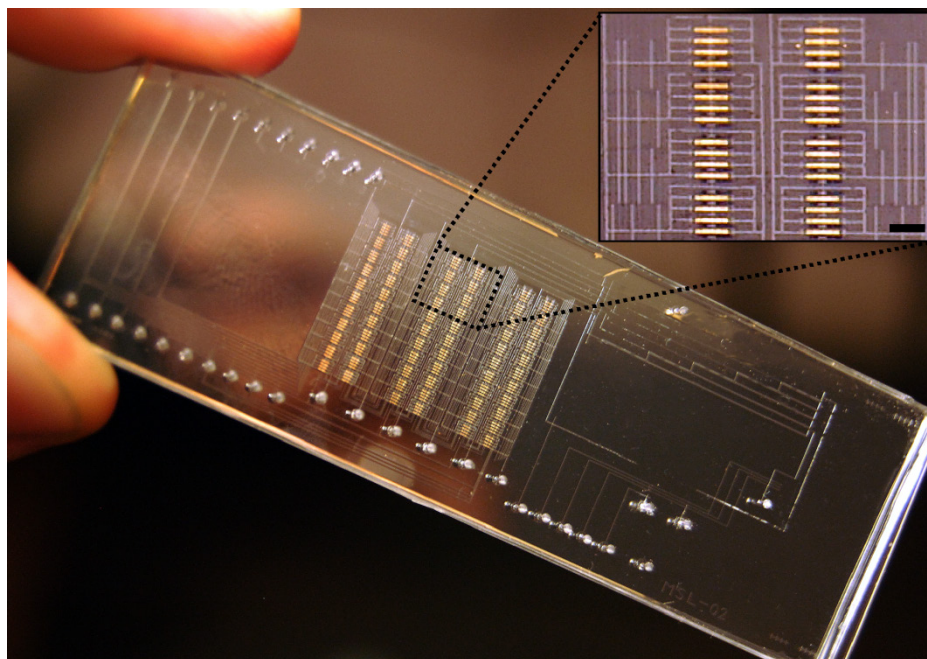


Figure 4-2 Photograph of the microfluidic chip bonded to a gold patterned glass slide. (Inset) A close-up of the marked region of the microarray; scale bar: 650 μ m.

4.2.4 INSTRUMENTATION

A custom-made solenoid valve controller with 32 valves was used to actuate the PDMS microvalves and drive fluid flow throughout the chip. The controller was driven by LabVIEW software (National Instruments, Austin, TX). To detect the biomolecular reactions within the chambers of the device by SPRi, a custom SPRi instrument was fabricated. The chip was placed on a layer of refractive index matching fluid ($n_d = 1.7300$, Series M, Cargille Labs, NJ) on the surface of an equilateral SF10 glass prism. An incoming collimated p -polarized LED light beam ($\lambda = 626$ nm) passed through the prism and illuminated the surface of the chip. The reflected light was then filtered and collected by a CCD camera. The CCD camera and associated optical components were attached to one of two optical rails, which were controlled by two superimposed motorized rotation stages. The prism was fixed in place between the two optical rails using a custom prism mount. The two rotation stages were driven by a stage controller that adjusted their positions *in-sync*. The entire setup was constructed in an upright position in order to facilitate the use of microfluidic chips.

4.2.5 SPRi MEASUREMENTS

After bonding the PDMS chip to the gold-patterned substrate, PBS buffer was loaded in the wash buffer input port and injected for 5 min to prime the gold surface and to achieve a stable baseline measurement. Subsequently, a 15 μ M solution of streptavidin in PBS buffer was loaded in the sample input port and incubated on the gold spots for 10 min, followed by rinsing with PBS buffer to remove any unbound protein. A 15 μ M solution of biotinylated human α -thrombin in PBS was next immobilized on the streptavidin using the method above. Following immobilization, dilutions of a 3.3 μ M solution of anti-human α -thrombin

IgG in PBS buffer were flowed across the surface and rinsed with PBS buffer as previously described. The binding process was monitored in real-time and the results analyzed with BIAevaluation software (Biacore GE Health Sciences, Piscataway, NJ). The digital images were taken at equilibrium and numerically processed using Image J.⁴⁵²

4.2.6 SAMPLE RECOVERY

Both anti-human factor IX and anti-human α -thrombin monoclonal antibodies were fluorescently labeled using the DyLight 488 and DyLight 594 microscale labeling kits, respectively, following the manufacturer's instructions (Pierce, Rockford, IL). Glycerol was first dialyzed from the antibody solutions prior to labeling using 20K MWCO dialyzing columns (Pierce, Rockford, IL) for 1 hr in 1 L of Nanopure water. A 10 μ M solution of human factor IX in PBS was first immobilized into 44 element-addressable chambers in the microfluidic SPRi chip by physical adsorption to the gold spots for 10 min. Following this incubation, the sample input port was washed for 10 min with PBS and a 15 μ M solution of human α -thrombin in PBS was immobilized into 44 different element-addressable chambers using the same method. Fluorescently-labeled antibodies were continuously injected in the device and left to interact with their respective immobilized proteins for 10 min by selecting the corresponding set of chambers. The remaining IgG sample was collected at the output of the device after the 10 min incubation. Next, all chambers were purged with PBS for an additional 10 min to remove any unbound antibodies and the sample was collected at the output of the device. In order to recover the bound fraction of antibodies, a regeneration solution of 50 mM NaOH (25 °C) was injected, and the eluted fraction was collected at the output of the chip. The immobilization, binding and regeneration processes were all monitored in real-time using SPRi. Fluorescent measurements for every fraction were recorded using a fluorescence plate reader (Tecan Infinite M200,

Tecan Systems Inc., San Jose, CA) in a volume of 10 μL per well in a 384-well black glass bottom plate (Nunc, Rochester, NY).

4.3 RESULTS AND DISCUSSION

4.3.1 MICROSYSTEM DESIGN AND PERFORMANCE

The microfluidic device presented here was designed to allow simultaneous interrogations of multiple ligands against different analytes at different concentrations in parallel. The dimensions of the 264 chamber microarray presented in **Figure 4-1** were selected to maximize the number of chambers within the size constraint exerted by the area of the prism of the SPR imager (25 x 25 mm). The flow velocity used to perform the SPR measurements was controlled at 3.5 mm s^{-1} ($12.6 \mu\text{l h}^{-1}$), resulting in a significant reduction in reagent consumption compared to traditional immunoassays.⁴⁵³ Compared to methods that employ molecules such as thiols to functionally modify entire gold surfaces, the use of patterned gold substrates allows the use of simple glass-to-PDMS bonding methods, while still providing a suitable bare gold sensor surface for SPR measurements inside each individual chamber.

4.3.2 MICRODILUTION NETWORK

The functionality of the serial dilution network was tested by injecting 45 mM fluorescein (FITC) at the sample input port and ddH₂O at the diluent input port. Both fluids entered the dilution network and were mixed together by the chaotic advection micromixers present in the channels. A portion of the fluorescent dye was routed towards the chamber array, while the remaining portion was further diluted in a cascade-like fashion until the last channel was reached. This design achieves a 1:1 mixing ratio at each stage of the dilution network. The concentration of FITC is therefore reduced by one half at every step, yielding a dynamic range of

2⁵. **Figure 4-3** presents the fluorescence images of all six chamber stacks. Image analysis shows exponentially-decreasing concentrations of FITC loaded in the chamber array. The average intensities for all 4 chambers were calculated and agree well with the theoretical predictions. The small uncertainty (relative standard deviation = 0.092) for each measurement indicates a high reproducibility for the formation of serial dilutions, and is due to the tight control over the amount of sample and diluents injected in the device.

4.3.3 PROOF-OF-CONCEPT: α -THROMBIN IMMUNOASSAY

A human α -thrombin immunoassay was conducted to investigate the ability of the chip to detect binding events and to yield reliable kinetic information. The element-addressability of the chip was exploited in these experiments, as the immobilization of biotinylated human α -thrombin was performed sequentially in a pre-defined pattern (**Figure 4-4A, D**). Anti-human α -thrombin was injected at different concentrations over the entire sensor surface and allowed to react with the immobilized protein (**Figure 4-4B**). An image subtraction process ensured that the intensity of the signal detected was solely due to IgG binding to thrombin by removing background signal. The difference image (**Figure 4-4C**) clearly demonstrates the binding of the antibody. Moreover, the serial dilution loading pattern described above is clearly represented, with exponentially decreasing concentrations from 1.3 μ M to 42 nM. An intensity profile of the marked region (**Figure 4-4C**) is graphically represented in **Figure 4-4E** with the binding intensity varying as a function of IgG concentration.

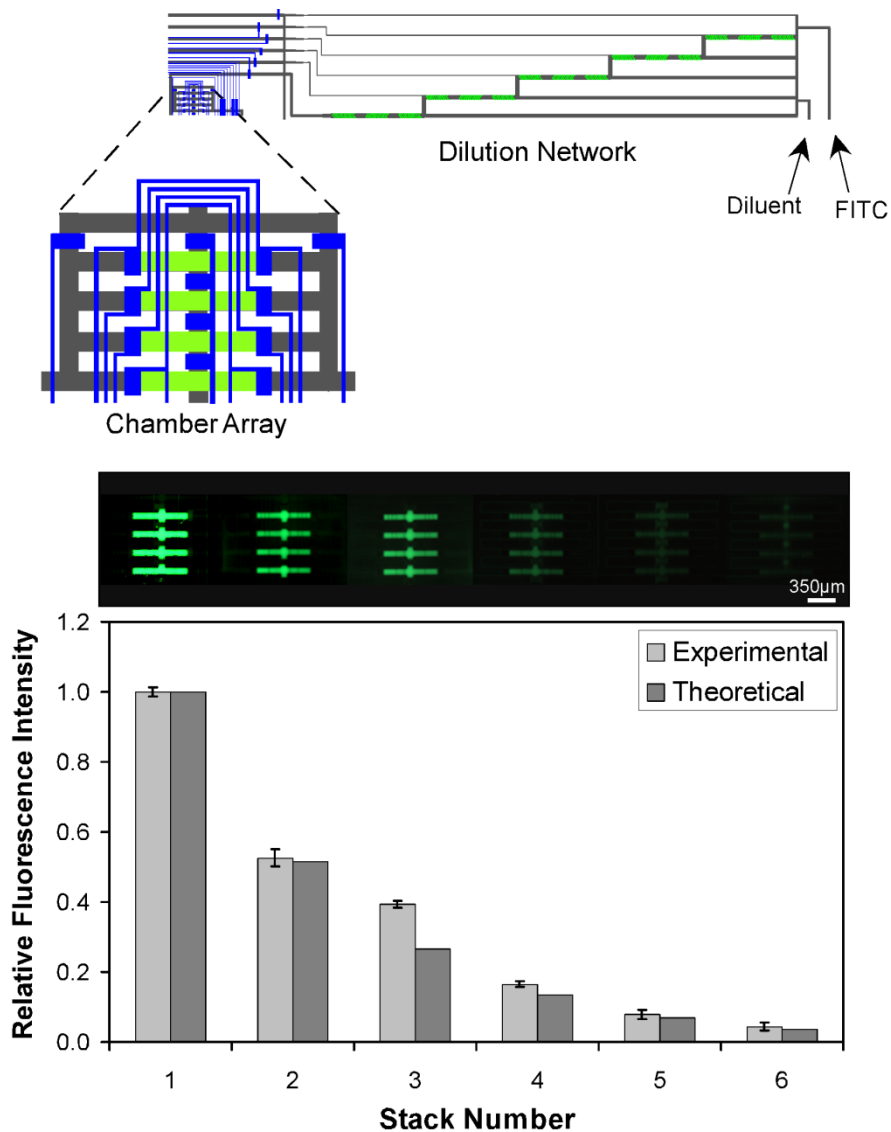


Figure 4-3 Serial dilutions from the chaotic advection micromixers on the chip. Top: schematic diagram of the serial dilution network. Bottom: fluorescence images and intensities of six different concentrations of fluorescein created by the dilution network from a stock solution of fluorescein (45 mM). The mean intensity of fluorescence was determined for all 4 chambers within a group.

Real-time binding kinetics of immunoreactions was recorded using SPR imaging. **Figure 4-5** presents sensorgrams for the binding kinetics of anti-thrombin IgG to surface immobilized thrombin on the gold spots indicated in **Figure 4-4C**. Because the concentrations of antibodies used were higher than earlier

experiments, sudden increases and decreases in the signal are observed. One stack of the chip was loaded with 1X PBS buffer as a baseline subtraction reference. Regions of interest (ROIs) of a consistent size were selected around the gold spots for each concentration. The signals were acquired at 1 Hz and were time-averaged using a moving window average of 4 s in order to improve the S/N ratio. The association was left to equilibrate for 10 min before washing the unbound antibodies with PBS buffer for the dissociation phase. Individually fitted curves are shown for every concentration and the quality of the fit is highly satisfactory, with residuals fluctuating closely around zero (**Figure 4-6**). Based on this result, the Langmuir monovalent binding model used to fit the curves accurately represents the binding interaction observed between the antibody and thrombin. Furthermore, no mass transfer effects are observed in the data, further validating the design of this device to yield reaction rate-limited kinetics. The equilibrium dissociation constant was determined from the fitted curves and was found to be 5.0 ± 1.9 nM. This value is within the same order of magnitude as specified by the manufacturer (14 nM).⁴⁵⁴

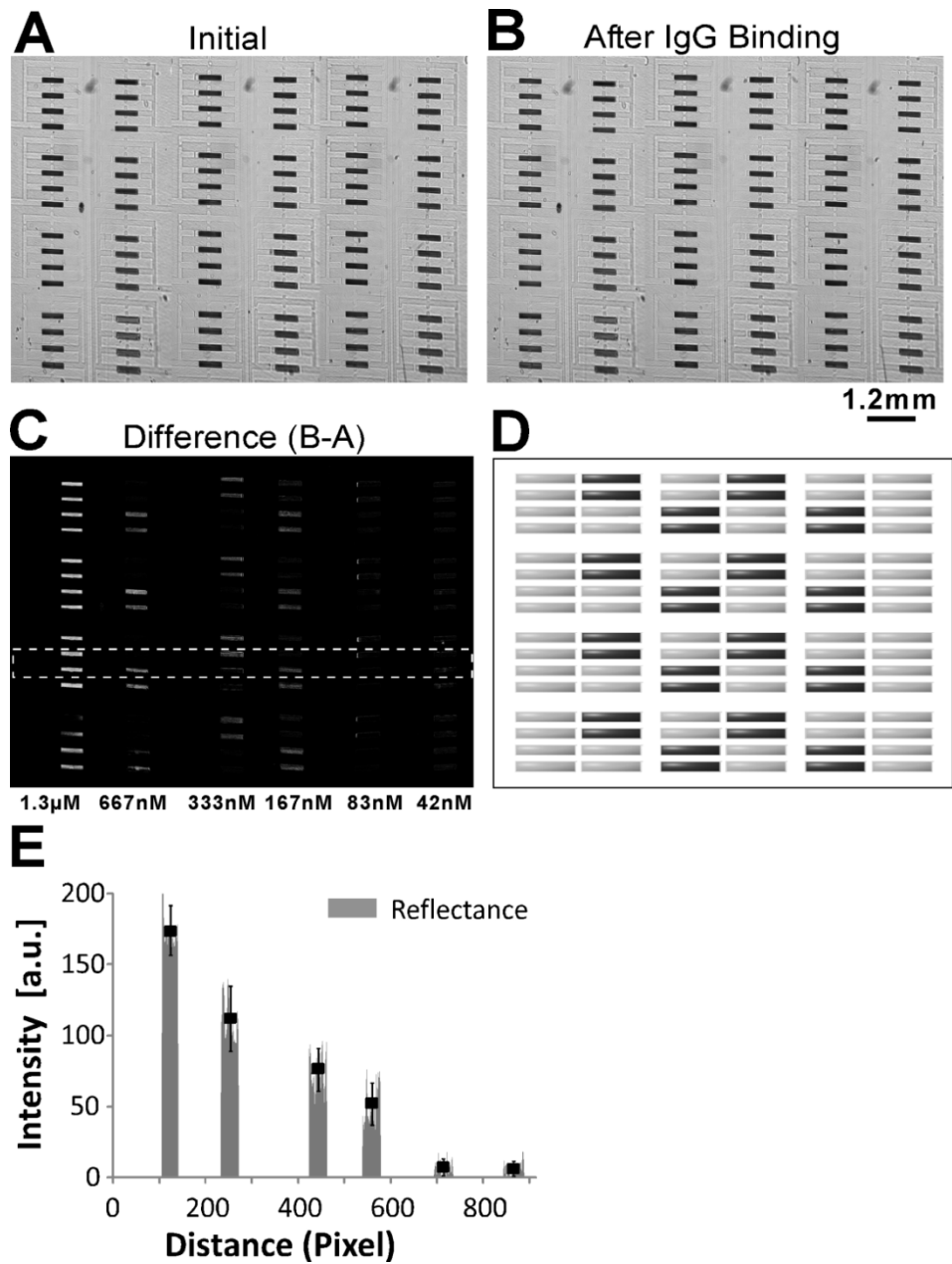


Figure 4-4 SPR images collected with the microfluidic chip (A) before the injection of anti-thrombin IgG; (B) after injection of anti-thrombin IgG; (C) difference image obtained for anti-human α -thrombin. Human α -thrombin was loaded in a pattern (D) to confirm the element addressability of the design (E) Intensity profile of the region marked in (C).

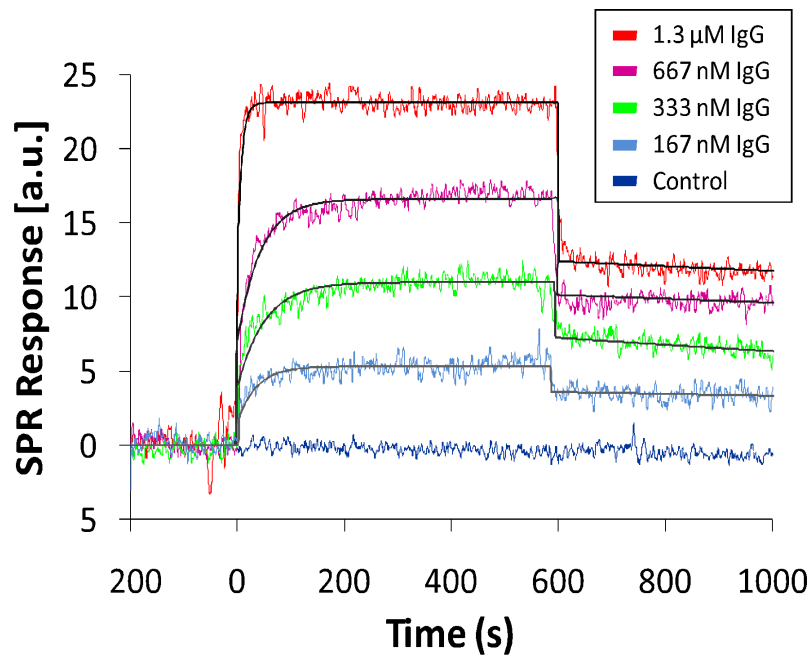


Figure 4-5 SPRi sensorgrams of anti-human α -thrombin binding to surface-immobilized thrombin on the microfluidic chip. The fitted curves yield an equilibrium dissociation constant of 5.0 ± 1.9 nM.

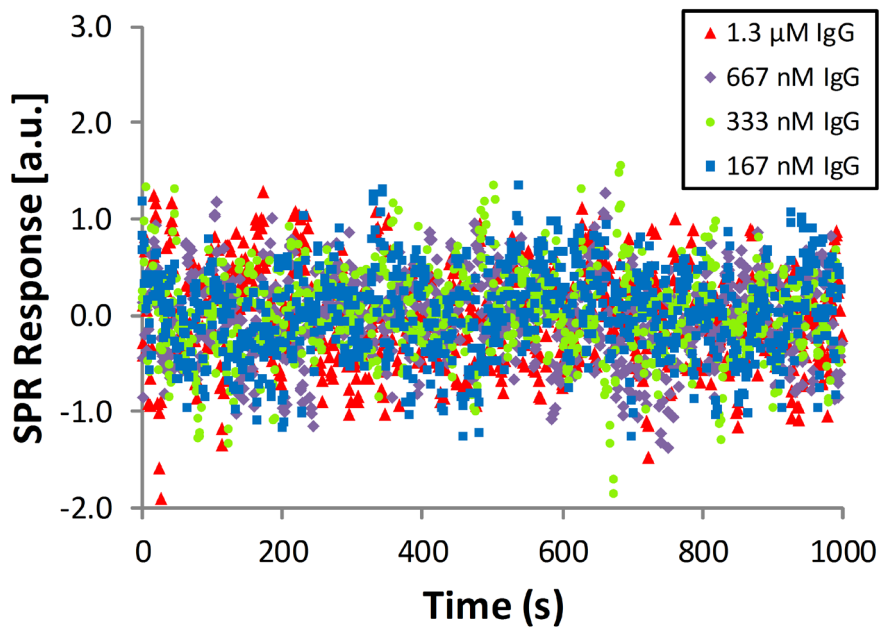


Figure 4-6 Residual plot of fittings for SPRi data shown in **Figure 4-5**.

4.3.4 MULTIPLE INTERACTIONS WITH SAMPLE RECOVERY

Two immunoassays were conducted simultaneously using the microfluidic SPRi chip and samples were recovered after the binding reactions to demonstrate the ability of our system to accommodate parallel experiments. Human factor IX proteins were immobilized in 44 element-addressable chambers followed by human α -thrombin proteins in 44 different chambers (88 chambers total). Two separate fluorescently-labeled antibodies with affinity for the immobilized proteins were subsequently injected in the device (anti-human factor IX labelled with DyLight 488; anti-human α -thrombin labelled with DyLight 594). **Figure 4-7** presents the results of the interaction and sample recovery process. **Figure 4-7A**, Step 1 corresponds to protein immobilization on the gold spots, as can be seen by the difference in baselines. Following protein immobilization, fluorescently labeled IgGs were injected across the surface and left to interact with the proteins (Step 2a) and any unbound or loosely-bound IgG were washed away (Step 2b). Upon reaching the new equilibrium, a regeneration solution was injected in the chambers to release the bound antibodies in solution (Step 3), resulting in collection of the bound fraction as well as regenerating the protein-derivatized surface. At regular intervals of the binding reactions, indicated by arrows in **Figure 4-7A**, antibody fractions were collected at the output of the device for further analysis. These fractions include the original dilution of fluorescently-labeled IgG; fraction I corresponding to the amount of excess IgG collected after the gold surfaces were saturated; fraction II, corresponding to any unbound IgG after washing; and fraction III, corresponding to the recovered IgG eluted from the protein-derivatized gold spots after regeneration.

Figure 4-7B and **C** present the concentration of fluorescently-labeled IgG collected at the output of the chip for both anti-human factor IX (DyLight 488) and anti-human α -thrombin (DyLight 594), respectively. The concentration values were calculated from a standard curve generated for both DyLight 488 and DyLight 594

fluorescent dyes (**Figure 4-8**). **Figure 4-7B** presents the concentration values measured for the interaction of anti-human factor IX to immobilized human factor IX. The values were also measured for anti-human α -thrombin as a negative control to ensure there was no leakage between chambers and stacks in the device. **Figure 4-7C** presents the interaction of anti-human α -thrombin to immobilized human α -thrombin. The values for anti-human factor IX were also measured. In both cases, the original amount of IgG injected in the device at the start of the interaction (**Figure 4-7A**, Step 2a) was recorded, and all other fluorescence values were normalized to this concentration. By subtracting the fluorescence measurements of the collected fraction from those of the original fraction, we calculated the amount of IgG retained in the device from fraction I to be 1.42 μ M and 2.60 μ M for anti-human factor IX and anti-human α -thrombin, respectively. Fraction II measured 0.96 μ M and 1.53 μ M for factor IX and thrombin IgG, respectively, corresponding to the dissociation phase (**Figure 4-7A**, Step 2b). As expected, fraction III – the regeneration step – (**Figure 4-7A**, Step 3) yielded an increase in the amount of IgG recovered from the gold surface (1.65 μ M for factor IX and 2.19 μ M for thrombin IgG).

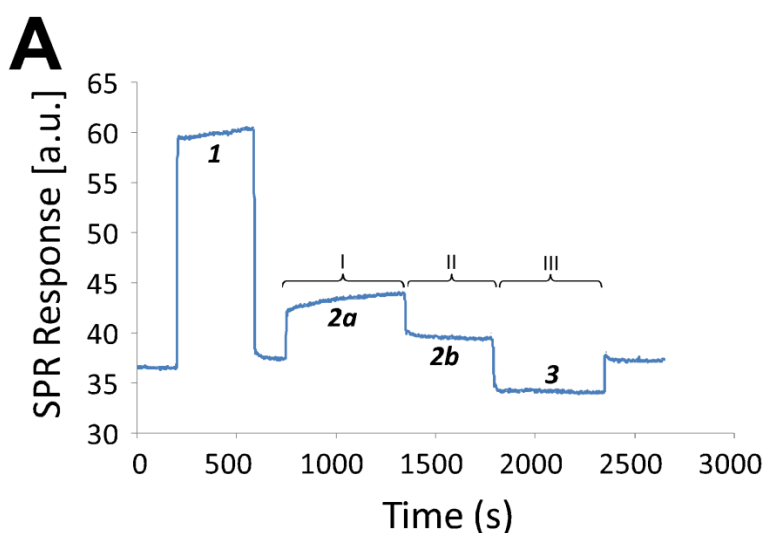


Figure 4-7 Recovery of surface-bound fluorescently-labeled antibodies from the microfluidic SPRi chip. (A) SPRi sensorgram of the interaction process and collected fraction marked as I, II and III. Step 1 – protein immobilization on the gold surface, Step 2a,b – association and dissociation phase of the protein-IgG complex, Step 3 – regeneration phase.

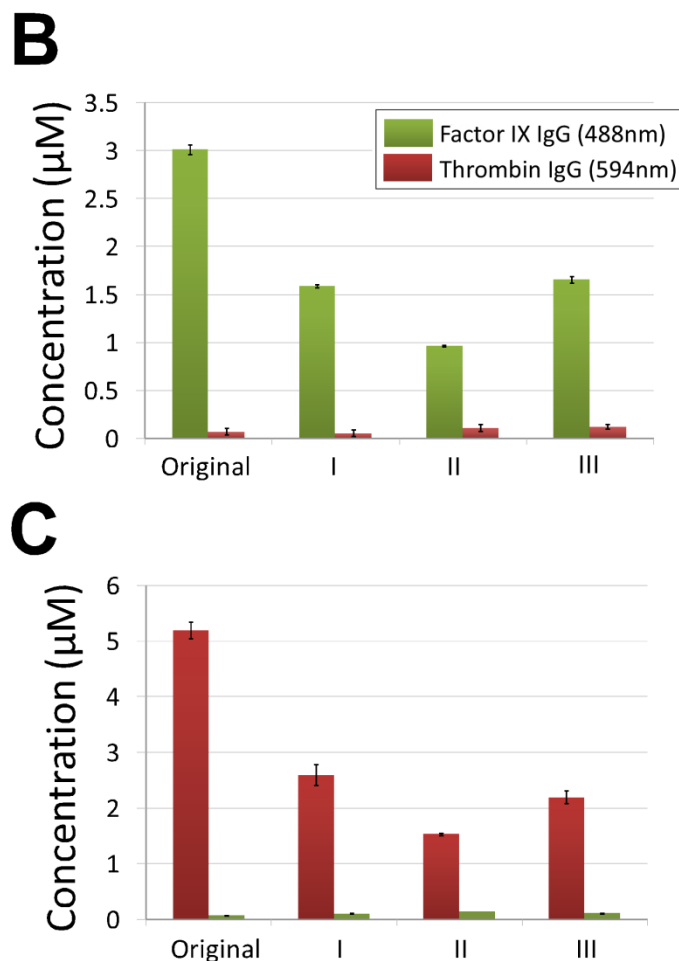


Figure 4-7 [continued from previous] (B) Fluorescence measurements of collected fractions of human factor IX IgG at each step of the interaction process. Excitation wavelengths of 488 nm (493/518 Ex/Em) and 594 nm (593/618 Ex/Em) correspond to labeled anti-human factor IX and anti-human α -thrombin, respectively. (C) Fluorescence measurements of collected fractions of human α -thrombin IgG at each step of the interaction process.

These results demonstrate the ability of the device to recover bound species from individual chambers for downstream processing as well as the possibility to accommodate the interrogation of multiple ligands to multiple analytes. As most devices previously reported are of a static flow cell design, they are only capable of interrogating multiple ligands to a single analyte, with very limited capabilities to isolate samples.^{433,455-458} However, with the integration of element-addressability as

presented here, it is possible to dynamically deliver and recover samples in a controlled fashion, adding an entire new level of functionality for SPRi measurements. By being able to deliver and recover specific samples in an array, the immobilization of multiple ligands and the interrogation of each to multiple analytes is now feasible. We anticipate many applications of this technology due to this capability to incorporate downstream processing of the recovered samples, including identification of proteins through mass spectrometry and sequencing of bound DNA molecules.

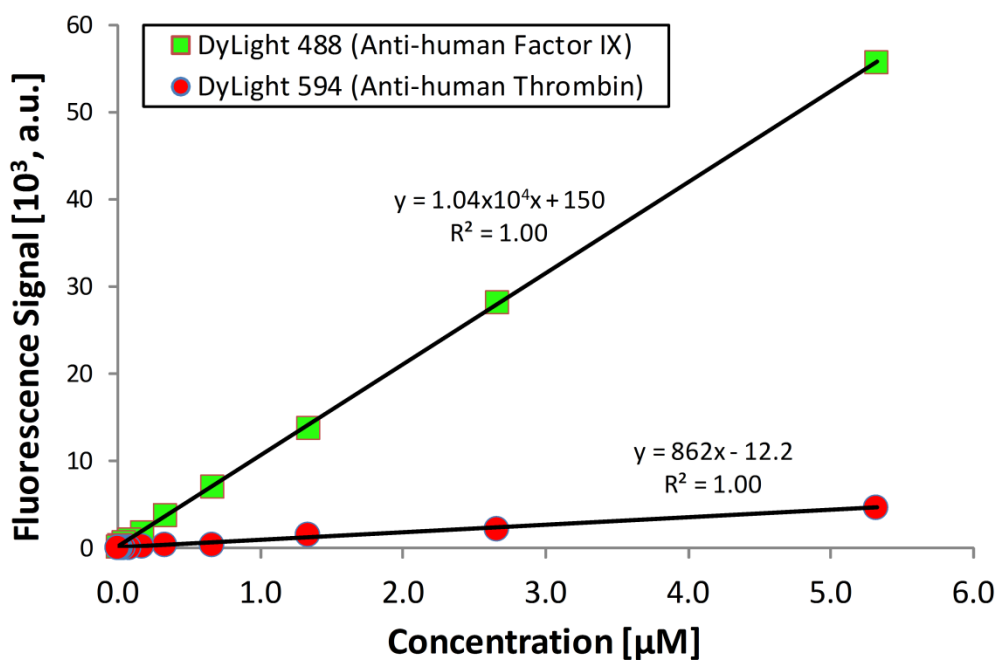


Figure 4-8 Standard curves for fluorescence quantitation of recovered labelled-antibody fractions from microfluidic SPRi arrays.

4.4 CONCLUDING REMARKS

A new platform for biological reagent affinity and specificity screening was presented, and its ability to accommodate the interrogation of multiple ligands to multiple analyte streams in a highly integrated fashion was reported. The device presented distinguishes itself from other SPRi arrays by combining the use of high-density microfluidic element-addressable chambers with integrated on-chip parallel dilutions of target analytes. A unique combination of microvalves enables independent access to each of the 700-pL chambers comprising the array, therefore enabling reagent conservation capabilities of potentially rare samples. Greater control over the reaction conditions was thereby achieved compared to previous approaches.

Effective detection of an anti-human α -thrombin IgG to surface-immobilized thrombin provided initial validation studies where the use of streptavidin as an immobilization and surface passivation molecule allowed for proper spatial arrangement of biotinylated thrombin. The resulting kinetic analysis confirmed the ability of this device in providing accurate binding information across parallel experiments by reporting corresponding binding affinities. Additionally, the microfluidic arrays were investigated for their suitability in accommodating parallel screenings of potential antibody (or aptamer) panels. A controlled mixture of both human α -thrombin and human factor IX IgGs was investigated for binding specificity to each of their respective surface-immobilized targets across multiple replicate chambers. The ability to recover the contents of each replicate chamber following binding interaction was assessed. Results confirmed that such recovery of rare samples for downstream processing is readily achievable with no cross-contamination.

The novel technology presented here should therefore enable multiplexed investigations of binding and specificity across different analytes in a single experiment, making it a particular attractive and valuable complement to both the

Hi-Fi SELEX aptamer discovery platform and current high-throughput platforms for antibody discovery.

Chapter 5

CONCLUSIONS AND OUTLOOK

*“The important thing is not to stop questioning.
Curiosity has its own reasons for existence”*

— Albert Einstein (1955)⁴⁵⁹

Advances in DNA technologies, including next-generation sequencing (NGS) platforms for detecting germline and somatic point mutations as well as other genetic variations, are providing an abundance of information related to human diseases and targets for treating them. Major research programs aimed at discovering drug targets—including the growing catalogue of somatic mutations (COSMIC)⁴⁶⁰ prognostic of cancer risk and progression—are well under way and will continue to provide insights into targeted treatment strategies. Many of those targeted therapies will undoubtedly be based on biologic affinity reagents, as evidenced by the explosive growth of monoclonal antibodies (mAbs) as therapeutics. Biologic affinity ligands will likewise continue to find use as key reagents in diagnostic systems, laboratory and preparative-scale purification systems, *in vivo* and *ex vivo* cellular imaging technologies, as well as several other applications. Indeed, both antibody (Singulex’s Errena® Immunoassay system; Olink’s Proseek® platform) and aptamer-based (SomaLogic’s SOMAScan™ platform) instruments are now available for detecting clinically actionable

biomarkers of specific life-threatening diseases, including cancers as well as various inflammatory, gastrointestinal, autoimmune and cardiovascular conditions.

However, the discovery of affinity ligands is challenging, especially those that present therapeutic value. Significant gaps in knowledge currently prohibit their *de novo* design, necessitating the use of more empirical *in vivo* and *in vitro* screening methods that do not require advanced knowledge of the specific epitope and binding mechanism through which the molecule must interact with the target. These technologies generally succeed through their ability to screen vast libraries of potential binding partners against a particular target of interest. Binding affinity is typically applied as the selective pressure, with binding specificity and biological/therapeutic activity rarely considered in the initial selection process. Nevertheless, many useful affinity reagents have been discovered using such platforms. This is particularly true for mAbs, in part because the demand on the screening platform is considerably lessened by the tremendous evolutionary “pre”-selection of mAbs specific to the target that occurs within the immunized animal.

However, a number of limitations to current platforms for mAb or aptamer discovery have been described in this thesis. In particular, the systematic studies presented in **Chapters 2 and 3** reveal a set of primary mechanisms limiting the performance of current SELEX platforms, including (i) loss of high-affinity members from the library due to various ways in which the flanking sequences can interfere with aptamer fold and function, (ii) excessive non-specific retention of undesirable library members that serves to limit per round partition efficiencies and diminish the chances by which a pool of high-affinity binders can be discovered, (iii) formation of partially complementary heteroduplexes that lead to excessive accumulation of HMW contaminants during PCR amplification of retained members, and (iv) incomplete regeneration of the sense-strand (aptamer) population from the pool of dsDNA amplicons. These limitations were shown to introduce significant biases into the *in vitro* selection process. As a result,

therapeutically-relevant members present within the initial semi-combinatorial population can inadvertently be removed from the pool, irrespective of their binding potential.

Identifying factors affecting the reliability and overall performance of SELEX has allowed a number of strategies and techniques to be developed to mitigate their influence without the need for highly specialized equipment generally unavailable in most labs interested in aptamer discovery. Ergo, the methods reported in this thesis differ markedly from CE-SELEX and M-SELEX; two platforms which rely on the use of specialized equipment to address a single limitation to successful aptamer selection, namely, low per-round *PE*.

Here, a powerful new platform for DNA aptamer discovery has been developed by establishing a compatible set of new techniques and methods that collectively address every limitation to aptamer selection identified above. Enhancements to the semi-combinatorial DNA library were made so as to block fixed-region interference effects that commonly arise during selection. Non-fouling surfaces were engineered and optimized to enable target display and library partitioning at incubation conditions that favour selective enrichment of tight-binding members by greatly reducing all non-specific retention events. Furthermore, a high-ionic-strength wash step was introduced to further reduce non-specific retention and enrich aptamers which bind the target through a more balanced ensemble of intermolecular forces that is not dominated by long-range Coulombic interactions. Simple PCR-based methods were then created to enable accurate quantification of retained library sequence diversity and mean binding affinity after each selection round. Traditional bulk PCR amplifications were replaced by a droplet digital PCR protocol that was optimized to eliminate the accumulation of HMW contaminants, therefore enabling large quantities of high-quality amplicons to be generated in their fully complementary format. This, in turn, permitted stoichiometric recovery of sense strands from the amplicon pool by λ -exonuclease digestion. The resulting

novel highly integrated platform for the reliable selection of clinically-relevant aptamers in a high-fidelity fashion (Hi-Fi SELEX) was shown to hold superior or at least commensurate performance compared to the most advanced selection platforms currently available.

Finally, recent advances to hybridoma-based and other platforms for reliably screening large immune repertoires have enabled more successful identification of antibody pools presenting high affinity and suitable binding kinetics. However, considerable further value could be realized through development of methods that permit efficient label-free screening of binding specificities. The same argument holds for aptamer discovery; indeed, in this case, no technologies enabling efficient specificity screenings of potential lead aptamer candidates have been described previously. The microfluidic SPRi arrays presented and demonstrated at the proof-of-concept level in **Chapter 4** provide a label-free binding and specificity screening platform which is compatible with both classes of affinity reagents considered in this thesis. Though admittedly specialized in design and operation, these arrays compensate for potential implementation obstacles by offering a unique approach to characterizing binding affinity and specificity by leveraging the capacity for microfluidic SPRi-based systems to provide binding kinetic data in a multiplexed manner at reasonable throughputs. The acquisition of such information can further refine the panel of lead compounds by excluding those, for instance, which transiently bind the target. Furthermore, these arrays are cost-efficient, in large part by virtue of their small (pL) sample volume demand and label-free approach to binding analysis. The integration of novel microfluidic arrays into current SPRi technology therefore offers the potential to discriminate mAbs or DNA aptamers based on binding affinity, binding kinetics, and/or binding specificity.

5.1 PROPOSED FUTURE DEVELOPMENTS

The Hi-Fi SELEX platform collectively reported in **Chapters 2** and **3** has the potential to improve both the speed and the reliability of aptamer discovery, as evidenced through its successful application in identifying panels of tight-binding aptamers against a number of clinically-relevant targets. However, as illustrated in **Figure 1-9**, further parsing of those panels through secondary screens that characterize other critical attributes (e.g. specificity, functional activity, stability, etc.) is required to isolate truly promising lead compounds. These additional screening processes remain onerous. Complementary cost-effective high-throughput technologies must therefore be developed to simplify these essential tasks, including technologies that leverage NGS or other array-based systems to enable multiplexing (such as the ones employed for QPASS).¹⁷¹ Indeed, a potentially fruitful avenue for improving therapeutic aptamer discovery would be through effective integration of functional screens into a high-throughput selection pipeline so as to selectively retain members that present specificities to biochemically-relevant epitopes. The unique provisions afforded by Hi-Fi SELEX, including the flanking sequence blocking strategy described in **Chapter 2**, should aid this process by increasing hit-rates and isolating minimal aptamer sequences to the random region of the library.

An intriguing use of the Hi-Fi SELEX platform could be toward the discovery of aptamers against therapeutic targets for which previous attempts at affinity reagent discovery have failed.²⁶¹ The enhancements provided by Hi-Fi SELEX could be leveraged in order both to elucidate the reasons for those failures and to isolate new pools of candidates via a unique screening approach. Moreover, though developed for DNA aptamer screening, the Hi-Fi SELEX platform could be applied to other library formats (e.g. RNA-based libraries, libraries harboring modified nucleotides) to establish multiple paths to discovery of useful aptamers. Although the literature on the potential value for incorporating modified nucleotides in

SELEX libraries is currently quite scarce, it is known that the incorporation of LNAs into a (previously discovered) aptamer does not in general compromise affinity.^{254,461} As a result, incorporation of LNAs into selection libraries may improve discovery by increasing the diversity of candidate aptamers, as well as the thermal stability of folds (creating the potential for harsher screening environments), especially when the competent library format (**Chapter 2**) is employed and the LNA content is restricted to within the random region.

Though not specifically addressed in this thesis, significant biases in the incorporation of adenosines into retained library amplicons have been reported for several library formats (i.e. RNA-based),^{462,463} irrespective of the partition conditions utilized. This may be related to the bulk PCR artifacts identified in this thesis, but the precise mechanism(s) is(are) not known. Library amplification by ddPCR could provide insights into the ways in which nucleotide biases occur, as the various cross-hybridization reactions that are observed during bulk PCR amplification of libraries can be minimized in the ddPCR format. Robust guidelines for conducting Hi-Fi SELEX using either a standard or an expanded genetic alphabet could therefore be developed.

Current theories describing library partitioning during SELEX offer guidelines for optimizing aptamer:target concentration ratios (namely, *PE*).^{199,200,285,367} Regrettably, each applies only to SELEX processes in which the library incubation and wash steps utilize the same solvent. Work in this thesis has provided evidence of the value of employing more stringent wash conditions, creating the need to develop more general models of the partition process. Highly advanced models capable of predicting optimal incubation/wash/elution conditions (e.g. time, pH, ionic strength) in relation to the biochemical properties of a given target (e.g. a protein's isoelectric point) have been developed for ion-exchange^{464,465} and other modes of chromatography,⁴⁶⁶⁻⁴⁶⁹ and those models could certainly be adapted for use in optimizing Hi-Fi SELEX screening protocols.

The Hi-Fi SELEX platform currently operates as a single selection pipeline. In principle, however, it could be multiplexed to allow parallel aptamer screenings given the microtitre plate format used for partitioning and washing steps. Likewise, the digital PCR strategy used in Hi-Fi SELEX to amplify and regenerate the retained library could be extended to permit parallel selections, particularly if template loading per well (i.e. higher CPDs) or the total number of droplets could be increased. The latter approach might be possible utilizing new dPCR technologies (e.g. Rain Dance's RainDrop platform), though the cost of implementing such technologies to achieve high-throughput Hi-Fi SELEX may prove prohibitive, at least in academic settings.

Finally, the microfluidic SPRi arrays developed in **Chapter 4** could present further opportunities to accelerate screening and selection of aptamers and antibodies. Refinements to those arrays could serve to improve loading capacities, while more simplified architecture could enhance their operation and enable greater densification of parallel operations. Moreover, though the current optical set-up is effective in monitoring antibody-binding events, further refinements to the analytical sensitivity (LOD) could improve detection of smaller ligands, such as aptamers, while also enhancing the instrument's ability to interrogate large panels of analytes. Further research into the ability to conduct high-fidelity aptamer screenings on such devices could also advance the field by providing high-throughput, element-addressability capabilities for measuring binding kinetics *in situ*. Such developments could thereby further streamline aptamer discovery efforts.

BIBLIOGRAPHY

1. Shell B (2005) *Sensational Scientists: The Journeys and Discoveries of 24 Men and Women of Science*, Raincoast Books, Vancouver, p. 146
2. Herrmann D (1998) *Helen Keller: A Life*, The University of Chicago Press, Chicago, p. 222
3. Sagan C (1979) *Broca's Brain: Reflections on the Romance of Science*, The Random House Publishing Group, New York, p. 16
4. Berson SA, Yalow RS, Bauman A, Rothschild MA, and Newerly K (1956) Insulin-I131 metabolism in human subjects: demonstration of insulin binding globulin in the circulation of insulin treated subjects. *The Journal of Clinical Investigation* **35**, 170-90.
5. Yalow RS, and Berson SA (1959) Assay of Plasma Insulin in Human Subjects by Immunological Methods. *Nature* **184**, 1648-49.
6. Kohler G, and Milstein C (1975) Continuous cultures of fused cells secreting antibody of predefined specificity. *Nature* **256**, 495-97.
7. Edwards BM, Barash SC, Main SH, Choi GH, Minter R, Ullrich S, Williams E, Du Fou L, Wilton J, Albert VR, Ruben SM, and Vaughan TJ (2003) The Remarkable Flexibility of the Human Antibody Repertoire; Isolation of Over One Thousand Different Antibodies to a Single Protein, BlyS. *J. Mol. Biol.* **334**, 103-18.
8. Xing PX, Russell S, Prenzoska J, and McKenzie JF (1994) Discrimination between alternatively spliced STP-A and -B isoforms of CD46. *Immunology* **83**, 122-27.
9. Raska M, Czernekova L, Moldoveanu Z, Zachova K, Elliott M, Novak Z, Hall S, Hoelscher M, Maboko L, Brown R, Smith P, Mestecky J, and Novak J (2014) Differential glycosylation of envelope gp120 is associated with differential recognition of HIV-1 by virus-specific antibodies and cell infection. *AIDS Res. Ther.* **11**, 1-16.
10. Mould DR, and Sweeney KR (2007) The pharmacokinetics and pharmacodynamics of monoclonal antibodies--mechanistic modeling applied to drug development. *Curr Opin Drug Discov Devel* **10**, 84-96.

11. Chapman AP, Antoniow P, Spitali M, West S, Stephens S, and King DJ (1999) Therapeutic antibody fragments with prolonged in vivo half-lives. *Nat Biotech* **17**, 780-83.
12. Oldham RK, and Dillman RO (2008) Monoclonal Antibodies in Cancer Therapy: 25 Years of Progress. *J. Clin. Oncol.* **26**, 1774-77.
13. Nelson AL, Dhimolea E, and Reichert JM (2010) Development trends for human monoclonal antibody therapeutics. *Nat Rev Drug Discov* **9**, 767-74.
14. Chames P, Van Regenmortel M, Weiss E, and Baty D (2009) Therapeutic antibodies: successes, limitations and hopes for the future. *Br. J. Pharmacol.* **157**, 220-33.
15. Ruigrok VJ, Levisson M, Eppink MH, Smidt H, and van der Oost J (2011) Alternative affinity tools: more attractive than antibodies? *Biochem. J.* **436**, 1-13.
16. Skerra A (2007) Alternative non-antibody scaffolds for molecular recognition. *Curr. Opin. Biotechnol.* **18**, 295-304.
17. Jayasena SD (1999) Aptamers: An Emerging Class of Molecules That Rival Antibodies in Diagnostics. *Clin. Chem.* **45**, 1628-50.
18. Ozer A, Pagano JM, and Lis JT (2014) New Technologies Provide Quantum Changes in the Scale, Speed, and Success of SELEX Methods and Aptamer Characterization. *Mol Ther Nucleic Acids* **3**, e183.

19. Lander ES, Linton LM, Birren B, Nusbaum C, Zody MC, Baldwin J, Devon K, Dewar K, Doyle M, FitzHugh W, Funke R, Gage D, Harris K, Heaford A, Howland J, Kann L, Lehoczky J, LeVine R, McEwan P, McKernan K, Meldrim J, Mesirov JP, Miranda C, Morris W, Naylor J, Raymond C, Rosetti M, Santos R, Sheridan A, Sougnez C, Stange-Thomann N, Stojanovic N, Subramanian A, Wyman D, Rogers J, Sulston J, Ainscough R, Beck S, Bentley D, Burton J, Clee C, Carter N, Coulson A, Deadman R, Deloukas P, Dunham A, Dunham I, Durbin R, French L, Grafham D, Gregory S, Hubbard T, Humphray S, Hunt A, Jones M, Lloyd C, McMurray A, Matthews L, Mercer S, Milne S, Mullikin JC, Mungall A, Plumb R, Ross M, Shownkeen R, Sims S, Waterston RH, Wilson RK, Hillier LW, McPherson JD, Marra MA, Mardis ER, Fulton LA, Chinwalla AT, Pepin KH, Gish WR, Chissole SL, Wendl MC, Delehaunty KD, Miner TL, Delehaunty A, Kramer JB, Cook LL, Fulton RS, Johnson DL, Minx PJ, Clifton SW, Hawkins T, Branscomb E, Predki P, Richardson P, Wenning S, Slezak T, Doggett N, Cheng JF, Olsen A, Lucas S, Elkin C, Uberbacher E, Frazier M, Gibbs RA, Muzny DM, Scherer SE, Bouck JB, Sodergren EJ, Worley KC, Rives CM, Gorrell JH, Metzker ML, Naylor SL, Kucherlapati RS, Nelson DL, Weinstock GM, Sakaki Y, Fujiyama A, Hattori M, Yada T, Toyoda A, Itoh T, Kawagoe C, Watanabe H, Totoki Y, Taylor T, Weissenbach J, Heilig R, Saurin W, Artiguenave F, Brottier P, Bruls T, Pelletier E, Robert C, Wincker P, Smith DR, Doucette-Stamm L, Rubenfield M, Weinstock K, Lee HM, Dubois J, Rosenthal A, Platzer M, Nyakatura G, Taudien S, Rump A, Yang H, Yu J, Wang J, Huang G, Gu J, Hood L, Rowen L, Madan A, Qin S, Davis RW, Federspiel NA, Abola AP, Proctor MJ, Myers RM, Schmutz J, Dickson M, Grimwood J, Cox DR, Olson MV, Kaul R, Raymond C, Shimizu N, Kawasaki K, Minoshima S, Evans GA, Athanasiou M, Schultz R, Roe BA, Chen F, Pan H, Ramser J, Lehrach H, Reinhardt R, McCombie WR, de la Bastide M, Dedhia N, Blocker H, Hornischer K, Nordsiek G, Agarwala R, Aravind L, Bailey JA, Bateman A, Batzoglou S, Birney E, Bork P, Brown DG, Burge CB, Cerutti L, Chen HC, Church D, Clamp M, Copley RR, Doerks T, Eddy SR, Eichler EE, Furey TS, Galagan J, Gilbert JG, Harmon C, Hayashizaki Y, Haussler D, Hermjakob H, Hokamp K, Jang W, Johnson LS, Jones TA, Kasif S, Kasprzyk A, Kennedy S, Kent WJ, Kitts P, Koonin EV, Korf I, Kulp D, Lancet D, Lowe TM, McLysaght A, Mikkelsen T, Moran JV, Mulder N, Pollara VJ, Ponting CP, Schuler G, Schultz J, Slater G, Smit AF, Stupka E, Szustakowski J, Thierry-Mieg D, Thierry-Mieg J, Wagner L, Wallis J, Wheeler R, Williams A, Wolf YI, Wolfe KH, Yang SP, Yeh RF, Collins F, Guyer MS, Peterson J, Felsenfeld A, Wetterstrand KA, Patrinos A, Morgan MJ, de Jong P, Catanese JJ, Osoegawa K, Shizuya H, Choi S, and Chen YJ (2001) Initial sequencing and analysis of the human genome. *Nature* **409**, 860-921.

20. Venter JC, Adams MD, Myers EW, Li PW, Mural RJ, Sutton GG, Smith HO, Yandell M, Evans CA, Holt RA, Gocayne JD, Amanatides P, Ballew RM, Huson DH, Wortman JR, Zhang Q, Kodira CD, Zheng XH, Chen L, Skupski M, Subramanian G, Thomas PD, Zhang J, Gabor Miklos GL, Nelson C, Broder S, Clark AG, Nadeau J, McKusick VA, Zinder N, Levine AJ, Roberts RJ, Simon M, Slayman C, Hunkapiller M, Bolanos R, Delcher A, Dew I, Fasulo D, Flanigan M, Florea L, Halpern A, Hannenhalli S, Kravitz S, Levy S, Mobarry C, Reinert K, Remington K, Abu-Threideh J, Beasley E, Biddick K, Bonazzi V, Brandon R, Cargill M, Chandramouliswaran I, Charlab R, Chaturvedi K, Deng Z, Francesco VD, Dunn P, Eilbeck K, Evangelista C, Gabrielian AE, Gan W, Ge W, Gong F, Gu Z, Guan P, Heiman TJ, Higgins ME, Ji R-R, Ke Z, Ketchum KA, Lai Z, Lei Y, Li Z, Li J, Liang Y, Lin X, Lu F, Merkulov GV, Milshina N, Moore HM, Naik AK, Narayan VA, Neelam B, Nusskern D, Rusch DB, Salzberg S, Shao W, Shue B, Sun J, Wang ZY, Wang A, Wang X, Wang J, Wei M-H, Wides R, Xiao C, Yan C, Yao A, Ye J, Zhan M, Zhang W, Zhang H, Zhao Q, Zheng L, Zhong F, Zhong W, Zhu SC, Zhao S, Gilbert D, Baumhueter S, Spier G, Carter C, Cravchik A, Woodage T, Ali F, An H, Awe A, Baldwin D, Baden H, Barnstead M, Barrow I, Beeson K, Busam D, Carver A, Center A, Cheng ML, Curry L, Danaher S, Davenport L, Desilets R, Dietz S, Dodson K, Doup L, Ferriera S, Garg N, Gluecksmann A, Hart B, Haynes J, Haynes C, Heiner C, Hladun S, Hostin D, Houck J, Howland T, Ibegwam C, Johnson J, Kalush F, Kline L, Koduru S, Love A, Mann F, May D, McCawley S, McIntosh T, McMullen I, Moy M, Moy L, Murphy B, Nelson K, Pfannkoch C, Pratts E, Puri V, Qureshi H, Reardon M, Rodriguez R, Rogers Y-H, Romblad D, Ruhfel B, Scott R, Sitter C, Smallwood M, Stewart E, Strong R, Suh E, Thomas R, Tint NN, Tse S, Vech C, Wang G, Wetter J, Williams S, Williams M, Windsor S, Winn-Deen E, Wolfe K, Zaveri J, Zaveri K, Abril JF, Guigó R, Campbell MJ, Sjolander KV, Karlak B, Kejariwal A, Mi H, Lazareva B, Hatton T, Narechania A, Diemer K, Muruganujan A, Guo N, Sato S, Bafna V, Istrail S, Lippert R, Schwartz R, Walenz B, Yooseph S, Allen D, Basu A, Baxendale J, Blick L, Caminha M, Carnes-Stine J, Caulk P, Chiang Y-H, Coyne M, Dahlke C, Mays AD, Dombroski M, Donnelly M, Ely D, Esparham S, Fosler C, Gire H, Glanowski S, Glasser K, Glodek A, Gorokhov M, Graham K, Gropman B, Harris M, Heil J, Henderson S, Hoover J, Jennings D, Jordan C, Jordan J, Kasha J, Kagan L, Kraft C, Levitsky A, Lewis M, Liu X, Lopez J, Ma D, Majoros W, McDaniel J, Murphy S, Newman M, Nguyen T, Nguyen N, Nodell M, Pan S, Peck J, Peterson M, Rowe W, Sanders R, Scott J, Simpson M, Smith T, Sprague A, Stockwell T, Turner R, Venter E, Wang M, Wen M, Wu D, Wu M, Xia A, Zandieh A, and Zhu X (2001) The Sequence of the Human Genome. *Science* **291**, 1304-51.
21. Gonzaga-Jauregui C, Lupski JR, and Gibbs RA (2012) Human Genome Sequencing in Health and Disease. *Annu. Rev. Med.* **63**, 35-61.
22. Botstein D, and Risch N (2003) Discovering genotypes underlying human phenotypes: past successes for mendelian disease, future approaches for complex disease. *Nat. Genet.* **33**, 228-37.

23. The Human Proteome Organization (HUPO) (2010) A Gene-centric Human Proteome Project: HUPO-The Human Proteome organization. *Mol. Cell. Proteomics* **9**, 427-29.
24. Kim M-S, Pinto SM, Getnet D, Nirujogi RS, Manda SS, Chaerkady R, Madugundu AK, Kelkar DS, Isserlin R, Jain S, Thomas JK, Muthusamy B, Leal-Rojas P, Kumar P, Sahasrabuddhe NA, Balakrishnan L, Advani J, George B, Renuse S, Selvan LDN, Patil AH, Nanjappa V, Radhakrishnan A, Prasad S, Subbannayya T, Raju R, Kumar M, Sreenivasamurthy SK, Marimuthu A, Sathe GJ, Chavan S, Datta KK, Subbannayya Y, Sahu A, Yelamanchi SD, Jayaram S, Rajagopalan P, Sharma J, Murthy KR, Syed N, Goel R, Khan AA, Ahmad S, Dey G, Mudgal K, Chatterjee A, Huang T-C, Zhong J, Wu X, Shaw PG, Freed D, Zahari MS, Mukherjee KK, Shankar S, Mahadevan A, Lam H, Mitchell CJ, Shankar SK, Satishchandra P, Schroeder JT, Sirdeshmukh R, Maitra A, Leach SD, Drake CG, Halushka MK, Prasad TSK, Hruban RH, Kerr CL, Bader GD, Iacobuzio-Donahue CA, Gowda H, and Pandey A (2014) A draft map of the human proteome. *Nature* **509**, 575-81.
25. Mehan MR, Ostroff R, Wilcox SK, Steele F, Schneider D, Jarvis TC, Baird GS, Gold L, and Janjic N (2013) Highly multiplexed proteomic platform for biomarker discovery, diagnostics, and therapeutics. *Advances in experimental medicine and biology* **735**, 283-300.
26. Vasan RS (2006) Biomarkers of Cardiovascular Disease: Molecular Basis and Practical Considerations. *Circulation* **113**, 2335-62.
27. Hewitt SM, Dear J, and Star RA (2004) Discovery of Protein Biomarkers for Renal Diseases. *Journal of the American Society of Nephrology* **15**, 1677-89.
28. Madu CO, and Lu Y (2010) Novel diagnostic biomarkers for prostate cancer. *Journal of Cancer* **1**, 150-77.
29. Polanski M, and Anderson NL (2007) A list of candidate cancer biomarkers for targeted proteomics. *Biomarker insights* **1**, 1-48.
30. Tuerk C, and Gold L (1990) Systematic evolution of ligands by exponential enrichment: RNA ligands to bacteriophage T4 DNA polymerase. *Science* **249**, 505-10.
31. Ellington AD, and Szostak JW (1990) In vitro selection of RNA molecules that bind specific ligands. *Nature* **346**, 818-22.
32. Robertson DL, and Joyce GF (1990) Selection in vitro of an RNA enzyme that specifically cleaves single-stranded DNA. *Nature* **344**, 467-68.
33. Song K-M, Lee S, and Ban C (2011) Aptamers and Their Biological Applications. *Sensors* **12**, 612-31.

34. Keefe AD, Pai S, and Ellington A (2010) Aptamers as therapeutics. *Nat Rev Drug Discov* **9**, 537-50.
35. Sassanfar M, and Szostak JW (1993) An RNA motif that binds ATP. *Nature* **364**, 550-53.
36. Wang J, Jiang H, and Liu F (2000) In vitro selection of novel RNA ligands that bind human cytomegalovirus and block viral infection. *RNA* **6**, 571-83.
37. Daniels DA, Chen H, Hicke BJ, Swiderek KM, and Gold L (2003) A tenascin-C aptamer identified by tumor cell SELEX: Systematic evolution of ligands by exponential enrichment. *Proceedings of the National Academy of Sciences* **100**, 15416-21.
38. Mannironi C, Di Nardo A, Fruscoloni P, and Tocchini-Valentini GP (1997) In Vitro Selection of Dopamine RNA Ligands. *Biochemistry* **36**, 9726-34.
39. Jenison R, Gill S, Pardi A, and Polisky B (1994) High-resolution molecular discrimination by RNA. *Science* **263**, 1425-29.
40. Leva S, Lichte A, Burmeister J, Muhn P, Jahnke B, Fesser D, Erfurth J, Burgstaller P, and Klussmann S (2002) GnRH Binding RNA and DNA Spiegelmers: A Novel Approach toward GnRH Antagonism. *Chemistry & Biology* **9**, 351-59.
41. Hesselberth JR, Robertson MP, Knudsen SM, and Ellington AD (2003) Simultaneous detection of diverse analytes with an aptazyme ligase array. *Anal. Biochem.* **312**, 106-12.
42. Jeong S, Eom T-Y, Kim S-J, Lee S-W, and Yu J (2001) In Vitro Selection of the RNA Aptamer against the Sialyl Lewis X and Its Inhibition of the Cell Adhesion. *Biochem. Biophys. Res. Commun.* **281**, 237-43.
43. Cruz-Toledo J, McKeague M, Zhang X, Giamberardino A, McConnell E, Francis T, DeRosa MC, and Dumontier M (2012) Aptamer base: a collaborative knowledge base to describe aptamers and SELEX experiments. *Database* **2012**, bas006.
44. Cerchia L, Esposito CL, Camorani S, Catuogno S, and Franciscis Vd (2011) Coupling Aptamers to Short Interfering RNAs as Therapeutics. *Pharmaceuticals* **4**, 1434-49.
45. Sundaram P, Kurniawan H, Byrne ME, and Wower J (2013) Therapeutic RNA aptamers in clinical trials. *Eur. J. Pharm. Sci.* **48**, 259-71.
46. Esposito CL, Catuogno S, de Franciscis V, and Cerchia L (2011) New insight into clinical development of nucleic acid aptamers. *Discov. Med.* **61**, 487-96.
47. Ni X, Castanares M, Mukherjee A, and Lupold SE (2011) Nucleic acid aptamers: clinical applications and promising new horizons. *Curr. Med. Chem.* **18**, 4206-14.

48. Stark BC, Kole R, Bowman EJ, and Altman S (1978) Ribonuclease P: an enzyme with an essential RNA component. *Proceedings of the National Academy of Sciences* **75**, 3717-21.
49. Kruger K, Grabowski PJ, Zaug AJ, Sands J, Gottschling DE, and Cech TR (1982) Self-splicing RNA: Autoexcision and autocyclization of the ribosomal RNA intervening sequence of tetrahymena. *Cell* **31**, 147-57.
50. Breaker RR, and Joyce GF (1994) A DNA enzyme that cleaves RNA. *Chem. Biol.* **1**, 223-29.
51. Hirao I, Kimoto M, and Yamashige R (2012) Natural versus Artificial Creation of Base Pairs in DNA: Origin of Nucleobases from the Perspectives of Unnatural Base Pair Studies. *Acc. Chem. Res.* **45**, 2055-65.
52. Lemieux S, and Major F (2002) RNA canonical and non-canonical base pairing types: a recognition method and complete repertoire. *Nucleic Acids Res.* **30**, 4250-63.
53. Mukherjee S, Bansal M, and Bhattacharyya D (2006) Conformational specificity of non-canonical base pairs and higher order structures in nucleic acids: crystal structure database analysis. *J. Comput. Aided Mol. Des.* **20**, 629-45.
54. Tok JB-H, Cho J, and Rando RR (2000) RNA aptamers that specifically bind to a 16S ribosomal RNA decoding region construct. *Nucleic Acids Res.* **28**, 2902-10.
55. Horn WT, Convery MA, Stonehouse NJ, Adams CJ, Liljas L, Phillips SE, and Stockley PG (2004) The crystal structure of a high affinity RNA stem-loop complexed with the bacteriophage MS2 capsid: further challenges in the modeling of ligand-RNA interactions. *RNA* **10**, 1776-82.
56. Jiang L, and Patel DJ (1998) Solution structure of the tobramycin-RNA aptamer complex. *Nat. Struct. Mol. Biol.* **5**, 769-74.
57. Robertson SA, Harada K, Frankel AD, and Wemmer DE (2000) Structure Determination and Binding Kinetics of a DNA Aptamer-Argininamide Complex. *Biochemistry* **39**, 946-54.
58. Bing T, Yang X, Mei H, Cao Z, and Shangguan D (2010) Conservative secondary structure motif of streptavidin-binding aptamers generated by different laboratories. *Bioorg. Med. Chem.* **18**, 1798-805.
59. Carothers JM, Davis JH, Chou JJ, and Szostak JW (2006) Solution structure of an informationally complex high-affinity RNA aptamer to GTP. *RNA* **12**, 567-79.
60. Tuerk C, MacDougall S, and Gold L (1992) RNA pseudoknots that inhibit human immunodeficiency virus type 1 reverse transcriptase. *Proceedings of the National Academy of Sciences* **89**, 6988-92.

61. Baker ES, Dupuis NF, and Bowers MT (2009) DNA Hairpin, Pseudoknot, and Cruciform Stability in a Solvent-Free Environment. *The Journal of Physical Chemistry B* **113**, 1722-27.
62. Boiziau C, Dausse E, Yurchenko L, and Toulmé J-J (1999) DNA Aptamers Selected Against the HIV-1trans-Activation-responsive RNA Element Form RNA-DNA Kissing Complexes. *J. Biol. Chem.* **274**, 12730-37.
63. Barbault F, Huynh-Dinh T, Paoletti J, and Lancelot G (2002) A new peculiar DNA structure: NMR solution structure of a DNA kissing complex. *J. Biomol. Struct. Dyn.* **19**, 649-58.
64. Huizenga DE, and Szostak JW (1995) A DNA Aptamer That Binds Adenosine and ATP. *Biochemistry* **34**, 656-65.
65. Wang KY, Krawczyk SH, Bischofberger N, Swaminathan S, and Bolton PH (1993) The tertiary structure of a DNA aptamer which binds to and inhibits thrombin determines activity. *Biochemistry* **32**, 11285-92.
66. Nakano S-i, Fujimoto M, Hara H, and Sugimoto N (1999) Nucleic acid duplex stability: influence of base composition on cation effects. *Nucleic Acids Research* **27**, 2957-65.
67. Williams AP, Longfellow CE, Freier SM, Kierzek R, and Turner DH (1989) Laser temperature-jump, spectroscopic, and thermodynamic study of salt effects on duplex formation by dGCATGC. *Biochemistry* **28**, 4283-91.
68. Murphy MC, Rasnik I, Cheng W, Lohman TM, and Ha T (2004) Probing single-stranded DNA conformational flexibility using fluorescence spectroscopy. *Biophys. J.* **86**, 2530-7.
69. Russo Krauss I, Merlino A, Randazzo A, Novellino E, Mazzarella L, and Sica F (2012) High-resolution structures of two complexes between thrombin and thrombin-binding aptamer shed light on the role of cations in the aptamer inhibitory activity. *Nucleic Acids Res.* **40**, 8119-28.
70. Zichel R, Chearwae W, Pandey GS, Golding B, and Sauna ZE (2012) Aptamers as a Sensitive Tool to Detect Subtle Modifications in Therapeutic Proteins. *PLoS One* **7**, e31948.
71. Förster U, Weigand JE, Trojanowski P, Suess B, and Wachtveitl J (2011) Conformational dynamics of the tetracycline-binding aptamer. *Nucleic Acids Res.* **40**, 1807-17.
72. Lin CH, and Patel DJ (1996) Encapsulating an amino acid in a DNA fold. *Nat. Struct. Mol. Biol.* **3**, 1046-50.

73. Long SB, Long MB, White RR, and Sullenger BA (2008) Crystal structure of an RNA aptamer bound to thrombin. *RNA* **14**, 2504-12.
74. Bianchini M, Radrizzani M, Brocardo MG, Reyes GB, Gonzalez Solveyra C, and Santa-Coloma TA (2001) Specific oligobodies against ERK-2 that recognize both the native and the denatured state of the protein. *J. Immunol. Methods* **252**, 191-7.
75. Murphy MB, Fuller ST, Richardson PM, and Doyle SA (2003) An improved method for the in vitro evolution of aptamers and applications in protein detection and purification. *Nucleic Acids Res.* **31**, e110.
76. Conrad R, Keranen LM, Ellington AD, and Newton AC (1994) Isozyme-specific inhibition of protein kinase C by RNA aptamers. *J. Biol. Chem.* **269**, 32051-4.
77. Kimoto M, Shirouzu M, Mizutani S, Koide H, Kaziro Y, Hirao I, and Yokoyama S (2002) Anti-(Raf-1) RNA aptamers that inhibit Ras-induced Raf-1 activation. *Eur. J. Biochem.* **269**, 697-704.
78. Zimmermann GR, Jenison RD, Wick CL, Simorre JP, and Pardi A (1997) Interlocking structural motifs mediate molecular discrimination by a theophylline-binding RNA. *Nat. Struct. Biol.* **4**, 644-9.
79. Hermann T, and Patel DJ (2000) Adaptive Recognition by Nucleic Acid Aptamers. *Science* **287**, 820-25.
80. Jenison RD, Gill SC, Pardi A, and Polisky B (1994) High-Resolution Molecular Discrimination by RNA. *Science* **263**, 1425-29.
81. Patel DJ, Suri AK, Jiang F, Jiang L, Fan P, Kumar RA, and Nonin S (1997) Structure, recognition and adaptive binding in RNA aptamer complexes. *J. Mol. Biol.* **272**, 645-64.
82. McKeague M, Bradley CR, Girolamo AD, Visconti A, Miller JD, and DeRosa MC (2010) Screening and Initial Binding Assessment of Fumonisin B1 Aptamers. *Int. J. Mol. Sci.* **11**, 4864-81.
83. Blackburn GM, Gait MJ, Loakes D, and Williams DM, eds. (2006). *Nucleic Acids in Chemistry and Biology*. 3rd ed. Cambridge, UK: The Royal Society of Chemistry. 503 p.
84. Ballin JD, Prevas JP, Ross CR, Toth EA, Wilson GM, and Record MT (2010) Contributions of the Histidine Side Chain and the N-terminal α -Amino Group to the Binding Thermodynamics of Oligopeptides to Nucleic Acids as a Function of pH. *Biochemistry* **49**, 2018-30.

85. Kuo T-C, Lee P-C, Tsai C-W, and Chen W-Y (2013) Salt bridge exchange binding mechanism between streptavidin and its DNA aptamer – thermodynamics and spectroscopic evidences. *J. Mol. Recognit.* **26**, 149-59.
86. Lee JH, Jucker F, and Pardi A (2008) Imino proton exchange rates imply an induced-fit binding mechanism for the VEGF165-targeting aptamer, Macugen. *FEBS Lett.* **582**, 1835-9.
87. Huang R-H, Fremont DH, Diener JL, Schaub RG, and Sadler JE (2009) A Structural Explanation for the Antithrombotic Activity of ARC1172, a DNA Aptamer that Binds von Willebrand Factor Domain A1. *Structure* **17**, 1476-84.
88. Seeman NC, Rosenberg JM, and Rich A (1976) Sequence-specific recognition of double helical nucleic acids by proteins. *Proceedings of the National Academy of Sciences* **73**, 804-08.
89. Ahmad S, and Sarai A (2011) Analysis of electric moments of RNA-binding proteins: implications for mechanism and prediction. *BMC Struct. Biol.* **11**, 8.
90. Franks F (1965) Hydrophobic hydration and the effect of hydrogen bonding solutes on the structure of water. *Ann. N. Y. Acad. Sci.* **125**, 277-89.
91. Dill KA (1990) Dominant forces in protein folding. *Biochemistry* **29**, 7133-55.
92. Frank HS, and Evans MW (1945) Free Volume and Entropy in Condensed Systems III. Entropy in Binary Liquid Mixtures; Partial Molal Entropy in Dilute Solutions; Structure and Thermodynamics in Aqueous Electrolytes. *The Journal of Chemical Physics* **13**, 507-32.
93. Silverstein KAT, Dill KA, and Haymet ADJ (2001) Hydrophobicity in a simple model of water: Entropy penalty as a sum of competing terms via full, angular expansion. *The Journal of Chemical Physics* **114**, 6303-14.
94. Spyarakis F, Cozzini P, Bertoli C, Marabotti A, Kellogg G, and Mozzarelli A (2007) Energetics of the protein-DNA-water interaction. *BMC Structural Biology* **7**, 4.
95. Jordan SR, and Pabo CO (1988) Structure of the lambda complex at 2.5 Å resolution: details of the repressor-operator interactions. *Science* **242**, 893-9.
96. Luscombe NM, Laskowski RA, and Thornton JM (2001) Amino acid–base interactions: a three-dimensional analysis of protein–DNA interactions at an atomic level. *Nucleic Acids Research* **29**, 2860-74.
97. Kool ET (2001) Hydrogen bonding, base stacking, and steric effects in dna replication. *Annu. Rev. Biophys. Biomol. Struct.* **30**, 1-22.

98. Ng EWM, and Adamis AP (2006) Anti-VEGF Aptamer (Pegaptanib) Therapy for Ocular Vascular Diseases. *Ann. N. Y. Acad. Sci.* **1082**, 151-71.
99. Famulok M, and Mayer G (2005) Intramers and aptamers: applications in protein-function analyses and potential for drug screening. *Chembiochem* **6**, 19-26.
100. Shastri A, McGregor LM, Liu Y, Harris V, Nan H, Mujica M, Vasquez Y, Bhattacharya A, Ma Y, Aizenberg M, Kuksenok O, Balazs AC, Aizenberg J, and He X (2015) An aptamer-functionalized chemomechanically modulated biomolecule catch-and-release system. *Nat. Chem.* **in press**.
101. Jayasena S (1999) Aptamers: An Emerging Class of Molecules That Rival Antibodies in Diagnostics. *Clin. Chem.* **45**, 1628-50.
102. Ellington A, and Pollard JD (2001) Synthesis and Purification of Oligonucleotides, in "Curr. Protoc. Mol. Biol.", John Wiley & Sons, Inc., p. 2.11.1-25
103. Verma S, and Eckstein F (1998) Modified Oligonucleotides: Synthesis and Strategy for Users. *Annu. Rev. Biochem.* **67**, 99-134.
104. Keefe AD, and Cload ST (2008) SELEX with modified nucleotides. *Curr. Opin. Chem. Biol.* **12**, 448-56.
105. Ng EWM, Shima DT, Calias P, Cunningham ET, Guyer DR, and Adamis AP (2006) Pegaptanib, a targeted anti-VEGF aptamer for ocular vascular disease. *Nat Rev Drug Discov* **5**, 123-32.
106. Vaught JD, Bock C, Carter J, Fitzwater T, Otis M, Schneider D, Rolando J, Waugh S, Wilcox SK, and Eaton BE (2010) Expanding the Chemistry of DNA for in Vitro Selection. *Journal of the American Chemical Society* **132**, 4141-51.
107. von Behring E, and Kitasato S (1890) [The mechanism of diphtheria immunity and tetanus immunity in animals]. *Deutsch med Wochenschr* **16**, 1113-14.
108. Ehrlich P (1891) [Experimental studies on immunity I. About ricin.]. *Deutsch med Wochenschr* **17**, 976-79.
109. Ehrlich P (1891) [Experimental studies on immunity II. About abrin.]. *Deutsch med Wochenschr* **17**, 1218-19.
110. Hage DS (1999) Affinity Chromatography: A Review of Clinical Applications. *Clinical Chemistry* **45**, 593-615.
111. Matos LL, Trufelli DC, de Matos MG, and da Silva Pinhal MA (2010) Immunohistochemistry as an important tool in biomarkers detection and clinical practice. *Biomarker insights* **5**, 9-20.

112. Pei X, Zhang B, Tang J, Liu B, Lai W, and Tang D (2013) Sandwich-type immunosensors and immunoassays exploiting nanostructure labels: A review. *Analytica Chimica Acta* **758**, 1-18.
113. Lequin RM (2005) Enzyme Immunoassay (EIA)/Enzyme-Linked Immunosorbent Assay (ELISA). *Clinical Chemistry* **51**, 2415-18.
114. Wild D, ed. (2013). *The Immunoassay Handbook: Theory and Applications of Ligand Binding, ELISA and Related Techniques*. Fourth ed. Oxford: Elsevier.
115. Reichert JM (2012) Marketed therapeutic antibodies compendium. *mAbs* **4**, 413-15.
116. U.S. Food & Drug Administration (FDA) Eletronic Orange Book: <http://www.accessdata.fda.gov/scripts/cder/ob/>. Accessed February 2015.
117. Chan AC, and Carter PJ (2010) Therapeutic antibodies for autoimmunity and inflammation. *Nat. Rev. Immunol.* **10**, 301-16.
118. Scott AM, Wolchok JD, and Old LJ (2012) Antibody therapy of cancer. *Nat Rev Cancer* **12**, 278-87.
119. Feige MJ, Hendershot LM, and Buchner J (2010) How antibodies fold. *Trends in Biochemical Sciences* **35**, 189-98.
120. Bork P, Holm L, and Sander C (1994) The immunoglobulin fold. Structural classification, sequence patterns and common core. *J Mol Biol* **242**, 309-20.
121. Al-Lazikani B, Lesk AM, and Chothia C (1997) Standard conformations for the canonical structures of immunoglobulins. *J. Mol. Biol.* **273**, 927-48.
122. North B, Lehmann A, and Dunbrack RL (2011) A new clustering of antibody CDR loop conformations. *J. Mol. Biol.* **406**, 228-56.
123. Jerne NK (1974) Towards a network theory of the immune system. *Ann. Immunol. (Paris)* **125c**, 373-89.
124. Burry RW (2010) Antibodies, in "Immunocytochemistry", Springer, New York, p. 7-16
125. Raff MC (1973) T and B Lymphocytes and Immune Responses. *Nature* **242**, 19-23.
126. Ganusov VV, and De Boer RJ (2007) Do most lymphocytes in humans really reside in the gut? *Trends Immunol.* **28**, 514-18.
127. Schroeder Jr HW, and Cavacini L (2010) Structure and function of immunoglobulins. *J. Allergy Clin. Immunol.* **125**, S41-S52.

128. Benjamin DC, Berzofsky JA, East IJ, Gurd FRN, Hannum C, Leach SJ, Margoliash E, Michael JG, Miller A, Prager EM, Reichlin M, Sercarz EE, Smith-Gill SJ, Todd PE, and Wilson AC (1984) The Antigenic Structure of Proteins: A Reappraisal. *Annual Review of Immunology* **2**, 67-101.
129. Kunik V, Peters B, and Ofran Y (2012) Structural consensus among antibodies defines the antigen binding site. *PLoS Comput. Biol.* **8**, e1002388.
130. Jemmerson R (1987) Antigenicity and native structure of globular proteins: low frequency of peptide reactive antibodies. *Proc. Natl. Acad. Sci. U. S. A.* **84**, 9180-4.
131. Yokota A, Tsumoto K, Shiroishi M, Kondo H, and Kumagai I (2003) The Role of Hydrogen Bonding via Interfacial Water Molecules in Antigen-Antibody Complexation: The HyHEL-10-HEL Interaction. *J. Biol. Chem.* **278**, 5410-18.
132. Dougan DA, Malby RL, Gruen LC, Kortt AA, and Hudson PJ (1998) Effects of substitutions in the binding surface of an antibody on antigen affinity. *Protein Eng.* **11**, 65-74.
133. Braden BC, Dall'Acqua W, Eisenstein E, Fields BA, Goldbaum FA, Malchiodi EL, Mariuzza RA, Schwarz FP, Ysern X, and Poljak RJ (1995) Protein motion and lock and key complementarity in antigen-antibody reactions. *Pharm. Acta Helv.* **69**, 225-30.
134. Rini JM, Schulze-Gahmen U, and Wilson IA (1992) Structural evidence for induced fit as a mechanism for antibody-antigen recognition. *Science* **255**, 959-65.
135. Reverberi R, and Reverberi L (2007) Factors affecting the antigen-antibody reaction. *Blood Transfusion* **5**, 227-40.
136. Yu J, Kane S, Wu J, Benedettini E, Li D, Reeves C, Innocenti G, Wetzel R, Crosby K, Becker A, Ferrante M, Cheung WC, Hong X, Chirieac LR, Sholl LM, Haack H, Smith BL, Polakiewicz RD, Tan Y, Gu T-L, Loda M, Zhou X, and Comb MJ (2009) Mutation-Specific Antibodies for the Detection of EGFR Mutations in Non-Small-Cell Lung Cancer. *Clin. Cancer Res.* **15**, 3023-28.
137. Capper D, Zentgraf H, Balss J, Hartmann C, and von Deimling A (2009) Monoclonal antibody specific for IDH1 R132H mutation. *Acta Neuropathol.* **118**, 599-601.
138. Capper D, Preusser M, Habel A, Sahn F, Ackermann U, Schindler G, Pusch S, Mechtersheimer G, Zentgraf H, and von Deimling A (2011) Assessment of BRAF V600E mutation status by immunohistochemistry with a mutation-specific monoclonal antibody. *Acta Neuropathol.* **122**, 11-19.
139. Jin M, and Khan AI (2010) Procalcitonin: Uses in the Clinical Laboratory for the Diagnosis of Sepsis. *Lab Medicine* **41**, 173-77.
140. Waldmann TA (2003) Immunotherapy: past, present and future. *Nat Med* **9**, 269-77.

141. Winter G, and Milstein C (1991) Man-made antibodies. *Nature* **349**, 293-9.
142. Chames P, Van Regenmortel M, Weiss E, and Baty D (2009) Therapeutic antibodies: successes, limitations and hopes for the future. *Br. J. Pharmacol.* **157**, 220-33.
143. Jakobovits A (1995) Production of fully human antibodies by transgenic mice. *Curr Opin Biotechnol* **6**, 561-6.
144. Heinis C, Rutherford T, Freund S, and Winter G (2009) Phage-encoded combinatorial chemical libraries based on bicyclic peptides. *Nat Chem Biol* **5**, 502-07.
145. Sun H, Zhu X, Lu PY, Rosato RR, Tan W, and Zu Y (2014) Oligonucleotide Aptamers: New Tools for Targeted Cancer Therapy. *Mol Ther Nucleic Acids* **3**, e182.
146. Alley SC, Okeley NM, and Senter PD (2010) Antibody–drug conjugates: targeted drug delivery for cancer. *Current Opinion in Chemical Biology* **14**, 529-37.
147. Sano K, Mitsunaga M, Nakajima T, Choyke PL, and Kobayashi H (2012) In vivo breast cancer characterization imaging using two monoclonal antibodies activatably labeled with near infrared fluorophores. *Breast cancer research : BCR* **14**, R61.
148. Atreya R, Neumann H, Neufert C, Waldner MJ, Billmeier U, Zopf Y, Willma M, App C, Munster T, Kessler H, Maas S, Gebhardt B, Heimke-Brinck R, Reuter E, Dorje F, Rau TT, Uter W, Wang TD, Kiesslich R, Vieth M, Hannappel E, and Neurath MF (2014) In vivo imaging using fluorescent antibodies to tumor necrosis factor predicts therapeutic response in Crohn's disease. *Nat Med* **20**, 313-18.
149. Bee C, Abdiche YN, Pons J, and Rajpal A (2013) Determining the Binding Affinity of Therapeutic Monoclonal Antibodies towards Their Native Unpurified Antigens in Human Serum. *PLoS One* **8**, e80501.
150. Fodey TL, Greer NM, and Crooks SR (2009) Antibody production: Low dose immunogen vs. low incorporation hapten using salmeterol as a model. *Anal. Chim. Acta* **637**, 328-32.
151. Rajak P, Vijayalakshmi MA, and Jayaprakash NS (2013) Production and characterization of monoclonal antibodies (mAbs) against human serum albumin (HSA) for the development of an immunoaffinity system with oriented anti-HSA mAbs as immobilized ligand. *J. Pharm. Biomed. Anal.* **78-79**, 154-60.
152. Schillberg S, Twyman RM, and Fischer R (2005) Opportunities for recombinant antigen and antibody expression in transgenic plants - technology assessment. *Vaccine* **23**, 1764-69.
153. McCafferty J, Griffiths AD, Winter G, and Chiswell DJ (1990) Phage antibodies: filamentous phage displaying antibody variable domains. *Nature* **348**, 552-54.

154. Winter G, Griffiths AD, Hawkins RE, and Hoogenboom HR (1994) Making Antibodies by Phage Display Technology. *Annu. Rev. Immunol.* **12**, 433-55.
155. Almagro JC, and Fransson J (2008) Humanization of antibodies. *Front. Biosci.* **13**, 1619-33.
156. Hudson PJ, and Souriau C (2003) Engineered antibodies. *Nat. Med.* **9**, 129-34.
157. Prechl J, Tchorbanov A, Horvath A, Baiu DC, Hazenbos W, Rajnavolgyi E, Kurucz I, Capel PJ, and Erdei A (1999) Targeting of influenza epitopes to murine CR1/CR2 using single-chain antibodies. *Immunopharmacology* **42**, 159-65.
158. Chowdhury PS, and Wu H (2005) Tailor-made antibody therapeutics. *Methods* **36**, 11-24.
159. Van Ness J, Laemmli UK, and Pettijohn DE (1984) Immunization in vitro and production of monoclonal antibodies specific to insoluble and weakly immunogenic proteins. *Proceedings of the National Academy of Sciences* **81**, 7897-901.
160. Falkenberg FW, Weichert H, Krane M, Bartels I, Palme M, Nagels HO, and Fiebig H (1995) In vitro production of monoclonal antibodies in high concentration in a new and easy to handle modular minifermenter. *J. Immunol. Methods* **179**, 13-29.
161. Schwab I, and Nimmerjahn F (2013) Intravenous immunoglobulin therapy: how does IgG modulate the immune system? *Nat Rev Immunol* **13**, 176-89.
162. Hinton PR, Xiong JM, Johlfs MG, Tang MT, Keller S, and Tsurushita N (2006) An engineered human IgG1 antibody with longer serum half-life. *Journal of immunology (Baltimore, Md. : 1950)* **176**, 346-56.
163. Cheng C, Chen YH, Lennox KA, Behlke MA, and Davidson BL (2013) In vivo SELEX for Identification of Brain-penetrating Aptamers. *Mol Ther Nucleic Acids* **2**, e67.
164. Mukhopadhyay R (2005) Aptamers Are Ready for the Spotlight. *Anal. Chem.* **77**, 114 A-18 A.
165. Bruno J (2013) A Review of Therapeutic Aptamer Conjugates with Emphasis on New Approaches. *Pharmaceuticals* **6**, 340-57.
166. Richardson FC, Tennant BC, Meyer DJ, Richardson KA, Mann PC, McGinty GR, Wolf JL, Zack PM, and Bendele RA (1999) An Evaluation of the Toxicities of 2' - Fluorouridine and 2'-Fluorocytidine-HCl in F344 Rats and Woodchucks (*Marmota monax*). *Toxicol. Pathol.* **27**, 607-17.
167. The EyeTech Study Group (2002) Preclinical and Phase 1A Clinical Evaluation of An Anti-Vegf Pegylated Aptamer (Eye001) for the Treatment of Exudative Age-Related Macular Degeneration. *Retina* **22**, 143-52.

168. Wlotzka B, Leva S, Eschgfäller B, Burmeister J, Kleinjung F, Kaduk C, Muhn P, Hess-Stumpp H, and Klussmann S (2002) In vivo properties of an anti-GnRH Spiegelmer: An example of an oligonucleotide-based therapeutic substance class. *Proceedings of the National Academy of Sciences* **99**, 8898-902.
169. Kaufman J, and Kalaitzandonakes N (2011) The economic potential of plant-made pharmaceuticals in the manufacture of biologic pharmaceuticals. *J Commer Biotechnol* **17**, 173-82.
170. Gold L, and Jayasena SD (1990) "Nucleic acid ligand inhibitors to DNA polymerases ". US Patent 5,693,502
171. Cho M, Soo Oh S, Nie J, Stewart R, Eisenstein M, Chambers J, Marth JD, Walker F, Thomson JA, and Soh HT (2013) Quantitative selection and parallel characterization of aptamers. *Proceedings of the National Academy of Sciences* **110**, 18460-65.
172. Bock LC, Griffin LC, Latham JA, Vermaas EH, and Toole JJ (1992) Selection of single-stranded DNA molecules that bind and inhibit human thrombin. *Nature* **355**, 564-66.
173. Harris LJ, Larson SB, Hasel KW, and McPherson A (1997) Refined structure of an intact IgG2a monoclonal antibody. *Biochemistry* **36**, 1581-97.
174. Schultze P, Macaya RF, and Feigon J (1994) Three-dimensional solution structure of the thrombin-binding DNA aptamer d(GGTTGGTGTGGTTGG). *J Mol Biol* **235**, 1532-47.
175. Singhal A, Haynes CA, and Hansen CL (2010) Microfluidic measurement of antibody-antigen binding kinetics from low-abundance samples and single cells. *Anal Chem* **82**, 8671-9.
176. Fitzgerald V, Manning B, O'Donnell B, O'Reilly B, O'Sullivan D, O'Kennedy R, and Leonard P (2015) Exploiting Highly Ordered Subnanoliter Volume Microcapillaries as Microtools for the Analysis of Antibody Producing Cells. *Anal. Chem.* **87**, 997-1003.
177. Debs BE, Utharala R, Balyasnikova IV, Griffiths AD, and Merten CA (2012) Functional single-cell hybridoma screening using droplet-based microfluidics. *Proceedings of the National Academy of Sciences* **109**, 11570-75.
178. Xu Y, Roach W, Sun T, Jain T, Prinz B, Yu T-Y, Torrey J, Thomas J, Bobrowicz P, Vásquez M, Wittrup KD, and Krauland E (2013) Addressing polyspecificity of antibodies selected from an in vitro yeast presentation system: a FACS-based, high-throughput selection and analytical tool. *Protein Engineering Design and Selection* **26**, 663-70.

179. Schofield D, Pope A, Clementel V, Buckell J, Chapple S, Clarke K, Conquer J, Crofts A, Crowther S, Dyson M, Flack G, Griffin G, Hooks Y, Howat W, Kolb-Kokocinski A, Kunze S, Martin C, Maslen G, Mitchell J, O'Sullivan M, Perera R, Roake W, Shadbolt SP, Vincent K, Warford A, Wilson W, Xie J, Young J, and McCafferty J (2007) Application of phage display to high throughput antibody generation and characterization. *Genome Biol.* **8**, R254.
180. Tickle S, Adams R, Brown D, Griffiths M, Lightwood D, and Lawson A (2009) High-Throughput Screening for High Affinity Antibodies. *Journal of the Association for Laboratory Automation* **14**, 303-07.
181. Jin A, Ozawa T, Tajiri K, Obata T, Kondo S, Kinoshita K, Kadowaki S, Takahashi K, Sugiyama T, Kishi H, and Muraguchi A (2009) A rapid and efficient single-cell manipulation method for screening antigen-specific antibody-secreting cells from human peripheral blood. *Nat. Med.* **15**, 1088-92.
182. Love JC, Ronan JL, Grotenbreg GM, van der Veen AG, and Ploegh HL (2006) A microengraving method for rapid selection of single cells producing antigen-specific antibodies. *Nat Biotech* **24**, 703-07.
183. Mills DR, Peterson RL, and Spiegelman S (1967) An extracellular Darwinian experiment with a self-duplicating nucleic acid molecule. *Proc. Natl. Acad. Sci. U. S. A.* **58**, 217-24.
184. Market E, and Papavasiliou FN (2003) V(D)J Recombination and the Evolution of the Adaptive Immune System. *PLoS Biol* **1**, e16.
185. McBride LJ, and Caruthers MH (1983) An investigation of several deoxynucleoside phosphoramidites useful for synthesizing deoxyoligonucleotides. *Tetrahedron Lett.* **24**, 245-48.
186. Bartel DP, Zapp ML, Green MR, and Szostak JW (1991) HIV-1 rev regulation involves recognition of non-Watson-Crick base pairs in viral RNA. *Cell* **67**, 529-36.
187. Lorenz C, von Pelchrzim F, and Schroeder R (2006) Genomic systematic evolution of ligands by exponential enrichment (Genomic SELEX) for the identification of protein-binding RNAs independent of their expression levels. *Nat. Protoc.* **1**, 2204-12.
188. Zimmermann B, Bilusic I, Lorenz C, and Schroeder R (2010) Genomic SELEX: A discovery tool for genomic aptamers. *Methods* **52**, 125-32.
189. Kuwahara M, and Obika S (2013) In vitro selection of BNA (LNA) aptamers. *Artificial DNA, PNA & XNA* **4**, 39-48.
190. Klusmann S, Nolte A, Bald R, Erdmann VA, and Furste JP (1996) Mirror-image RNA that binds D-adenosine. *Nature biotechnology* **14**, 1112-5.

191. Thiel WH, Bair T, Wyatt Thiel K, Dassie JP, Rockey WM, Howell CA, Liu XY, Dupuy AJ, Huang L, Owczarzy R, Behlke MA, McNamara JO, and Giangrande PH (2011) Nucleotide Bias Observed with a Short SELEX RNA Aptamer Library. *Nucleic Acid Therapeutics* **21**, 253-63.
192. Hall B, Micheletti JM, Satya P, Ogle K, Pollard J, and Ellington AD (2001) Design, Synthesis, and Amplification of DNA Pools for In Vitro Selection, in "Curr. Protoc. Mol. Biol.", John Wiley & Sons, Inc., p. 24.2.1-27
193. Legiewicz M, Lozupone C, Knight R, and Yarus M (2005) Size, constant sequences, and optimal selection. *RNA* **11**, 1701-09.
194. SantaLucia J, Jr., and Hicks D (2004) The thermodynamics of DNA structural motifs. *Annu Rev Biophys Biomol Struct* **33**, 415-40.
195. Stoltenburg R, Reinemann C, and Strehlitz B (2007) SELEX - A (r)evolutionary method to generate high-affinity nucleic acid ligands. *Biomolecular Engineering* **24**, 381-403.
196. Stovall GM, Cox JC, and Ellington AD (2004) Automated Optimization of Aptamer Selection Buffer Conditions. *Journal of the Association for Laboratory Automation* **9**, 117-22.
197. Oh SS, Ahmad KM, Cho M, Kim S, Xiao Y, and Soh HT (2011) Improving Aptamer Selection Efficiency through Volume Dilution, Magnetic Concentration, and Continuous Washing in Microfluidic Channels. *Anal. Chem.* **83**, 6883-89.
198. McKeague M, and DeRosa MC (2012) Challenges and Opportunities for Small Molecule Aptamer Development. *Journal of Nucleic Acids* **2012**, 20.
199. Irvine D, Tuerk C, and Gold L (1991) Selexion : Systematic evolution of ligands by exponential enrichment with integrated optimization by non-linear analysis. *J. Mol. Biol.* **222**, 739-61.
200. Vant-Hull B, Payano-Baez A, Davis RH, and Gold L (1998) The mathematics of SELEX against complex targets. *J. Mol. Biol.* **278**, 579-97.
201. Klussmann S (2006) *The Aptamer Handbook: Functional Oligonucleotides and Their Applications*, ed. Weinheim, Germany
202. Pinto A, Polo PN, Henry O, Redondo MC, Svobodova M, and O'Sullivan CK (2014) Label-free detection of gliadin food allergen mediated by real-time apta-PCR. *Anal. Bioanal. Chem.* **406**, 515-24.
203. Lou X, Qian J, Xiao Y, Viel L, Gerdon AE, Lagally ET, Atzberger P, Tarasow TM, Heeger AJ, and Soh HT (2009) Micromagnetic selection of aptamers in microfluidic channels. *Proceedings of the National Academy of Sciences* **106**, 2989-94.

204. Nieuwlandt D (2000) In vitro selection of functional nucleic acid sequences. *Curr. Issues Mol. Biol.* **2**, 9-16.
205. Musheev MU, and Krylov SN (2006) Selection of aptamers by systematic evolution of ligands by exponential enrichment: addressing the polymerase chain reaction issue. *Anal. Chim. Acta* **564**, 91-6.
206. Kai E, Sumikura K, Ikebukuro K, and Karube I (1998) Purification of single stranded DNA from asymmetric PCR product using the SMART system. *Biotechnology Techniques* **12**, 935-39.
207. Pagratis NC (1996) Rapid preparation of single stranded DNA from PCR products by streptavidin induced electrophoretic mobility shift. *Nucleic Acids Research* **24**, 3645-46.
208. Williams KP, and Bartel DP (1995) PCR product with strands of unequal length. *Nucleic Acids Research* **23**, 4220-21.
209. Civit L, Fragoso A, and O'Sullivan CK (2012) Evaluation of techniques for generation of single-stranded DNA for quantitative detection. *Analytical Biochemistry* **431**, 132-38.
210. Avci-Adali M, Paul A, Wilhelm N, Ziemer G, and Wendel HP (2009) Upgrading SELEX technology by using lambda exonuclease digestion for single-stranded DNA generation. *Molecules* **15**, 1-11.
211. Jones LA, Clancy LE, Rawlinson WD, and White PA (2006) High-affinity aptamers to subtype 3a hepatitis C virus polymerase display genotypic specificity. *Antimicrob. Agents Chemother.* **50**, 3019-27.
212. Meyer S, Maufort JP, Nie J, Stewart R, McIntosh BE, Conti LR, Ahmad KM, Soh HT, and Thomson JA (2013) Development of an efficient targeted cell-SELEX procedure for DNA aptamer reagents. *PLoS One* **8**, e71798.
213. Citartan M, Tang T-H, Tan S-C, and Gopinath SB (2011) Conditions optimized for the preparation of single-stranded DNA (ssDNA) employing lambda exonuclease digestion in generating DNA aptamer. *World Journal of Microbiology and Biotechnology* **27**, 1167-73.
214. Rotherham LS, Maserumule C, Dheda K, Theron J, and Khati M (2012) Selection and Application of ssDNA Aptamers to Detect Active TB from Sputum Samples. *PLoS ONE* **7**, e46862.
215. Ayel E, and Escudé C (2009) In vitro selection of oligonucleotides that bind double-stranded DNA in the presence of triplex-stabilizing agents. *Nucleic Acids Res.* **38**, e31.

216. Meng H-W, Pagano JM, White BS, Toyoda Y, Min IM, Craighead HG, Shalloway D, Lis JT, Xiao K, and Jin MM (2014) Discovering Aptamers by Cell-SELEX against Human Soluble Growth Factors Ectopically Expressed on Yeast Cell Surface. *PLoS ONE* **9**, e93052.
217. Marshall KA, and Ellington AD (2000) In vitro selection of RNA aptamers, in "Methods Enzymol.", Academic Press. Vol. **Volume 318**, p. 193-214
218. Wilson DS, and Szostak JW (1999) In vitro selection of functional nucleic acids. *Annu. Rev. Biochem.* **68**, 611-47.
219. Bridonneau P, Gold L, Hicke B, and Parma DH (1998) "High affinity nucleic acid ligands to lectins". US Patent 6,001,988
220. Dean TR, Allen SV, and Miller ES (2005) In vitro selection of phage RB69 RegA RNA binding sites yields UAA triplets. *Virology* **336**, 26-36.
221. McKeague M, Bradley CR, De Girolamo A, Visconti A, Miller JD, and DeRosa MC (2010) Screening and Initial Binding Assessment of Fumonisin B(1) Aptamers. *Int. J. Mol. Sci.* **11**, 4864-81.
222. Simmons SC, McKenzie EA, Harris LK, Aplin JD, Brenchley PE, Velasco-Garcia MN, and Missailidis S (2012) Development of Novel Single-Stranded Nucleic Acid Aptamers against the Pro-Angiogenic and Metastatic Enzyme Heparanase (HPSE1). *PLoS ONE* **7**, e37938.
223. Rozenblum GT, Kaufman T, and Vitullo AD (2014) Myelin Basic Protein and a Multiple Sclerosis-related MBP-peptide Bind to Oligonucleotides. *Mol Ther Nucleic Acids* **3**, e192.
224. Wochner A, Cech B, Menger M, Erdmann VA, and Glokler J (2007) Semi-automated selection of DNA aptamers using magnetic particle handling. *Biotechniques* **43**, 344-53.
225. Nagarkatti R, de Araujo FF, Gupta C, and Debrabant A (2014) Aptamer Based, Non-PCR, Non-Serological Detection of Chagas Disease Biomarkers in *Trypanosoma cruzi* Infected Mice. *PLoS Negl. Trop. Dis.* **8**, e2650.
226. Hoinka J, Zotenko E, Friedman A, Sauna ZE, and Przytycka TM (2012) Identification of sequence-structure RNA binding motifs for SELEX-derived aptamers. *Bioinformatics* **28**, i215-23.
227. Fukusho S, Furusawa H, and Okahata Y (2000) In vitro selection and analysis of RNA aptamer recognize arginine-rich motif (ARM) model peptide on a QCM. *Nucleic Acids Symp. Ser.* **44**, 187-88.
228. Gold L, and Tuerk C (1995) "Nucleic acid ligands". US Patent 5,475,096

229. Thiel KW, and Giangrande PH (2009) Therapeutic Applications of DNA and RNA Aptamers. *Oligonucleotides* **19**, 209-22.
230. Brody EN, and Gold L (2000) Aptamers as therapeutic and diagnostic agents. *J. Biotechnol.* **74**, 5-13.
231. Jolma A, Kivioja T, Toivonen J, Cheng L, Wei G, Enge M, Taipale M, Vaquerizas JM, Yan J, Sillanpää MJ, Bonke M, Palin K, Talukder S, Hughes TR, Luscombe NM, Ukkonen E, and Taipale J (2010) Multiplexed massively parallel SELEX for characterization of human transcription factor binding specificities. *Genome Res.* **20**, 861-73.
232. Djordjevic M (2007) SELEX experiments: New prospects, applications and data analysis in inferring regulatory pathways. *Biomolecular Engineering* **24**, 179-89.
233. Lakhin AV, Tarantul VZ, and Gening LV (2013) Aptamers: Problems, Solutions and Prospects. *Acta Naturae* **5**, 34-43.
234. Gold L, Zichi DA, Jenison RD, and Schneider DJ (2003) "Method for the automated generation of nucleic acid ligands". US Patent 6,569,620
235. Biesecker G, Jayasena S, Gold L, Smith D, and Kirschenheuter G (2002) "Systematic evolution of ligands by exponential enrichment: blended selex". US Patent 6,465,189
236. Bowser M, and Mendonsa S (2004) "In vitro evolution of functional RNA and DNA using electrophoretic selection". US Patent Application 20040018530
237. Gold L, Eaton B, Smith D, Wecker M, and Jensen K (2001) "Systematic evolution of ligands by exponential enrichment: Chemi-SELEX". US Patent 6,300,074
238. Burke D, Eaton BE, Gold L, and Tarasow T (1998) "Systematic evolution of ligands by exponential enrichment: chimeric selex". US Patent 5,773,598
239. Smith JD, and Gold L (2003) "Conditional-selex". US Patent 6,506,887
240. Gold L, Jenison RD, and Polisky B (1996) "High-affinity nucleic acid ligands that discriminate between theophylline and caffeine". US Patent 5,580,737
241. Gold L, Schneider DJ, and Vanderslice R (1999) "Flow cell SELEX". US Patent 5,861,254
242. Krylov S, and Berezovski M (2010) "Non-equilibrium capillary electrophoresis of equilibrium mixtures (NECEEM)-based methods for drug and diagnostic development". US Patent 7,672,786
243. Eaton BE, and Gold L (1998) "Parallel selex". US Patent 5,723,289

244. Atkinson B, Gold L, Jensen K, Koch T, Ringquist S, and Willis M (1999) "Systematic evolution of ligands by exponential enrichment: photoselection of nucleic acid ligands and solution selex". US Patent 6,001,577
245. Gold L, Zichi DA, and Smith JD (2002) "Modified SELEX processes without purified protein". US Patent 6,376,190
246. Gold L, and Ringquist S (1996) "Systematic evolution of ligands by exponential enrichment: Solution SELEX". US Patent 5,567,588
247. Chen H, Gold L, Jensen KB, Morris KN, and Stephens A (2000) "Systematic evolution of ligands by exponential enrichment: tissue selex". US Patent 6,114,120
248. Sullenger BA, and Rusconi CP (2007) "RNA aptamers and methods for identifying the same". US Patent 7,312,325
249. Smith JD, and Gold L (2002) "Transcription-free selex". US Patent 6,387,620
250. Pagratis N, Gold L, Shtatland T, and Javornik B (2001) "Truncation selex method". US Patent 6,261,774
251. Sefah K, Yang Z, Bradley KM, Hoshika S, Jimenez E, Zhang L, Zhu G, Shanker S, Yu F, Turek D, Tan W, and Benner SA (2014) In vitro selection with artificial expanded genetic information systems. *Proc. Natl. Acad. Sci. U. S. A.* **111**, 1449-54.
252. Davies DR, Gelinis AD, Zhang C, Rohloff JC, Carter JD, O'Connell D, Waugh SM, Wolk SK, Mayfield WS, Burgin AB, Edwards TE, Stewart LJ, Gold L, Janjic N, and Jarvis TC (2012) Unique motifs and hydrophobic interactions shape the binding of modified DNA ligands to protein targets. *Proc. Natl. Acad. Sci. U. S. A.* **109**, 19971-6.
253. Kuwahara M, and Obika S (2013) In vitro selection of BNA (LNA) aptamers. *Artif DNA PNA XNA* **4**, 39-48.
254. Forster C, Zydek M, Rothkegel M, Wu Z, Gallin C, Gessner R, Lisdat F, and Furste JP (2012) Properties of an LNA-modified ricin RNA aptamer. *Biochem. Biophys. Res. Commun.* **419**, 60-5.
255. Weng C-H, Huang C-J, and Lee G-B (2012) Screening of Aptamers on Microfluidic Systems for Clinical Applications. *Sensors* **12**, 9514-29.
256. Darmostuk M, Rimpelová S, Gbelcová H, and Ruml T (2015) Current approaches in SELEX: An update to aptamer selection technology. *Biotechnology Advances* **in press**.
257. Janas T, and Janas T (2011) The selection of aptamers specific for membrane molecular targets. *Cell. Mol. Biol. Lett.* **16**, 25-39.

258. Gevertz J, Gan HH, and Schlick T (2005) In vitro RNA random pools are not structurally diverse: A computational analysis. *RNA* **11**, 853-63.
259. Bartel DP, and Szostak JW (1993) Isolation of new ribozymes from a large pool of random sequences. *Science* **261**, 1411-8.
260. Shoji A, Kuwahara M, Ozaki H, and Sawai H (2007) Modified DNA Aptamer That Binds the (R)-Isomer of a Thalidomide Derivative with High Enantioselectivity. *J. Am. Chem. Soc.* **129**, 1456-64.
261. Gold L, Ayers D, Bertino J, Bock C, Bock A, Brody EN, Carter J, Dalby AB, Eaton BE, Fitzwater T, Flather D, Forbes A, Foreman T, Fowler C, Gawande B, Goss M, Gunn M, Gupta S, Halladay D, Heil J, Heilig J, Hicke B, Husar G, Janjic N, Jarvis T, Jennings S, Katilius E, Keeney TR, Kim N, Koch TH, Kraemer S, Kroiss L, Le N, Levine D, Lindsey W, Lollo B, Mayfield W, Mehan M, Mehler R, Nelson SK, Nelson M, Nieuwlandt D, Nikrad M, Ochsner U, Ostroff RM, Otis M, Parker T, Pietrasiewicz S, Resnicow DI, Rohloff J, Sanders G, Sattin S, Schneider D, Singer B, Stanton M, Sterkel A, Stewart A, Stratford S, Vaught JD, Vrkljan M, Walker JJ, Watrobka M, Waugh S, Weiss A, Wilcox SK, Wolfson A, Wolk SK, Zhang C, and Zichi D (2010) Aptamer-Based Multiplexed Proteomic Technology for Biomarker Discovery. *PLoS One* **5**, e15004.
262. Kraemer S, Vaught JD, Bock C, Gold L, Katilius E, Keeney TR, Kim N, Saccomano NA, Wilcox SK, Zichi D, and Sanders GM (2011) From SOMAmer-Based Biomarker Discovery to Diagnostic and Clinical Applications: A SOMAmer-Based, Streamlined Multiplex Proteomic Assay. *PLoS One* **6**, e26332.
263. Pan W, and Clawson G (2009) The Shorter the Better: Reducing Fixed Primer Regions of Oligonucleotide Libraries for Aptamer Selection. *Molecules* **14**, 1353-69.
264. Pan W, Xin P, and Clawson GA (2008) Minimal primer and primer-free SELEX protocols for selection of aptamers from random DNA libraries. *Biotechniques* **44**, 351-60.
265. Legiewicz M, and Yarus M (2005) A More Complex Isoleucine Aptamer with a Cognate Triplet. *J. Biol. Chem.* **280**, 19815-22.
266. Zhang Z, Guo L, Guo A, Xu H, Tang J, Guo X, and Xie J (2010) In vitro lectin-mediated selection and characterization of rHuEPO-a-binding ssDNA aptamers. *Bioorg. Med. Chem.* **18**, 8016-25.
267. Nonaka Y, Sode K, and Ikebukuro K (2010) Screening and Improvement of an Anti-VEGF DNA Aptamer. *Molecules* **15**, 215-25.
268. Chang Y-C, Kao W-C, Wang W-Y, Wang W-Y, Yang R-B, and Peck K (2009) Identification and characterization of oligonucleotides that inhibit Toll-like receptor 2-associated immune responses. *The FASEB Journal* **23**, 3078-88.

269. Vater A, Jarosch F, Buchner K, and Klussmann S (2003) Short bioactive Spiegelmers to migraine associated calcitonin gene related peptide rapidly identified by a novel approach: Tailored SELEX. *Nucleic Acids Res.* **31**, e130.
270. Lai Y-T, and DeStefano JJ (2011) A primer-free method that selects high-affinity single-stranded DNA aptamers using thermostable RNA ligase. *Anal. Biochem.* **414**, 246-53.
271. Jarosch F, Buchner K, and Klussmann S (2006) In vitro selection using a dual RNA library that allows primerless selection. *Nucleic Acids Res.* **34**, e86.
272. Shtatland T, Gill SC, Javornik BE, Johansson HE, Singer BS, Uhlenbeck OC, Zichi DA, and Gold L (2000) Interactions of Escherichia coli RNA with bacteriophage MS2 coat protein: genomic SELEX. *Nucleic Acids Res.* **28**, e93.
273. Gopinath S (2007) Methods developed for SELEX. *Anal. Bioanal. Chem.* **387**, 171-82.
274. Kong HY, and Byun J (2013) Nucleic Acid aptamers: new methods for selection, stabilization, and application in biomedical science. *Biomol. Ther. (Seoul)* **21**, 423-34.
275. Mosing RK, and Bowser MT (2007) Microfluidic selection and applications of aptamers. *J Sep Sci* **30**, 1420-6.
276. Kulbachinskiy AV (2007) Methods for selection of aptamers to protein targets. *Biochemistry (Mosc.)* **72**, 1505-18.
277. Weng C-H, Huang C-J, and Lee G-B (2012) Screening of Aptamers on Microfluidic Systems for Clinical Applications. *Sensors (Basel, Switzerland)* **12**, 9514-29.
278. Shi H, Fan X, Ni Z, and Lis JT (2002) Evolutionary dynamics and population control during in vitro selection and amplification with multiple targets. *RNA* **8**, 1461-70.
279. Cox JC, Hayhurst A, Hesselberth J, Bayer TS, Georgiou G, and Ellington AD (2002) Automated selection of aptamers against protein targets translated in vitro: from gene to aptamer. *Nucleic Acids Res.* **30**, e108-e08.
280. Buddai SK, Layzer JM, Lu G, Rusconi CP, Sullenger BA, Monroe DM, and Krishnaswamy S (2010) An anticoagulant RNA aptamer that inhibits proteinase-cofactor interactions within prothrombinase. *J. Biol. Chem.* **285**, 5212-23.
281. Lakamp AS, and Ouellette MM (2011) A ssDNA Aptamer That Blocks the Function of the Anti-FLAG M2 Antibody. *Journal of Nucleic Acids* **2011**, 1-11.
282. Mayer G, and Hover T (2009) In vitro selection of ssDNA aptamers using biotinylated target proteins. *Methods Mol. Biol.* **535**, 19-32.

283. Murphy MB, Fuller ST, Richardson PM, and Doyle SA (2003) An improved method for the in vitro evolution of aptamers and applications in protein detection and purification. *Nucleic Acids Res.* **31**, e110-e10.
284. Balogh Z, Lautner G, Bardóczy V, Komorowska B, Gyurcsányi RE, and Mészáros T (2010) Selection and versatile application of virus-specific aptamers. *The FASEB Journal* **24**, 4187-95.
285. Wang J, Rudzinski JF, Gong Q, Soh HT, and Atzberger PJ (2012) Influence of Target Concentration and Background Binding on In Vitro Selection of Affinity Reagents. *PLoS One* **7**, e43940.
286. Berezovski MV, Musheev MU, Drabovich AP, Jitkova JV, and Krylov SN (2006) Non-SELEX: selection of aptamers without intermediate amplification of candidate oligonucleotides. *Nat. Protocols* **1**, 1359-69.
287. Biesecker G, Dihel L, Enney K, and Bendele RA (1999) Derivation of RNA aptamer inhibitors of human complement C5. *Immunopharmacology* **42**, 219-30.
288. Tasset DM, Kubik MF, and Steiner W (1997) Oligonucleotide inhibitors of human thrombin that bind distinct epitopes. *J. Mol. Biol.* **272**, 688-98.
289. Green LS, Jellinek D, Bell C, Beebe LA, Feistner BD, Gill SC, Jucker FM, and Janjić Na (1995) Nuclease-resistant nucleic acid ligands to vascular permeability factor/vascular endothelial growth factor. *Chem. Biol.* **2**, 683-95.
290. Davis KA, Lin Y, Abrams B, and Jayasena SD (1998) Staining of cell surface human CD4 with 2'-F-pyrimidine-containing RNA aptamers for flow cytometry. *Nucleic Acids Res.* **26**, 3915-24.
291. Liu Y, Kuan CT, Mi J, Zhang X, Clary BM, Bigner DD, and Sullenger BA (2009) Aptamers selected against the unglycosylated EGFRvIII ectodomain and delivered intracellularly reduce membrane-bound EGFRvIII and induce apoptosis. *Biol. Chem.* **390**, 137-44.
292. Hoehlig K, Maasch C, Shushakova N, Buchner K, Huber-Lang M, Purschke WG, Vater A, and Klussmann S (2013) A Novel C5a-neutralizing Mirror-image (L-)Aptamer Prevents Organ Failure and Improves Survival in Experimental Sepsis. *Mol. Ther.* **21**, 2236-46.
293. Daniels DA, Sohal AK, Rees S, and Grisshammer R (2002) Generation of RNA aptamers to the G-protein-coupled receptor for neurotensin, NTS-1. *Anal. Biochem.* **305**, 214-26.
294. Lupold SE, Hicke BJ, Lin Y, and Coffey DS (2002) Identification and characterization of nuclease-stabilized RNA molecules that bind human prostate cancer cells via the prostate-specific membrane antigen. *Cancer Res.* **62**, 4029-33.

295. Ahmad KM, Oh SS, Kim S, McClellan FM, Xiao Y, and Soh HT (2011) Probing the Limits of Aptamer Affinity with a Microfluidic SELEX Platform. *PLoS One* **6**, e27051.
296. Cho M, Xiao Y, Nie J, Stewart R, Csordas AT, Oh SS, Thomson JA, and Soh HT (2010) Quantitative selection of DNA aptamers through microfluidic selection and high-throughput sequencing. *Proceedings of the National Academy of Sciences* **107**, 15373-78.
297. Huang CJ, Lin HI, Shiesh SC, and Lee GB (2010) Integrated microfluidic system for rapid screening of CRP aptamers utilizing systematic evolution of ligands by exponential enrichment (SELEX). *Biosens. Bioelectron.* **25**, 1761-6.
298. Mallikaratchy P, Stahelin RV, Cao Z, Cho W, and Tan W (2006) Selection of DNA ligands for protein kinase C-delta. *Chemical Communications* **30**, 3229-31.
299. Drabovich A, Berezovski M, and Krylov SN (2005) Selection of Smart Aptamers by Equilibrium Capillary Electrophoresis of Equilibrium Mixtures (ECEEM). *J. Am. Chem. Soc.* **127**, 11224-25.
300. Nitsche A, Kurth A, Dunkhorst A, Pänke O, Sielaff H, Junge W, Muth D, Scheller F, Stöcklein W, Dahmen C, Pauli G, and Kage A (2007) One-step selection of Vaccinia virus-binding DNA aptamers by MonoLEX. *BMC Biotechnol.* **7**, 48-48.
301. Latulippe DR, Szeto K, Ozer A, Duarte FM, Kelly CV, Pagano JM, White BS, Shalloway D, Lis JT, and Craighead HG (2013) Multiplexed Microcolumn-Based Process for Efficient Selection of RNA Aptamers. *Anal. Chem.* **85**, 3417-24.
302. Drabovich A, Berezovski M, and Krylov SN (2005) Selection of smart aptamers by equilibrium capillary electrophoresis of equilibrium mixtures (ECEEM). *J. Am. Chem. Soc.* **127**, 11224-5.
303. Berezovski M, Drabovich A, Krylova SM, Musheev M, Okhonin V, Petrov A, and Krylov SN (2005) Nonequilibrium capillary electrophoresis of equilibrium mixtures: a universal tool for development of aptamers. *J. Am. Chem. Soc.* **127**, 3165-71.
304. Berezovski M, Drabovich A, Krylova SM, Musheev M, Okhonin V, Petrov A, and Krylov SN (2005) Nonequilibrium Capillary Electrophoresis of Equilibrium Mixtures: A Universal Tool for Development of Aptamers. *J. Am. Chem. Soc.* **127**, 3165-71.
305. Yang J, and Bowser MT (2013) Capillary Electrophoresis-SELEX Selection of Catalytic DNA Aptamers for a Small-Molecule Porphyrin Target. *Anal. Chem.* **85**, 1525-30.
306. Li Y, Geyer CR, and Sen D (1996) Recognition of anionic porphyrins by DNA aptamers. *Biochemistry* **35**, 6911-22.

307. Mosing RK, Mendonsa SD, and Bowser MT (2005) Capillary Electrophoresis-SELEX Selection of Aptamers with Affinity for HIV-1 Reverse Transcriptase. *Anal. Chem.* **77**, 6107-12.
308. Kasahara Y, Irisawa Y, Ozaki H, Obika S, and Kuwahara M (2013) 2',4'-BNA/LNA aptamers: CE-SELEX using a DNA-based library of full-length 2'-O,4'-C-methylene-bridged/linked bicyclic ribonucleotides. *Bioorg. Med. Chem. Lett.* **23**, 1288-92.
309. Mosing RK, and Bowser MT (2008) CE-SELEX: Isolating Aptamers Using Capillary Electrophoresis, in "Handbook of Capillary and Microchip Electrophoresis and Associated Microtechniques", CRC Press, p. 825-36
310. Qian J, Lou X, Zhang Y, Xiao Y, and Soh HT (2009) Generation of Highly Specific Aptamers via Micromagnetic Selection. *Anal. Chem.* **81**, 5490-95.
311. Stoltenburg R, Reinemann C, and Strehlitz B (2005) FluMag-SELEX as an advantageous method for DNA aptamer selection. *Anal. Bioanal. Chem.* **383**, 83-91.
312. Davis JH, and Szostak JW (2002) Isolation of high-affinity GTP aptamers from partially structured RNA libraries. *Proceedings of the National Academy of Sciences* **99**, 11616-21.
313. Bittker JA, Le BV, and Liu DR (2002) Nucleic acid evolution and minimization by nonhomologous random recombination. *Nat. Biotechnol.* **20**, 1024-29.
314. Marshall KA, and Ellington AD (2000) In vitro selection of RNA aptamers. *Methods Enzymol.* **318**, 193-214.
315. Haas MJ (2009) Apt screening with microfluidics. *SciBX* **2**, 1-2.
316. Hamula CLA, Guthrie JW, Zhang H, Li X-F, and Le XC (2006) Selection and analytical applications of aptamers. *TrAC Trends in Analytical Chemistry* **25**, 681-91.
317. Ozer A, White BS, Lis JT, and Shalloway D (2013) Density-dependent cooperative non-specific binding in solid-phase SELEX affinity selection. *Nucleic Acids Res.* **41**, 7167-75.
318. Tok J, Lai J, Leung T, and Li SF (2010) Selection of aptamers for signal transduction proteins by capillary electrophoresis. *Electrophoresis* **31**, 2055-62.
319. Szeto K, Latulippe DR, Ozer A, Pagano JM, White BS, Shalloway D, Lis JT, and Craighead HG (2013) RAPID-SELEX for RNA Aptamers. *PLoS One* **8**, e82667.
320. Civit L, Fragoso A, and O'Sullivan CK (2012) Evaluation of techniques for generation of single-stranded DNA for quantitative detection. *Anal. Biochem.* **431**, 132-38.

321. Svobodova M, Pinto A, Nadal P, and CK OS (2012) Comparison of different methods for generation of single-stranded DNA for SELEX processes. *Anal. Bioanal. Chem.* **404**, 835-42.
322. Lee G, Yoo J, Leslie BJ, and Ha T (2011) Single-molecule analysis reveals three phases of DNA degradation by an exonuclease. *Nat. Chem. Biol.* **7**, 367-74.
323. Thompson JR, Marcelino LA, and Polz MF (2002) Heteroduplexes in mixed-template amplifications: formation, consequence and elimination by 'reconditioning PCR'. *Nucleic Acids Res.* **30**, 2083-88.
324. Nakano M, Komatsu J, Matsuura S-i, Takashima K, Katsura S, and Mizuno A (2003) Single-molecule PCR using water-in-oil emulsion. *J. Biotechnol.* **102**, 117-24.
325. Shao K, Ding W, Wang F, Li H, Ma D, and Wang H (2011) Emulsion PCR: A High Efficient Way of PCR Amplification of Random DNA Libraries in Aptamer Selection. *PLoS One* **6**, e24910.
326. Williams R, Peisajovich SG, Miller OJ, Magdassi S, Tawfik DS, and Griffiths AD (2006) Amplification of complex gene libraries by emulsion PCR. *Nat Meth* **3**, 545-50.
327. Margulies M, Egholm M, Altman WE, Attiya S, Bader JS, Bemben LA, Berka J, Braverman MS, Chen Y-J, Chen Z, Dewell SB, Du L, Fierro JM, Gomes XV, Godwin BC, He W, Helgesen S, Ho CH, Irzyk GP, Jando SC, Alenquer MLI, Jarvie TP, Jirage KB, Kim J-B, Knight JR, Lanza JR, Leamon JH, Lefkowitz SM, Lei M, Li J, Lohman KL, Lu H, Makhijani VB, McDade KE, McKenna MP, Myers EW, Nickerson E, Nobile JR, Plant R, Puc BP, Ronan MT, Roth GT, Sarkis GJ, Simons JF, Simpson JW, Srinivasan M, Tartaro KR, Tomasz A, Vogt KA, Volkmer GA, Wang SH, Wang Y, Weiner MP, Yu P, Begley RF, and Rothberg JM (2005) Genome sequencing in microfabricated high-density picolitre reactors. *Nature* **437**, 376-80.
328. Schütze T, Wilhelm B, Greiner N, Braun H, Peter F, Mörl M, Erdmann VA, Lehrach H, Konthur Z, Menger M, Arndt PF, and Glökler J (2011) Probing the SELEX Process with Next-Generation Sequencing. *PLoS One* **6**, e29604.
329. Hoon S, Zhou B, Janda KD, Brenner S, and Scolnick J (2011) Aptamer selection by high-throughput sequencing and informatic analysis. *Biotechniques* **51**, 413-16.
330. Mosing RK, and Bowser MT (2009) Isolating Aptamers Using Capillary Electrophoresis-SELEX (CE-SELEX), in "Nucleic Acid and Peptide Aptamers: Methods and Protocols". Vol. **535**, p. 33-43
331. Cox JC, Hayhurst A, Hesselberth J, Bayer TS, Georgiou G, and Ellington AD (2002) Automated selection of aptamers against protein targets translated in vitro: from gene to aptamer. *Nucl. Acids Res.* **30**, e108.

332. Ogawa N, and Biggin M (2012) High-Throughput SELEX Determination of DNA Sequences Bound by Transcription Factors In Vitro, in "Gene Regulatory Networks", Humana Press. Vol. **786**, p. 51-63
333. Eulberg D, Buchner K, Maasch C, and Klussmann S (2005) Development of an automated in vitro selection protocol to obtain RNA-based aptamers: identification of a biostable substance P antagonist. *Nucleic Acids Res.* **33**, e45.
334. Dausse E, Taouji S, Evade L, Di Primo C, Chevet E, and Toulme J-J (2011) HAPIScreen, a method for high-throughput aptamer identification. *Journal of Nanobiotechnology* **9**, 1-10.
335. Drolet DW, Jenison RD, Smith DE, Pratt D, and Hicke BJ (1999) A high throughput platform for systematic evolution of ligands by exponential enrichment (SELEX). *Comb. Chem. High Throughput Screen.* **2**, 271-8.
336. Rhodes A, Deakin A, Spaul J, Coomber B, Aitken A, Life P, and Rees S (2000) The Generation and Characterization of Antagonist RNA Aptamers to Human Oncostatin M. *J. Biol. Chem.* **275**, 28555-61.
337. Gopinath SC, Sakamaki Y, Kawasaki K, and Kumar PK (2006) An efficient RNA aptamer against human influenza B virus hemagglutinin. *J. Biochem.* **139**, 837-46.
338. Singhal A, Haynes CA, and Hansen CL (2010) Microfluidic Measurement of Antibody–Antigen Binding Kinetics from Low-Abundance Samples and Single Cells. *Anal. Chem.* **82**, 8671-79.
339. Varadarajan N, Kwon DS, Law KM, Ogunniyi AO, Anahtar MN, Richter JM, Walker BD, and Love JC (2012) Rapid, efficient functional characterization and recovery of HIV-specific human CD8+ T cells using microengraving. *Proc. Natl. Acad. Sci. U. S. A.* **109**, 3885-90.
340. Yoshimoto N, Kida A, Jie X, Kurokawa M, Iijima M, Niimi T, Maturana AD, Nikaido I, Ueda HR, Tatematsu K, Tanizawa K, Kondo A, Fujii I, and Kuroda Si (2013) An automated system for high-throughput single cell-based breeding. *Sci. Rep.* **3**, 1191.1-9.
341. Dijkstra EW (1974) Trip report E.W.Dijkstra, Edinburgh and Newcastle, 1 - 6 September 1974. (EWD448), in "The Manuscripts of Edsger W. Dijkstra (1930 - 2002)",
342. Wen J-D, and Gray DM (2004) Selection of genomic sequences that bind tightly to Ff gene 5 protein: primer-free genomic SELEX. *Nucleic Acids Res.* **32**, e182.
343. Pollard J, Bell SD, and Ellington AD (2001) Design, Synthesis, and Amplification of DNA Pools for Construction of Combinatorial Pools and Libraries, *Current Protocols in Molecular Biology*, John Wiley & Sons, Inc., p. 24.2.1.

344. Tran DT, Janssen KPF, Pollet J, Lammertyn E, Ann J, Van Schepdael A, and Lammertyn J (2010) Selection and Characterization of DNA Aptamers for Egg White Lysozyme. *Molecules* **15**, 1127-40.
345. Mehta J, Rouah-Martin E, Van Dorst B, Maes B, Herrebout W, Scippo M-L, Dardenne F, Blust R, and Robbens J (2012) Selection and Characterization of PCB-Binding DNA Aptamers. *Anal. Chem.* **84**, 1669-76.
346. Hamula CLA, Zhang H, Guan LL, Li X-F, and Le XC (2008) Selection of Aptamers against Live Bacterial Cells. *Anal. Chem.* **80**, 7812-19.
347. Janssen KPF, Knez K, Pollet J, Roberts SJ, Schrooten J, and Lammertyn J (2011) Assay design considerations for use of affinity aptamer amplification in ultra-sensitive protein assays using capillary electrophoresis. *Analytical Methods* **3**, 2156-59.
348. Bing T, Yang X, Mei H, Cao Z, and Shangguan D (2010) Conservative secondary structure motif of streptavidin-binding aptamers generated by different laboratories. *Bioorganic & Medicinal Chemistry* **18**, 1798-805.
349. Potty ASR, Kourentzi K, Fang H, Jackson GW, Zhang X, Legge GB, and Willson RC (2009) Biophysical characterization of DNA aptamer interactions with vascular endothelial growth factor. *Biopolymers* **91**, 145-56.
350. Harlow K, and Pfundheller HM (2010) Thermo Scientific Nunc Immobilizer Amino Surface: Protocol for Coupling Proteins. *Exiqon Laboratories, Denmark Tech Note No. 43*.
351. Moreau MJJ, and Schaeffer PM (2012) A polyplex qPCR-based binding assay for protein-DNA interactions. *Analyst* **137**, 4111-13.
352. Zuker M (2003) Mfold web server for nucleic acid folding and hybridization prediction. *Nucleic Acids Res.* **31**, 3406-15.
353. Gold L, and Janjic N (1998) "High-affinity oligonucleotide ligands to vascular endothelial growth factor (VEGF)". US Patent 5,811,533
354. Kanakaraj I, Chen W-H, Poongavanam M, Dhamane S, Stagg LJ, Ladbury JE, Kourentzi K, Strych U, and Willson RC (2013) Biophysical characterization of VEGF-aHt DNA aptamer interactions. *Int. J. Biol. Macromol.* **57**, 69-75.
355. Cox JC, Hayhurst A, Hesselberth J, Bayer TS, Georgiou G, and Ellington AD (2002) Automated selection of aptamers against protein targets translated in vitro: from gene to aptamer. *Nucleic Acids Res* **30**, e108.

356. Xiao Z, Levy-Nissenbaum E, Alexis F, Lupták A, Teply BA, Chan JM, Shi J, Digga E, Cheng J, Langer R, and Farokhzad OC (2012) Engineering of Targeted Nanoparticles for Cancer Therapy Using Internalizing Aptamers Isolated by Cell-Uptake Selection. *ACS Nano* **6**, 696-704.
357. Latulippe DR, Szeto K, Ozer A, Duarte FM, Kelly CV, Pagano JM, White BS, Shalloway D, Lis JT, and Craighead HG (2013) Multiplexed microcolumn-based process for efficient selection of RNA aptamers. *Anal. Chem.* **85**, 3417-24.
358. Wang C, Yang G, Luo Z, and Ding H (2009) In vitro selection of high-affinity DNA aptamers for streptavidin. *Acta Biochimica et Biophysica Sinica* **41**, 335-40.
359. Kikuchi K, Umehara T, Fukuda K, Hwang J, Kuno A, Hasegawa T, and Nishikawa S (2003) RNA Aptamers Targeted to Domain II of Hepatitis C Virus IRES That Bind to Its Apical Loop Region. *J. Biochem.* **133**, 263-70.
360. Wilson R, Cossins A, Nicolau DV, and Sotiris M (2013) The Selection of DNA Aptamers for Two Different Epitopes of Thrombin Was Not Due to Different Partitioning Methods. *Nucleic Acid Ther.* **23**, 88-92.
361. Tahiri-Alaoui A, Frigotto L, Manville N, Ibrahim J, Romby P, and James W (2002) High affinity nucleic acid aptamers for streptavidin incorporated into bi-specific capture ligands. *Nucleic Acids Res.* **30**, e45.
362. Niebel Br, Wosnitza CI, and Famulok M (2013) RNA-aptamers that modulate the RhoGEF activity of Tiam1. *Bioorg. Med. Chem.* **21**, 6239-46.
363. Dua P, Kang HS, Hong S-M, Tsao M-S, Kim S, and Lee D-k (2013) Alkaline Phosphatase ALPPL-2 Is a Novel Pancreatic Carcinoma-Associated Protein. *Cancer Res.* **73**, 1934-45.
364. Wochner A, Menger M, Orgel D, Cech B, Rimmele M, Erdmann VA, and Glökler J (2008) A DNA aptamer with high affinity and specificity for therapeutic anthracyclines. *Anal. Biochem.* **373**, 34-42.
365. Choi EW, Nayak LV, and Bates PJ (2010) Cancer-selective antiproliferative activity is a general property of some G-rich oligodeoxynucleotides. *Nucleic Acids Res.* **38**, 1623-35.
366. Descartes R (1637) *Discours de la Méthode*, (Berthier L, Ed.), Librairie de la Bibliothèque Nationale
367. Levine HA, and Nilsen-Hamilton M (2007) A mathematical analysis of SELEX. *Comput. Biol. Chem.* **31**, 11-35.

368. Burke DH, Scates L, Andrews K, and Gold L (1996) Bent Pseudoknots and Novel RNA Inhibitors of Type 1 Human Immunodeficiency Virus (HIV-1) Reverse Transcriptase. *J. Mol. Biol.* **264**, 650-66.
369. Stoltenburg R, Nikolaus N, and Strehlitz B (2012) Capture-SELEX: Selection of DNA Aptamers for Aminoglycoside Antibiotics. *Journal of Analytical Methods in Chemistry* **2012**, 14.
370. Mendonsa SD, and Bowser MT (2004) In Vitro Evolution of Functional DNA Using Capillary Electrophoresis. *J. Am. Chem. Soc.* **126**, 20-21.
371. Kavanagh D, and Goodship THJ (2011) Atypical Hemolytic Uremic Syndrome, Genetic Basis, and Clinical Manifestations. *ASH Education Program Book* **2011**, 15-20.
372. Jha P, Bora PS, and Bora NS (2007) The role of complement system in ocular diseases including uveitis and macular degeneration. *Mol. Immunol.* **44**, 3901-08.
373. Arend WP, Mehta G, Antonioli AH, Takahashi M, Takahashi K, Stahl GL, Holers VM, and Banda NK (2013) Roles of Adipocytes and Fibroblasts in Activation of the Alternative Pathway of Complement in Inflammatory Arthritis in Mice. *The Journal of Immunology* **190**, 6423-33.
374. Thurman JM, and Holers VM (2006) The Central Role of the Alternative Complement Pathway in Human Disease. *The Journal of Immunology* **176**, 1305-10.
375. Vanbrabant J, Leirs K, Vanschoenbeek K, Lammertyn J, and Michiels L (2014) reMelting curve analysis as a tool for enrichment monitoring in the SELEX process. *Analyst* **139**, 589-95.
376. Ouellet E, Lagally ET, Cheung KC, and Haynes CA (2014) A simple method for eliminating fixed-region interference of aptamer binding during SELEX. *Biotechnology and Bioengineering* **111**, 2265-79.
377. Wilson R, Bourne C, Chaudhuri RR, Gregory R, Kenny J, and Cossins A (2014) Single-Step Selection of Bivalent Aptamers Validated by Comparison with SELEX Using High-Throughput Sequencing. *PLoS One* **9**, e100572.
378. Hünninger T, Wessels H, Fischer C, Paschke-Kratzin A, and Fischer M (2014) Just in Time-Selection: A Rapid Semiautomated SELEX of DNA Aptamers Using Magnetic Separation and BEAMing. *Anal. Chem.* **86**, 10940-47.
379. Ouellet E, Lagally ET, Cheung KC, and Haynes CA (2014) A simple method for eliminating fixed-region interference of aptamer binding during SELEX. *Biotechnol. Bioeng.* **111**, 2265-79.

380. Ajikumar PK, Ng JK, Tang YC, Lee JY, Stephanopoulos G, and Too HP (2007) Carboxyl-terminated dendrimer-coated bioactive interface for protein microarray: high-sensitivity detection of antigen in complex biological samples. *Langmuir* **23**, 5670-77.
381. Chen A, Kozak D, Battersby BJ, Forrest RM, Scholler N, Urban N, and Trau M (2009) Antifouling surface layers for improved signal-to-noise of particle-based immunoassays. *Langmuir* **25**, 13510-15.
382. Kizhakkedathu JN, Creagh AL, Shenoi RA, Rossi NAA, Brooks DE, Chan T, Lam J, Dandepally SR, and Haynes CA (2010) High Molecular Weight Polyglycerol-Based Multivalent Mannose Conjugates. *Biomacromolecules* **11**, 2567-75.
383. Lai BFL, Creagh AL, Janzen J, Haynes CA, Brooks DE, and Kizhakkedathu JN (2010) The induction of thrombus generation on nanostructured neutral polymer brush surfaces. *Biomaterials* **31**, 6710-18.
384. Gong P, and Grainger DW (2007) Nonfouling surfaces: a review of principles and applications for microarray capture assay designs. *Methods Mol. Biol.* **381**, 59-92.
385. Cattani-Scholz A, Pedone D, Blobner F, Abstreiter G, Schwartz J, Tornow M, and Andruzzi L (2009) PNA-PEG Modified Silicon Platforms as Functional Bio-Interfaces for Applications in DNA Microarrays and Biosensors. *Biomacromolecules* **10**, 489-96.
386. Schlapak R, Pammer P, Armitage D, Zhu R, Hinterdorfer P, Vaupel M, Frühwirth T, and Howorka S (2005) Glass Surfaces Grafted with High-Density Poly(ethylene glycol) as Substrates for DNA Oligonucleotide Microarrays. *Langmuir* **22**, 277-85.
387. Poncin-Epaillard F, Vrlinic T, Debarnot D, Mozetic M, Coudreuse A, Legeay G, El Moulaj B, and Zorzi W (2012) Surface Treatment of Polymeric Materials Controlling the Adhesion of Biomolecules. *Journal of Functional Biomaterials* **3**, 528-43.
388. Jensen SP, Rasmussen SE, and Jakobsen MH (1996) Photochemical Coupling of Peptides to Polystyrene MicroWell Plates. *Innovations & Perspectives in Solid Phase Synthesis & Combinatorial Chemical Libraries* **1996**, 419-22.
389. Jakobsen MH, and Koch T (2000) "Method of photochemical immobilization of ligands using quinones". US Patent 6,033,784
390. Jensen MA, and Straus N (1993) Effect of PCR conditions on the formation of heteroduplex and single-stranded DNA products in the amplification of bacterial ribosomal DNA spacer regions. *Genome Res.* **3**, 186-94.
391. Baker M (2012) Digital PCR hits its stride. *Nat Meth* **9**, 541-44.

392. Yufa R, Krylova SM, Bruce C, Bagg EA, Schofield CJ, and Krylov SN (2014) Emulsion PCR Significantly Improves Nonequilibrium Capillary Electrophoresis of Equilibrium Mixtures-Based Aptamer Selection: Allowing for Efficient and Rapid Selection of Aptamer to Unmodified ABH2 Protein. *Analytical Chemistry* **87**, 1411-19.
393. Little JW (1967) An Exonuclease Induced by Bacteriophage λ : II. Nature Of The Enzymatic Reaction. *J. Biol. Chem.* **242**, 679-86.
394. Sriprakash KS, Lundh N, MM-O H, and Radding CM (1975) The specificity of lambda exonuclease. Interactions with single-stranded DNA. *J. Biol. Chem.* **250**, 5438-45.
395. Hindson BJ, Ness KD, Masquelier DA, Belgrader P, Heredia NJ, Makarewicz AJ, Bright IJ, Lucero MY, Hiddessen AL, Legler TC, Kitano TK, Hodel MR, Petersen JF, Wyatt PW, Steenblock ER, Shah PH, Bousse LJ, Troup CB, Mellen JC, Wittmann DK, Erndt NG, Cauley TH, Koehler RT, So AP, Dube S, Rose KA, Montesclaros L, Wang S, Stumbo DP, Hodges SP, Romine S, Milanovich FP, White HE, Regan JF, Karlin-Neumann GA, Hindson CM, Saxonov S, and Colston BW (2011) High-Throughput Droplet Digital PCR System for Absolute Quantitation of DNA Copy Number. *Anal. Chem.* **83**, 8604-10.
396. Heyries KA, Tropini C, VanInsberghe M, Doolin C, Petriv OI, Singhal A, Leung K, Hughesman CB, and Hansen CL (2011) Megapixel digital PCR. *Nat Meth* **8**, 649-51.
397. Rouah-Martin E, Mehta J, van Dorst B, de Saeger S, Dubruel P, Maes B, Lemiere F, Goormaghtigh E, Daems D, Herrebout W, van Hove F, Blust R, and Robbens J (2012) Aptamer-Based Molecular Recognition of Lysergamine, Metergoline and Small Ergot Alkaloids. *Int. J. Mol. Sci.* **13**, 17138-59.
398. Chen C-hB, Chernis GA, Hoang VQ, and Landgraf R (2003) Inhibition of heregulin signaling by an aptamer that preferentially binds to the oligomeric form of human epidermal growth factor receptor-3. *Proceedings of the National Academy of Sciences* **100**, 9226-31.
399. Rusconi CP, Roberts JD, Pitoc GA, Nimjee SM, White RR, Quick Jr G, Scardino E, Fay WP, and Sullenger BA (2004) Antidote-mediated control of an anticoagulant aptamer in vivo. *Nat Biotech* **22**, 1423-28.
400. Dey AK, Griffiths C, Lea SM, and James W (2005) Structural characterization of an anti-gp120 RNA aptamer that neutralizes R5 strains of HIV-1. *RNA* **11**, 873-84.
401. Britten RJ, and Kohne DE (1968) Repeated sequences in DNA. Hundreds of thousands of copies of DNA sequences have been incorporated into the genomes of higher organisms. *Science* **161**, 529-40.

402. Mencin N, Šmuc T, Vraničar M, Mavri J, Hren M, Galeša K, Krkoč P, Ulrich H, and Šolar B (2014) Optimization of SELEX: Comparison of different methods for monitoring the progress of in vitro selection of aptamers. *J. Pharm. Biomed. Anal.* **91**, 151-59.
403. Dwight ZL, Palais R, and Wittwer CT (2012) uAnalyze: web-based high-resolution DNA melting analysis with comparison to thermodynamic predictions. *IEEE/ACM Trans. Comput. Biol. Bioinform.* **9**, 1805-11.
404. Palais RA, and Wittwer CT (2011) "Melting curve analysis with exponential background subtraction". US Patent 8 068 992
405. Lyon E, Millson A, Lowery MC, Woods R, and Wittwer CT (2001) Quantification of HER2/neu Gene Amplification by Competitive PCR Using Fluorescent Melting Curve Analysis. *Clin. Chem.* **47**, 844-51.
406. Dragan AI, Casas-Finet JR, Bishop ES, Strouse RJ, Schenerman MA, and Geddes CD (2010) Characterization of PicoGreen Interaction with dsDNA and the Origin of Its Fluorescence Enhancement upon Binding. *Biophys. J.* **99**, 3010-19.
407. Croy JE, Fast JL, Grimm NE, and Wuttke DS (2008) Deciphering the mechanism of thermodynamic accommodation of telomeric oligonucleotide sequences by the *Schizosaccharomyces pombe* protection of telomeres 1 (Pot1pN) protein. *Biochemistry* **47**, 4345-58.
408. Teller E (1962) *The Legacy of Hiroshima*, First ed. New York p. 146
409. Kretschmann E, and Raether H (1968) Radiative decay of nonradiative surface plasmons excited by light. *Z. Naturforsch. A* **23**, 2135.
410. Otto A (1968) Excitation of nonradiative surface plasma waves in silver by the method of frustrated total reflection. *Zeitschrift für Physik* **216**, 398-410.
411. Campbell CT, and Kim G (2007) SPR microscopy and its applications to high-throughput analyses of biomolecular binding events and their kinetics. *Biomaterials* **28**, 2380-92.
412. Schasfoort RBM, and Tudos AJ, eds. (2008). *Handbook of Surface Plasmon Resonance*. First ed. London: Royal Society of Chemistry. 426 p.
413. Rothenhausler B, and Knoll W (1988) Surface-plasmon microscopy. *Nature* **332**, 615-17.
414. Yeatman E, and Ash EA (1987) Surface plasmon microscopy. *Electronics Letters* **23**, 1091-92.

415. Piliarik M, Vaisocherová H, and Homola J (2005) A new surface plasmon resonance sensor for high-throughput screening applications. *Biosens. Bioelectron.* **20**, 2104-10.
416. Wassaf D, Kuang G, Kopacz K, Wu Q-L, Nguyen Q, Toews M, Cosic J, Jacques J, Wiltshire S, Lambert J, Pazmany CC, Hogan S, Ladner RC, Nixon AE, and Sexton DJ (2006) High-throughput affinity ranking of antibodies using surface plasmon resonance microarrays. *Anal. Biochem.* **351**, 241-53.
417. Shumaker-Parry JS, Zareie MH, Aebersold R, and Campbell CT (2004) Microspotting streptavidin and double-stranded DNA Arrays on gold for high-throughput studies of protein-DNA interactions by surface plasmon resonance microscopy. *Anal. Chem.* **76**, 918-29.
418. Li Y, Wark AW, Lee HJ, and Corn RM (2006) Single-Nucleotide Polymorphism Genotyping by Nanoparticle-Enhanced Surface Plasmon Resonance Imaging Measurements of Surface Ligation Reactions. *Anal. Chem.* **78**, 3158-64.
419. Malic L, Veres T, and Tabrizian M (2009) Biochip functionalization using electrowetting-on-dielectric digital microfluidics for surface plasmon resonance imaging detection of DNA hybridization. *Biosens. Bioelectron.* **24**, 2218-24.
420. Goodrich TT, Lee HJ, and Corn RM (2004) Direct Detection of Genomic DNA by Enzymatically Amplified SPR Imaging Measurements of RNA Microarrays. *J. Am. Chem. Soc.* **126**, 4086-87.
421. Wegner GJ, Lee HJ, Marriott G, and Corn RM (2003) Fabrication of Histidine-Tagged Fusion Protein Arrays for Surface Plasmon Resonance Imaging Studies of Protein-Protein and Protein-DNA Interactions. *Analytical Chemistry* **75**, 4740-46.
422. Shumaker-Parry JS, Aebersold R, and Campbell CT (2004) Parallel, Quantitative Measurement of Protein Binding to a 120-Element Double-Stranded DNA Array in Real Time Using Surface Plasmon Resonance Microscopy. *Anal. Chem.* **76**, 2071-82.
423. Li Y, Lee HJ, and Corn RM (2007) Detection of Protein Biomarkers Using RNA Aptamer Microarrays and Enzymatically Amplified Surface Plasmon Resonance Imaging. *Anal. Chem.* **79**, 1082-88.
424. Wegner GJ, Lee HJ, and Corn RM (2002) Characterization and Optimization of Peptide Arrays for the Study of Epitope-Antibody Interactions Using Surface Plasmon Resonance Imaging. *Analytical Chemistry* **74**, 5161-68.
425. Lee K-H, Su Y-D, Chen S-J, Tseng F-G, and Lee G-B (2007) Microfluidic systems integrated with two-dimensional surface plasmon resonance phase imaging systems for microarray immunoassay. *Biosens. Bioelectron.* **23**, 466-72.
426. Lausted C, Hu Z, and Hood L (2008) Quantitative Serum Proteomics from Surface Plasmon Resonance Imaging. *Mol. Cell. Proteomics* **7**, 2464-74.

427. Fu E, Chinowsky T, Nelson K, Johnston K, Edwards T, Helton K, Grow M, Miller JW, and Yager P (2007) SPR Imaging-Based Salivary Diagnostics System for the Detection of Small Molecule Analytes. *Ann. N. Y. Acad. Sci.* **1098**, 335-44.
428. Kretschmann E, and Raether H (1968) Radiative decay of non radiative surface plasmons excited by light. *Z. Naturforschung* **23**, 2135-36.
429. Im H, Lesuffleur A, Lindquist NC, and Oh S-H (2009) Plasmonic Nanoholes in a Multichannel Microarray Format for Parallel Kinetic Assays and Differential Sensing. *Anal. Chem.* **81**, 2854-59.
430. Gordon R, Sinton D, Kavanagh KL, and Brolo AG (2008) A New Generation of Sensors Based on Extraordinary Optical Transmission. *Acc. Chem. Res.* **41**, 1049-57.
431. Rich RL, and Myszka DG (2007) Higher-throughput, label-free, real-time molecular interaction analysis. *Anal. Biochem.* **361**, 1-6.
432. Boozer C, Kim G, Cong S, Guan H, and Londergan T (2006) Looking towards label-free biomolecular interaction analysis in a high-throughput format: a review of new surface plasmon resonance technologies. *Curr. Opin. Biotechnol.* **17**, 400-05.
433. Luo Y, Yu F, and Zare RN (2008) Microfluidic device for immunoassays based on surface plasmon resonance imaging. *Lab on a Chip* **8**, 694-700.
434. Chakrabarty KS, and Su F (2005) Design Automation Challenges for Microfluidics-Based Biochips, in "Design, Test, Integration and Packaging of MEMS/MOEMS Symposium", Proc IEEE, p. 260-65
435. Barry R, and Ivanov D (2004) Microfluidics in biotechnology. *Journal of Nanobiotechnology* **2**, 1-5.
436. Bange A, Halsall HB, and Heineman WR (2005) Microfluidic immunosensor systems. *Biosens. Bioelectron.* **20**, 2488-503.
437. DeMello AJ (2006) Control and detection of chemical reactions in microfluidic systems. *Nature* **442**, 394-402.
438. Khandurina J, and Guttman A (2002) Bioanalysis in microfluidic devices. *J. Chromatogr. A* **943**, 159-83.
439. Wang Z, Wilkop T, Xu D, Dong Y, Ma G, and Cheng Q (2007) Surface plasmon resonance imaging for affinity analysis of aptamer-protein interactions with PDMS microfluidic chips. *Anal. Bioanal. Chem.* **389**, 819-25.
440. Abbas A, Linman MJ, and Cheng Q (2011) New trends in instrumental design for surface plasmon resonance-based biosensors. *Biosens. Bioelectron.* **26**, 1815-24.

441. Kovarik ML, Gach PC, Ornoff DM, Wang Y, Balowski J, Farrag L, and Allbritton NL (2012) Micro total analysis systems for cell biology and biochemical assays. *Anal. Chem.* **84**, 516-40.
442. Guo X (2012) Surface plasmon resonance based biosensor technique: A review. *Journal of Biophotonics* **5**, 483-501.
443. Tokel O, Inci F, and Demirci U (2014) Advances in Plasmonic Technologies for Point of Care Applications. *Chem. Rev.* **114**, 5728-52.
444. Lee HJ, Goodrich TT, and Corn RM (2001) SPR Imaging Measurements of 1-D and 2-D DNA Microarrays Created from Microfluidic Channels on Gold Thin Films. *Anal. Chem.* **73**, 5525-31.
445. Bravman T, Bronner V, Lavie K, Notcovich A, Papalia GA, and Myszka DG (2006) Exploring "one-shot" kinetics and small molecule analysis using the ProteOn XPR36 array biosensor. *Anal. Biochem.* **358**, 281-88.
446. Rich RL, Cannon MJ, Jenkins J, Pandian P, Sundaram S, Magyar R, Brockman J, Lambert J, and Myszka DG (2008) Extracting kinetic rate constants from surface plasmon resonance array systems. *Anal. Biochem.* **373**, 112-20.
447. Thorsen T, Maerkl SJ, and Quake SR (2002) Microfluidic Large-Scale Integration. *Science* **298**, 580-84.
448. Unger MA, Chou H-P, Thorsen T, Scherer A, and Quake SR (2000) Monolithic Microfabricated Valves and Pumps by Multilayer Soft Lithography. *Science* **288**, 113-16.
449. Jiang X, Ng JMK, Stroock AD, Dertinger SKW, and Whitesides GM (2003) A Miniaturized, Parallel, Serially Diluted Immunoassay for Analyzing Multiple Antigens. *J. Am. Chem. Soc.* **125**, 5294-95.
450. Stroock AD, Dertinger SKW, Ajdari A, Mezic I, Stone HA, and Whitesides GM (2002) Chaotic Mixer for Microchannels. *Science* **295**, 647-51.
451. Duffy DC, McDonald JC, Schueller OJA, and Whitesides GM (1998) Rapid Prototyping of Microfluidic Systems in Poly(dimethylsiloxane). *Anal. Chem.* **70**, 4974-84.
452. Schneider CA, Rasband WS, and Eliceiri KW (2012) NIH Image to ImageJ: 25 years of image analysis. *Nat Meth* **9**, 671-75.
453. Gao Y, Lin FYH, Hu G, Sherman PM, and Li D (2005) Development of a novel electrokinetically driven microfluidic immunoassay for the detection of *Helicobacter pylori*. *Anal. Chim. Acta* **543**, 109-16.

454. Haematologic Technologies (2009) Anti-Human Thrombin (5020), http://www.haemtech.com/Antibodies/Anti_Human_Thrombin_5020.htm
455. Dong Y, Wilkop T, Xu D, Wang Z, and Cheng Q (2008) Microchannel chips for the multiplexed analysis of human immunoglobulin G–antibody interactions by surface plasmon resonance imaging. *Anal. Bioanal. Chem.* **390**, 1575-83.
456. Kanda V, Kariuki JK, Harrison DJ, and McDermott MT (2004) Label-Free Reading of Microarray-Based Immunoassays with Surface Plasmon Resonance Imaging. *Anal. Chem.* **76**, 7257-62.
457. Grasso G, D'Agata R, Zanolli L, and Spoto G (2009) Microfluidic networks for surface plasmon resonance imaging real-time kinetics experiments. *Microchem. J.* **93**, 82-86.
458. Liu J, Eddings MA, Miles AR, Bukasov R, Gale BK, and Shumaker-Parry JS (2009) In Situ Microarray Fabrication and Analysis Using a Microfluidic Flow Cell Array Integrated with Surface Plasmon Resonance Microscopy. *Anal. Chem.* **81**, 4296-301.
459. Miller W (1955) Death of a Genius, in "Life", p. 64.
460. Forbes SA, Beare D, Gunasekaran P, Leung K, Bindal N, Boutselakis H, Ding M, Bamford S, Cole C, Ward S, Kok CY, Jia M, De T, Teague JW, Stratton MR, McDermott U, and Campbell PJ (2015) COSMIC: exploring the world's knowledge of somatic mutations in human cancer. *Nucleic Acids Res.* **43**, D805-D11.
461. Elle IC, Karlsen KK, Terp MG, Larsen N, Nielsen R, Derbyshire N, Mandrup S, Ditzel HJ, and Wengel J (2015) Selection of LNA-containing DNA aptamers against recombinant human CD73. *Mol. Biosyst.* **in press**.
462. Thiel WH, Bair T, Wyatt Thiel K, Dassie JP, Rockey WM, Howell CA, Liu XY, Dupuy AJ, Huang L, Owczarzy R, Behlke MA, McNamara JO, and Giangrande PH (2011) Nucleotide bias observed with a short SELEX RNA aptamer library. *Nucleic Acid Ther.* **21**, 253-63.
463. Doessing H, Hansen L, Veedu R, Wengel J, and Vester B (2012) Amplification and Re-Generation of LNA-Modified Libraries. *Molecules* **17**, 13087-97.
464. Brooks CA, and Cramer SM (1992) Steric mass-action ion exchange: Displacement profiles and induced salt gradients. *AIChE J.* **38**, 1969-78.
465. Iyer H, Tapper S, Lester P, Wolk B, and van Reis R (1999) Use of the steric mass action model in ion-exchange chromatographic process development1. *J. Chromatogr. A* **832**, 1-9.
466. Francis P, von Lieres E, and Haynes CA (2011) Zonal rate model for stacked membrane chromatography. I: characterizing solute dispersion under flow-through conditions. *J. Chromatogr. A* **1218**, 5071-8.

467. Francis P, von Lieres E, and Haynes C (2012) Zonal rate model for stacked membrane chromatography part II: characterizing ion-exchange membrane chromatography under protein retention conditions. *Biotechnol. Bioeng.* **109**, 615-29.
468. Choy DY, Creagh AL, and Haynes C (2014) Improved isoelectric focusing chromatography on strong anion exchange media via a new model that custom designs mobile phases using simple buffers. *Biotechnol. Bioeng.* **111**, 552-64.
469. Choy DY, Creagh AL, von Lieres E, and Haynes C (2014) A new mixed-mode model for interpreting and predicting protein elution during isoelectric chromatofocusing. *Biotechnol. Bioeng.* **111**, 925-36.

Appendix A

PROTOCOLS AND PROCEDURES

A.1 SPRI DEVICE MOLD DESCRIPTION

The design of the device was created using CAD software and contains a total of 4 layers for fabrication divided onto 2 molds. The molds are fabricated on standard 4" silicon wafers using standard photolithography techniques.

1. The CONTROL mold contains a single layer of positive photoresist (e.g. Shipley SPR220-7.0) that is patterned to harbor rounded channels of uniform thickness (10 μm).
2. The second (FLOW) mold contains three layers of photoresist. The initial array is of uniform thickness (10 μm), patterned with positive photoresist. Subsequently, the integrated network of micromixers is fabricated by casting 2 additional layers of negative photoresist. The first of which is patterned (10 μm thickness) to complete the gaps from the previously patterned array (located in the area reserved for the dilution network). The other layer is patterned to reveal sets of 4 μm thick chevrons (micromixers) that sit atop the previously patterned channels.

The SPRi device described is a 2-layer “push-down” device containing several microvalves that actuate by interrupting the flow of fluids beneath. Fabricated PDMS devices are irreversibly bonded to a glass substrate comprising an array of patterned gold islands for SPR detection. The entire gold pattern design is shrunk by 1% to compensate for PDMS shrinkage after curing.

A.2 PDMS DEVICE FABRICATION

A.2.1 MOLD CLEANING AND PASSIVATION

It is advisable to examine the mold carefully prior to beginning the fabrication process in order to ensure the quality of the microfeatures contained. When properly cleaned and stored, molds can be reused multiple times.

1. Remove small dust particles using a filtered N₂ stream. Never touch any part of the photoresist pattern and Do NOT use any liquids or solvents to clean the wafer. Should residual PDMS remain from previous fabrications, it is advisable to repeat the fabrication protocol (see below) with a thicker layer as to efficiently remove any residues.
2. Unless otherwise passivated, bare mold must be treated with TMCS (trimethylchlorosilane) prior to beginning the fabrication process as to prevent adhesion of PDMS to the surface.

*Note: This portion of the process should be performed in a fume hood.
Incubate 0.5 ml of TMCS in a small vial along with each mold to be treated in a sealed container for 2-5 min. TMCS vapors will passivate the silicon surface.*

A.2.2 PDMS FABRICATION PROTOCOL

Notes: Part A refers to elastomer base; Part B refers to curing agent. This protocol has been optimized for fabricating devices with both GE RTV615 and Dow Corning Sylgard 184 silicone elastomer.

FOR THE CONTROL LAYER:

1. Add 25g Part A and 5g Part B (5:1) to a disposable cup and mix thoroughly.
2. Pour the PDMS mixture onto the CONTROL mold, placed inside a 4.5" dia. aluminum weighing pan.
3. Degas the poured PDMS in a desiccator. If smaller bubbles remain at the surface, a needle may be used to pop them, taking precaution to not disturb the wafer.
4. Level the wafer on the bottom of the aluminum pan by pressing down on the edges.
5. Let stand for 10 min and place in a levelled oven set at 80°C for 20 minutes.

FOR THE FLOW LAYER:

1. Add 15g Part A to 0.75g Part B (20:1) inside a falcon tube and mix thoroughly
2. Degas the mixture in a desiccator
3. Set the FLOW wafer at the centre of a vacuum chuck, mounted onto a spinner instrument (e.g. Laurell WS-650 series) and ensure proper mounting
4. Carefully pour the PDMS mixture onto the centre of the FLOW mold as to prevent the trapping of air pockets and spin at 500 rpm for 5 s to ensure an even spread, followed by a ramp up to 2500 rpm in 10 s and spin at this velocity for 60 s. Aim to achieve a height of 20 μm

Note: This parameter will change per instrument and should be optimized with a spin curve

5. Carefully remove the wafer from the spinner (by the edges) and place in an aluminum weighing pan.
6. Let stand 10 min and place in a levelled oven set at 80°C for 20 minutes.

DEVICE ASSEMBLY

1. Take both molds out of the oven and carefully cut the PDMS 1 cm inside the perimeter of the CONTROL wafer using a surgical knife.
2. Carefully peel off the PDMS from the mold.
3. With the flow layer still in its aluminum pan, align the features of the peeled PDMS slab of the CONTROL layer to the ones found on the FLOW layer, as dictated by the original CAD design, with the aid of a stereomicroscope.

Note: Avoid repeated cycles of placing and peeling to ensure the integrity of the FLOW PDMS membrane. Do NOT try to peel off the spun PDMS membrane from the FLOW mold at this time.

4. After alignment, remove any remaining trapped air between the two PDMS layers by applying gentle pressure.
5. Cure the aligned device by placing the FLOW/CONTROL hybrid layers in the oven at 80°C for 2 hours.
6. Take the aligned mold out of the oven and cut the PDMS membrane of the FLOW layer around the edges of the mold
7. Carefully peel off the aligned monolith from the FLOW layer

Note: It is advisable to not put excessive pressure on the PDMS for the remainder of the fabrication steps as to prevent the adhesion of the thin membrane to the top layer, effectively sealing CONTROL channels.

8. Dice the layers into individual devices using a razor blade and punch holes for the access port where appropriate using a boring needle (e.g. Miltex® Biopsy punch).
9. Remove any remaining PDMS shards or dust with adhesive tape
10. Incubate devices on a flat substrate at 80°C for 2 days

A.3 GOLD SUBSTRATE FABRICATION

Note: This procedure should be performed on a wetbench in a class < 1000 clean room

1. Clean SF-10 glass substrates in piranha solution (5:1 H₂SO₄:H₂O₂) at 80°C.

USE EXTREME CAUTION! Proper PPE (safety goggles, face shield and chemical-resistant apron and gloves) must be worn at all times. No material other than glass containers and either Teflon or stainless steel tweezers may be used.

- a. Add 100 mL 96% sulfuric acid (H₂SO₄) to a second glass beaker
- b. Add 20 mL 30% hydrogen peroxide (H₂O₂) to a glass beaker
- c. Pour the H₂SO₄ solution into a Pyrex® crystallizing dish (125 mm x 65 mm)
- d. SLOWLY add the H₂O₂ solution to the H₂SO₄

Note: Although this order is counter-intuitive, piranha solutions may become extremely volatile for concentrations of H₂O₂ exceeding 50%. As such, the potential for explosion from this highly exothermic reaction is more significant than the order reversal of specific gravities.

- e. Carefully mix the solution using stainless steel or Teflon tweezers. Dish may be very hot. Allow solution to reasonably cool before applying additional heat.
- f. Place onto the surface of a hotplate set at 100°C. Solution temperature should hover around 80°C.
- g. Place an SF-10 glass slide and let incubate for 10 min.
- h. Remove dish from hotplate and place onto a glass plate.
- i. Immediately remove glass slide and transfer to a glass container filled with DI water to quench the reaction.
- j. Rinse glass slide with copious amounts of DI water. Blow dry with N₂
- k. Store in a dust-free environment until further use.

- l. Repeat the procedure from *f-k* for any remaining glass slides to be cleaned. Solution is effective up to 1 hr.
 - m. Let the used solution cool down and dispose according to local guidelines.
2. On one side of the SF-10 glass slide, sputter 50 Å chromium as an adhesion layer for the sputter deposition of 475 Å gold.
 3. Store in a dust-free environment until further use.
 4. Place a gold-coated slide on a hot plate at 120°C for 2 min. Let cool 2 min.
 5. Mount the slide (gold-face up) onto the vacuum chuck of a spinner (e.g. Laurell WS-650 series)
 6. Pour positive photoresist (e.g. Shipley SPR220-7.0) across the centre length of the slide. Let stand 1 min to allow spreading.
 7. Coat by spinning at 500 rpm for 5 s to ensure even spread, followed by a ramp up to 5500 rpm in 10 s and spinning at this velocity for 40 s. Aim to achieve a thickness of 6 μm
 8. Immediately remove coated slide from spinner and pre-bake on a hot plate at 115°C for 2 min
 9. Remove from hot plate and let stand for 5 min
 10. Mount coated slide onto the stage of a calibrated mask aligner (e.g. Canon PLA-501F)
 11. Place transparency mask (laser plotted at 20,000 dpi) on top of the slide and ensure uniform contact by mounting a 5" x 5" glass plate
 12. Expose photoresist to UV light ($\lambda = 405$ nm) for 65 s
 13. Remove setup from mask aligner and let exposed slide stand for 15 min to allow photoresist to relax
 14. Develop pattern (e.g. MF-24A Megaposit Developer) with gentle agitation for 2 min 15 s

Note: Time will vary depending on thickness of photoresist and exposure time; check pattern under stereomicroscope and continue development process in increments of 15 s. Do NOT over-develop

15. Immediately remove slide from developer solution and rinse in copious amounts of running DI water. Blow dry with nitrogen and check pattern under a stereomicroscope.
16. Post-bake photoresist on a hot plate at 115°C for 2 min.
17. Remove from hot plate and cool for 5 min.
18. Immerse pattern-coated slide in gold etchant (e.g. type TFA; Transene Company) for 17 s. *Do NOT over-etch.*
19. Immediately rinse with copious amounts of running DI water to quench the etching process. Blow dry with N₂
20. Immerse gold-etched slide in chromium etchant (e.g. type 1020; Transene Company) for < 2 s. *Do NOT over-etch.*
21. Immediately rinse with copious amounts of running DI water. Blow dry with N₂
22. Immerse patterned-glass slide in acetone with gentle agitation to strip remaining photoresist
23. Rinse gold-patterned slide with copious amounts of running DI water. Blow dry with N₂. Check gold pattern under stereomicroscope. Repeat steps 22-23 if photoresist residues remain.
24. Clean gold-patterned SF-10 glass substrate in piranha solution as described in step 1.
25. Store in a dust-free environment.

A.4 IRREVERSIBLE SPRI DEVICE BONDING

1. Ensure both the PDMS device and gold-patterned substrate are clean. Use adhesive tape to remove dust particles from PDMS devices and remove dust particles using a stream of N₂ for cleaned glass substrates.
2. Place a PDMS device (channels up) and a gold-patterned glass slide (pattern side up) on the clean tray of a UV-Ozone cleaner.

Note: Proper exhaust must be in place to remove excess O₃ produced in the chamber.

3. Expose bonding sides for 5 min. Remove from tray.
4. Immediately place a few μL of 100% ethanol on the gold-patterned glass slide (pattern side up) and bring the PDMS device (channels down) in contact with the substrate.
5. Using a stereomicroscope, align the device chambers with the gold pattern. The ethanol will help lubricate the two surfaces for alignment. Work quickly.
6. GENTLY apply pressure to the PDMS device to ensure proper contact with the gold slide.

Note: excessive pressure will cause the channels to collapse and bond shut.

7. Incubate in oven at 80°C for 2 min to evaporate ethanol
8. Remove from oven and GENTLY apply pressure on areas where air bubbles may be trapped.
9. Incubate in oven at 80°C for 1 hr to complete the bonding process. Alternatively, incubation at room temperature overnight will achieve the same results.

Note: Best performance is typically achieved when using > 3 days old fabricated devices.

Appendix B

CUSTOM-DESIGNED INTRUMENTATION

B.1 SURFACE PLASMON RESONANCE IMAGER

The following describes in detail the assembly and operation of the custom-built Kretschmann configured SPR imaging instrument used for this research. A complete list of the components can be found at the end of this section.

Unlike other custom built instruments, the one described here was built in a vertical position to allow for easy access and mounting of gold arrays. In short, this requires mounting two optical breadboards at a right angle, with the majority of the SPR setup fastened to the vertical breadboard: including two rotation stages, optical rails, optical posts and components as well as the LED light source and CCD detector. The prism is placed into a custom-built prism holder, atop an optical post. This holder is fastened to the horizontal breadboard, aligned with the central axis of the superimposed rotation stages. The entire setup is contained within a box to limit stray light and dust from impeding with the measurements. The following sections will describe in greater detail the assembly of such an instrument.

Initially, a large 24" X 36" anodized aluminum optical breadboard is laid flat on a stable surface. A second smaller 12" X 12" anodized aluminum optical

breadboard is vertically mounted on the larger one using right angle mounting brackets and 1/4"-20 cap screws. The first precision rotation stage (URS75BPP, Newport Corporation) is mounted at the top of the vertical breadboard with the position marking on the left hand side. At this point, the zero position should be aligned with the marked position, pointing toward the left. A top mounting plate and 12" optical rail are then attached to the rotation stage, with the optical rail pointing downward (overlapping the 90 degrees position), with enough clearance for rotation. Two 1" optical posts are then mounted on the upper right-hand and lower left-hand corners of the rotation stages to provide a mounting surface for the second. This should afford enough spacing between both rotation stages to ensure a full 90 degrees of unobstructed rotation of the previously mounted optical rail. The second rotation stage is then mounted on the posts directly atop the first one, this time with the marked zero position pointing towards the top. A second top mounting plate and optical rail are then attached to this stage in the same fashion as before, this time overlapping the 180 degrees position. Both optical rails should then be pointing downwards, when both rotation stages are at the zero position. Each rotation stages should be connected to their respective motion controller/driver (SMC100, Newport Corporation) and registered with the serial port of a computer. The bottom rotation stage should be registered as #1, and the top stage as #2, using the control software provided with the controller. Using the same software, rotate the position of the bottom stage -45 degrees, and +45 degrees for the top stage. The optical rails should now be pointing away from each other, as depicted in **Figure B-1**. Ultimately, the motion control will be controlled using custom-written LabVIEW™ software (National Instruments) with the libraries supplied by Newport Corporation in order to control the motion of both rotation stages *in-sync*, crucial for the proper operation of the SPR imager.

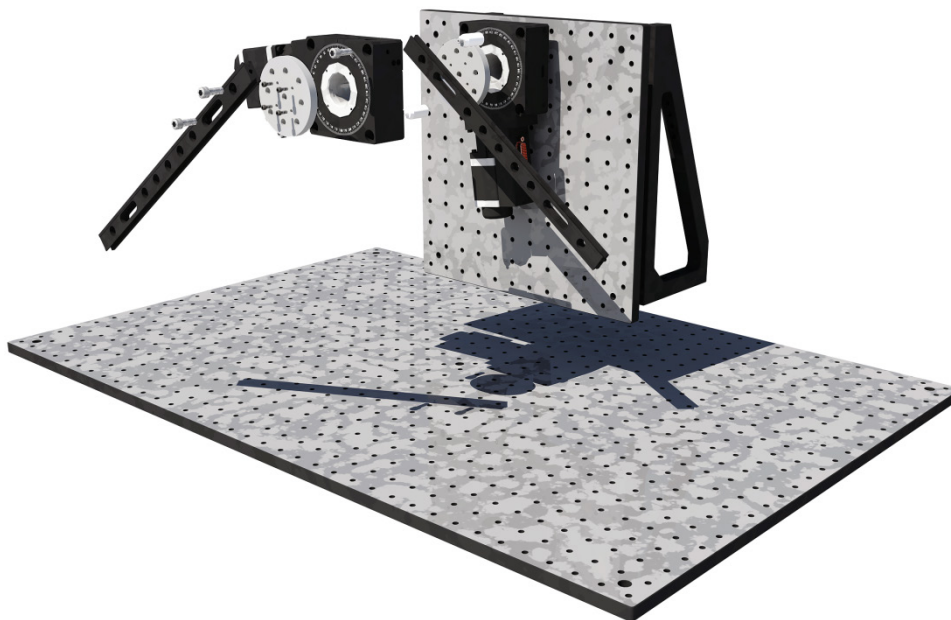


Figure B-1 Initial SPRi setup for mounting optical breadboards, rotation stages and optical rails. Depiction adapted from publicly available CAD drawings obtained from ThorLabs and Newport Corporation.

The illumination source and collimation optical components are mounted on the bottom optical rail, whereas the top optical rail will contain three components: a magnification lens, polarization and filter optics as well as the CCD camera with the imaging lens. Unless otherwise specified, all optical components and lens mounts are 1" in diameter.

A near infrared LED ($\lambda=626\text{nm}$; T-1 3/4 package) is used for SPR imaging due to its ability to provide better sensitivity and contrast ratio, as opposed to using lower wavelength illumination sources. Additionally, LEDs provide a safe, inexpensive and incoherent light source that can be easily operated as opposed to monochromatic laser sources. These more expensive options typically add a greater level of difficulty for their operation and require the use of complex optical components (including beam expanders, waveplates and phase retarders) in order to provide sufficient illumination of the entire surface and well as to eliminate

interference fringes that appear on SPR images due to their spatial coherence. To ensure proper collimation, the domed epoxy lens at the end of the LED casing needs to be cut off and filed smooth. This LED is then mounted to a lens mount along with two lens tubes containing a diffuser and a collimation lens. Both ends of the contraption are attached to a lens mount, which are then connected to 4" optical posts, and inserted into post holders mounted on the bottom optical rail. This will provide the SPR imager with a large uniform light beam.

A magnification lens is mounted in an adjustable lens holder in order to allow for fine-tuning the magnification of the SPR image being collected. This lens holder is attached to a 2" optical post, inserted into a post holder, mounted on the top optical rail. A linear polarizer ($\lambda = 400 - 700 \text{ nm}$) and band-pass filter ($\lambda = 630 \pm 2 \text{ nm}$; FWHM = $10 \pm 2 \text{ nm}$) are both inserted in a rotation mount, which is also mounted on the top railing the same fashion as the magnification lens. The rotation mount allows for manually switching between *s* and *p*-polarized light components from the LED by turning the polarizer 90 degrees. The filter allows for filtering the LED light as well as any stray light that may be interfering with the measurement. Finally, a 50mm imaging lens affixed to a monochromatic CCD camera with IEEE1394 connectivity (FO432SB, Foculus, NET GmbH) is also mounted on the rail using optical posts and mounts. A visual summary of the optical setup is shown in **Figure B-2**. All optical components should be aligned to be parallel to the optical rail axis on which they have been mounted. Additionally, Z-direction alignment can be performed by adjusting the insertion depth of optical posts in each post holder. Careful alignment is crucial for the proper operation of the imager.

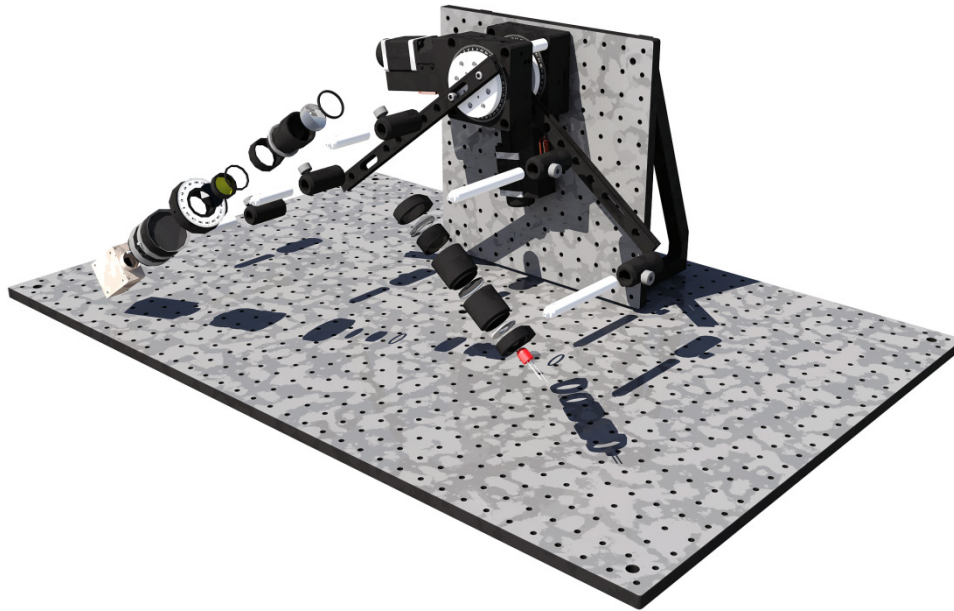


Figure B-2 Summary of SPRi optical components and their mounting order on the optical rails. Depiction adapted from publicly available CAD drawings obtained from ThorLabs and Newport Corporation.

An equilateral SF10 prism (30 X 30 mm) is mounted on a custom-built prism mount using modular riser plates by carefully inserting it from the top side, through the square opening. A clamping arm, attached to the bottom-side of the prism holder, ensures proper insertion and holds the prism in place. When properly inserted, the prism should be sitting a few millimetres above the surface of the plate, resting on the adjustable clamping arm. The entire contraption is attached to an 8" optical post and inserted into a post holder, which is fastened to the flat breadboard surface by using a clamping fork. A depiction of the prism holder is shown in **Figure B-3**.



Figure B-3 Custom-built prism holder depiction with equilateral prism and clamping arm.

With all optical components in place, these must be properly aligned to ensure proper SPR information gathering by the CCD camera by having the LED light pass through the diffuser and collimation lens assembly before being reflected at the prism surface back through the magnification lens, the band pass filter and polarizer assembly. Components on the optical rails can be aligned by adjusting the positions of each component along the optical rail axis as well as by adjusting the length of the post insertion into each post holder. Proper alignment will be achieved by having the center portion of the LED beam captured by the imaging lens of the CCD camera. Both the position and height of the prism also needs to be carefully adjusted in order to minimize image transitions and distortions when adjusting the rotation angle across several positions. The prism surface should be aligned with the center point of the top rotation stage, by adjusting the position of the clamping fork and the insertion length of the post inside the post holder. Once alignment is complete, clamping collars can be fastened to each post in order to secure the alignment positions.

The entire instrument will need to be contained inside a sturdy enclosure in order to both protect the optical components as well as to avoid external intrusions such as stray light or dust particles from entering the system and optical assemblies, interfering with the measurements while the instrument is in use. Construction rails are used to create a 20" X 24" X 12" enclosure, held together by construction cubes at each end. Sturdy blackout materials such as black hardboard

or posterboard is cut into shapes and inserted in the grooves of the construction rails to enclose the entire setup. A rectangular opening on the top panel is cut to allow access to the prism surface for operating the SPR imager. **Figure B-4** shows this construction in greater detail.

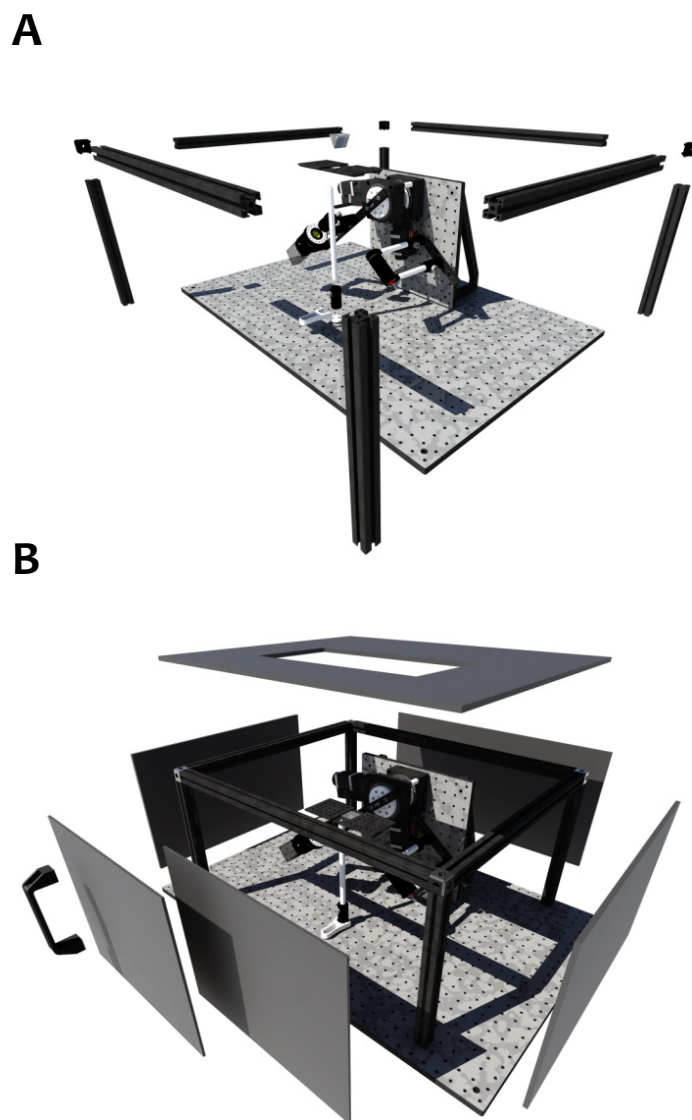


Figure B-4 SPR imager enclosure construction. (A) Construction rails are fastened together to form an enclosure large enough to contain the entire optical setup. (B) Blackout material is cut to dimension and inserted to enclose the imager. Depiction adapted from publicly available CAD drawings obtained from ThorLabs and Newport Corporation

A lid for the rectangular opening is also cut out of blackout material and placed when the imager is not in use. The LED is connected to a constant current source (described in section **B.2**) in order to minimize light intensity fluctuations over the course of an experiment and the CCD camera to the IEEE 1394 firewire port of a computer. A final depiction of the enclosed SPR imager is shown in **Figure B-5**. Custom written LabVIEW™ software (**Appendix C**) is used to operate the imager's hardware and perform data acquisition.



Figure B-5 Final depiction of the fully enclosed SPR imager with corresponding lid, providing access to the prism surface. The rotation stages and CCD camera are connected to a computer and the LED to a constant current source (not shown). Depiction adapted from publicly available CAD drawings obtained from ThorLabs and Newport Corporation

Components Source: ThorLabs

Qty	Description	Product No.
1	Aluminum Breadboard (24 X 36)	MB2436
1	Aluminum Breadboard (12X12)	MB12
1	1/4"-20 Hardware Kit	HW-KIT2
4	Rubber feet	RDF1
2	Mounting Brackets	VB01
4	Construction Rails (12")	XE25L12
2	Construction Rails (18")	XE25L24
2	Construction Rails (24")	XE25L18
3	Rail Clamp	CL6
2	Black Hard Board (3 sheets - 24" X 24")	TB4
1	Handles	BBH1
4	Corner Cube for Construction Rails	XE25W3
1	Low-Profile Screws	SH25LP38
2	Dovetail Optical Rails (12")	RLA1200
1	Dovetail Optical Rails (6")	RLA0600
2	1" Optical Post	TR1
1	2" Optical Post	TR2
3	4" Optical Post	TR4
2	6" Optical Post	TR6
1	8" Optical Post	TR8
5	Post Holder	PH2
6	Post Collar	R2
1	Pedestal Post holder	BE1
1	Small clamping fork	CF125
1	Right Angle Mounting Plate	AP90
2	Right Angle Bracket	AB90
1	Large Adjustable Clamping Arm	PM4
1	Rotation Mount	RSP1
1	0.5" SM1 Lens Tube	SM1L05
3	1" SM1 Lens Tube	SM1L10
1	1" SM1 Adjustable Lens Tube	SM1V10
1	SM1 Lens Tube Coupler	SM1T1
3	Fixed Lens Mount	LMR1
1	SM1 LED Mount	S1LEDM
1	630 nm Bandpass Filter	FB630-10

Components Source: Newport Corporation

Qty	Description	Product No.
2	Precision Rotation Stages	URS75BPP
2	Single-axis Stepper Motor Controller/Driver	SMC100PP
2	Round Mounting Plate	URS75TP
2	Modular Riser Plate	MRP3-0.125

Components Source: Edmund Optics

Qty	Description	Product No.
1	Linear Glass Polarizer 25mm Diameter	NT47-316
2	Plano-Convex Lens 25mm Diameter	NT45-508-INK
1	Double-Convex Lens 25mm Diameter	NT45-892-INK
1	25° Holographic Diffuser	HT54-498
1	Aspheric Lens 0.50 NA Near-IR	NT49-114
1	Megapixel 50mm FL Imaging Lens	NT56-790

Component Source: Ealing Catalog

Qty	Description	Product No.
1	Equilateral SF-10 Prism (30 X 30 mm)	24-2966

Component Source: Digi-Key

Qty	Description	Product No.
1	626 nm LED; 2.1V; 20mA	516-2457-1-ND

Component Source: AV Supply

Qty	Description	Product No.
1	FOculus 1/2" Firewire CCD Camera	FO432SB

B.2 CONSTANT CURRENT LED DRIVER

This section describes the specifications related to the design and assembly of a constant current LED driver for the SPR imager in order to provide low noise and stable light intensity for many hours of continuous operation. The schematic and the PCB were both designed in Eagle by colleague Bernard Coquinco based on specifications mutually discussed and agreed upon.

Important design requirements:

1. Footprint must be kept small to allow for proper mounting on optical rails
2. Power connector must be remote from LED connector to allow for proper placement in the SPR setup.
3. Power input must be able to accommodate a voltage range from 5 to 12 V.
4. LED connector must be compatible with T-1 3/4 package LEDs
5. A 20mA stable current source must be supplied to the LED at room temperature for many hours of continuous use.

The LT1763 Low-Noise Voltage Regulator used in combination with a 0.01 μ F bypass ceramic capacitor provides a stable 5V output voltage (20 μ V_{RMS} Noise) to the rest of the PCB.

The LM4140 Precision Voltage Reference (5V input) provides an ultra-low noise output of 2.048V capable of sourcing 8mA, meeting the low-noise requirements discussed previously in a SOIC package. The addition of input (0.1 μ F) and output (1 μ F) capacitors both improve stability and allows for proper sourcing or sinking load current demands.

The reference voltage is directly amplified by an output precision amplifier (op-amp), also bound by the low noise requirements. The LMP7701 met these constraints in a SOIC package. This single channel op-amp uses output of the LM4140 to supply a constant current source of 20mA to the LED for constant SPR illumination.

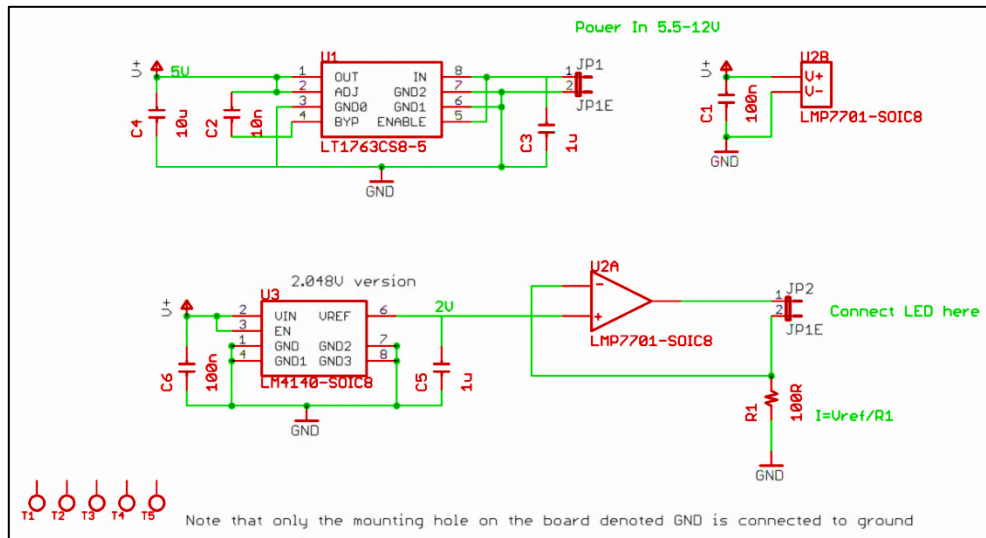
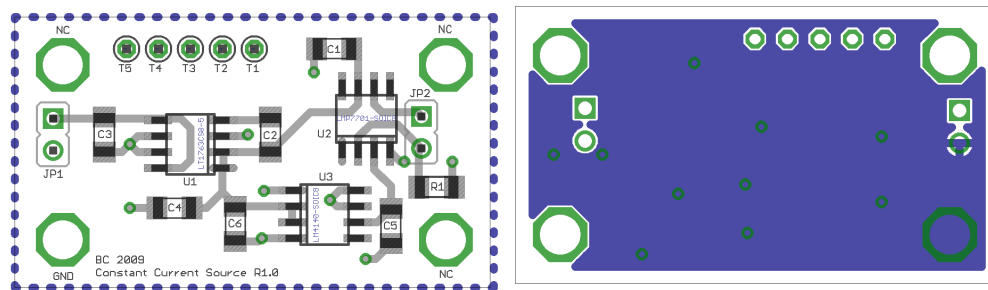


Figure B-6 LED constant current driver schematic. This was developed in collaboration with Bernard Coquinco and Dr. Eric Lagally (Michael Smith Laboratories – UBC Vancouver)

A



B

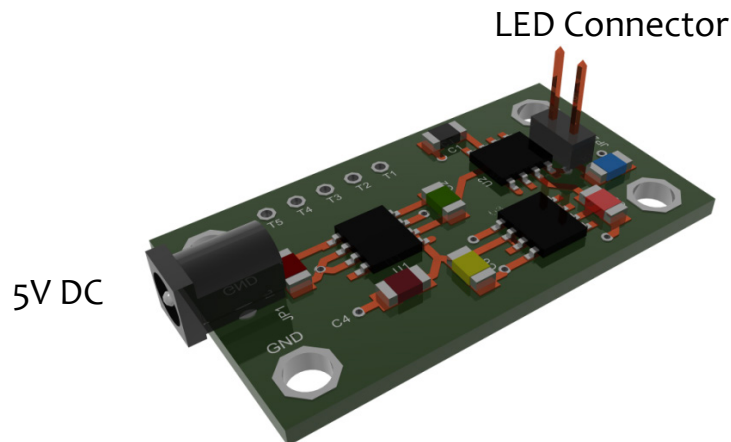


Figure B-7 LED driver circuit board diagram and electronic components. (A) Top view: Copper Layer (Blue), Vias (Green) and Connectors (Grey). Bottom view showing the ground mounting hole: Copper Layer (Blue), Vias (Green). Dimensions 20 mm X 35mm. (B) Representation of the assembled printed circuit board.

Appendix C

LABVIEW™ CODE FOR SPR IMAGER

C.1 DESCRIPTION OF LABVIEW™

LabVIEW™ (Laboratory Virtual Instrument Engineering Workbench) is a graphical programming platform published by National Instruments, typically used for data acquisition, instrument control and automation. Unlike text-based programming languages, LabVIEW™ uses a dataflow programming language (G) to create programs and subroutines known as Virtual Instruments (VIs).

Execution of a VI is determined by graphical structures on which several nodes and connector panels are connected by drawing wires. These wires carry the data flow to other parts of the VI as soon as it becomes available, ergo allowing parallel execution of multiple routines. Each VI is composed of three parts: the front panel, the block diagram and the connector panel.

The front panel provides a customizable graphical user interface (GUI), populated by either controls or indicators. Controls are inputs where a user can supply information to the VI whereas indicators are outputs, capable of displaying results given by the VI.

The block diagram contains the graphical source code which dictates the execution of the VI. All objects placed on the front panel appear in the block diagram as terminals. These terminals are able to be wired to other components and interact with structures and function nodes. National Instruments provides numerous libraries of functions and nodes, readily available for the development of VIs.

The connector panel represent the VI in the block diagram of other calling VIs where the front panel controls and indicators are depicted as input and output connectors, respectively.

The VI uses a hierarchical structure, where other VIs, often referred to as sub-VIs, can be called upon using its connector panel, to perform other tasks and functions, not provided by National Instruments. This allows for seamless integration and high levels of customization.

This dissertation uses National Instrument's LabVIEW™ to operate the Surface Plasmon Resonance imager hardware as well as to perform several functions linked to data acquisition. The NI Vision Assistant module, containing several drivers (including Legacy support) and IMAQ (image acquisition) VIs, is also required. The Main VI and each Sub-VI will be represented and discussed by the three components mentioned earlier.

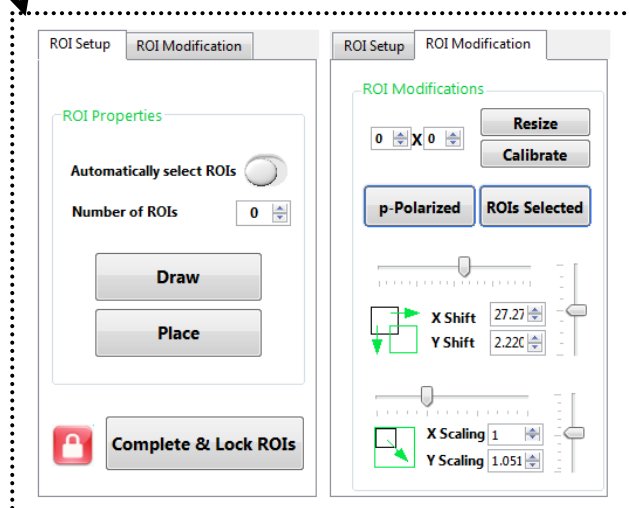
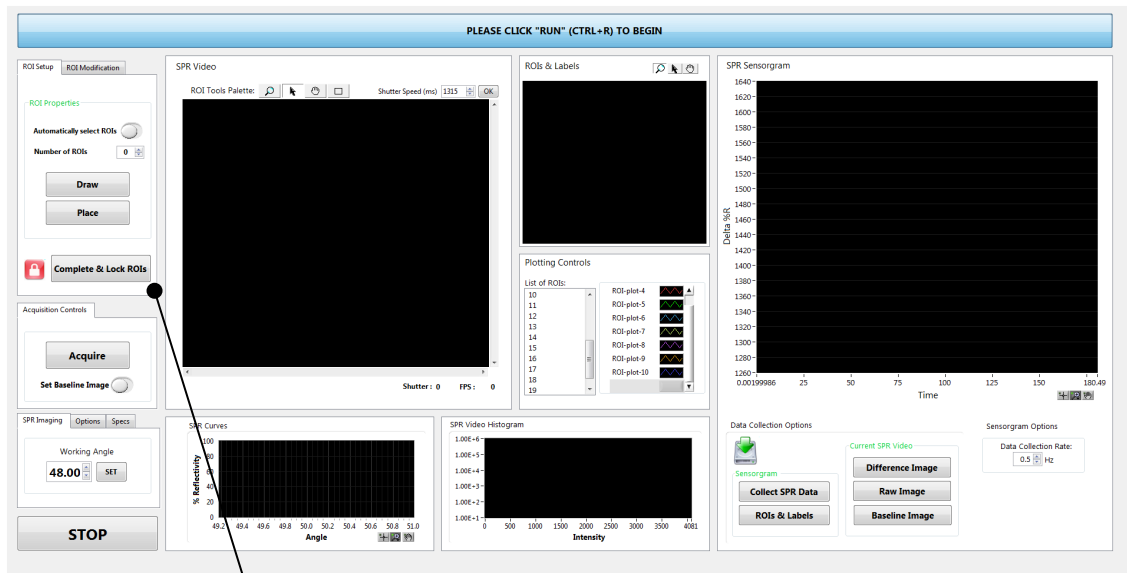
C.2 THE MAIN VI

CONNECTOR PANEL:

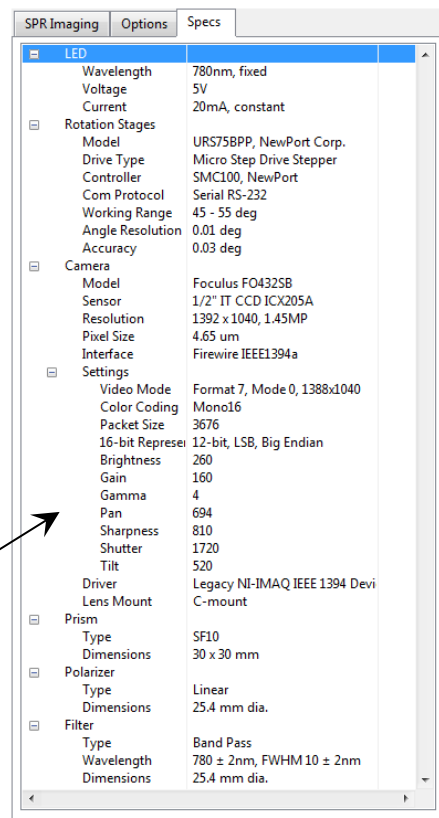
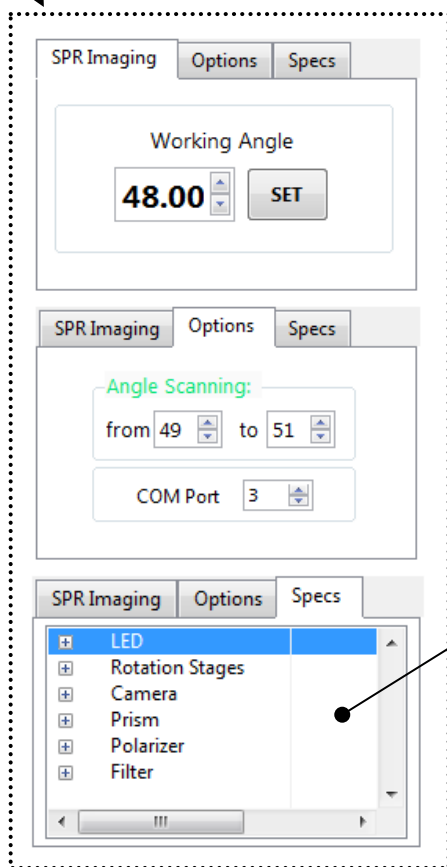
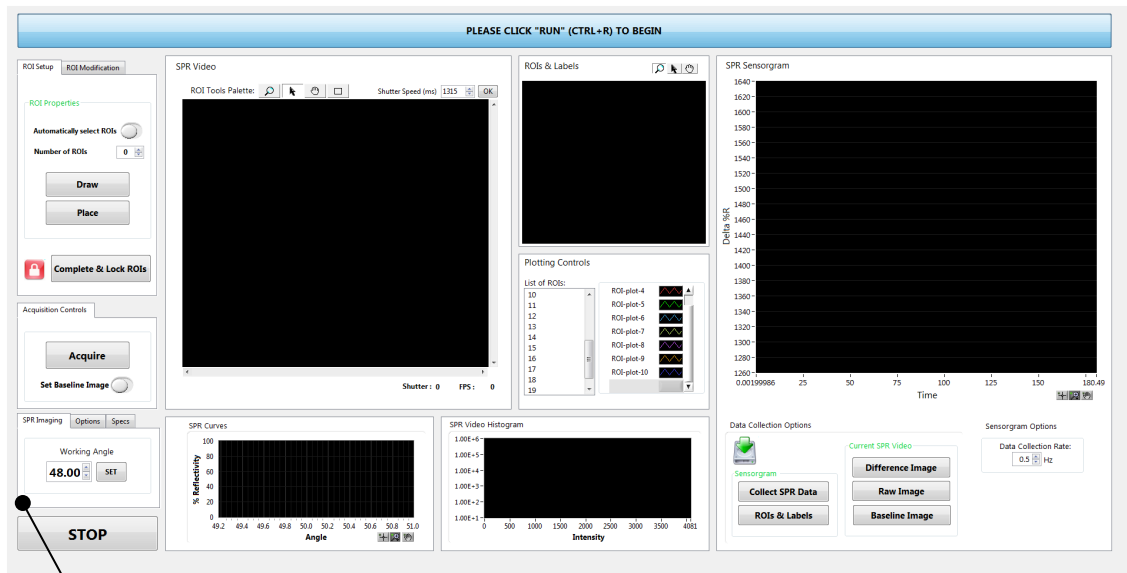
Near-IR SPR v4.0 (16-bit).vi



FRONT PANEL: GRAPHICAL USER INTERFACE (GUI)

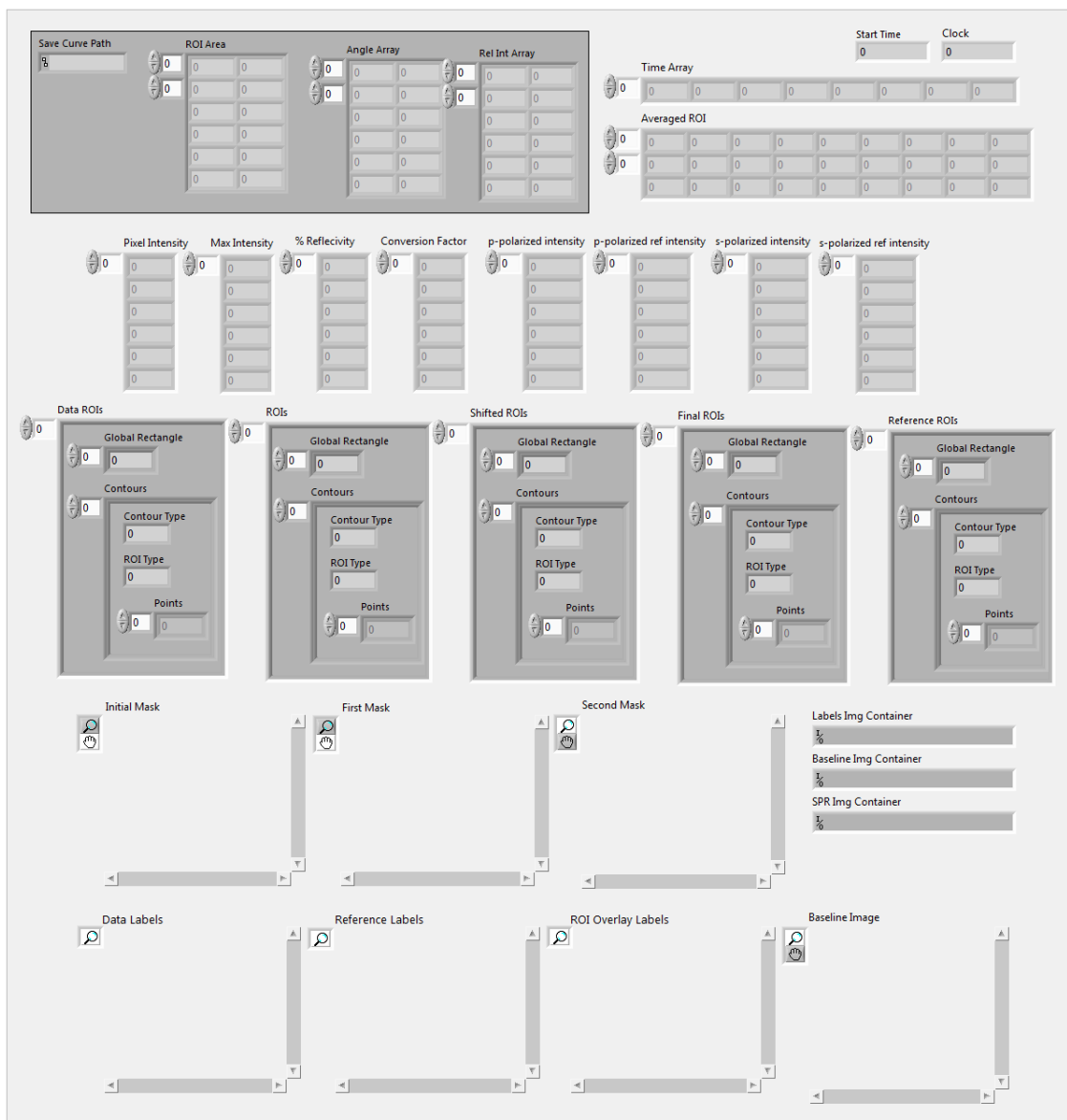


A set of controls for defining, modifying and controlling the Regions of Interest (ROI) to be analyzed on the SPR Video panel



A set of controls for defining the angular parameters for SPR imaging, the communication port for the rotation stages as well as technical specifications related to the instrument's hardware and software components

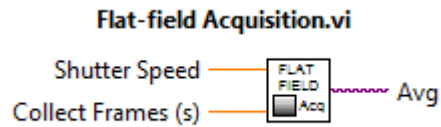
FRONT PANEL: CONTROLS AND INDICATORS



Various controls and indicators hidden from view necessary for initiating proper communication and function of sub-VIs

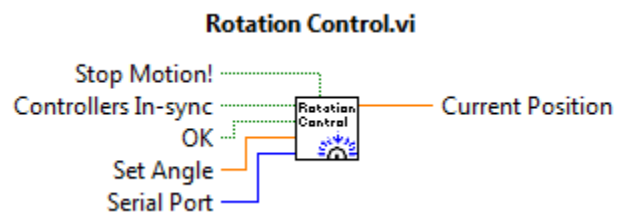
LIST OF SUB-VIS INVOKED ALONG WITH CONNECTOR PANEL AND SECTION REFERENCE:

(In order of Appearance)



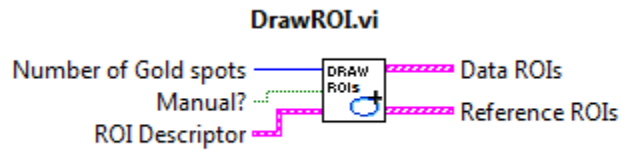
Appendix C.5

This sub-VI allows for acquiring a blank image for reference subtraction



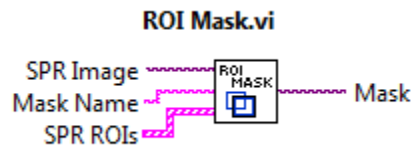
Appendix C.12

This sub-VI controls the rotation angle for both rotation stages



Appendix C.4

This sub-VI defines multiple regions of interest (ROIs) on the SPR image for analysis



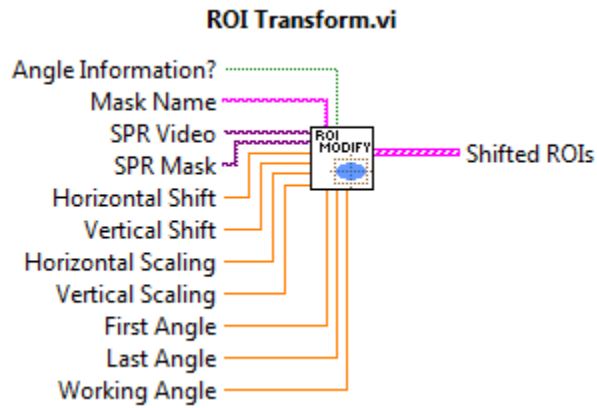
Appendix C.10

This sub-VI converts the regions of interest (ROIs) on the SPR image to an image mask



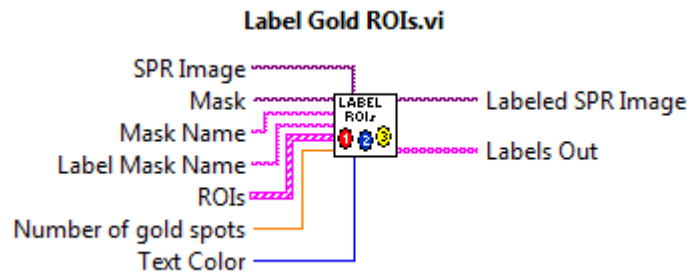
Appendix C.9

This sub-VI converts and image mask to individual regions of interest (ROIs)



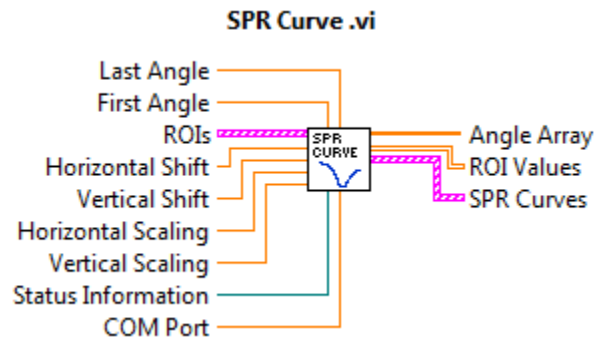
Appendix C.11

This sub-VI transforms the geometry of every region of interest (ROI) on the SPR image by shifting and scaling their dimensions



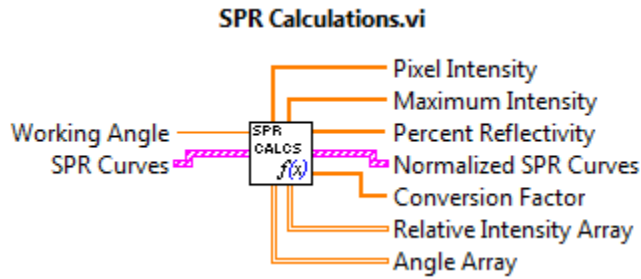
Appendix C.8

This sub-VI labels every region of interest (ROI) on the SPR image with a unique descriptor for future reference



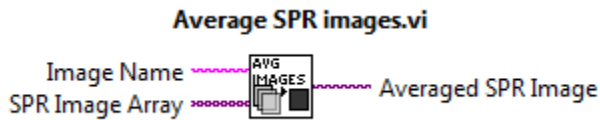
Appendix C.14

This sub-VI defines the SPR curve of every gold region delimited by a region of interest (ROI) and outputs each curve data in an array for plotting



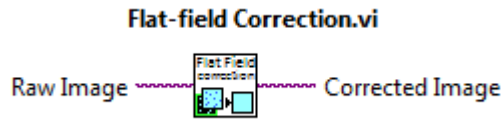
Appendix C.13

This sub-VI performed a number of calibrations and normalization for each SPR curve obtained from "SPR Curve.vi"



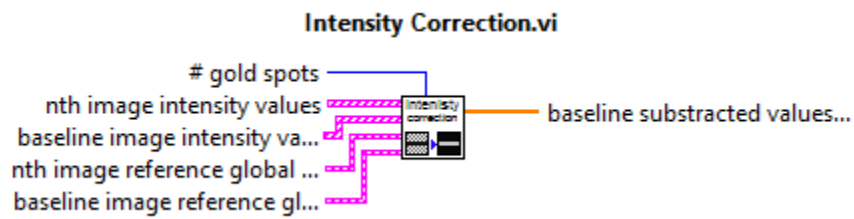
Appendix C.3

This sub-VI averages a series of collected SPR images by the CCD camera to minimize the noise signal from the sensor



Appendix C.6

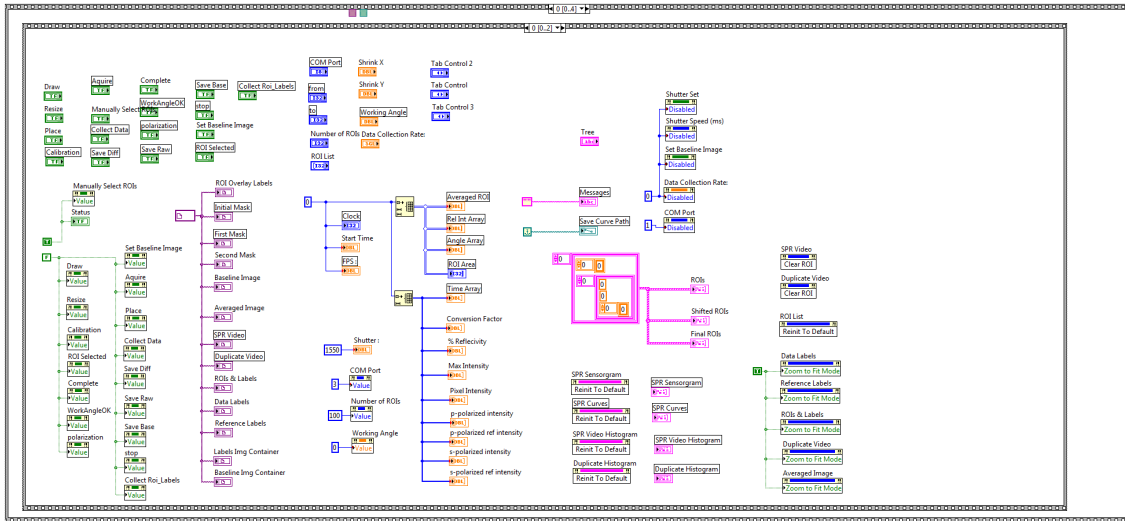
This sub-VI performs a field correction on the averaged SPR image collected by subtracting it to the reference image collected from “Flat-field Acquisition.vi”



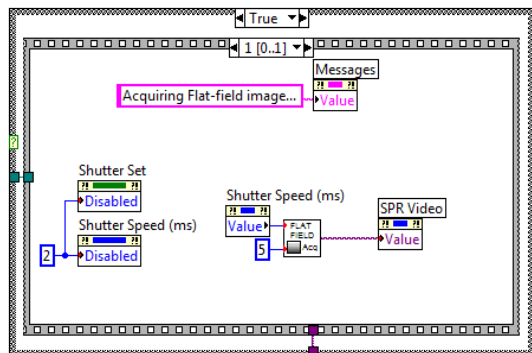
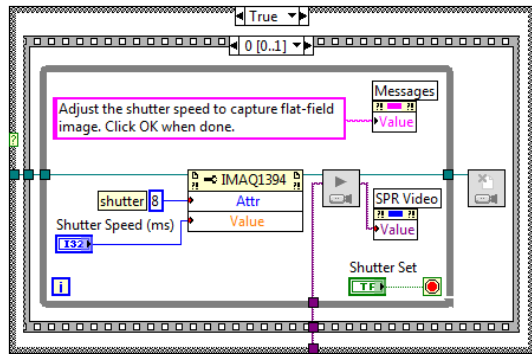
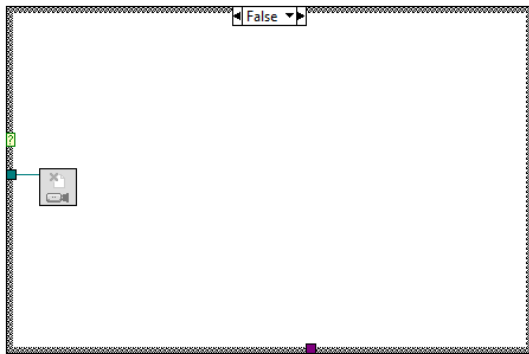
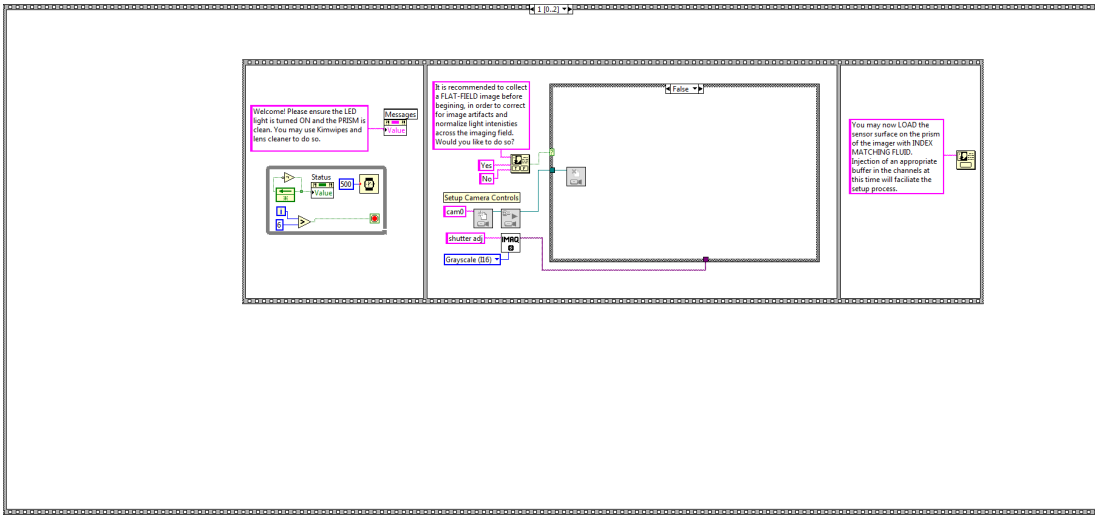
Appendix C.7

This sub-VI normalizes the p-polarized pixel intensity for each defined region of interest (ROI) to a series of reference ROI in order to correct for LED/CCD signal and temperature fluctuations

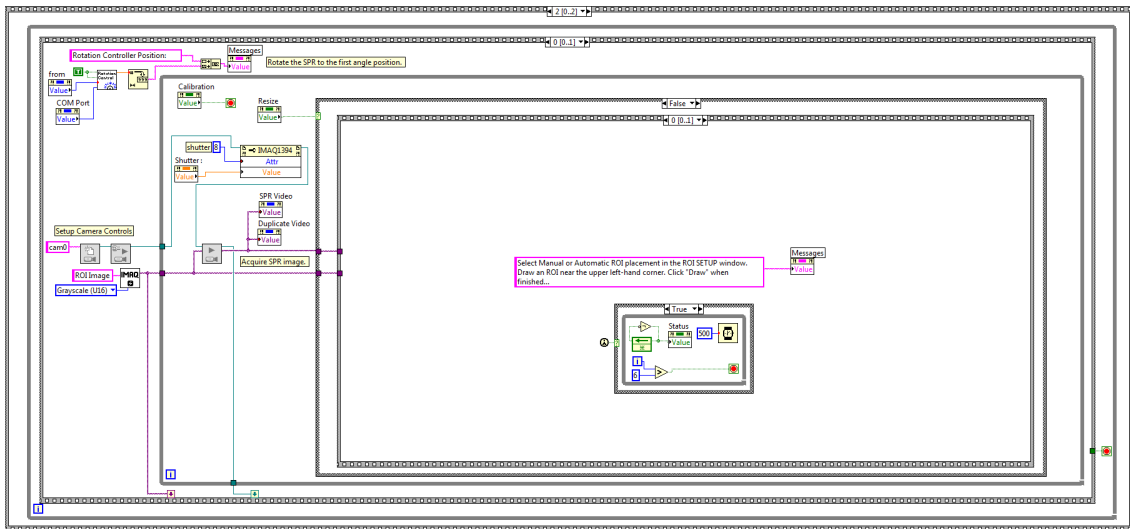
BLOCK DIAGRAM:



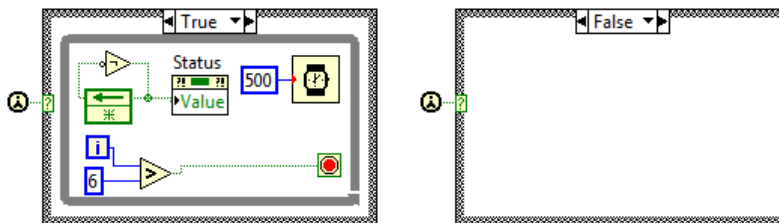
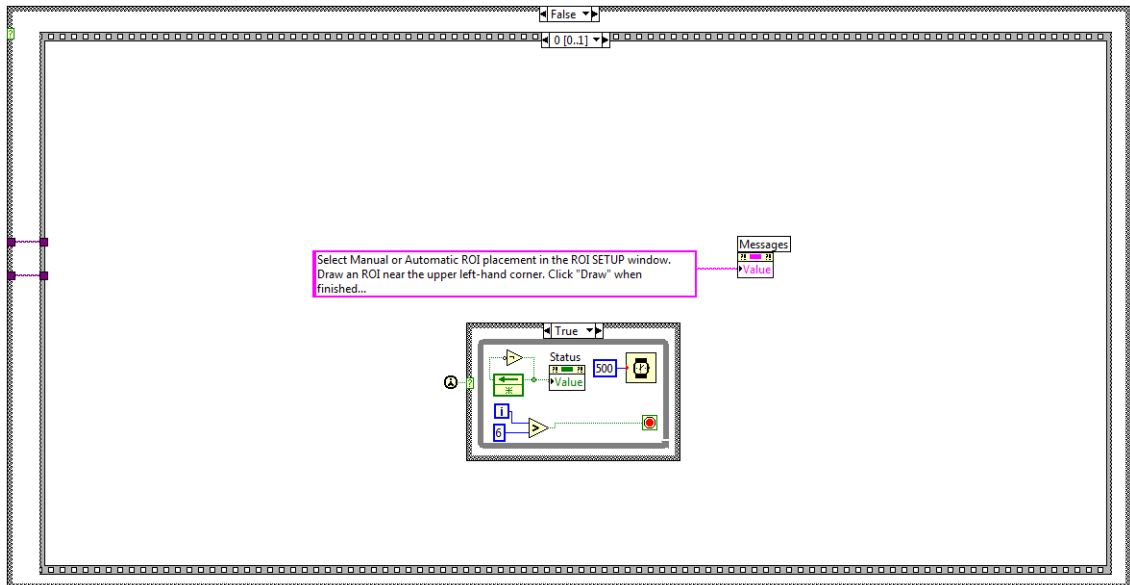
Initialize all controls and indicators



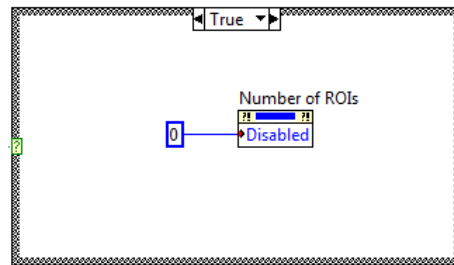
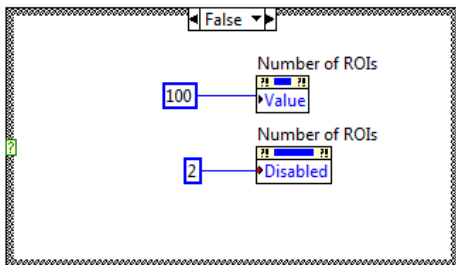
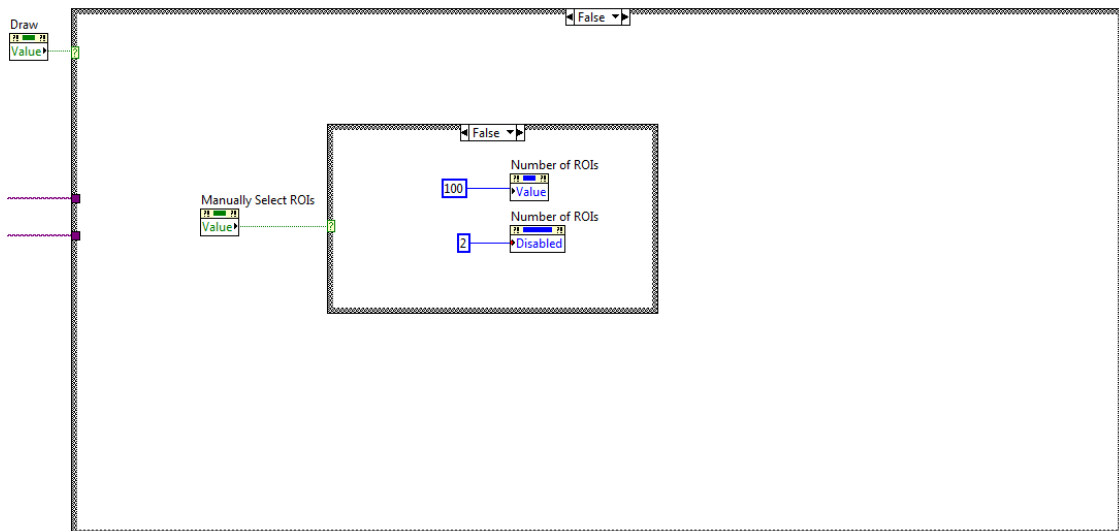
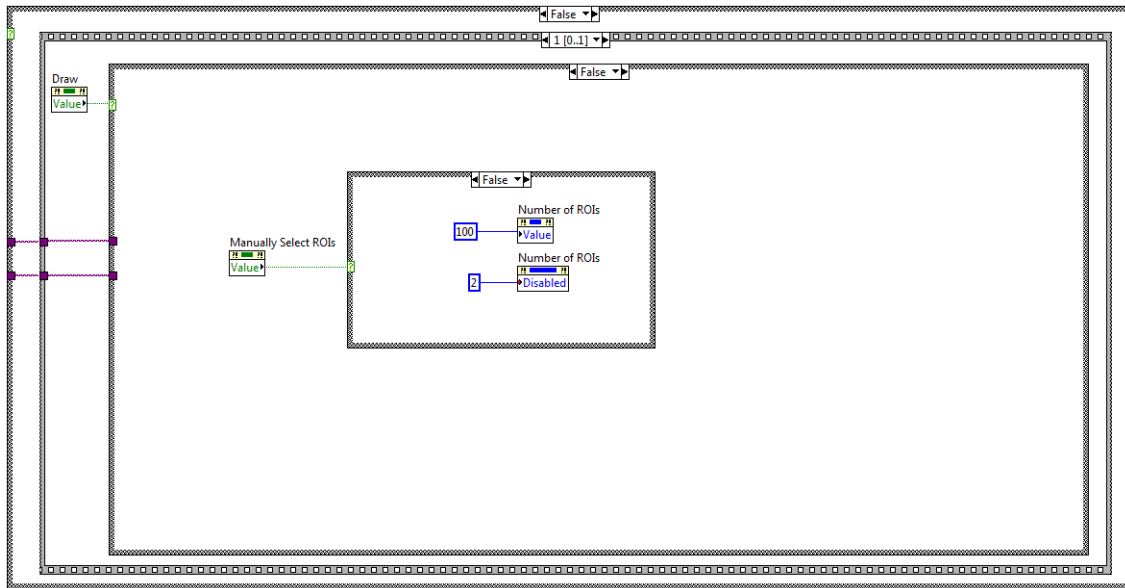
Inquire about collecting a reference image. Denial results in releasing access to CCD.
 Confirmation results in acquisition of the reference image through the "Flat-Field Acquisition" sub-VI



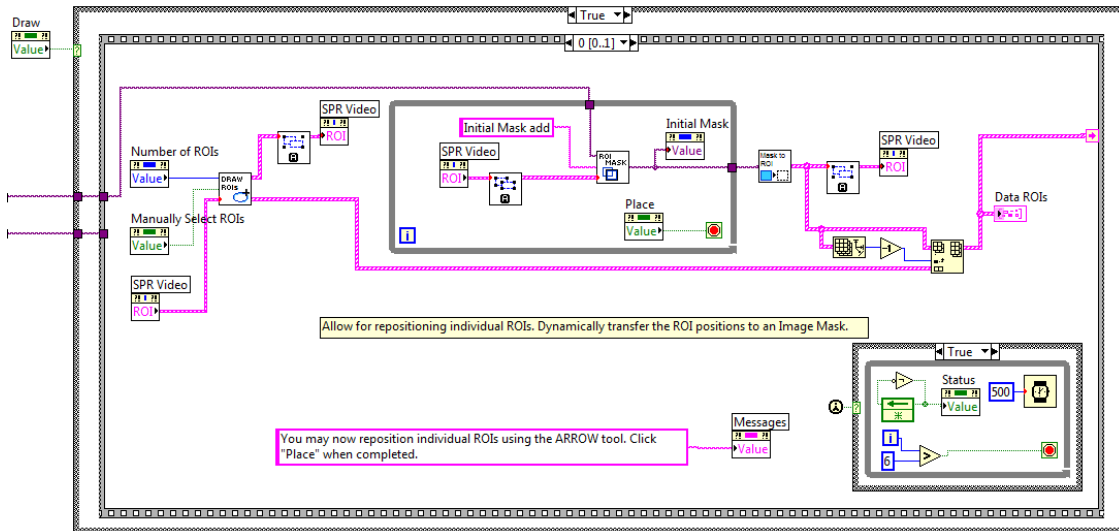
Initializes the rotation stages to the first angle (as defined in the "Options" tab) through the "Rotation Control" sub-VI. Initializes the CCD camera and begins acquisition of SPR Video.



Provides a message on the status bar of the front panel and blinks 3 times. Several instances of these are invoked throughout the Main VI and will not be addressed any further.

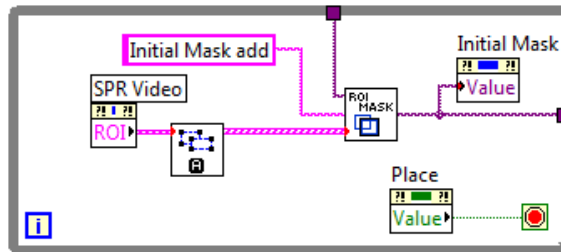


Set the number of gold areas to analyze either automatically or manually. The software waits for the user to draw a region of interest on the SPR Video to continue.

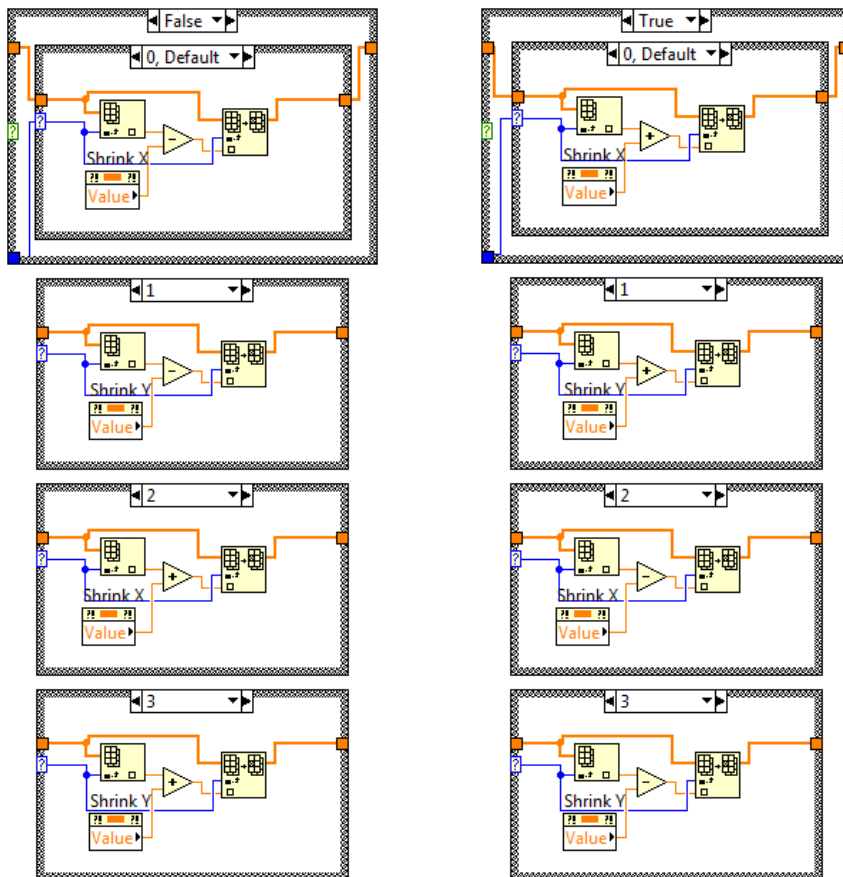
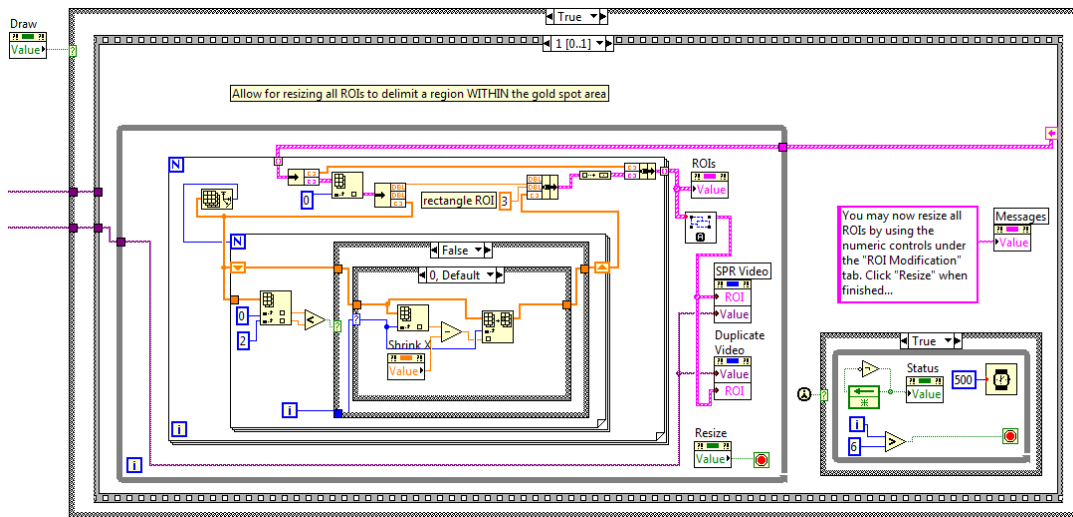


ROI Modifications Step 1 of 2:

After having drawn an ROI, the software automatically draws a number of identical ROIs (defined by the user) by invoking the "Draw ROIs" sub-VI.

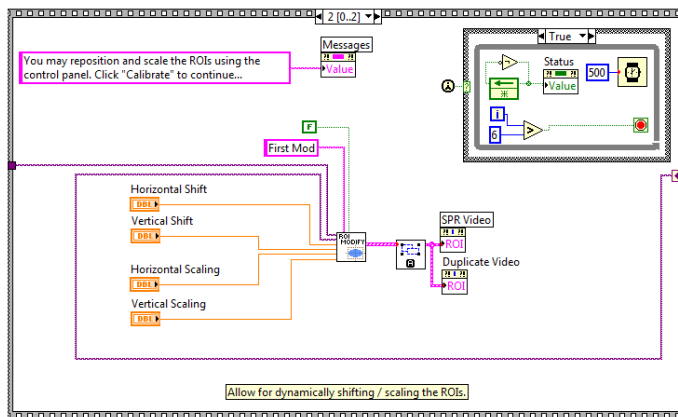
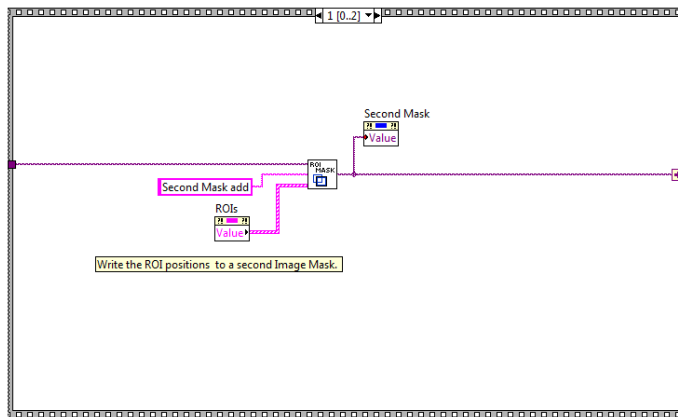
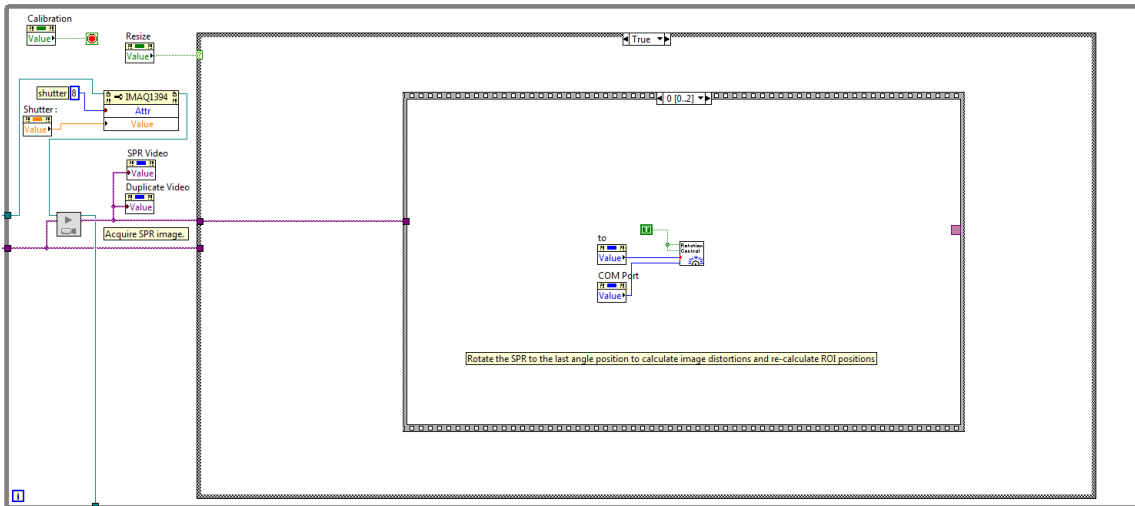


After drawing the ROIs, these are dynamically converted to an image mask by invoking the "ROI mask" sub-VI while the user repositions individually drawn ROIs.



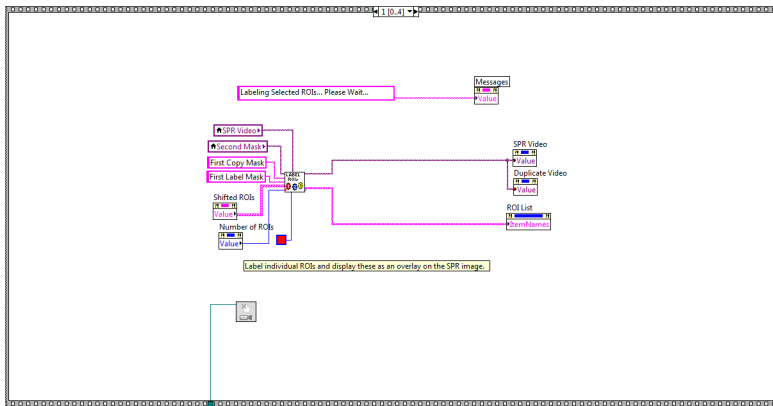
ROI Modifications Step 2 of 2:

After repositioning individual ROIs, these new positions are recorded and the ensemble of ROIs can now be dynamically scaled and shifted in order to refine their position. The modifications appear in real-time on the SPR Video. The User clicks "Resize" when complete.

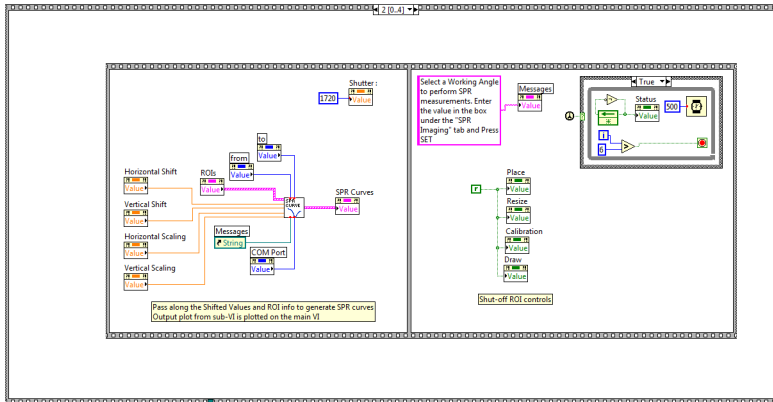


Clicking “Resize” activates the next sequence of events where the rotation stages rotate to the last angular position (defined in the “Options” tab) which will distort the SPR image.

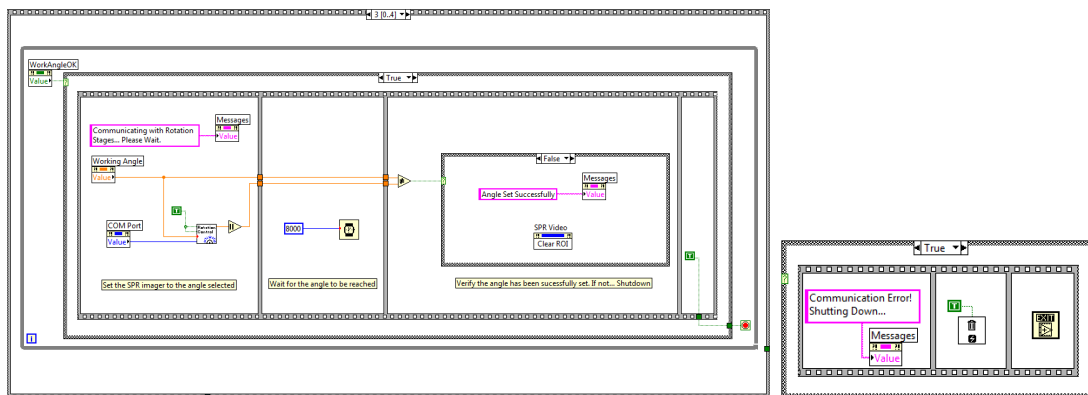
The user can now shift and scale the ensemble of ROIs to fit the area of this distorted image to calibrate the imager.



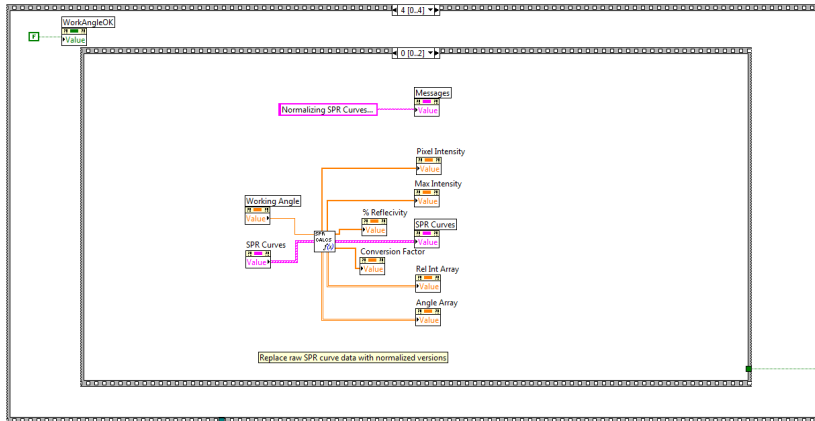
Individual ROIs are labeled with a unique identifier by invoking the “Label Gold ROIs” sub-VI, the output of which displays the labels on the SPR Video for reference.



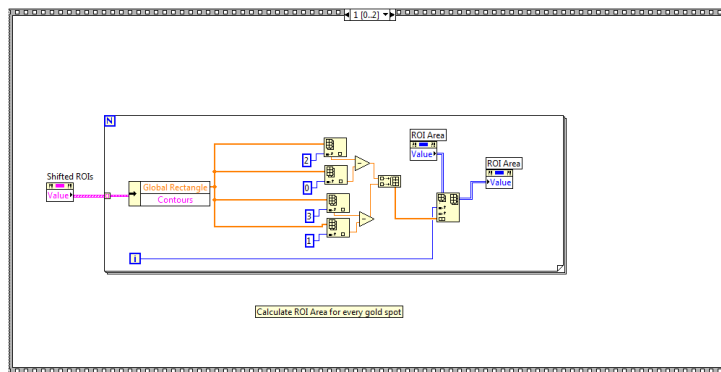
SPR curves are generated (via the “SPR Curve” sub-VI) for each labeled ROI on the SPR Video, along with the distortion parameters that were defined previously in order to keep the ROIs within the analysis area when performing angular scanning.



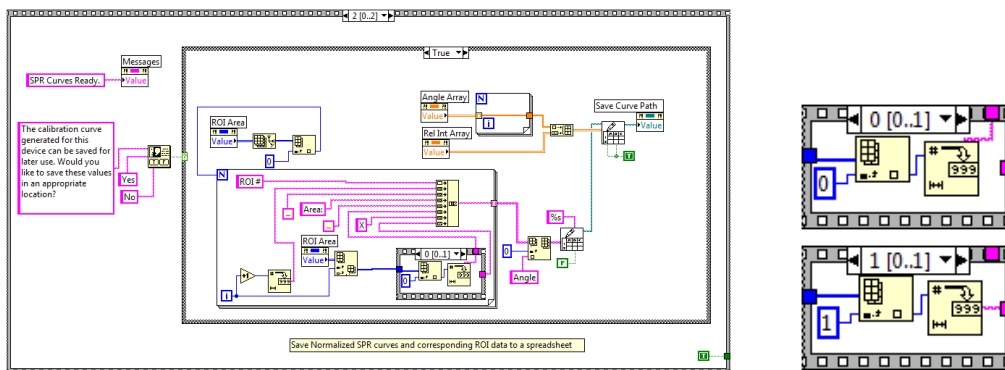
The user chooses a working angle from the SPR Curves, and the software checks the position of the stages to confirm the correct position. Otherwise, an error is generated.



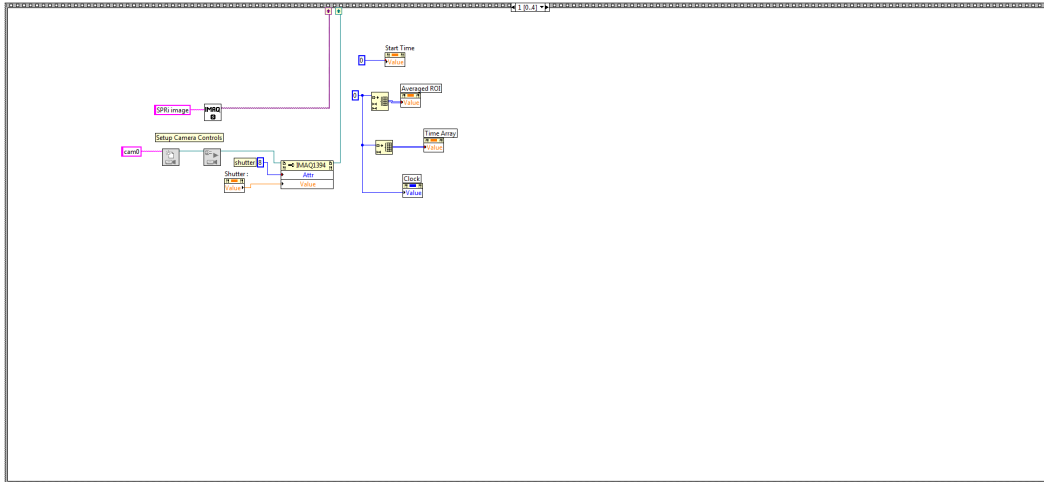
The generated SPR Curves are normalized to percent intensity values by invoking the "SPR Calculations" sub-VI



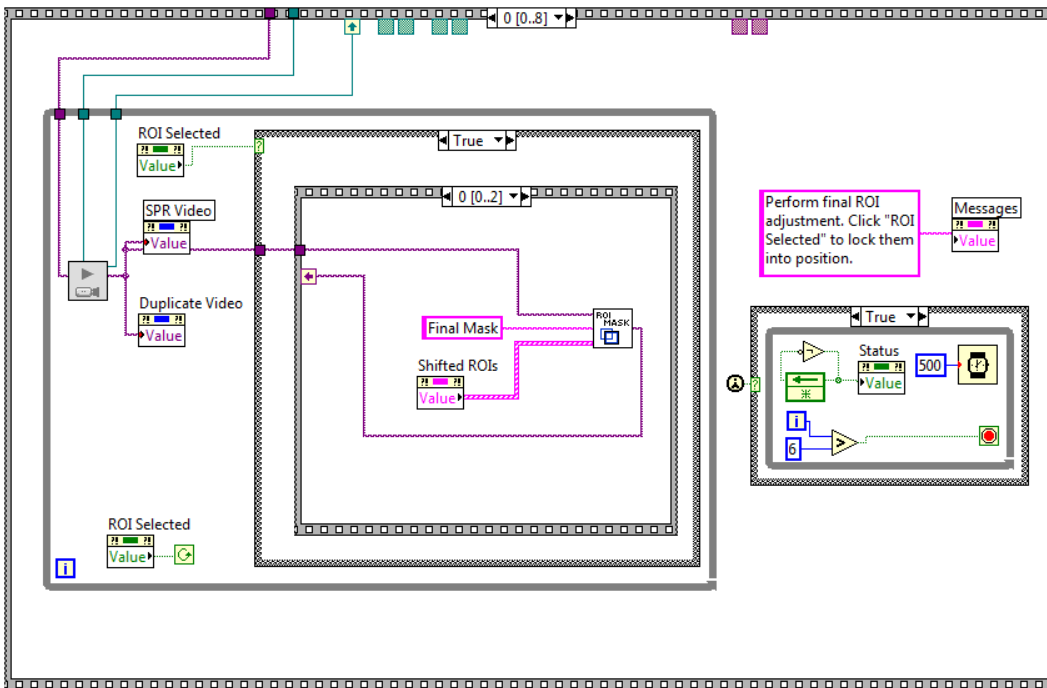
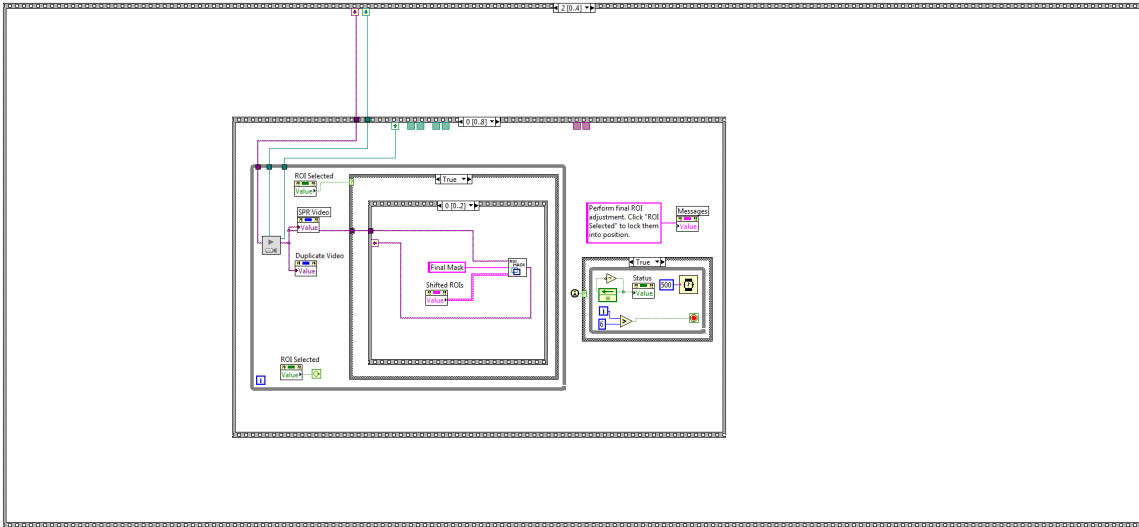
The area of each individual ROI is recorded

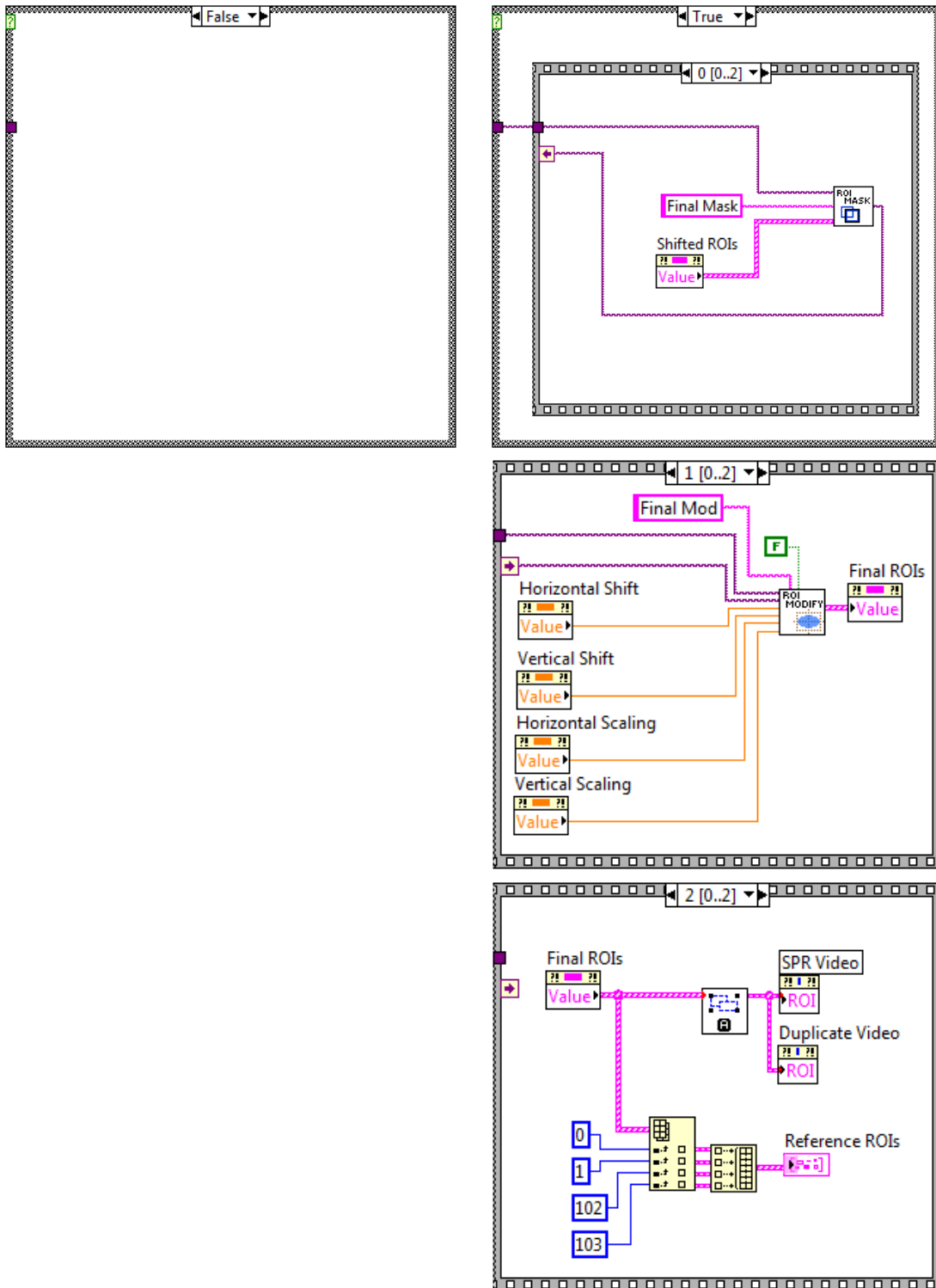


And the entire normalized data can be saved as an Excel Spreadsheet for future reference. Denial of this instance returns nothing.

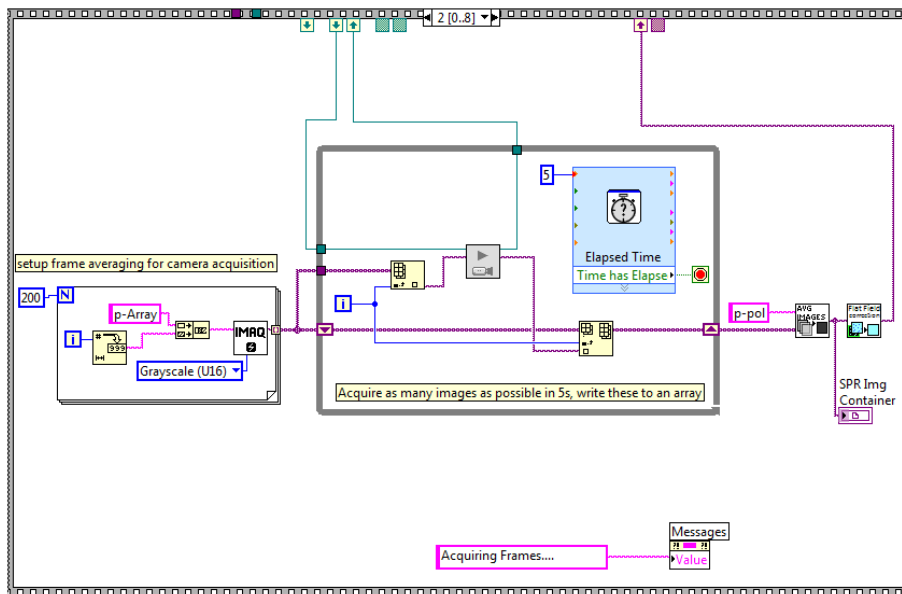
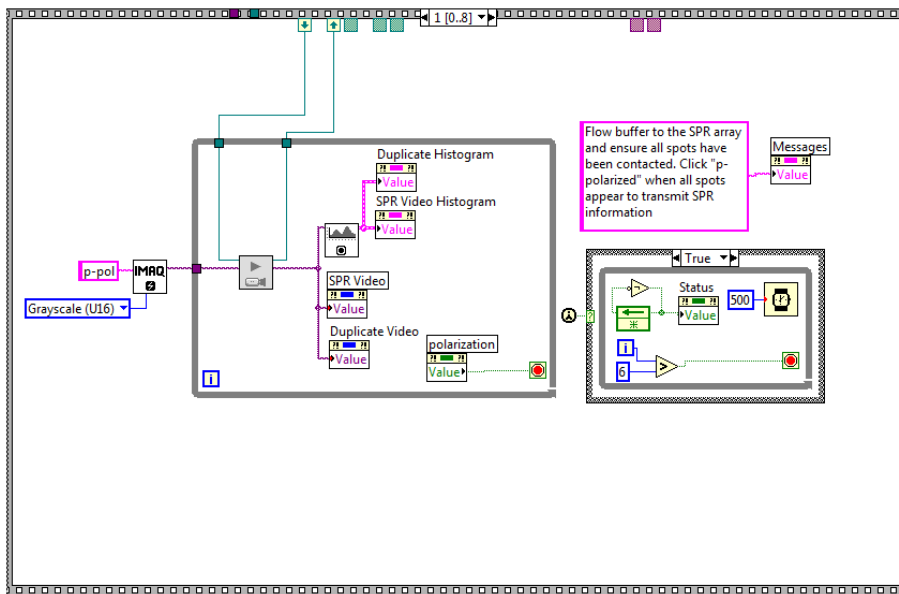


Once the initialization process is complete, the final phase of calibration can begin

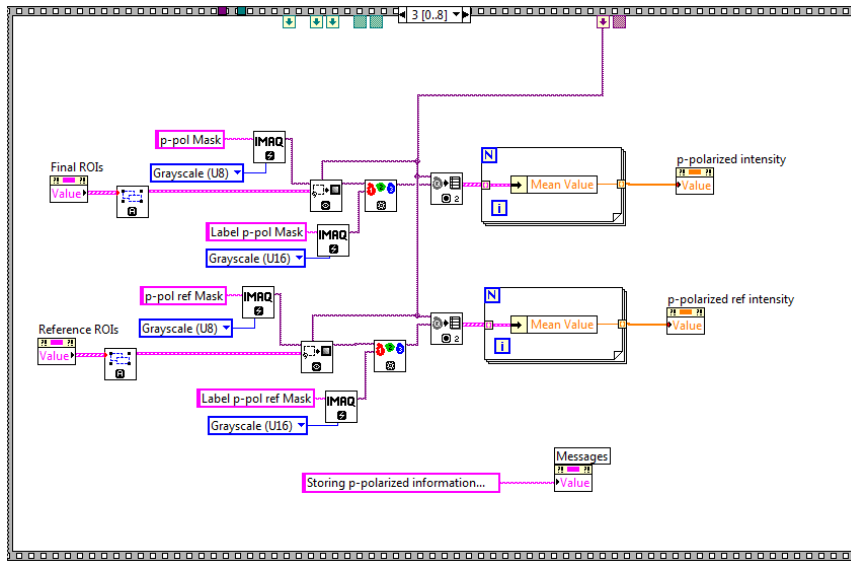




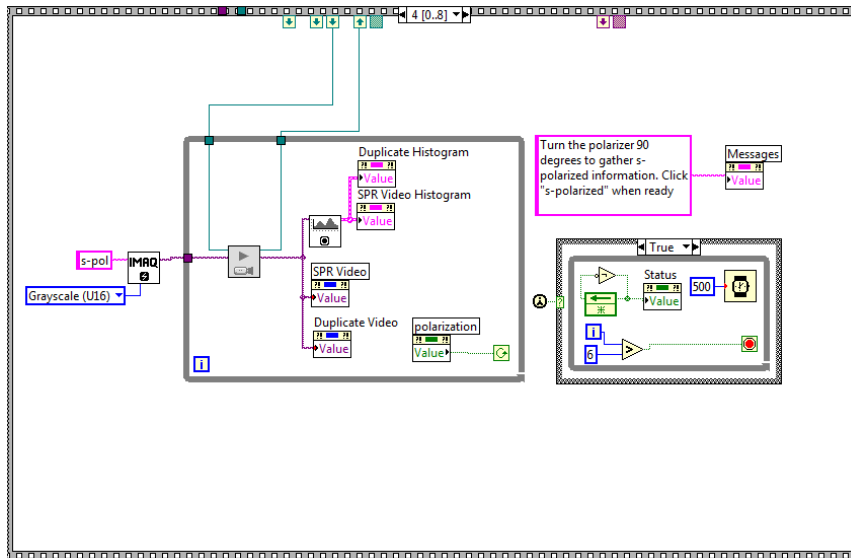
The user is allowed to make one final adjustment to the ensemble of ROIs before locking them into position for analysis.



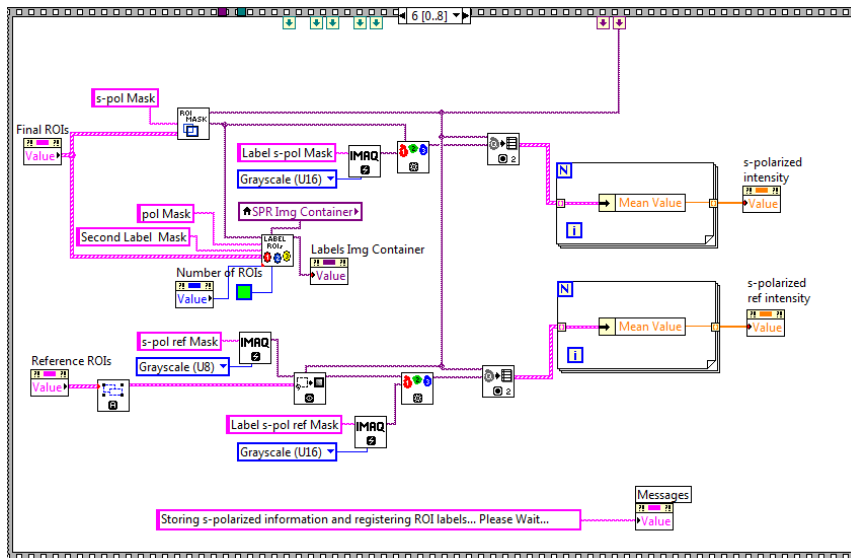
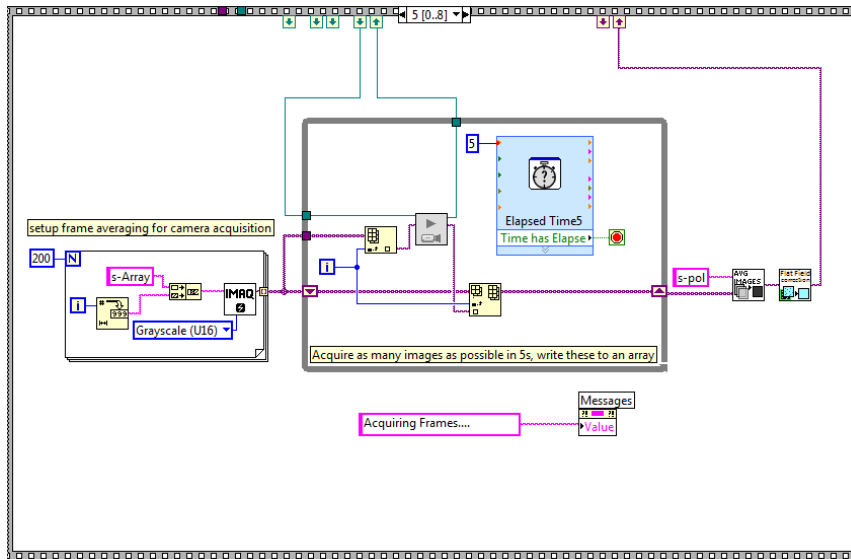
The imager acquires 5 seconds of frames under p-polarized lighting conditions. The totality of the acquired frames is averaged by invoking the "Average SPR Image" sub-VI and further corrected with the flat-field reference image taken at the beginning by invoking the "Flat-Field Correction" sub-VI.



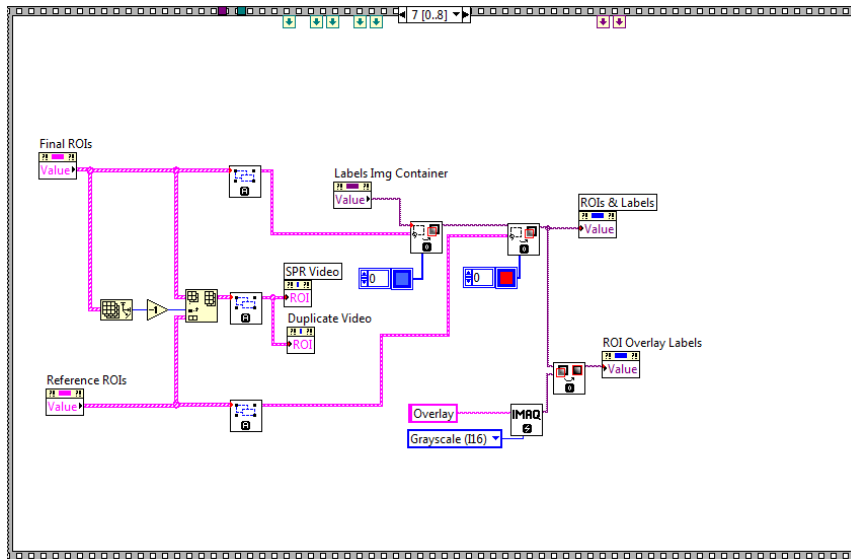
The mean pixel intensity of the corrected SPR image is measured for each individual ROI and stored in an array for future reference.



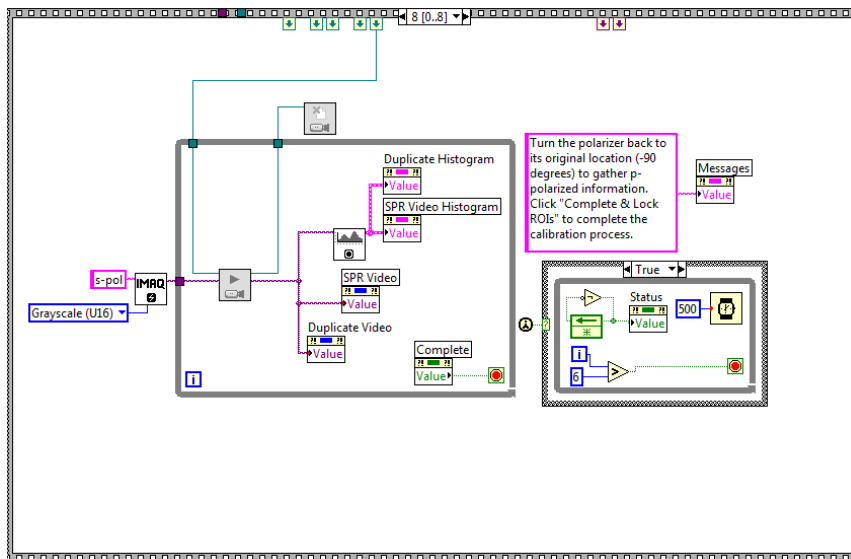
The user is instructed to turn the polarizer by 90° in order to acquire frames under s-polarized light conditions



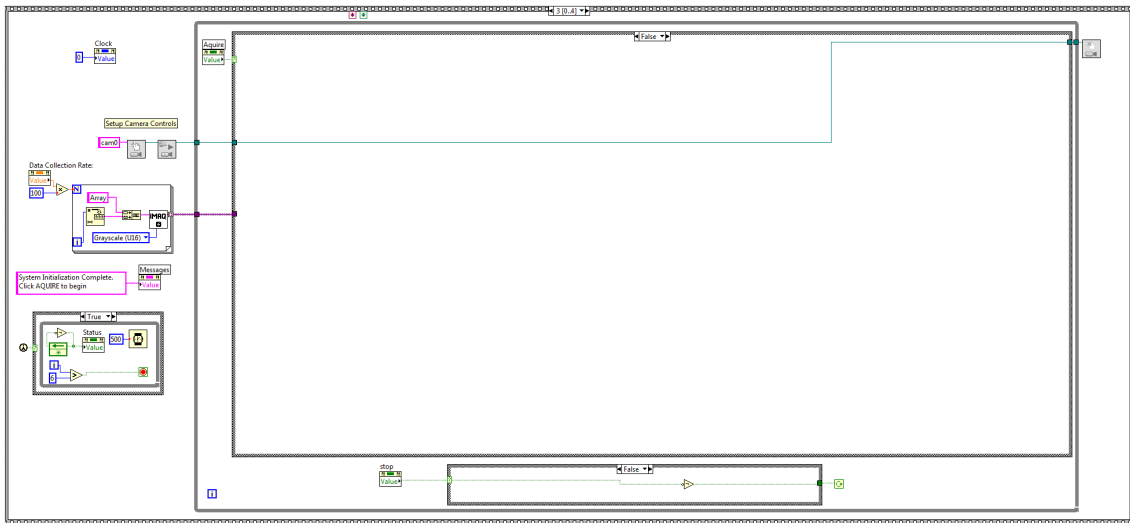
s-polarized light images are averaged, corrected and the intensities stored as mentioned previously. The software labels the individual analysis ROIs.



... and displays them along with the reference ROIs in the “ROIs & Labels” container on the Front Panel GUI.

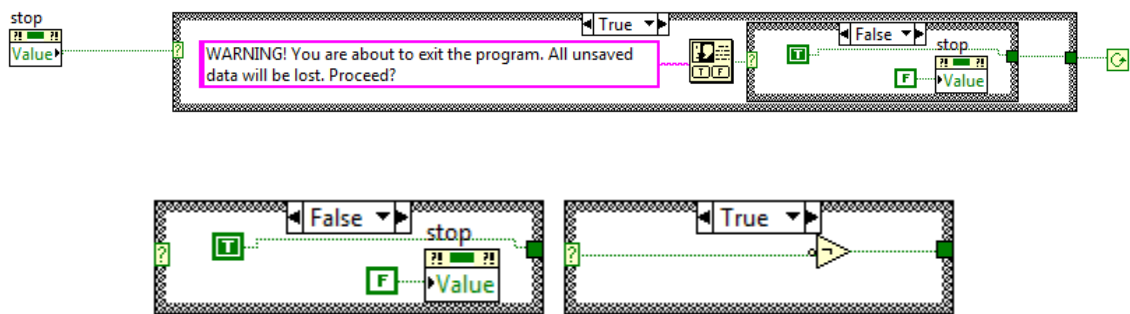


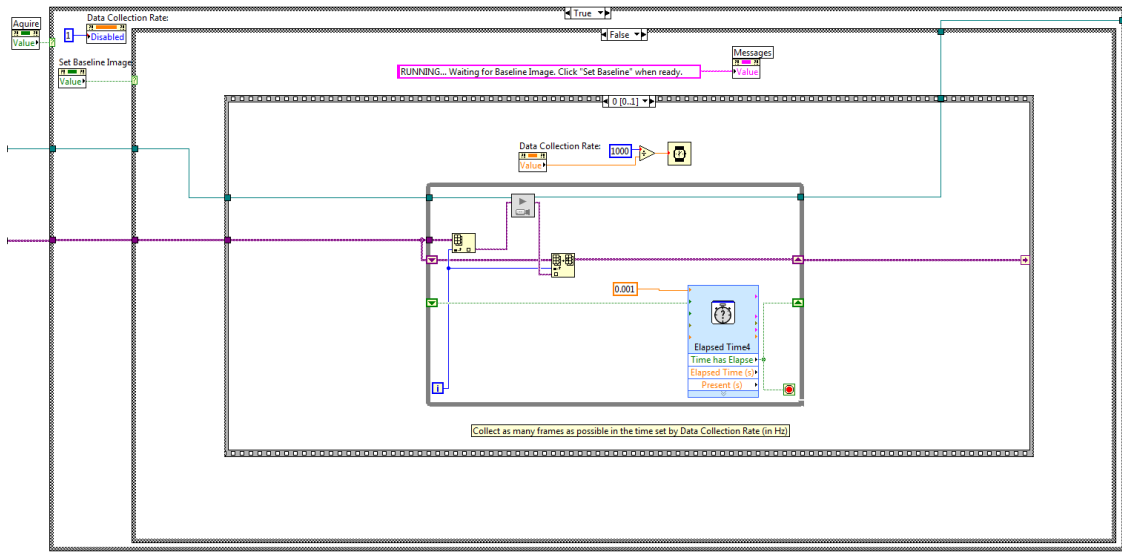
The user is instructed to turn the polarizer back to p-polarized lighting conditions. This final step concludes the initialization and calibration portion of the SPR imager.



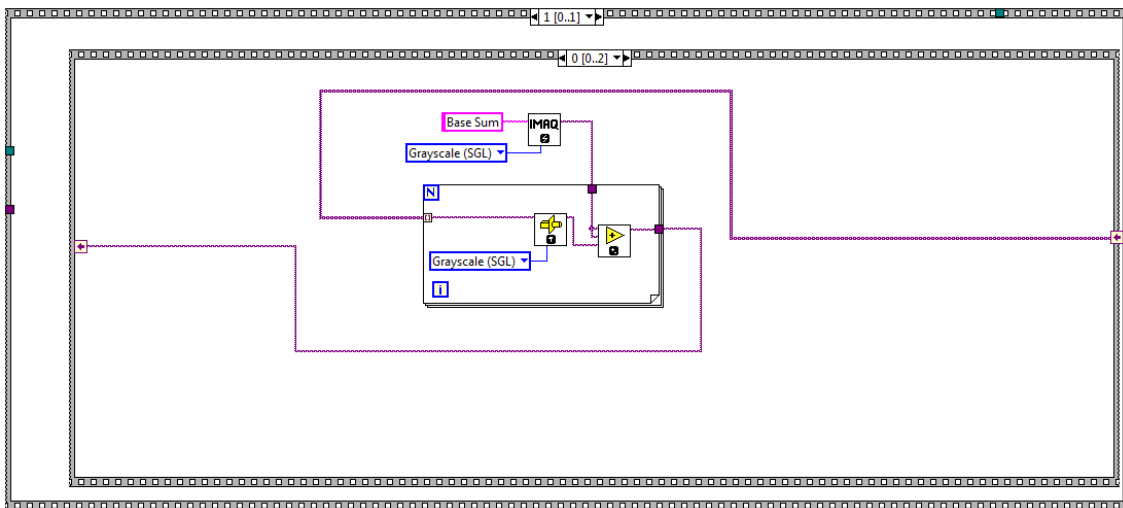
The system indicates that it is now ready for analysis and initializes the CCD camera and sets the data acquisition rate for acquiring SPR frames. The user is instructed to begin the acquisition of frames by clicking “Acquire” on the Front Panel GUI.

At any point, the user can stop the acquisition by pressing “STOP” on the Front Panel GUI and confirming the termination.

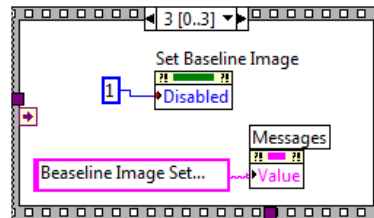
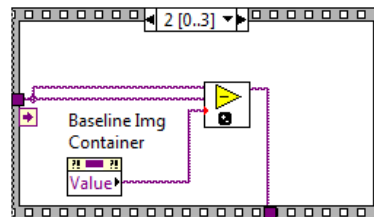
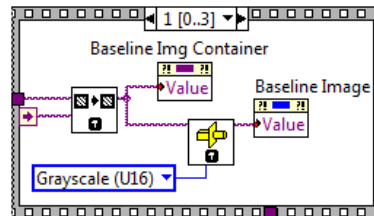
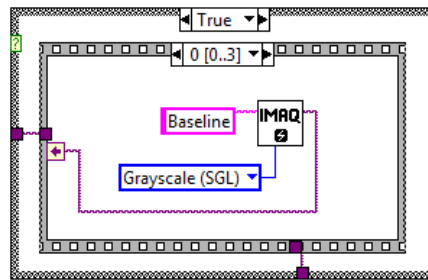
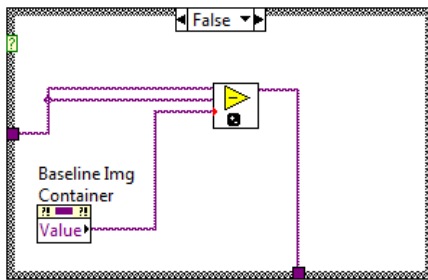
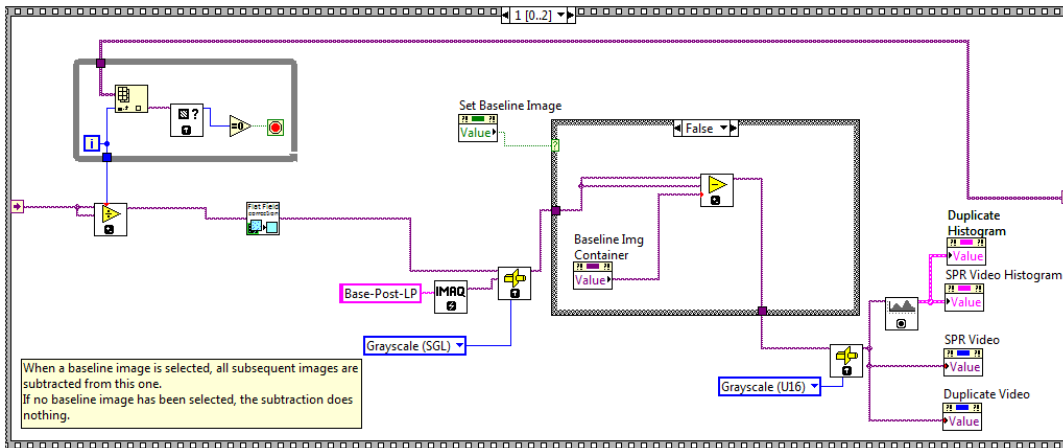




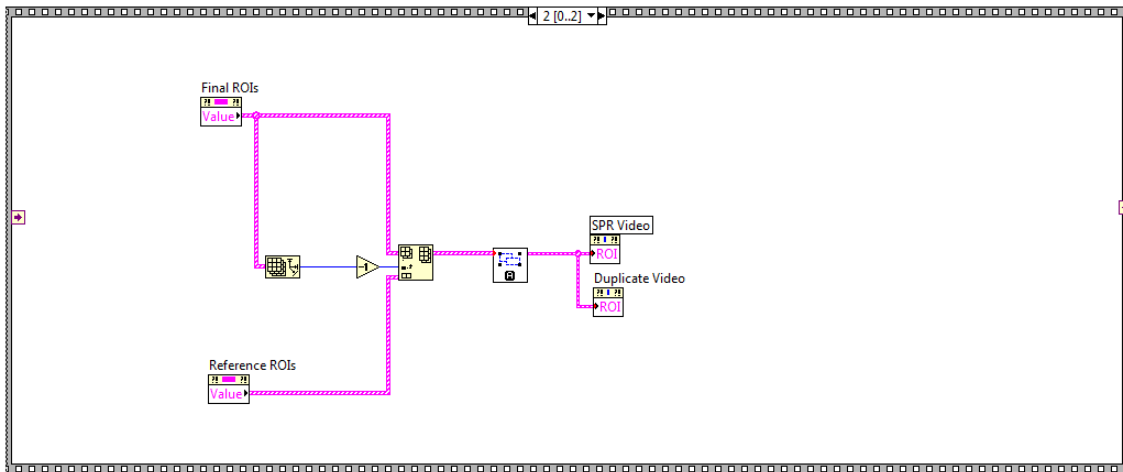
The imager acquires as many frames as possible within the time frame set by the data acquisition rate.



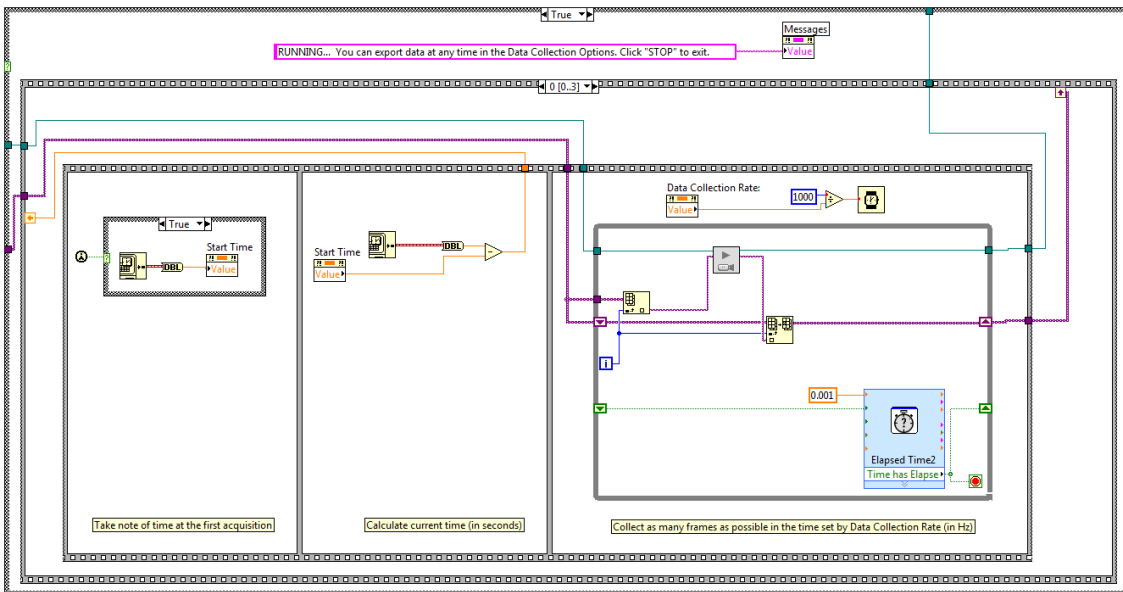
The acquired images are added together and stored in a new image called "Base Sum"



This “Base Sum” image is averaged and subsequently corrected for artifacts. This image is then directly displayed on the SPR Video of the GUI, unless the user chooses to set this image as the baseline for SPR analysis. At this point, the corrected image is stored into the Baseline Image container and is set as the reference image, to which all subsequent images acquired will be subtracted from.

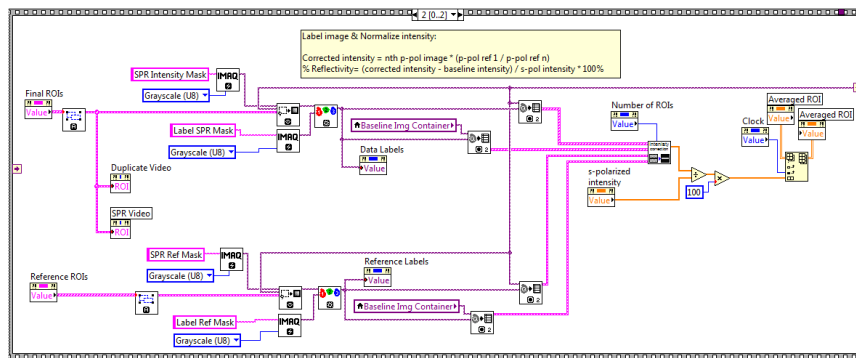
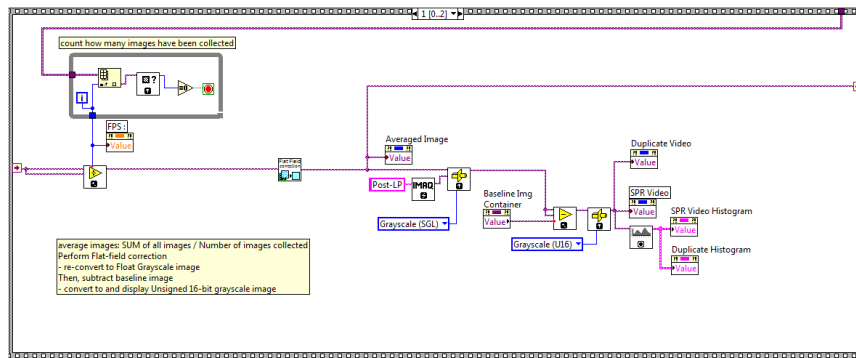
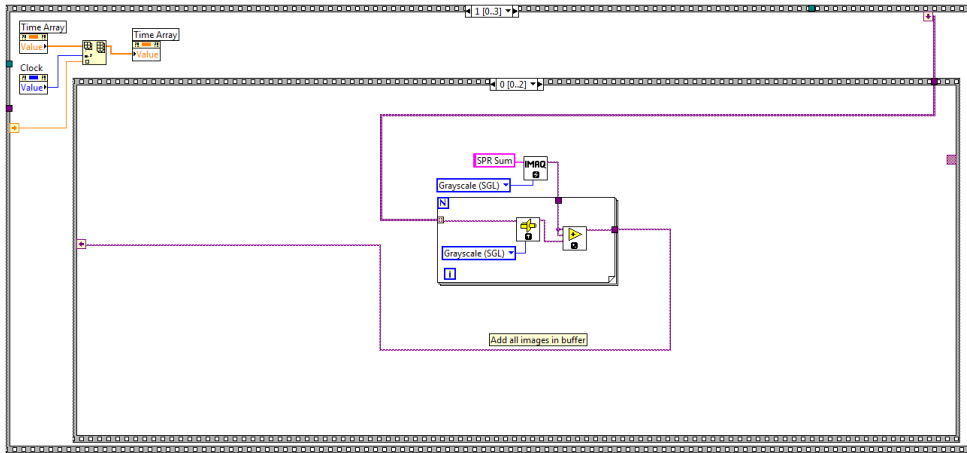


The data and reference ROIs are continuously displayed on the SPR Video for reference



SPR Imager Data Acquisition: Step 1 of 4

After setting the Baseline Image, the software uses the system time key to determine the real-time component of the SPR sensorgram, in seconds. A maximum amount of frames is acquired per data collection interval (typically 1 Hz).

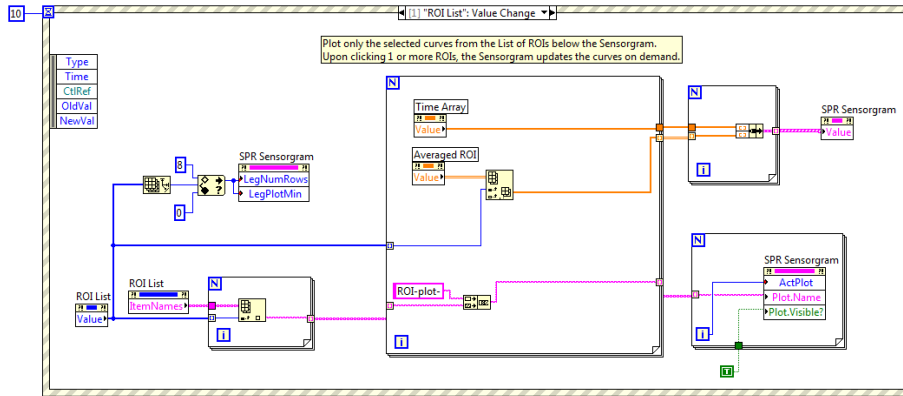
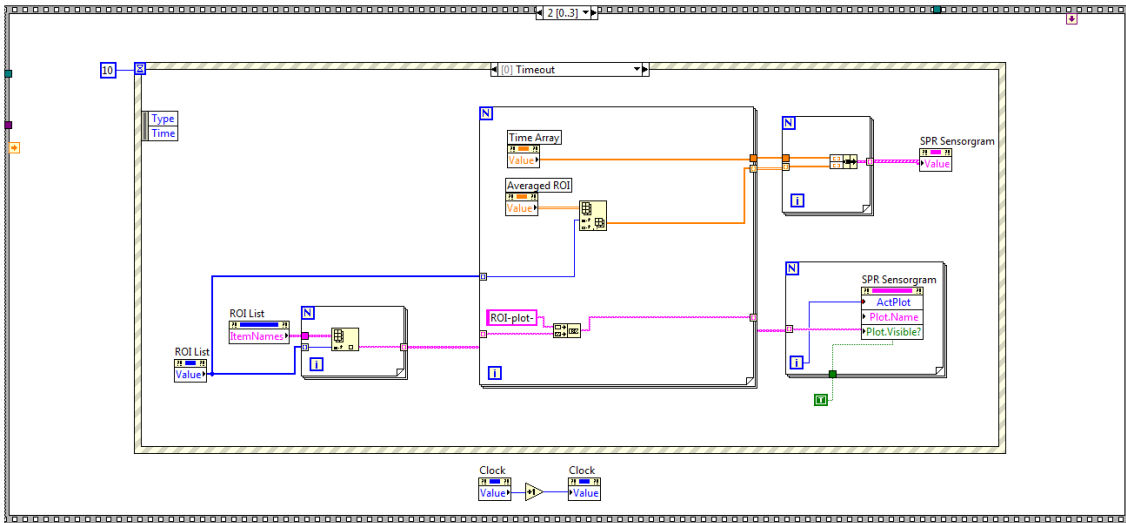


SPR Imer Data Acquisition: Step 2 of 4

The elapsed time is stored into a “Time Array” for plotting the sensorgram.

The acquired images are averaged, corrected and subtracted to the baseline image before being displayed on the SPR Video on the Front Panel GUI

Each ROI of the SPR image is labeled before having their respective pixel intensity measured. The pixel intensity values are converted to percent intensity by invoking the “Intensity Correction” sub-VI. The output of the normalization is stored into an array.

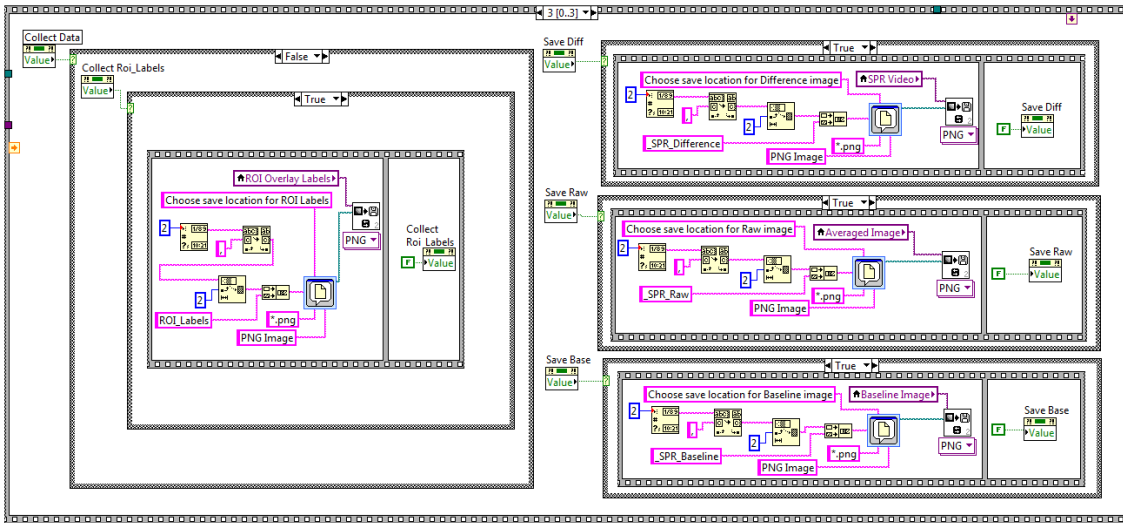


SPR Imager Data Acquisition: Step 3 of 4

The values acquired up to this point are stored into 2 arrays, a “Time” for the x-axis as well as an “Averaged ROI” array for the y-axis containing the normalized pixel intensity values.

The user can control which ROI to plot in real-time by selecting one or multiple ROI labels, the output of each are plotted in the “SPR Sensorgram” on the Front Panel GUI.

Should the user not change the selection from before, the “timeout” subroutine will keep plotting the same curves exactly as previously selected.



SPR Imer Data Acquisition: Step 4 of 4

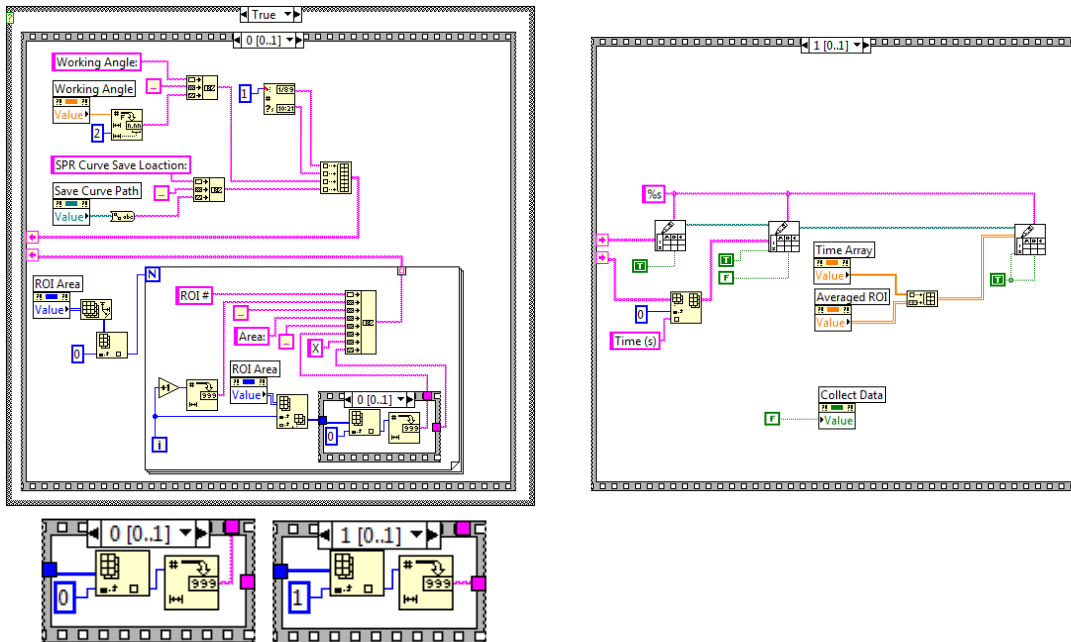
At any point during the acquisition, the user can chose to save the data and/or images.

The current averaged image can be saved by clicking “Raw Image”

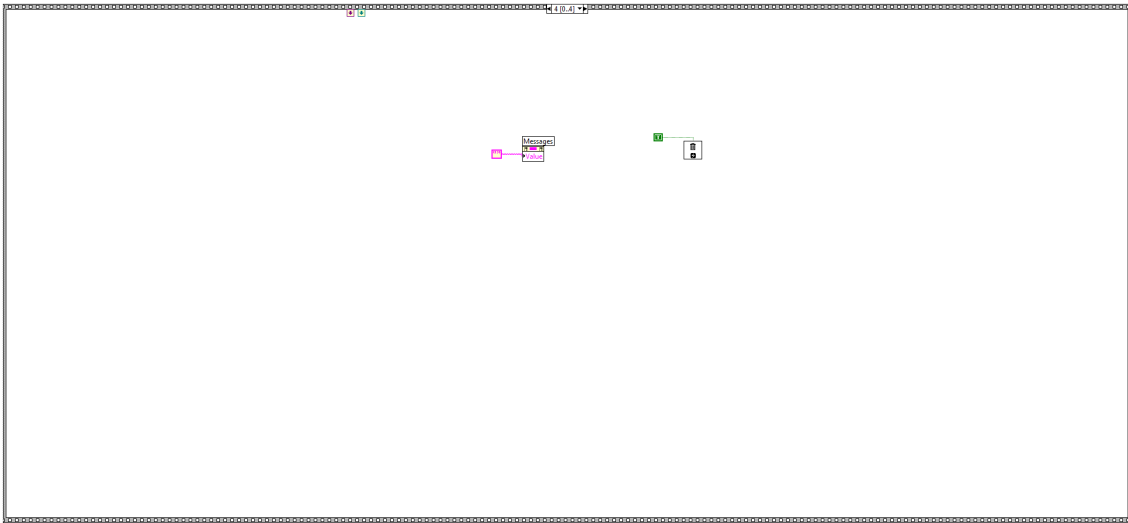
The current difference image can be saved by clicking “Difference Image”

The baseline image can be saved by clicking “Baseline Image”

The current position of each ROI and its label can be saved by clicking “ROIs & Labels”



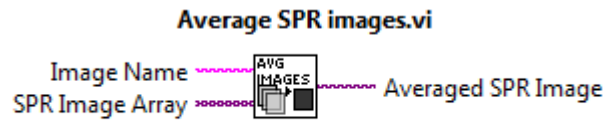
The area of each ROI, the working angle, the location of the SPR curves, and the SPR data are all packaged into a single Excel Spreadsheet for analysis.



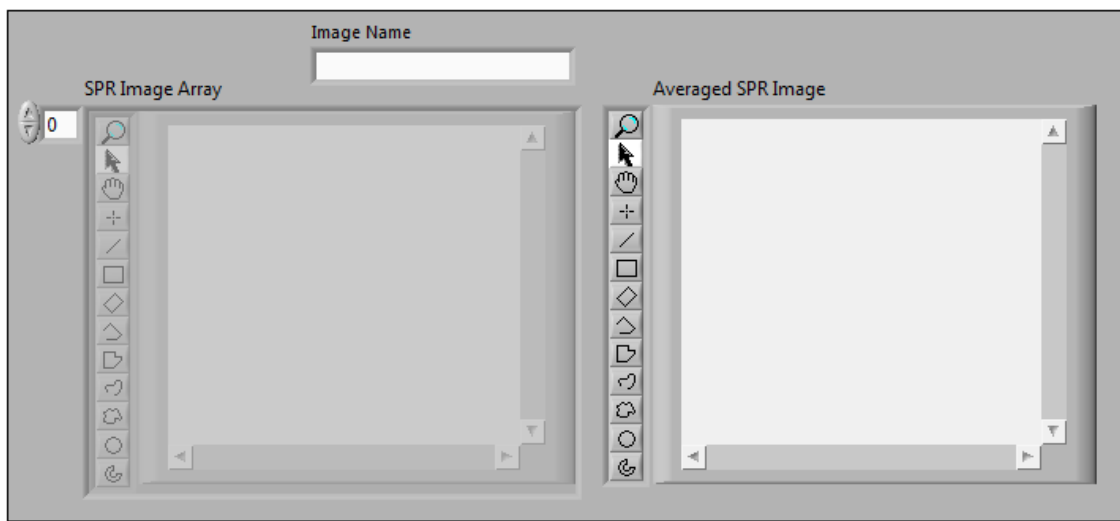
The program ends when the user clicks “STOP”, where the software executes a memory dump of all images stored.

C.3 AVERAGE SPR IMAGES.VI

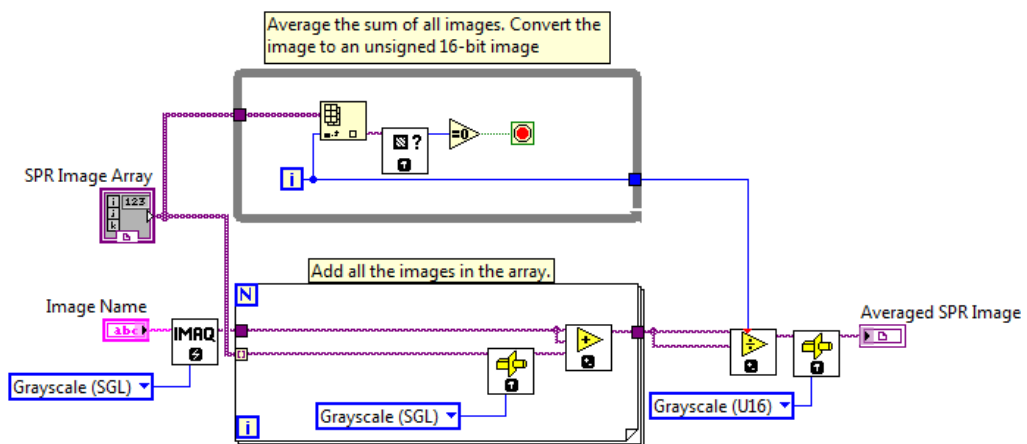
CONNECTOR PANEL:



FRONT PANEL:



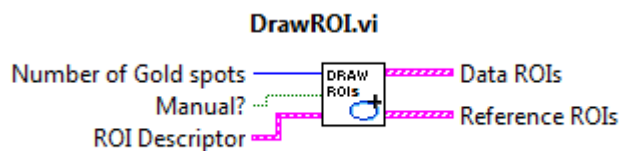
BLOCK DIAGRAM:



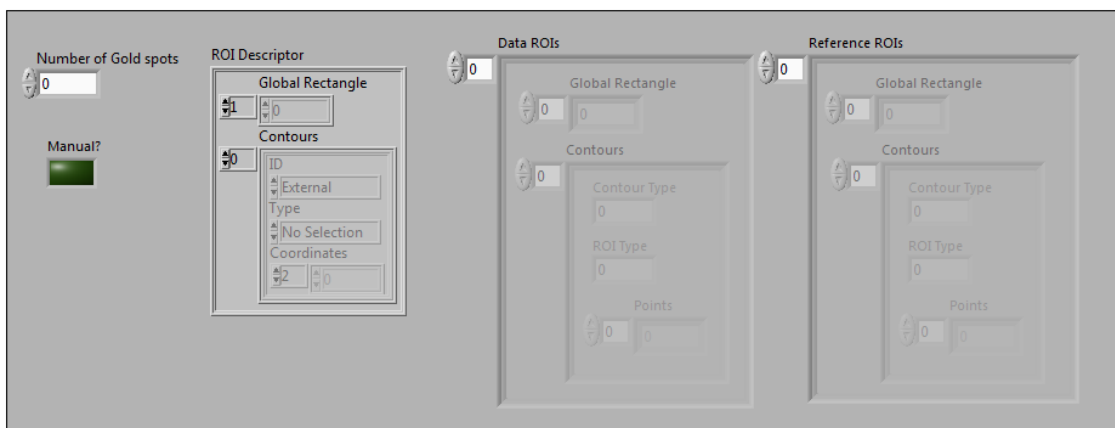
This sub-VI averages an array of acquired SPR images into a single 16-bit image for analysis

C.4 DRAW ROI.VI

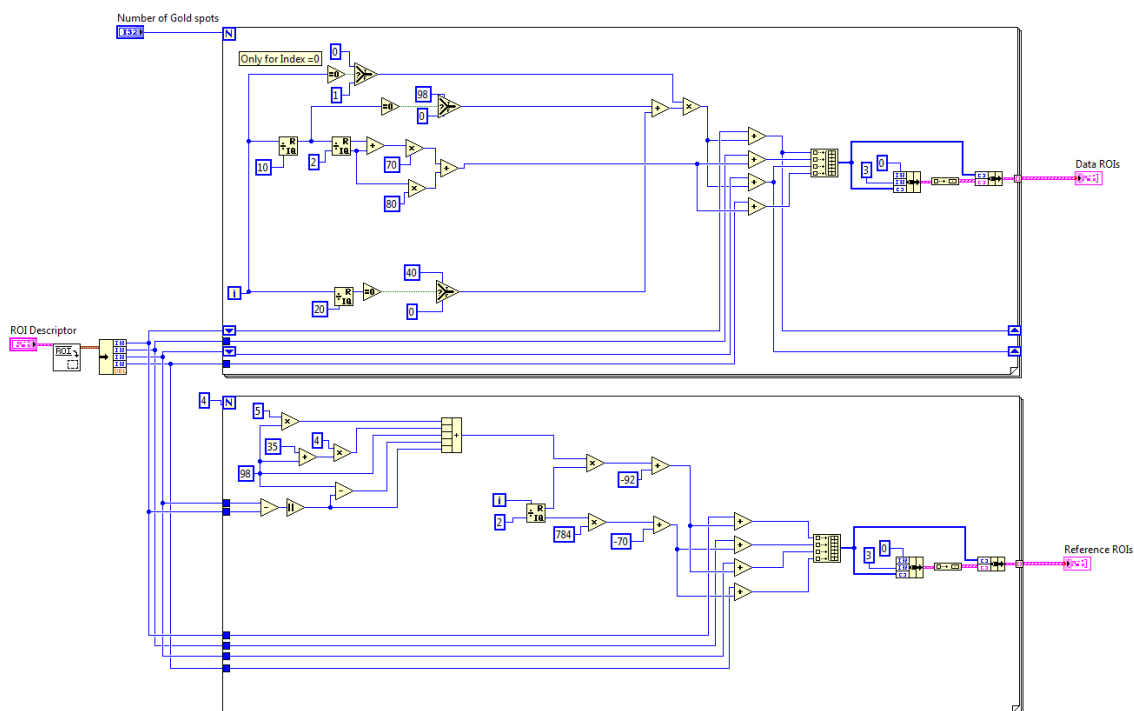
CONNECTOR PANEL:



FRONT PANEL:



BLOCK DIAGRAM:

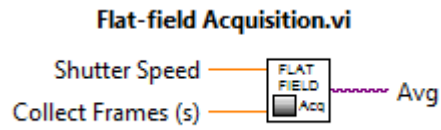


This sub-VI draws an array of regions of interest (ROI) identical in shape and size to a template, initially supplied by the “ROI Descriptor”. Each ROI within a single column (of 10) of the array will be vertically added below at 70 pixels spacing, starting from the initial position of the first ROI in the descriptor. Even numbered columns will be immediately added adjacent to the previous column of 10 ROIs, at 98 pixels to the right. Odd numbered columns will begin at 98+40 pixels to the right of the previously added column. A Reference ROI is also added to every corner of the ROI array. Two separate clusters are created, the first one containing the ROI array for analysis, and a second cluster containing the reference ROIs, both of which are returned to the Main VI.

Cluster of 3 elements: ID= external; Type = 3 (rectangular); Coordinates (top left corner & bottom right corner)

C.5 FLAT-FIELD ACQUISITION.VI

CONNECTOR PANEL:



FRONT PANEL:



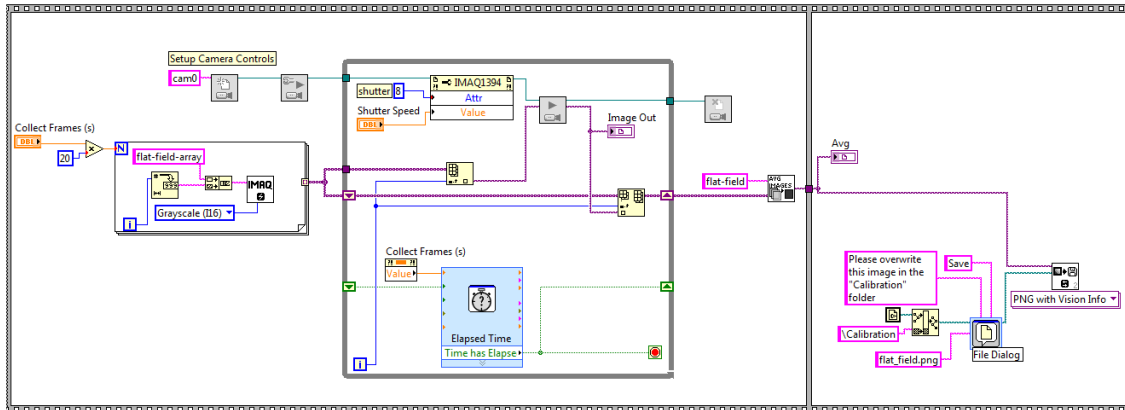
SUB-VI INVOKED ALONG WITH CONNECTOR PANEL AND SECTION REFERENCE



Appendix C.3

This sub-VI averages a series of collected SPR images by the CCD camera to minimize the noise signal from the sensor

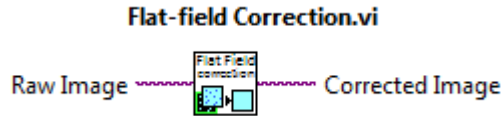
BLOCK DIAGRAM:



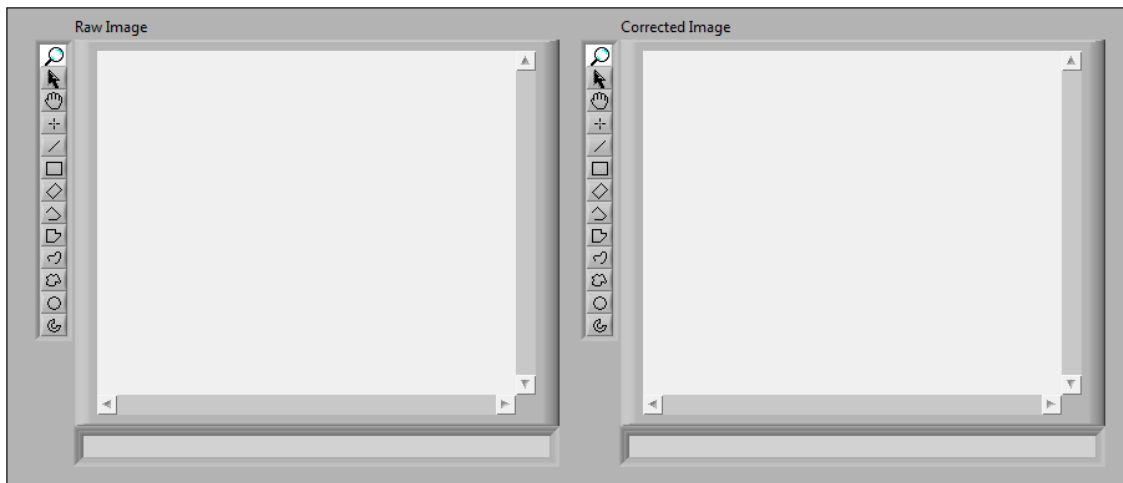
This sub-VI initializes the CCD camera as well as an array container for storing acquired images. The CCD acquires images for the duration prescribed by the control “collect frames (s)” where each image is sequentially stored in the “flat-field array”. At the end of the acquisition, images in the array are averaged and then saved in the “Calibration” folder for the Main VI’s reference.

C.6 FLAT-FIELD CORRECTION.VI

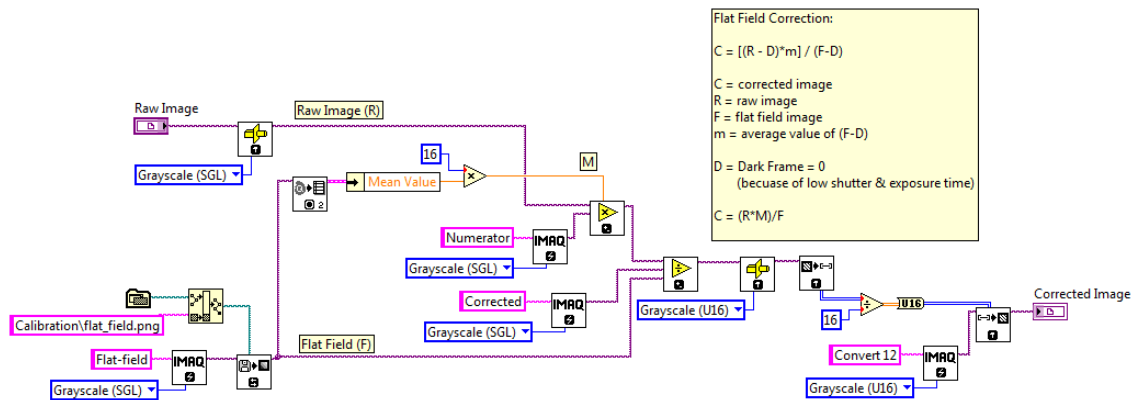
CONNECTOR PANEL:



FRONT PANEL:



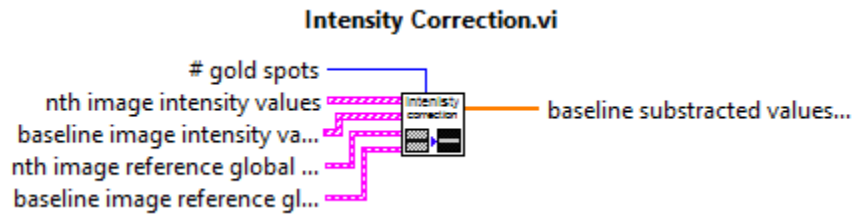
BLOCK DIAGRAM:



This sub-VI performs a reference subtraction of an averaged SPR image to a flat-field image to remove any image artifacts associated with the optical components, dust or physical anomalies on the SPR imager. The corrected image is returned to the Main VI.

C.7 INTENSITY CORRECTION.VI

CONNECTOR PANEL:



FRONT PANEL:

gold spots

100

nth image intensity values

0

0.00	Mean Value
0.00	Standard Variation
0.00	Minimal Value
0.00	Maximal Value
0.00	Area (calibrated)
0	Area (pixels)
0.00	%

Calibration Valid

baseline image intensity values

0

0.00	Mean Value
0.00	Standard Variation
0.00	Minimal Value
0.00	Maximal Value
0.00	Area (calibrated)
0	Area (pixels)
0.00	%

Calibration Valid

baseline subtracted values (gold spots)

0

0

0

0

0

0

0

0

0

nth image reference global values

0.00	Mean Value
0.00	Standard Variation
0.00	Minimal Value
0.00	Maximal Value
0.00	Area (calibrated)
0	Area (pixels)
0.00	%

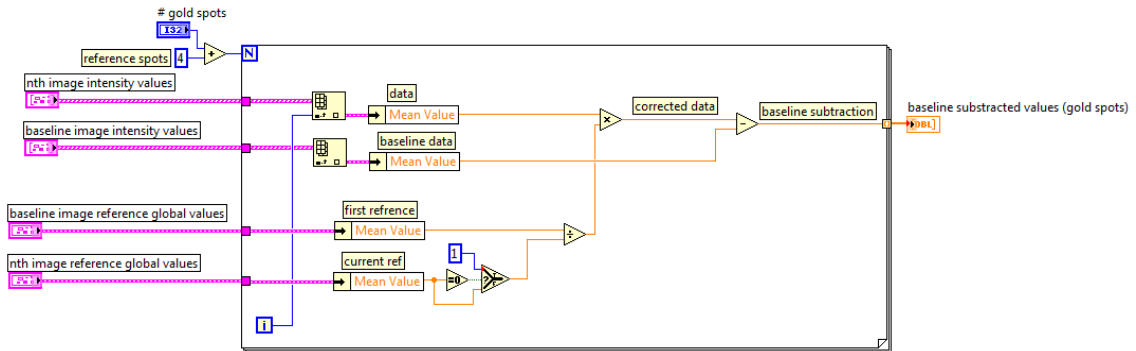
Calibration Valid

baseline image reference global values

0.00	Mean Value
0.00	Standard Variation
0.00	Minimal Value
0.00	Maximal Value
0.00	Area (calibrated)
0	Area (pixels)
0.00	%

Calibration Valid

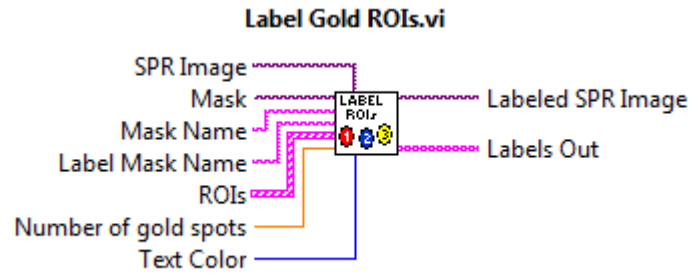
BLOCK DIAGRAM:



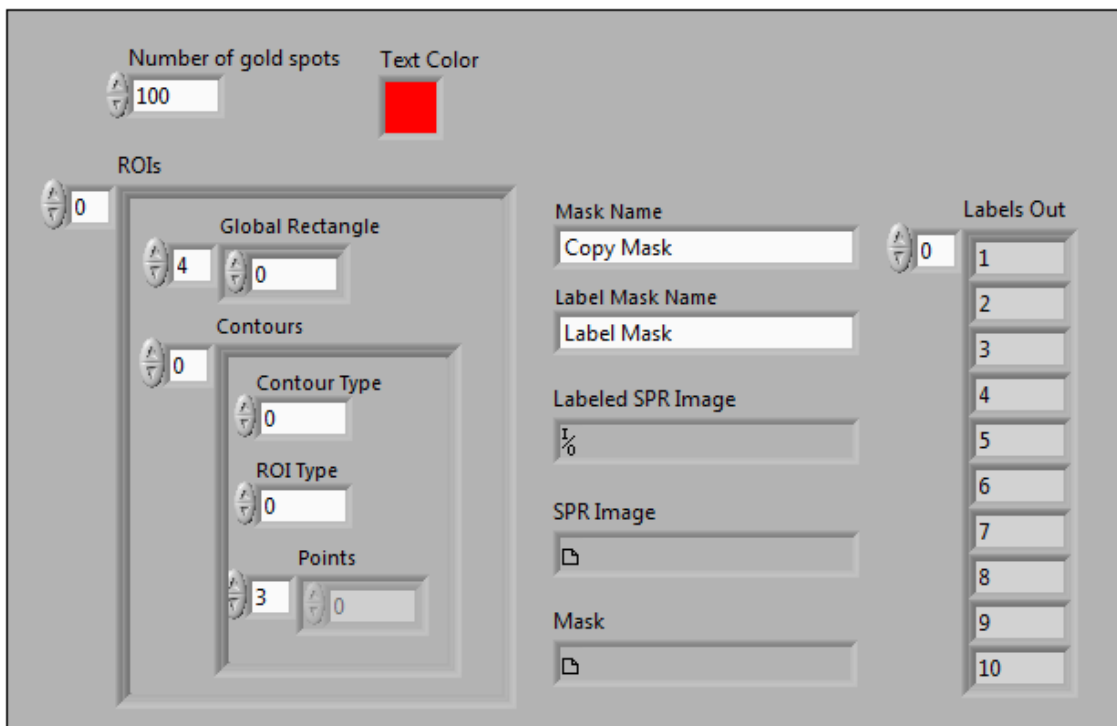
This sub-VI provides the difference pixel intensity for each region of interest (ROI) to be analyzed. The reference intensity values of the current image to be analyzed are compared to the same ones collected in the first image acquired. A normalization factor is calculated from this comparison, and applied to the entire image, correcting for fluctuations in LED intensity over time. The intensity-corrected image is then subtracted to the initial image acquired to obtain the difference SPR signal, which is returned to the Main VI

C.8 LABEL GOLD ROI.VI

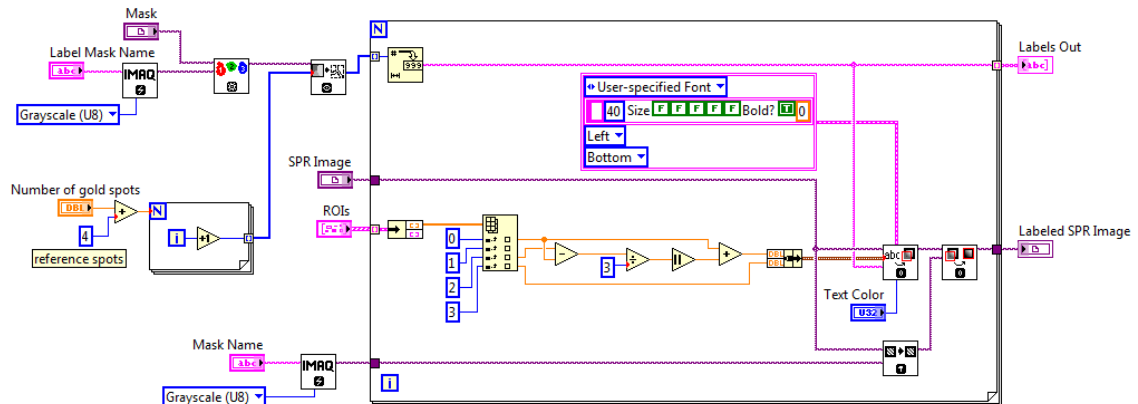
CONNECTOR PANEL:



FRONT PANEL:



BLOCK DIAGRAM:



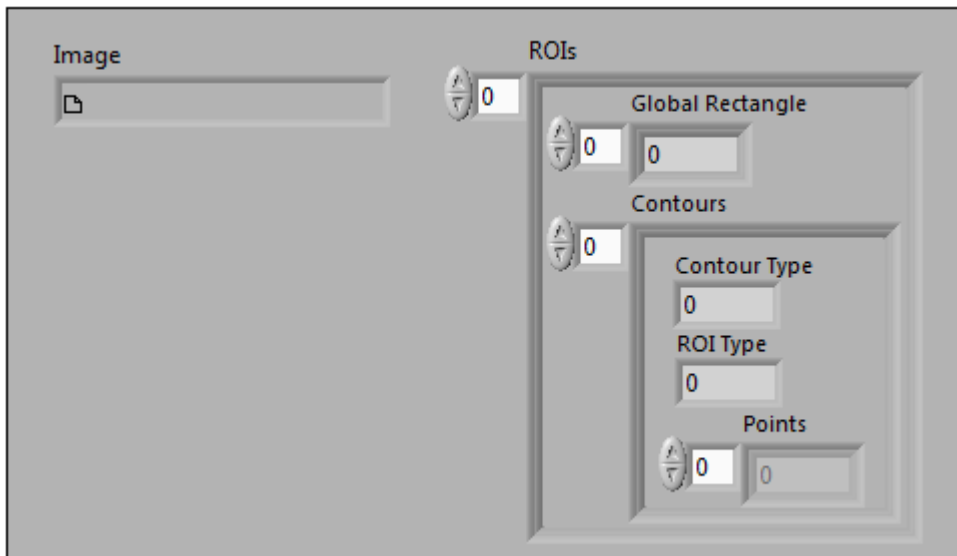
This sub-VI defines individual region of interest (ROI) area in an SPR image with a unique identifier that can be referenced in the future. Both a labeled SPR image and corresponding labels are provided to the Main VI.

C.9 MASK TO ROI.VI

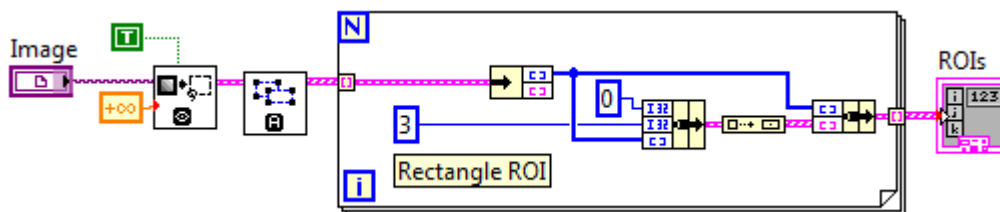
CONNECTOR PANEL:



FRONT PANEL:



BLOCK DIAGRAM:



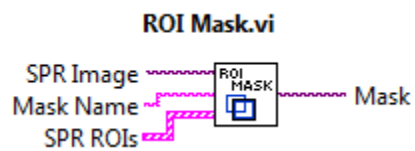
This sub-VI converts an image mask to an array of region of interest (ROI) descriptors, which is provided to the Main VI.

ROIs are a cluster of 3 elements:

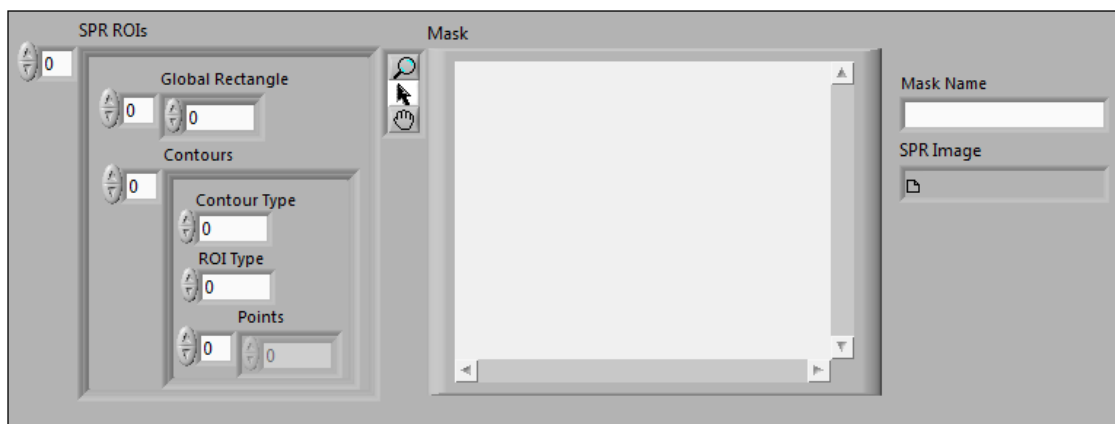
ID= external; Type = 3 (rectangular); Coordinates (top left corner & bottom right corner)

C.10 ROI MASK.VI

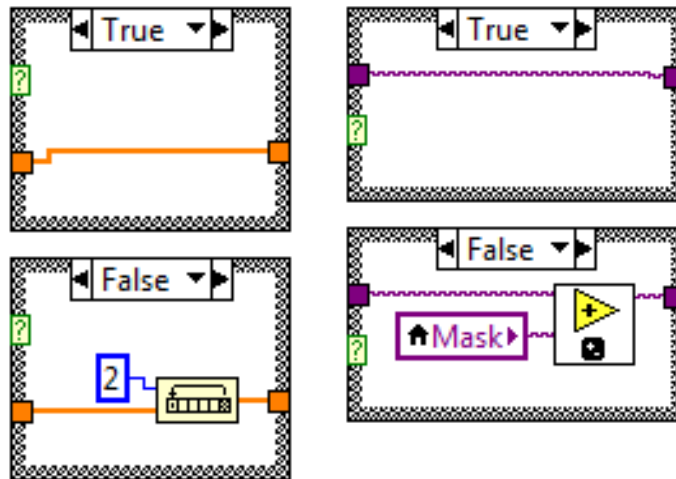
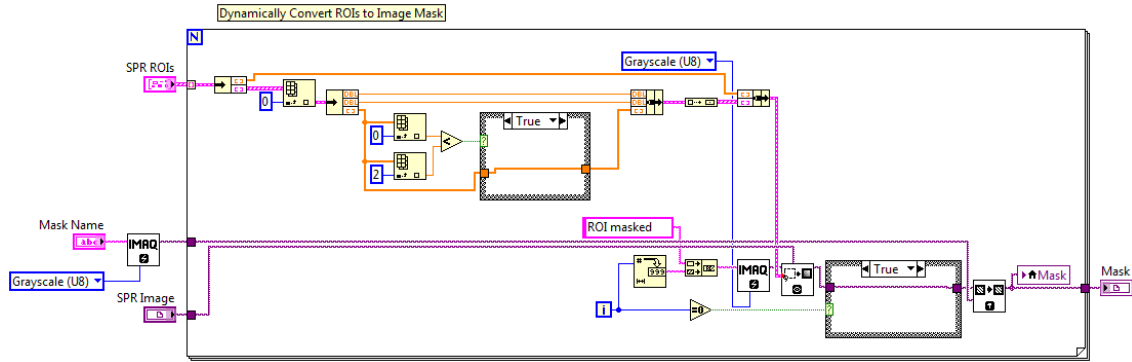
CONNECTOR PANEL:



FRONT PANEL:



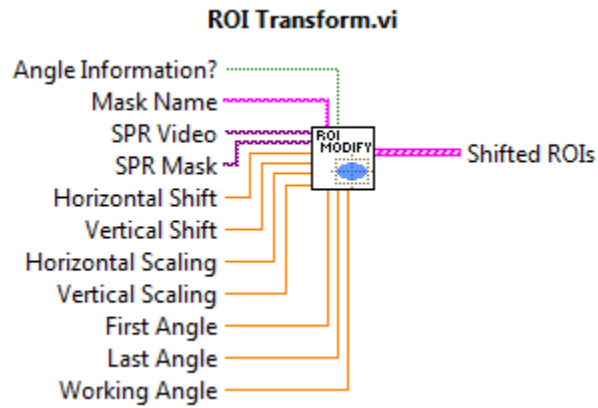
BLOCK DIAGRAM:



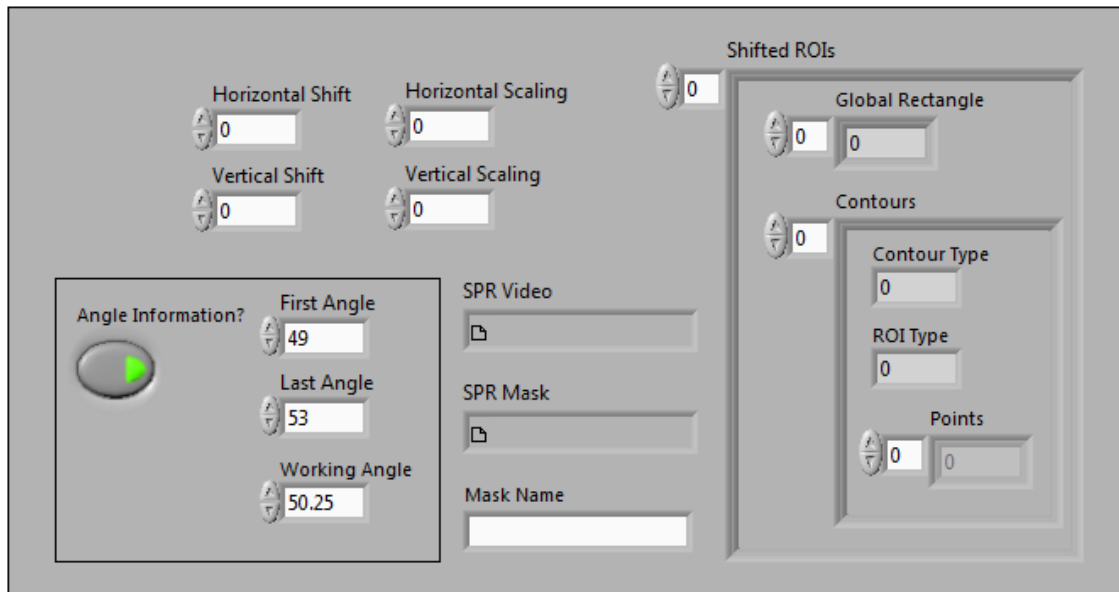
This sub-VI converts the regions of interest (ROIs) defined on the SPR image to an image mask for further manipulation. Each ROI area is sequentially added to an image mask, which is returned to the Main VI.

C.11 ROI TRANSFORM.VI

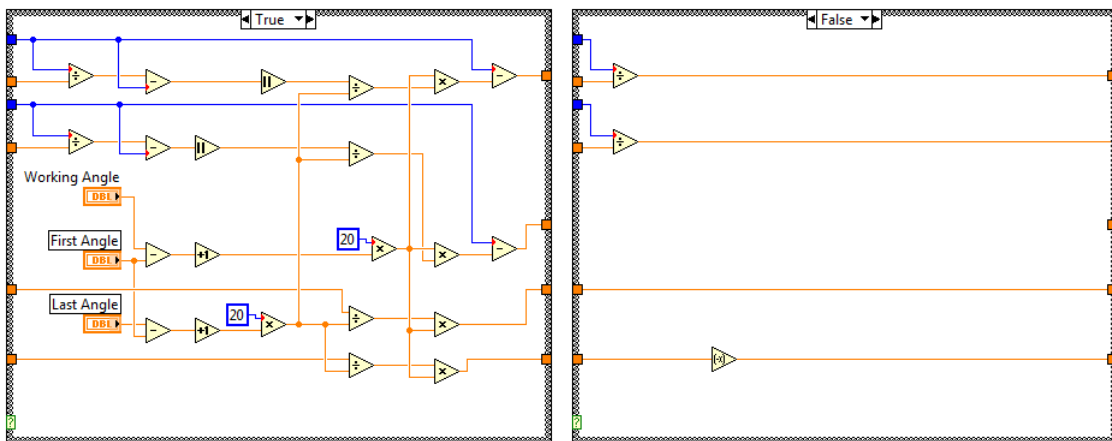
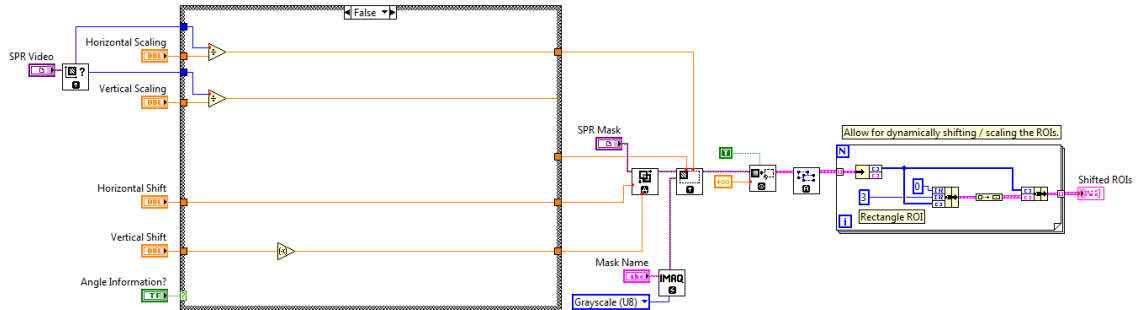
CONNECTOR PANEL:



FRONT PANEL:



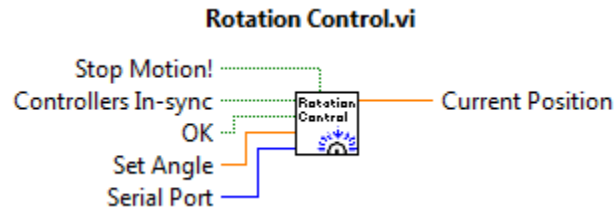
BLOCK DIAGRAM:



This sub-VI allows for scaling and resizing an SPR mask (containing ROI information) in order to accommodate variations in the PDMS microfluidic devices and/or physical or virtual distortions in the SPR image. The modified ROIs are provided to the Main VI.

C.12 ROTATION CONTROL.VI

CONNECTOR PANEL:

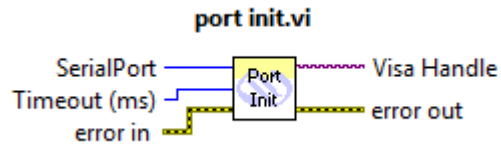


FRONT PANEL:



This panel displays the absolute position of each rotation stage and several parameters related to their movement. The rotation is always performed *in-sync*, moving away from each other.

LIST OF SUB-VIS CALLED WITHIN THIS SUB-VI:



This sub-VI initializes the RS-232 Communication protocol with each rotation stage

The following RS-232 parameters are fixed:

Baud Rate = 57600

Data Bits = 8

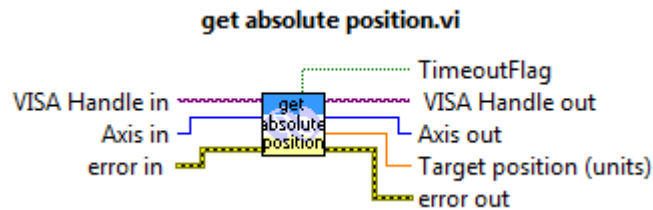
Parity = None

Stop Bits = 1

Flow Control = XON/XOFF

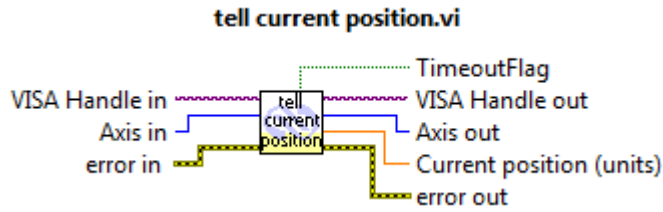
Termination Character = CR/LF

Note: This VI is available from Newport Corporation and will not be discussed any further.



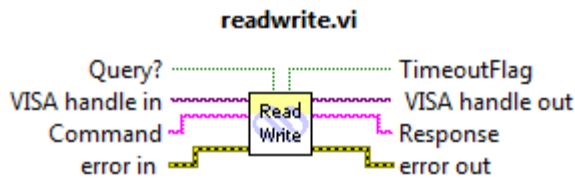
This sub-VI returns the absolute position for every rotation stage
(referenced from Axis in)

Note: This VI is available from Newport Corporation



This sub-VI returns the current position for every rotation stage (referenced from Axis in)

Note: This VI is available from Newport Corporation



This sub-VI allows for sending commands to the rotation stages via the SMC100 controller and to receive responses via the RS-232 communication port.

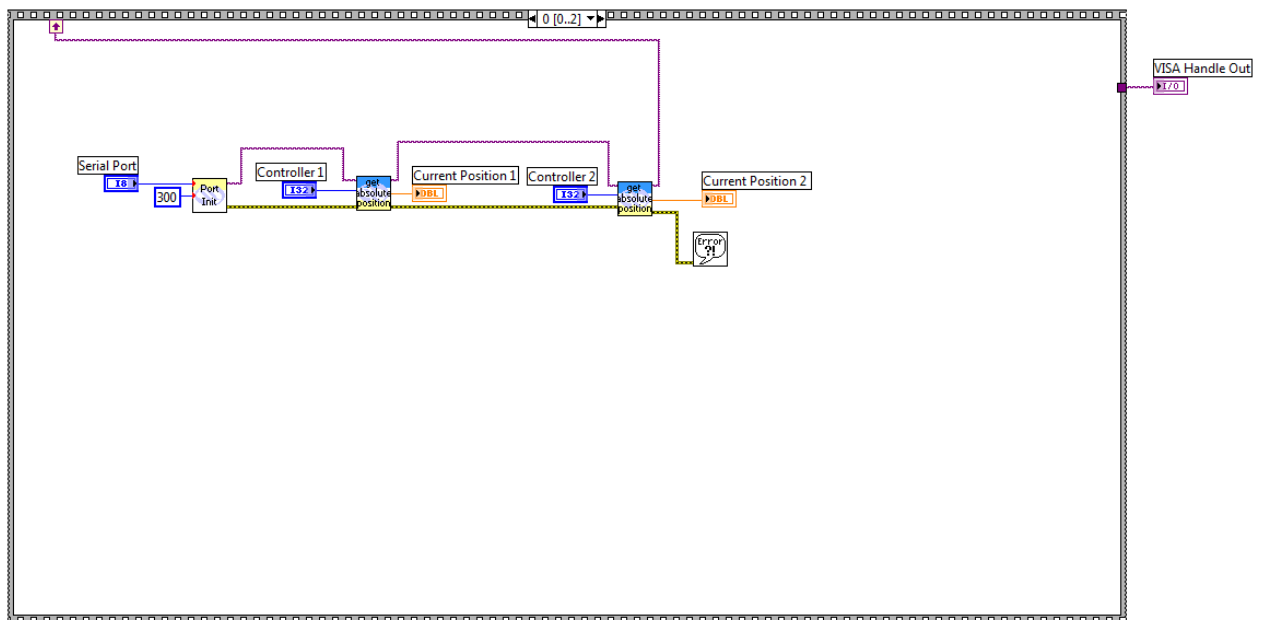
Note: This VI is available from Newport Corporation



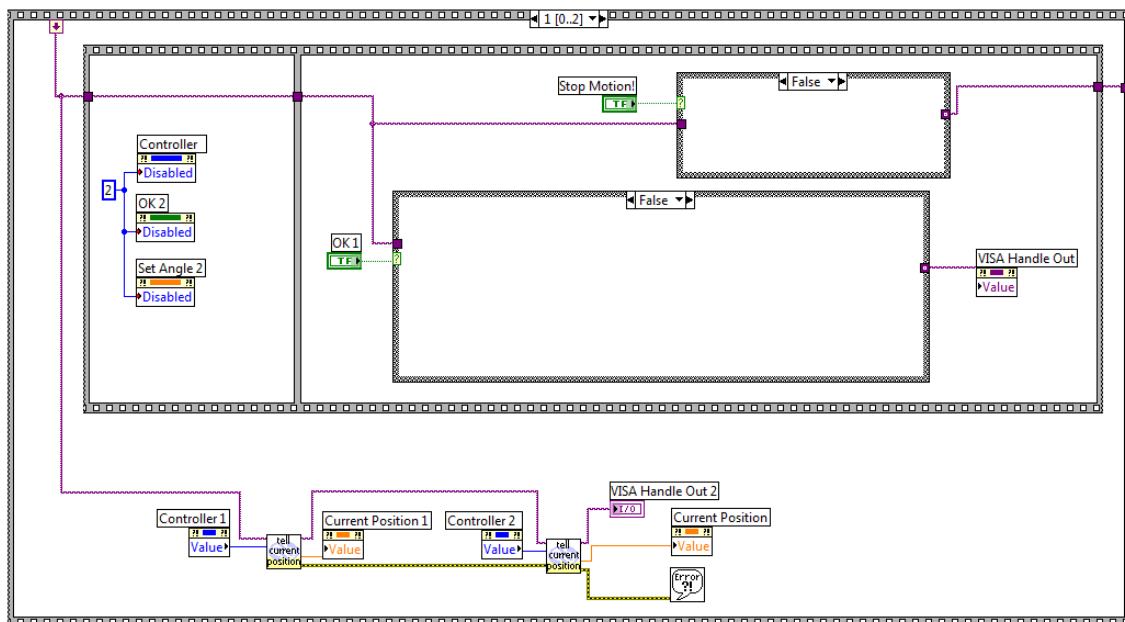
This sub-VI closes the RS-232 communication port.

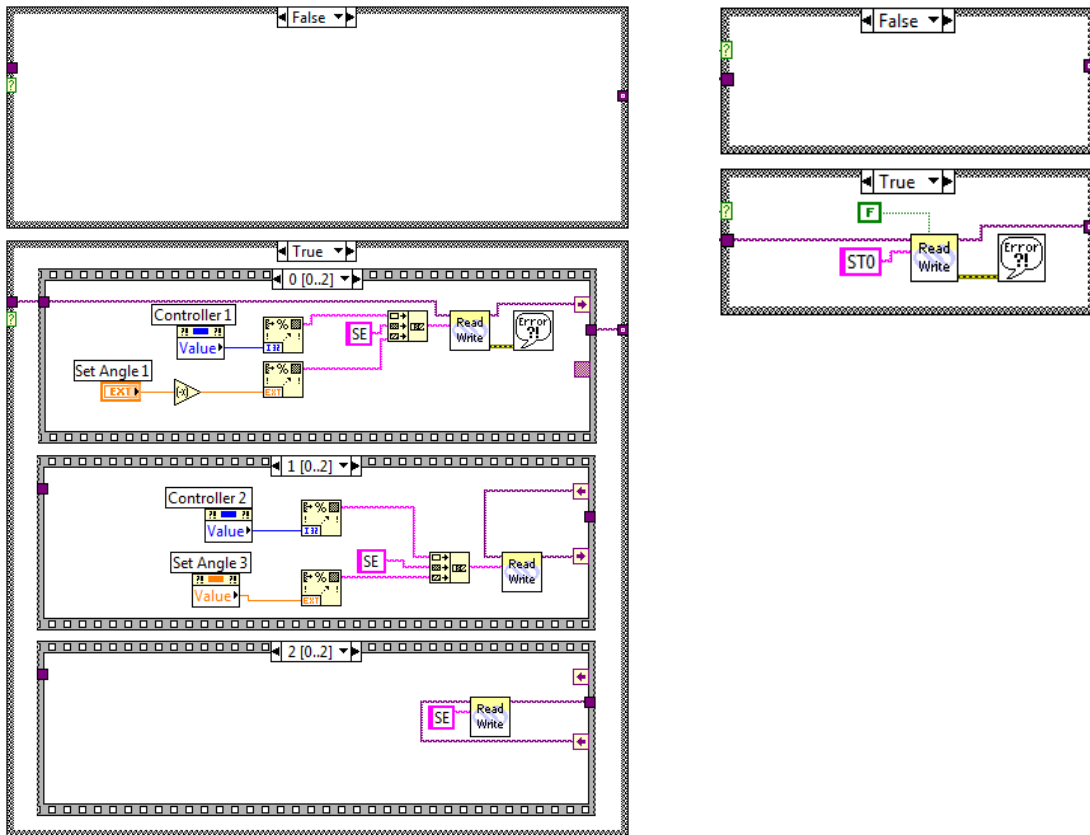
Note: This VI is available from Newport Corporation

BLOCK DIAGRAM:

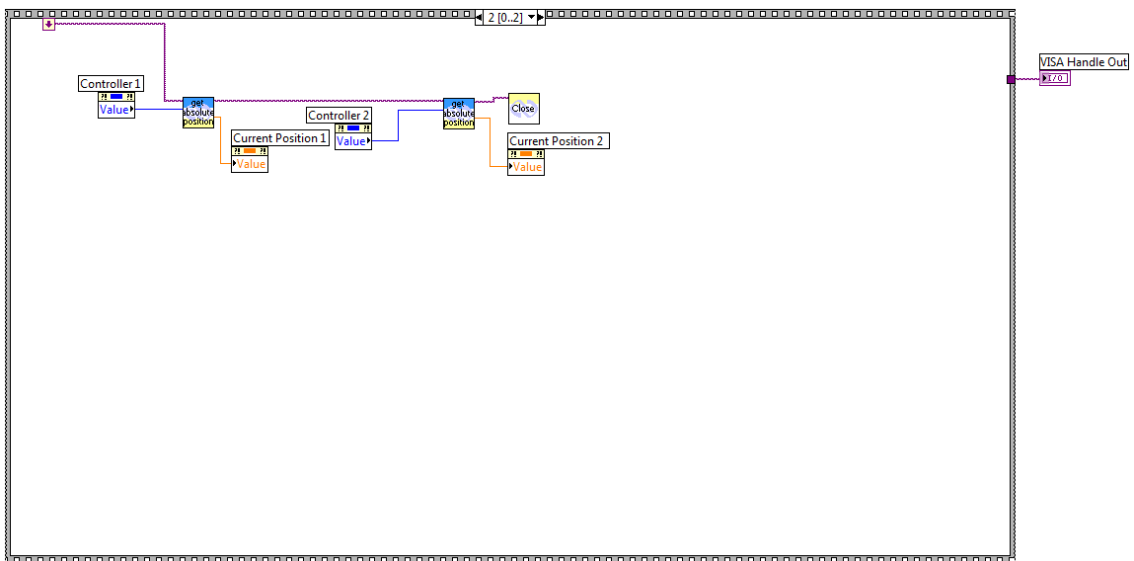


Initialize communication with both rotation stages and get their position





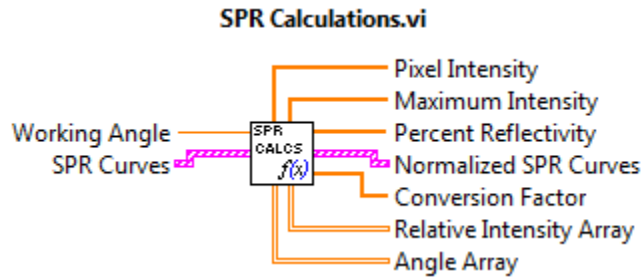
Write new angular position to both rotation stages and begin motion.
Update the current position in real-time.



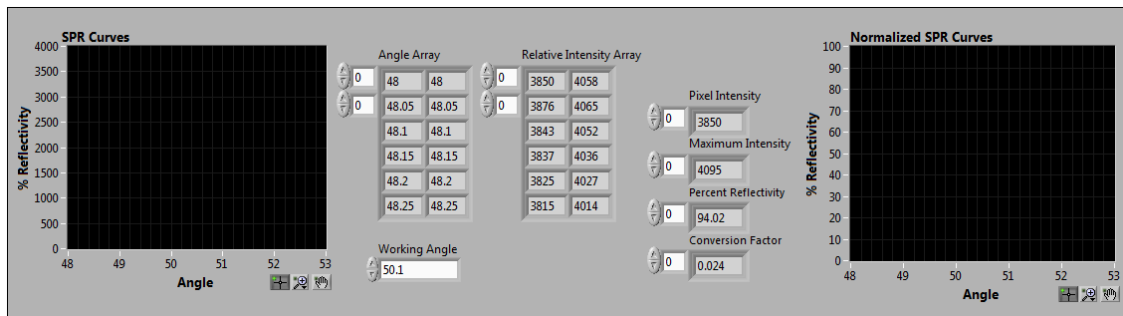
Read final angular position for each rotation stage and close the RS-232 communication port. The current rotation stage position is returned to the Main VI.

C.13 SPR CALCULATIONS.VI

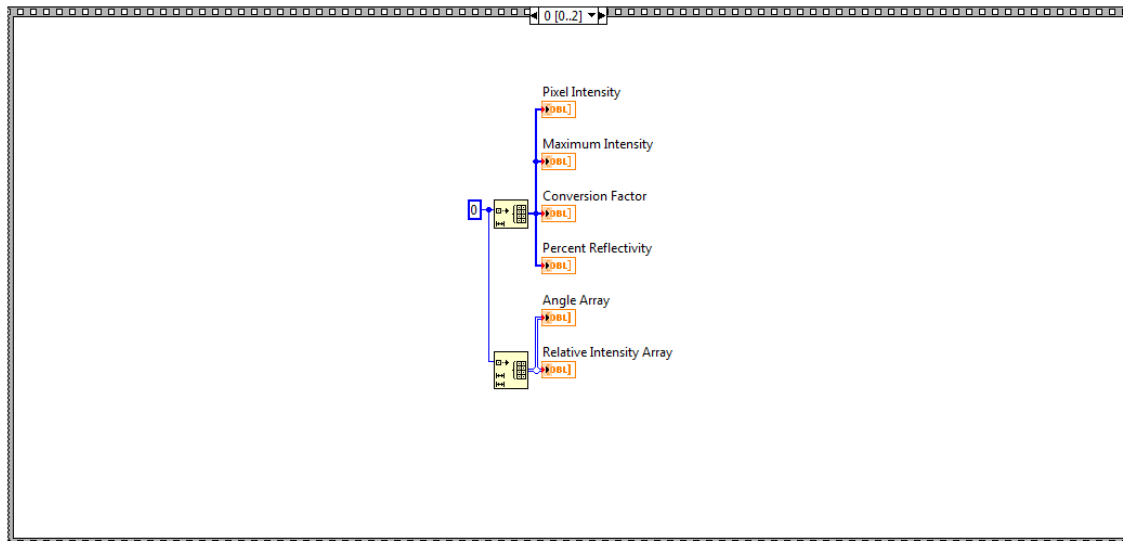
CONNECTOR PANEL:



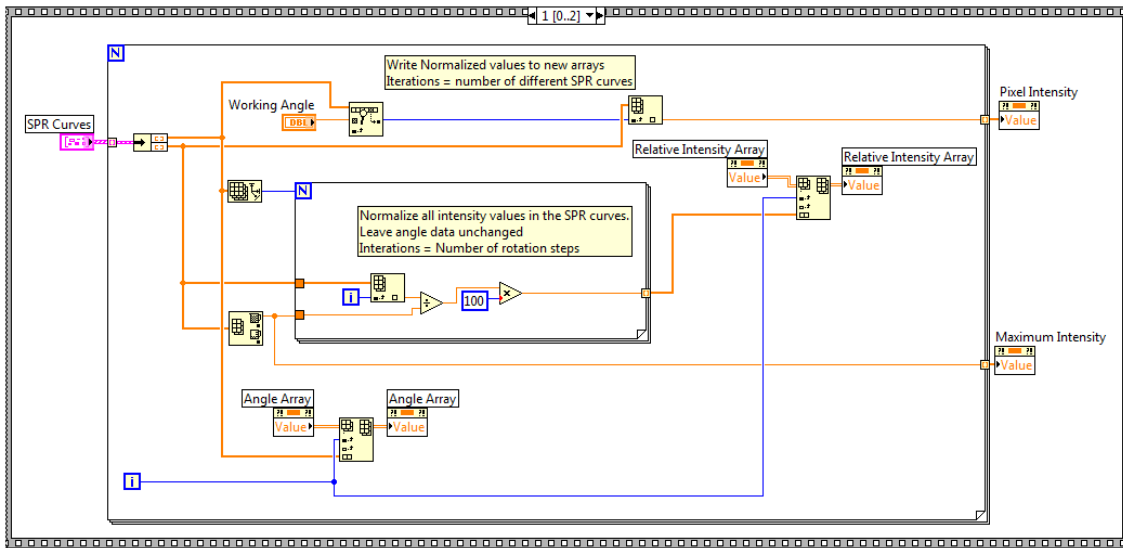
FRONT PANEL:



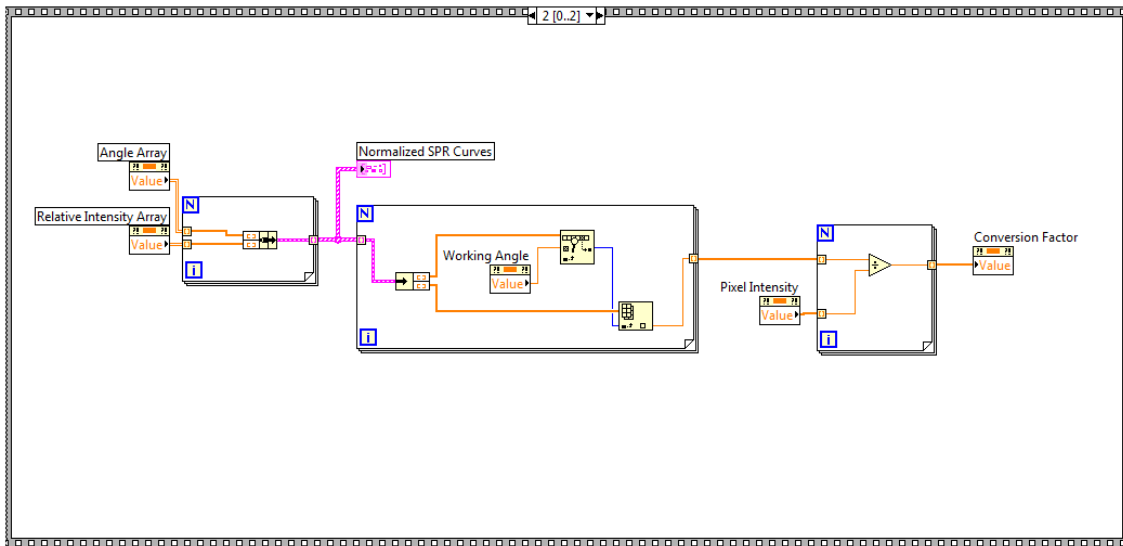
BLOCK DIAGRAM:



Initialize all values to zero



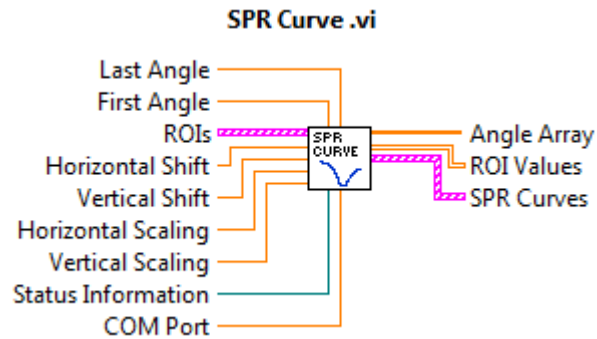
Normalizes each SPR Curve and re-write these values to an array



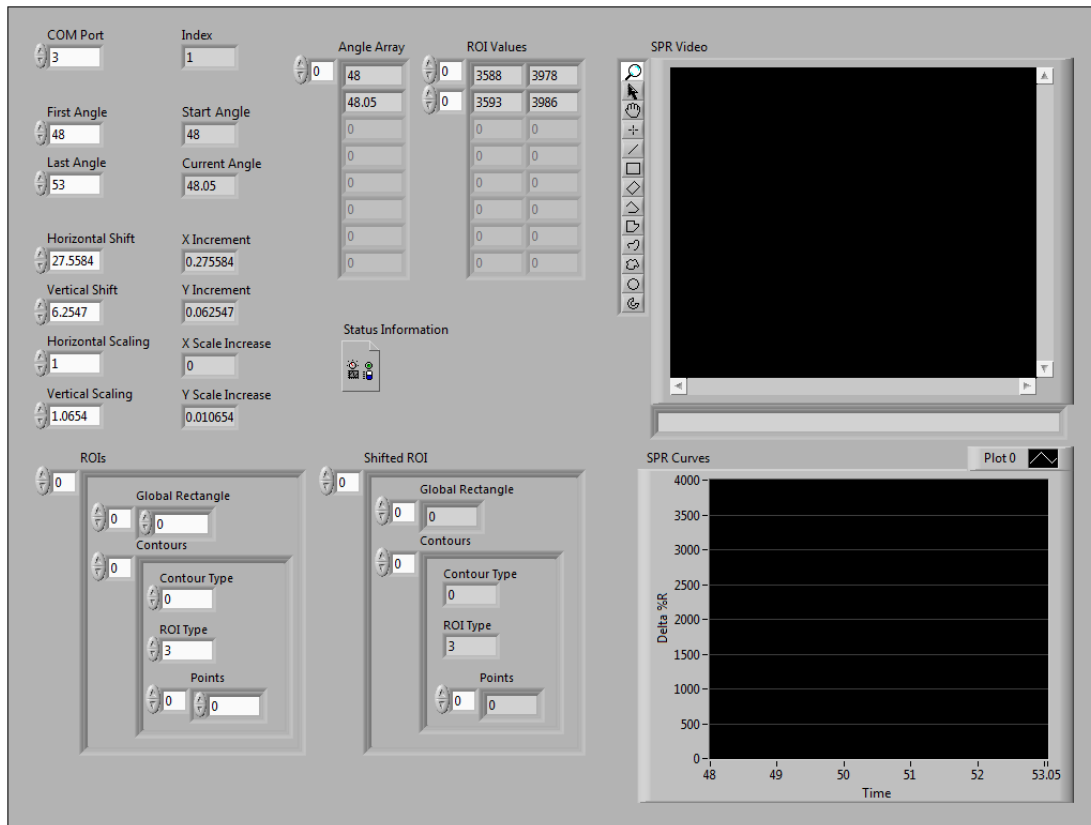
Plots normalized SPR curves in relation to the angular data and calculate the conversion factors

C.14 SPR CURVE.VI

CONNECTOR PANEL:



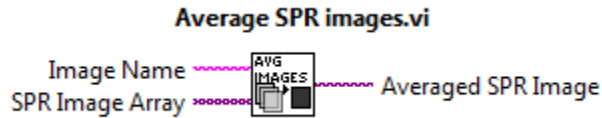
FRONT PANEL:



This sub-VI contains a number of controls and indicators for acquiring and SPR image at 0.05° interval, where the pixel intensities for every region of interest (ROI) area defined is averaged, measured and stored in an array of values for plotting the SPR curves.

LIST OF SUB-VIS INVOKED ALONG WITH CONNECTOR PANEL AND SECTION REFERENCE

(In order of Appearance)



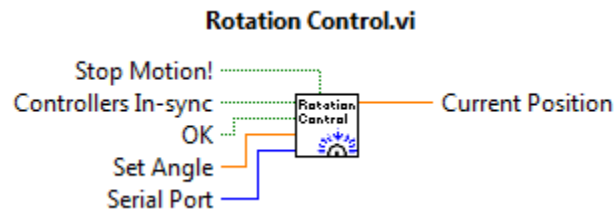
Appendix C.3

This sub-VI averages a series of collected SPR images by the CCD camera to minimize the noise signal from the sensor



Appendix C.10

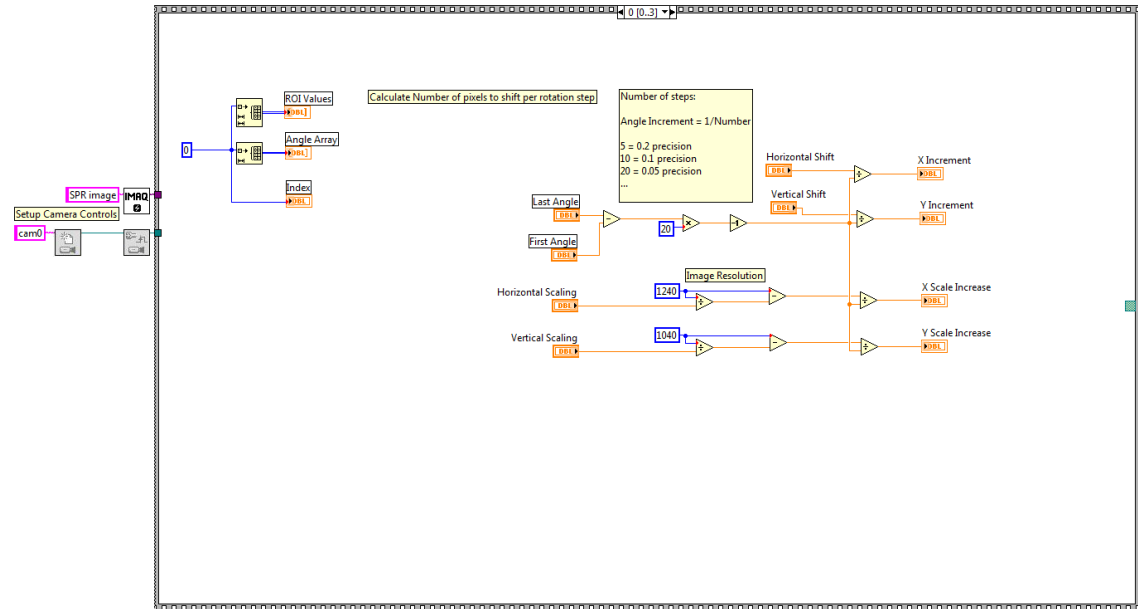
This sub-VI converts the regions of interest (ROIs) on the SPR image to an image mask



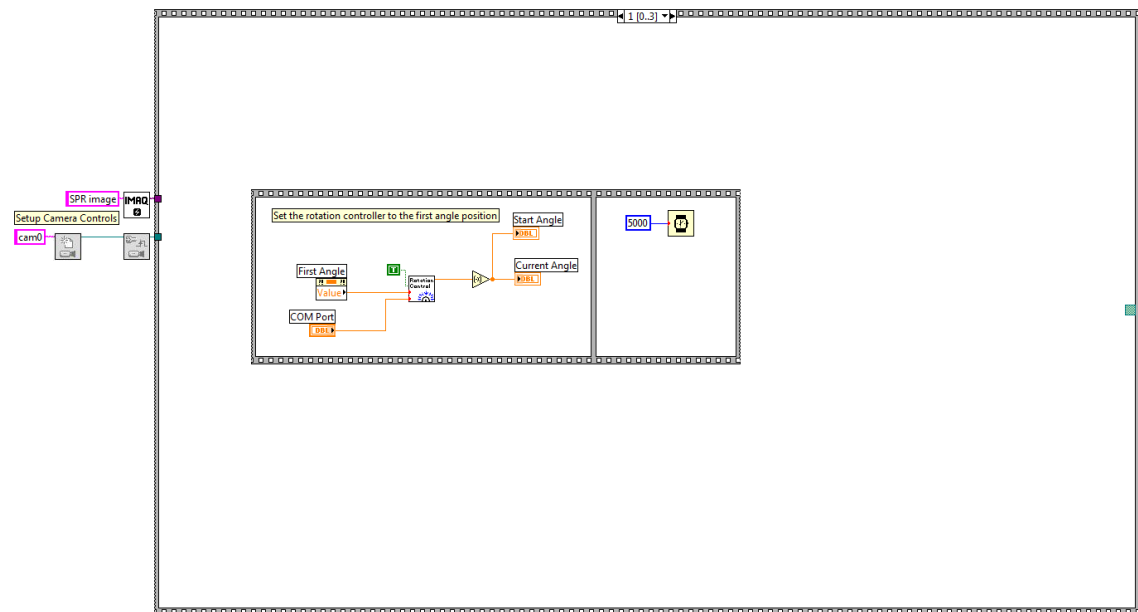
Appendix C.12

This sub-VI controls the rotation angle for both rotation stages

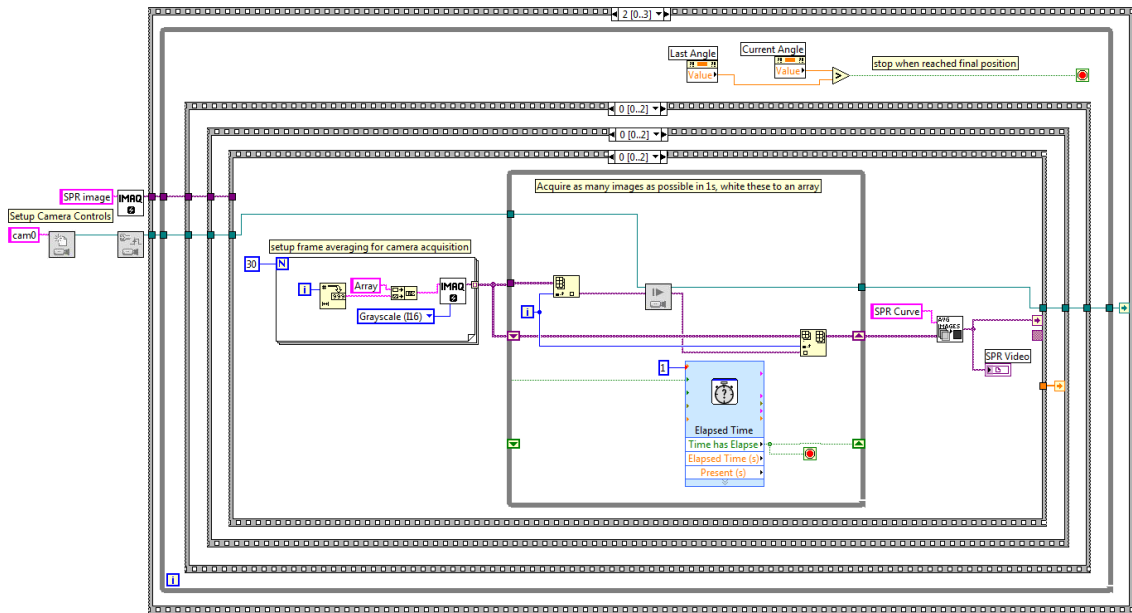
BLOCK DIAGRAM:



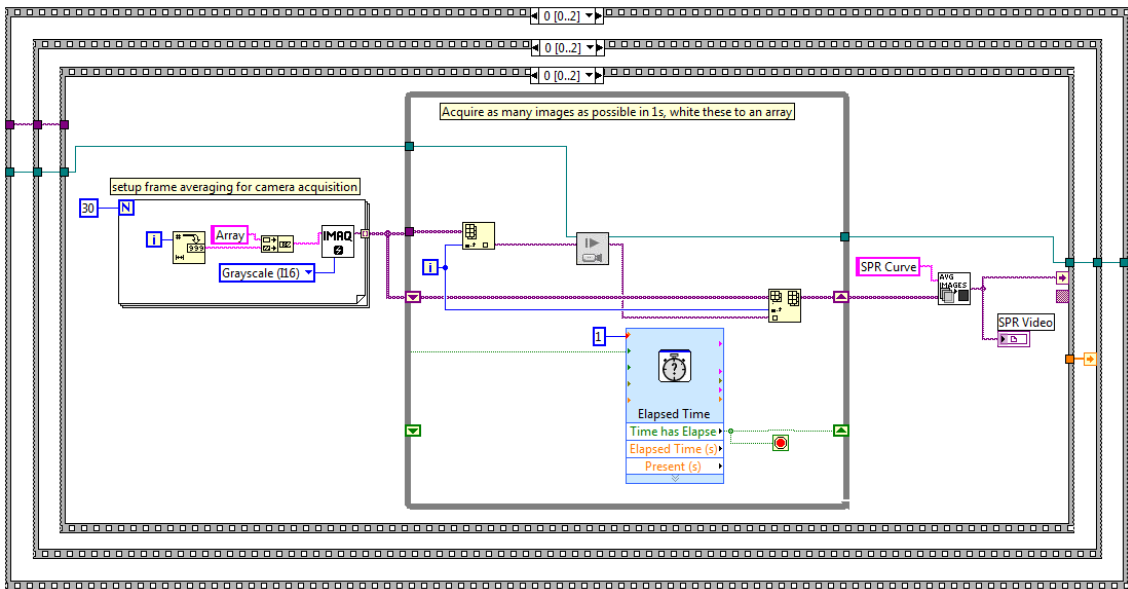
Initialize CCD camera acquisition parameters and angular precision



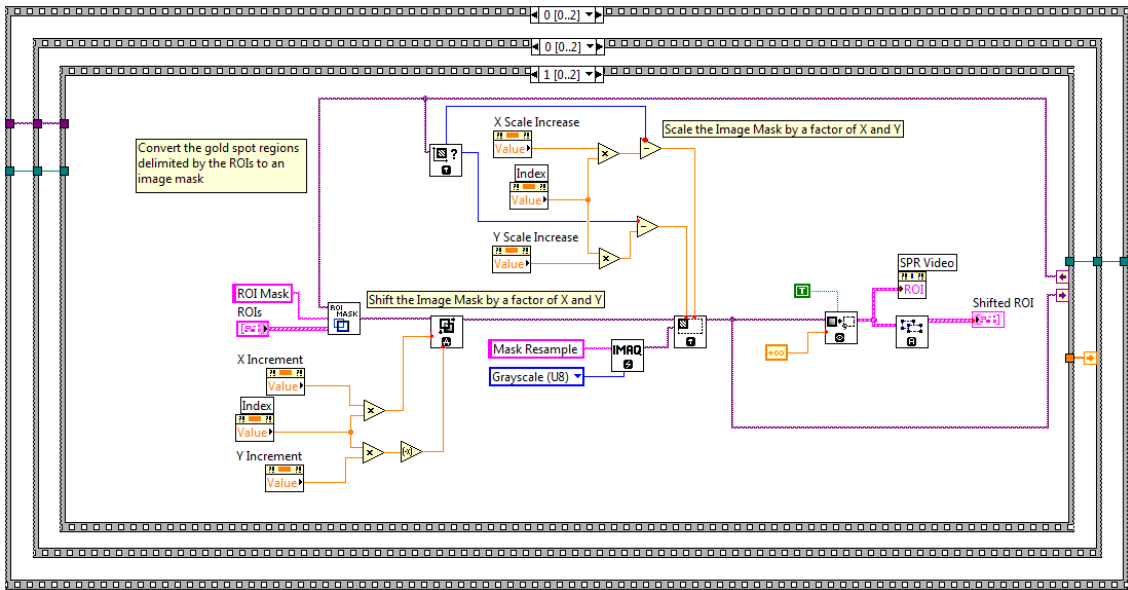
Set the rotation stages to the first angle position supplied by the Main VI, under the SPR Imaging "Options" Tab of the GUI.



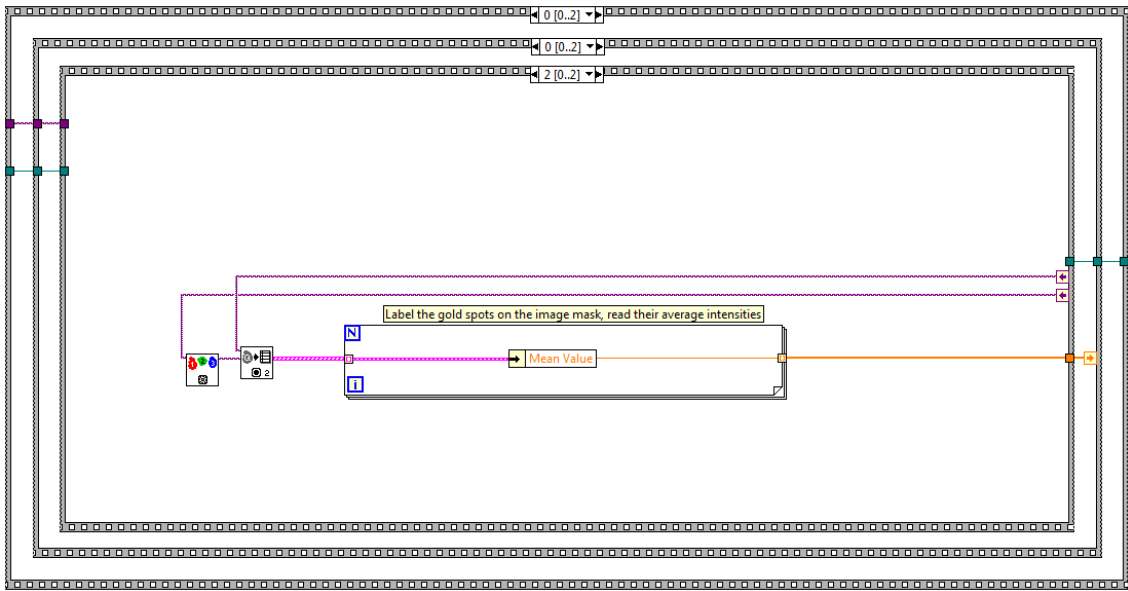
This structure and its subsequent steps (below) are iteratively executed until the last angle position has been reached



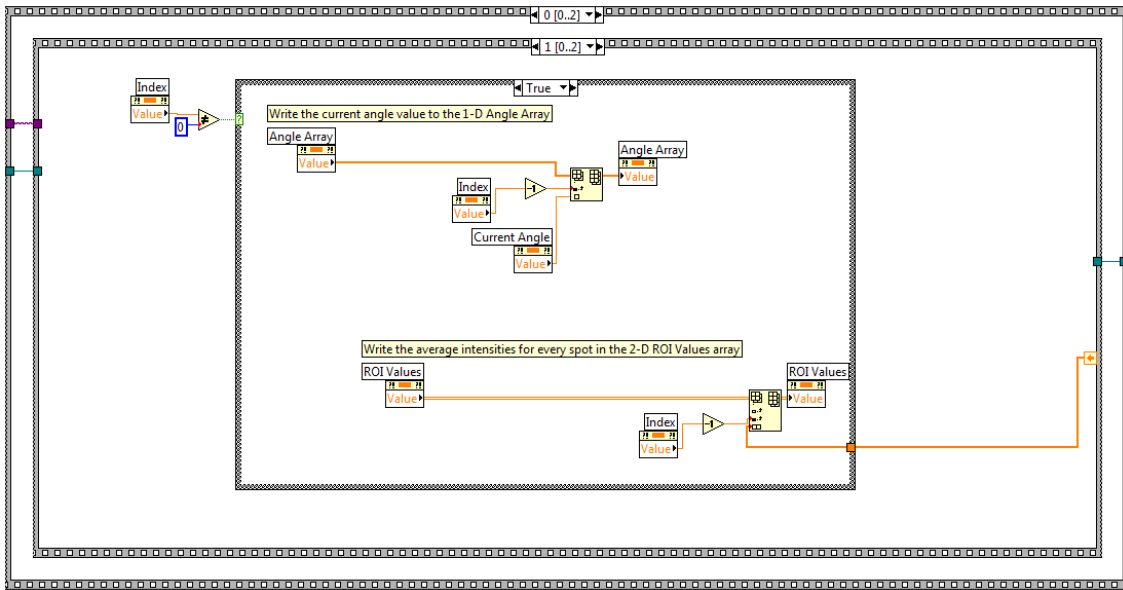
Step 1: Average multiple SPR frames acquired in 1 second



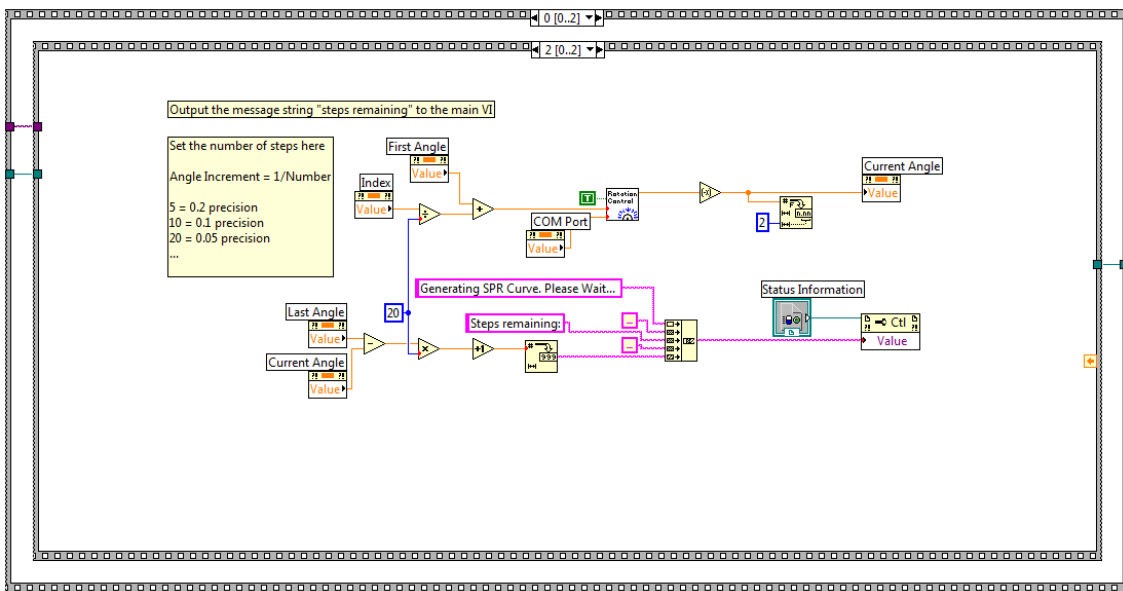
Step 2: Scale and modify the ROIs on the SPR image (initially supplied by the Main VI) according to the current angular position to compensate for the prism distortion



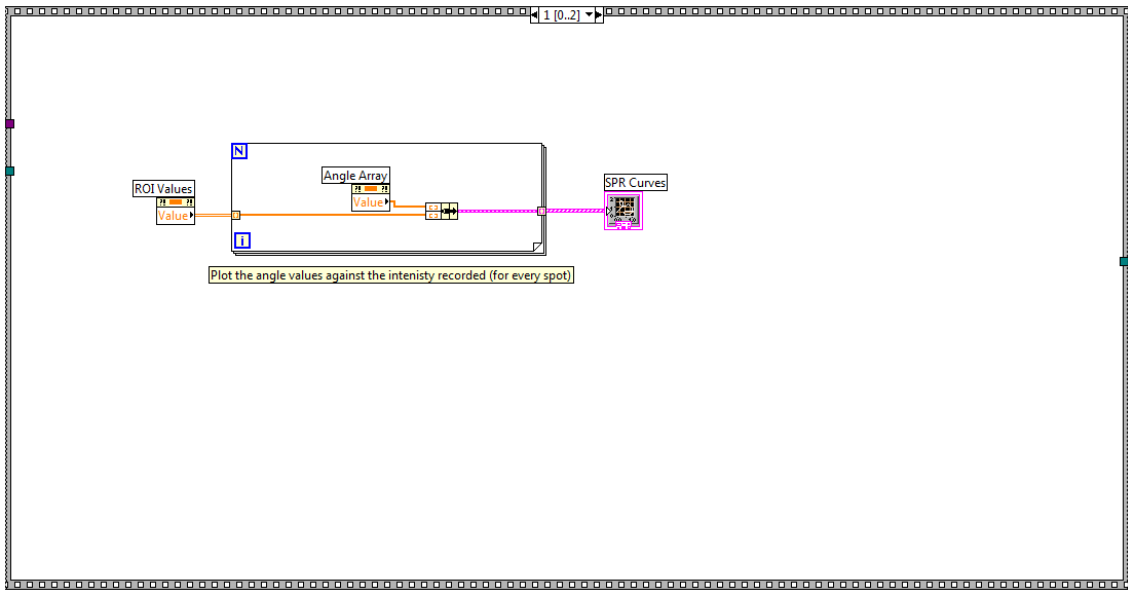
Step 3: Label the modified ROIs and read their average pixel intensities



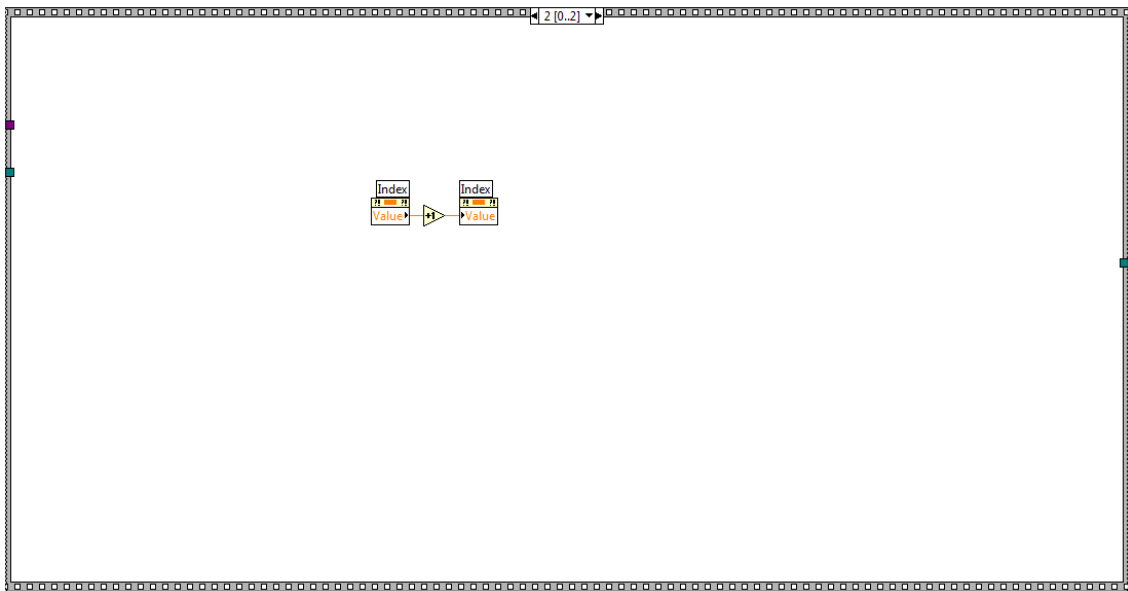
Step 4: Store both the current angular position and the mean intensity for all ROIs, unless this is the first iteration. False case returns nothing.



Step 5: Increment the angular position by 0.05° and return status of the operation to the GUI of the Main VI



Step 6: Plot the measured intensity values for each ROI in relation to the angular position



Step 7: Increment the Index by 1, and repeat at Step 1.

